Minimising Particulate Emissions From Sintering Operations

Matthew Hywell Thomas

Faculty of Science & Engineering

Swansea University

2023

A thesis presented to Swansea University for the fulfilment of the

requirements for the degree of Engineering Doctorate

Declaration

This work has not previously been accepted in substance for any degree and is not being concurrently submitted in candidature for any degree.

Signed: ███████

Date: 06/02/2023

STATEMENT 1

This thesis is the result of my own investigations, except where otherwise stated. Other sources are acknowledged by footnotes giving explicit references. A bibliography is appended.

Signed: ███████

Date: 06/02/2023

STATEMENT 2

I hereby give consent for my thesis, if accepted, to be available for electronic sharing.

Signed: ███████

Date: 06/02/2023

STATEMENT 3

The University's ethical procedures have been followed and, where appropriate, that ethical approval has been granted.

Signed: ███████

Date: 06/02/2023

Abstract

With the drive for manufacturing and foundation industries to move towards a circular economy, the steel industry is making step changes to its processes that aim to produce greener and cleaner products. The current work is focused on sintering, which can account for almost half of all particulate matter (PM) emissions produced during integrated steelmaking. Historic sintering data has been explored to understand the formation of particulate matter and has informed experimental trials, simulating the sintering process. It has shown that it is feasible to reduce PM emissions without incurring significant capital expenditures for a new end-of-line abatement. Prioritising trials was supported by an understanding of the main key levers from the historical data analysis of the sinter plant and a pilot-scale sinter rig that had been modified to capture PM emissions was commissioned and validated. To promote a more circular economy within the steel industry, experimental work showed that the use of new micropellets made from recycled materials would enhance sintering performance and reduce PM emissions. It was determined that the amount of chloride content emitted from PM emissions increased in the waste gas stream as well as decreasing the electrostatic precipitator (ESP) abatement efficiency and this influence can be reduced by washing recycled materials to remove undesirable volatile elements before sintering. It was also established that by manipulating the ratio of nuclei, adhering, and non-adhering particles in the sinter blend by controlling the size fractions, along with partially replacing raw materials, the particle size distribution can be optimised to reduce PM emissions.

Acknowledgements

Contents

List of Figures

List of Tables

1   Introduction

Iron ore sintering is a crucial step in preparing raw materials for the blast furnace during integrated steelmaking. The process involves mixing iron ores, fluxes, fossil fuels and recycled materials (e.g., sinter plant dust) to create a sinter blend which is then agglomerated at temperatures of 1300 – 1480 °C. Sintering these materials improves gas permeability and iron oxide reducibility which contributes to the improved performance and efficiency of blast furnaces.[1] During this process, by-products in the form of air pollutants such as gaseous COx, SOx, NOx, and harmful particulate matter are generated. Notably, the sintering process accounts for around 45 % of the total amount of particulates produced during steelmaking.[2] While recent studies have shown that effective particle removal rates may be achieved by utilising physical abatements such as high-quality filter bags and hybrid particulate collectors, [3,4] these require substantial investment and do not directly address the *production* of particulate matter at the source. Previous research has shown that particulate matter can be significantly affected by varying process parameters. In-bed regulating methods, such as increasing moisture content and granulation time, reducing coke breeze rate, and increasing recycled materials, have been shown to increase emissions during sintering [5]. Through a fundamental approach, it is hypothesised that a reduction in emissions could be achieved through process parameter optimisation, as opposed to the implementation of a physical abatement.

The integrated steel plant accumulates immense amounts of data in the various works areas. The blast furnaces are the primary driving force behind the fundamental financial performance of the steel plant. Therefore, the principal for the long-term future of the business is reliant on efficient and stable operations. Consistent raw materials are critical for the stable operation of the blast furnaces and with a focus on ferrous raw materials (sinter, pellets, and lump ores), coke, and injection coal. Sinter is made on-site by the sinter plant and is a continuous operation that is key for providing the blast furnaces with a consistent feed of raw materials. This work aims to identify key opportunities for decreasing PM emissions through extensive data analysis and prioritise further experimentation on a pilot-scale sinter rig. Simulation of physical sinter plant operations will also incorporate the capturing and monitoring of particulate emissions to enable an understanding of environmental output and process variables. Research findings through

data and experimental understanding will be iteratively optimised and finally, where successful, implemented in full-scale plant trials with online monitoring for real-time process interventions and data analysis.

The three main objectives for this project have been concluded and are:

1. Effects of the chemistry of the sinter blend upon performance (product output and environment e.g., PM emissions). Focusing on reduced chlorides by treatment of recycled materials, effects on sinter quality and implementing new innovative technology using a compilation of sinter process imitating equipment.

2. Pilot-scale sinter rig experiments with current and modified blends, Optimising process performance, analysis of the emissions from the rig and testing sinter quality.

3. Full-scale plant trials with the use of online monitors.

2   Literature Review

2.1   Overview of an integrated steel plant

The integrated steel plants are typically large sites with at least eleven miles in area with a production capacity of approximately five million tonnes per year[6] with the main processes in the steelworks being iron-making (sintering, blast furnace, coking and raw materials), steel-making (basic oxygen steel-making) and rolling mills, which were also the main contributors to PM_{10} emissions, accounting for 45% of the mass of particulates [7]. Authorities typically implement emission limit values (ELVs) for PM emissions on all sinter plants which target the main stacks. The consequence of non-compliance is the authority can fine and shut down the integrated steel plant, which highlights the importance of the work. Figure 2.1 shows a typical example of a measurement system often used around integrated steelworks which are typically used around steel works which are located close to communities. The filter dynamic measurement system (FDMS) is generally used and is usually located around the area and can measure the semi-volatile fraction of airborne PM. This can be important in the study of primary and secondary PM and to ensure there were no losses of these semi-volatile fractions due to sampling conditions. The dichots splits the incoming sample and separate the fine and coarse fractions providing a measurement of both sizes using its dual tapered element oscillating microbalance (TEOM) sensor design.[8]
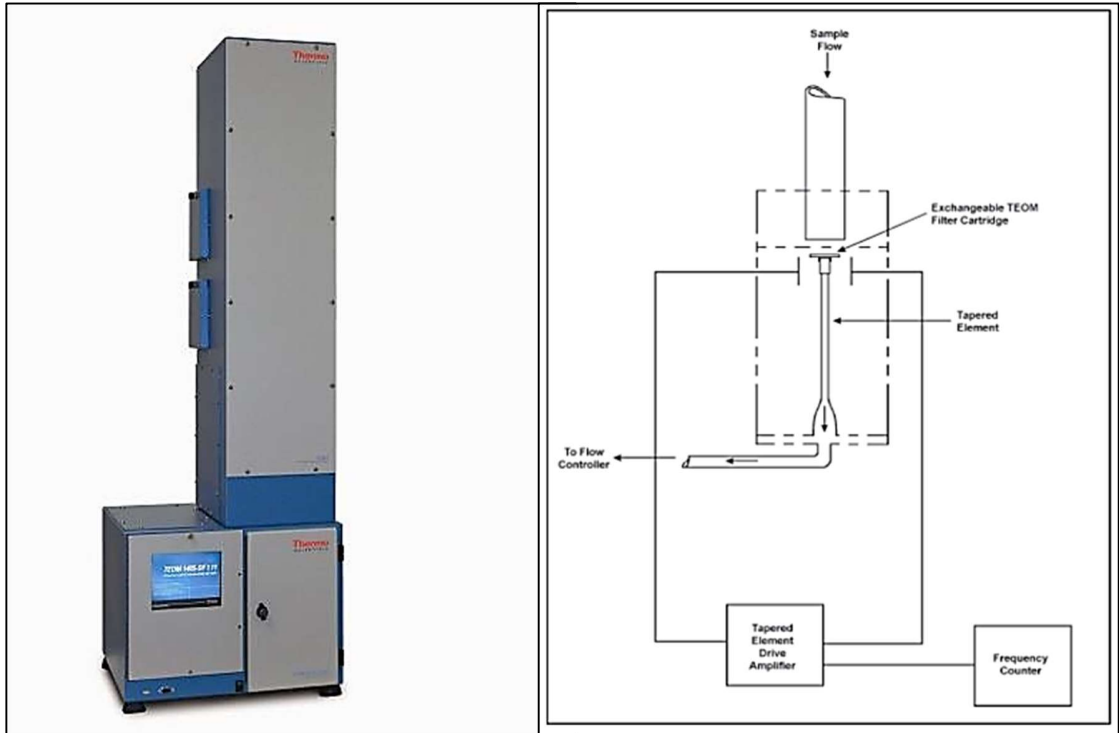
Figure 2.1 – Schematic of the filter dynamics measurement system (FDMS)[8]

2.2 The Steel Production Route

The iron and steel industries are highly material and energy-intensive with more than half of the mass input becoming outputs in the form of off-gases and solid wastes or by-products.[9] The iron and steel industry broadly consists of:

- Primary facilities that produce both iron and steel.
- Secondary steelmaking facilities.
- Iron production facilities.

2.3 Coke Plant

The coke oven plant (Figure 2.2) is where the coal is charged to airtight ovens by cooking the coal at temperatures of between 1200 -1300°C for around 18 hours to produce coke. At the end of the coking cycle, the coke is pushed out of the oven into a rail car and the red-hot coke is transported to a quenching tower where it is quenched by water.[10] The releases from the pushing operation are collected by a collection system and pass through

a water scrubber before being released from one of three stacks. Gas is driven off from the ovens during the coking cycle and is cooled (cleaned) and some by-products are removed, and the by-products are collected and either re-used or sold and clean gas is recycled within the site as fuel and excess gas may be vented through a flare stack which is ignited. Typical coke plant pollutant emissions are shown in Table 1 [11] which includes information from older plants before 1993 and newer plants after 1993 which contributed to the advancing of technology and the ability to analyse emissions.
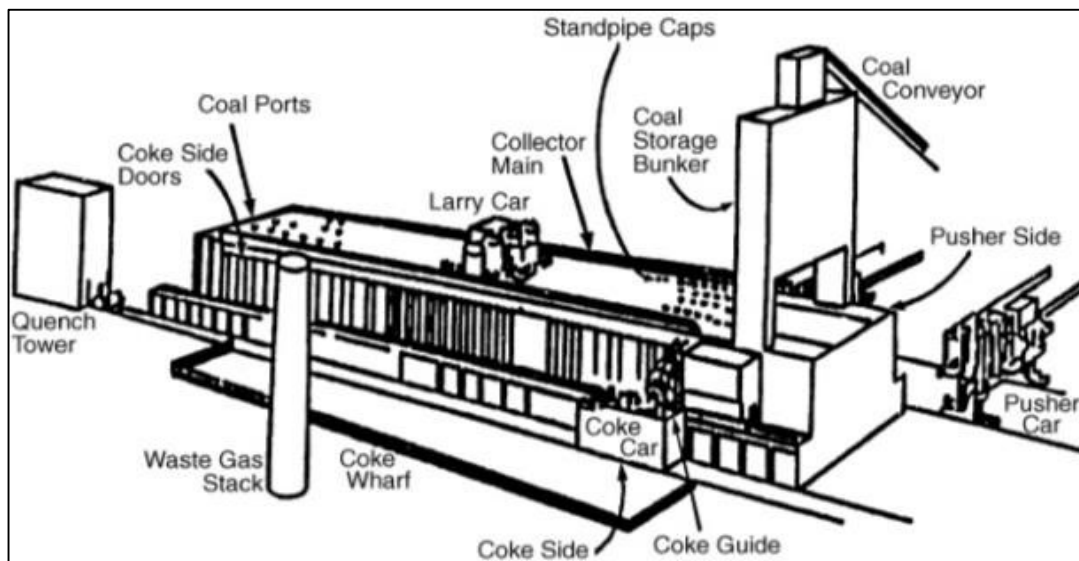
Figure 2.2 – A Typical coke oven plant[11]

Table 1 - Coke Plant typical pollutant emission levels[12]

Coke Operation	plant	PM (g/t LS)	CH₄ (g/t LS)	Ali. HC (gC/t LS)	Benzene (mg/t LS)	BaP (mg/t LS)	PAH (mg/t LS)	CO (g/t LS)	SO₂ (g/t LS)	H₂S (g/t LS)	NH₃ (g/t LS)	NOx (g/t LS)
Charging	Old plants	1-1.5	17	n/a	34	3.5	n/a	7-13	n/a	n/a	n/a	n/a
	Newer plants	0.1-3.5	0.025-25	0.003-10	2-100	0.007-1.5	n/a	0.02-24	0.003-3	n/a	<0.1	n/a
Carbonisation doors	Old plants	4	n/a	n/a	33.5	19	n/a	n/a	n/a	n/a	n/a	n/a
	Newer plants	0.1-2	1.5-2.5	0.3-8	70-4700	1.5-15	n/a	0.5-1.0	0.05-0.5	0.006-0.3	0.03-0.5	0.01-0.15
Lids	Old plants	n/a	n/a	n/a	270	3	n/a	n/a	n/a	n/a	n/a	n/a

	Newer plants	0.05-0.5	1.5-3.5	0.5-5	270-2200	3-5	n/a	0.3-3	0.05-0.3	0.005	0.03-0.1	0.01-0.005
Ascension pipes	Old plants	n/a	n/a	n/a	n/a	n/a	n/a	n/a	n/a	n/a	n/a	n/a
	Newer plants	<0.07	0.1-1	0.03-0.3	3-33	0.1-1	n/a	0.001-0.1	0.003-0.03	<0.005	<0.003	n/a

Legend: LS=liquid steel, ali.HC=Aliphatic hydrocarbons, BaP=Benzo(a)pyrene, PAH= Polycyclic aromatic hydrocarbons, n/a=not available

2.4 Granulated Coal Injection

Coal is delivered to the department by ship via a boom stacker to one of the stockyards delivered by road/rail and the coal is transported from the yard to the processing plants via a conveyor system. The coal is next crushed and dried in an inert atmosphere to temperatures over 100°C to reduce the moisture content to less than 1.5%.[13] The hot gases used to dry the coal are generated from a dual fuel burner; Blast furnace gas is the primary fuel with natural gas. The moisture and products of combustion are passed through a bag filter before being discharged via a stack (Figure 2.3). Typical emissions for granulated coal injection plant range from SO_2, NOx, CO, CO_2, and H_2O vapour.
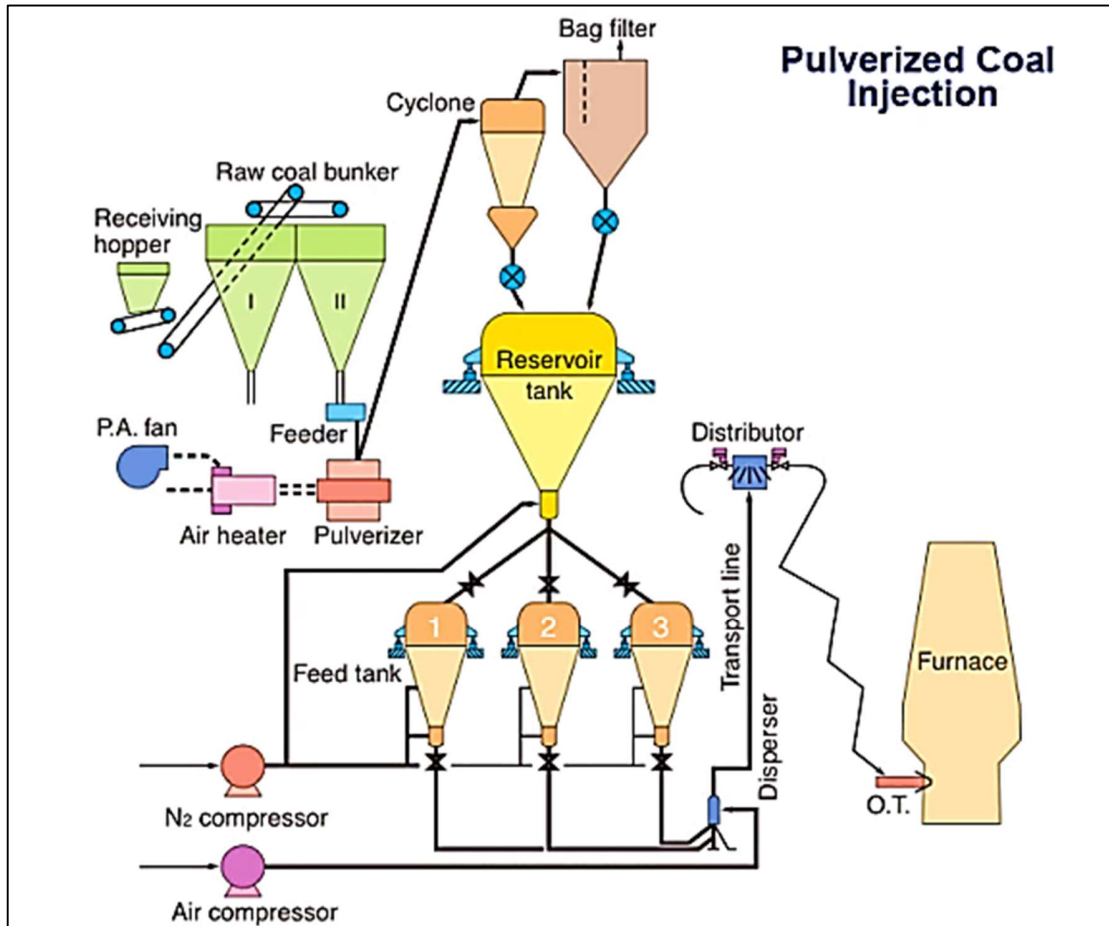
Figure 2.3 – A typical granulated coal injection plant [11]

2.5   Blast Furnace

The first step in the manufacturing of steels is by removing oxygen from the ore which is Fe chemically combined with O_2 or other non-metals from the earth's crust. The most workable ore is high in Fe_2O_3 and via reduction using CO gas which takes away the O_2 from the Fe_2O_3. The reaction of changing Fe_2O_3 into CO_2 (Equation 6) takes place due to each molecule of CO gaining an oxygen atom and this process is called redox. Another redox reaction (Equation 7) takes place with the remaining 20-30% of the iron by direct reduction (ore is directly reduced by the carbon). This is due to the furnace temperature being in the region of 1500 °C where the decomposition of limestone into calcium oxide (Equation 8) and this oxide helps to remove some of the acidic impurities from the ore (Equation 9). The blast furnace (Figure 2.4) operates continuously, and the furnace is

maintained at a full stock line level, by charging alternate layers of coke and ferrous materials such as iron ore and various fluxes.

Equation 1 – Blast furnace oxidisation reaction

$$Fe_2O_3(s) + 3CO(g) = 2Fe(l) + 3CO_2(g)$$
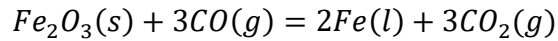
Equation 2 – Blast furnace direct reduction reaction

$$Fe_2O_3(s) + 3C(g) = 2Fe(l) + 3CO(g)$$
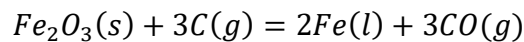
Equation 3 – Decomposition of limestone

$$CaCO_3(s) = CaO(s) + CO_2(g)$$
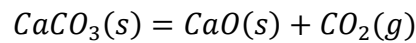
Equation 4 – Removal of acidic impurities

$$CaO(s) = SiO_2(s) + CaSiO_2(l)$$
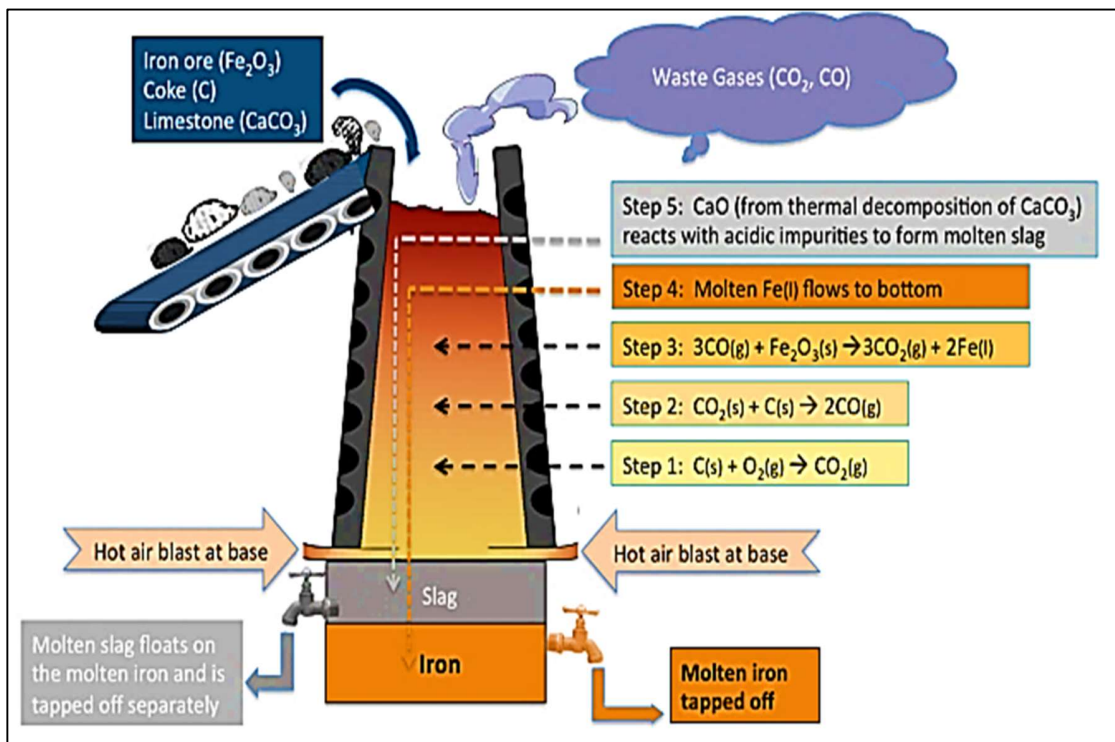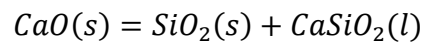
Figure 2.4 -A typical blast furnace diagram[14]

The most important requirement in blast furnace operation is that the pig iron and slag are fluid therefore both can be tapped from the furnace. The overall composition of the blast

furnace burden must produce pig iron of reproducible quality with the correct composition for subsequent steelmaking. The laboratory tests include tumble index (TI, % −6.3 mm), abrasion index (AI, % −0.5 mm), decrepitation index (DI, % −5.0 mm), reduction degradation index (RDI, % −3.15 mm), and reducibility index (RI). TI and AI (ISO 3271) are designed to measure lump resistance to physical breakdown during transportation, DI (ISO 8371) is a measure of lump resistance to thermal shock in the upper part of the blast furnace, RDI (ISO 4696) simulates physical breakdown during reduction, while RI (ISO 7215) is a measure of the ease with which iron oxides can be reduced (Figure 2.5).[15]
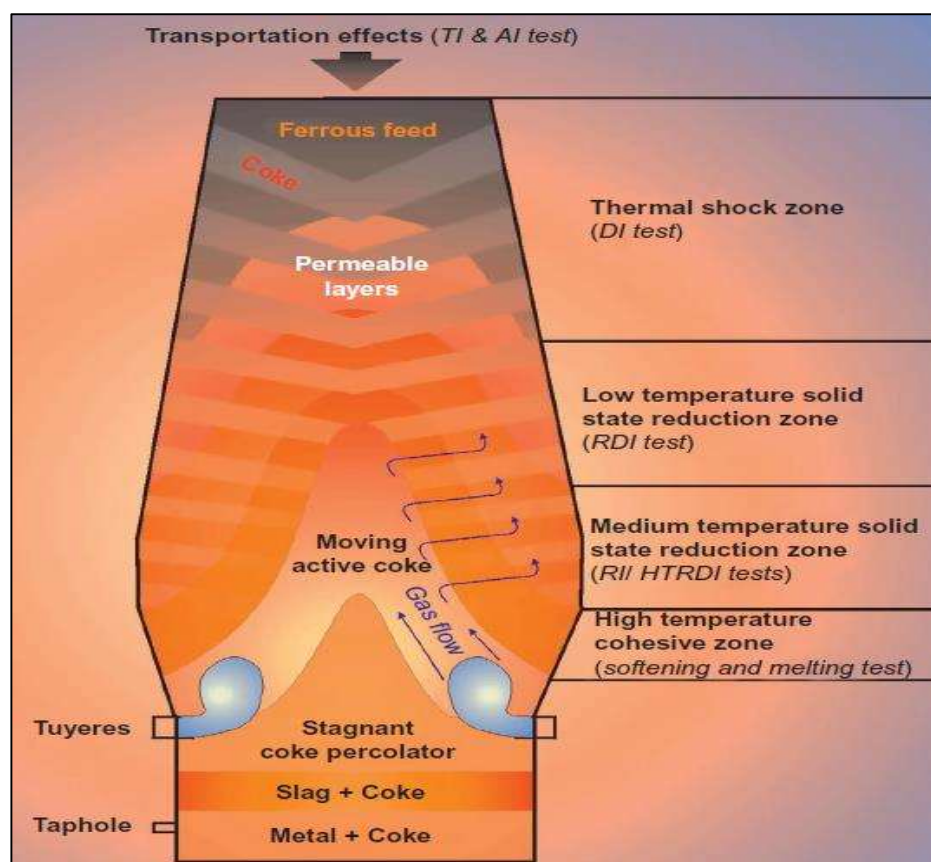
Figure 2.5 - Schematic cross-section through the blast furnace showing key zones and standard industry laboratory tests designed to simulate the respective zone.[15]

The lump properties of ore textural groups are consistent within and between the iron ore deposits examined, with minor quality differences due to differences in porosity (leaching). Key controls on lump metallurgical quality include the following:

- TI is interpreted to be a function of physical hardness, with less porous and dense martite-hematite textures being of higher TI and more porous, soft, goethite-bearing textures being of lower TI.

- AI is the complement of TI, as more porous and goethitic ores have higher AI.

- DI is highest where thermal shock results in the rapid evolution of mineral structural water, especially where goethite is locked within dense/low, open-porosity hematite/hydrohematite or where dense goethite is present.

- RDI tends to be high where there is a finely porous structure, and the minerals have few thick/solid interconnections.

- High lump reducibility is interpreted to be due to more porous ore textures.[15]

The blast furnace gas leaves the furnace top at usually about 2.0 bar pressure where gas is cooled/cleaned in the gas cleaning system and the cleaned gas is used as fuel for purposes such as coke ovens under firing, power plants or stoves. Excess gas can either be burnt or vented through several flare stacks or vents and typical blast furnace pollutant emission levels are shown in Table 2. The iron flows underneath a skimmer arrangement to ensure slag-free iron can pass into mobile torpedo ladles to allow transportation by rail to the basic oxygen steelmaking plant.

Table 2 - Blast furnace typical pollutant emission levels[12]

Operation/emission source	dust (g/ LS)	H_2S (g/t LS)	SO_2 (g/t LS)	NOx (g/t LS)	CO (g/t LS)
Charging zone	25/5-38	1s	1s	1s	1s
Coal preparation	15/2-54	1s	1s	1s	1s
BF cast house	12/2/79	5/0-3.4	12/2-250	4/1-27	1s
Slag granulation	n/a	14/1-300	13/1-142	1s	1s
Hot stoves	3-6	1s	45/15-375	41/100-550	29/50-2700

Legend: LS=liquid steel

2.6   Sinter Plant

The main aim of a sinter plant is to produce the main burden for the blast furnaces by bonding together fine materials that would otherwise be unsuitable for a direct charge to the furnaces. A sinter plant (Figure 2.6) is required to produce a strong product (sinter) by the correct control of chemistry and fuel additions, a product that is easily reduced in the

blast furnace process. Sinter is produced worldwide as it creates a product that has a good temperature profile that is highly reducible and has customised chemistry using fluxes that compensate for the other burden materials and the mandatory blast furnace slag chemistry is displayed in Figure 2.7. Waste materials from on-site can be recycled along with the use of various sources of iron ore fines which can be meticulously selected based on chemical analysis, cost, and commercial availability.
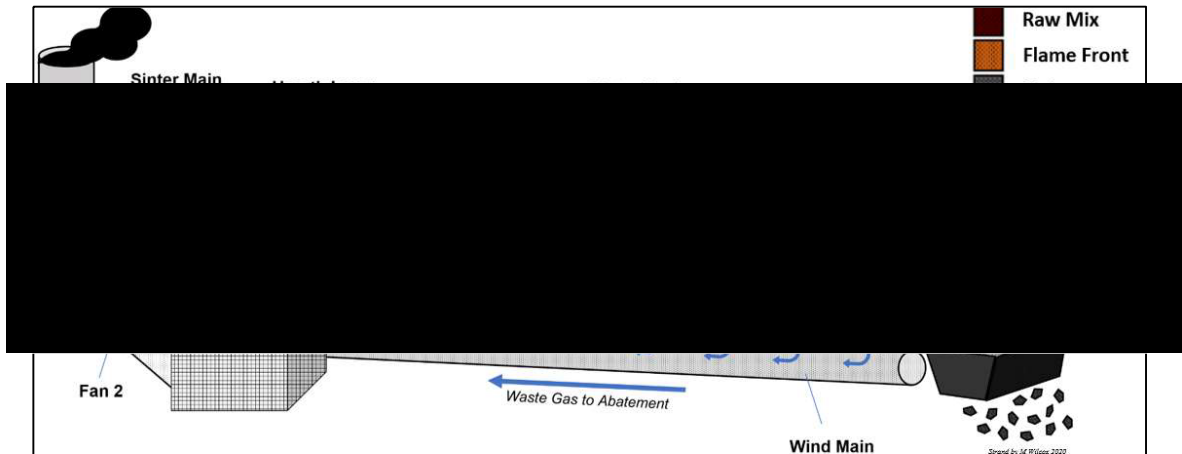
Figure 2.6 – A typical sinter plant strand with abatement and stack
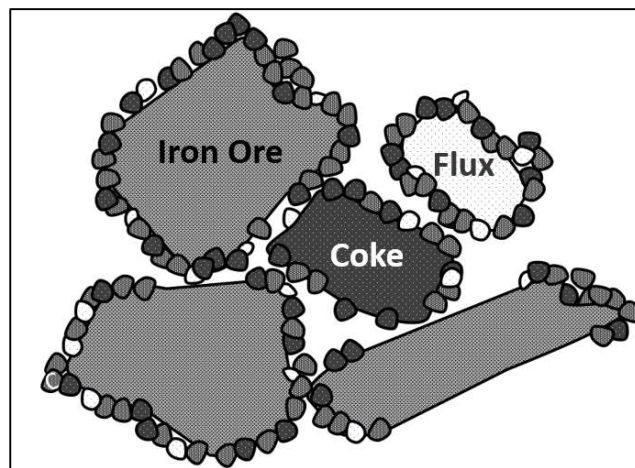
Figure 2.7 – Typical sinter mixture which includes coke, flux and iron ore.

Continuous opportunities for local and internal product use include the development of iron-recycled materials and alternative gangue sources for the sinter plant and blast furnace for basicity control. Also, alternative fuel sources for the sinter plant need to be used for site-wide waste streams and recycled materials need to be used to improve the circular economy within the steel plant. Technical boundaries can range from suitability (coking or sintering properties) to, quality of pellets, sinter, and coke for the blast furnace

process. Iron ores are mined around the world, their source determines their quality as shown in Table 3. Ideally, an iron producer requires a high iron (Fe) content from 60 to 65% with low levels of impurities where the impurities can be removed and absorbed into a slag formed by flux additions. The main two factors in material selection include the chemical composition, which is a necessity to satisfy the service level agreement between the sinter plant and blast furnace where the specification for sinter chemistry changes every four days with a new blend and another factor is that the mix of materials needs to be generated at minimum cost. The aim is to make one product at the end of sintering, using an array of raw materials (up to twenty-two materials) in the blend with various chemical compositions.

Table 3 – Applications of various iron ore that can be used in steel making.

Material	Fe content %	Morphology	Size in diameter	Application
Pellets	60 – 65%	Spherical	6-13mm	Pellets are made by tumbling iron ore fines with a blending agent to produce a green pellet, cured by heating.
Lump Ore	Up to 64%	Metamorphic	6 – 25mm	Lump ore is produced directly at the mine and has no further processing.
Sinter	52 – 60%	Amorphous with mixed shapes	6-25mm with 90% is typically <25mm	The sinter blend is heated therefore that the particles sinter together.

There are three stages in the planning process for material selection:
1. Ore selection – availability and chemistry specification are key levers.
2. Recycled material selection – major concerns include Zn, P and Alkali loading where K_2O levels are of interest flue to scab/scaffolding to the blast furnace refractories wall.
3. Flux selection – three fluxes: olivine (40% Si, 48% MgO), magstone (15-20% Mg, 30% limestone) and limestone.

Sinter consists of various mineral phases of varying composition and morphology consisting of hematite (Fe_2O_3), magnetite (Fe_3O_4) and calcium ferrites with silica and alumina and the different applications of iron ores are shown in Table 3. Hematite is a

direct-shipping ore with naturally high iron content, hematite ore must undergo only minimal crushing, screening, and blending processes before being dispatched for steel production. The mineral magnetite has higher iron content than the mineral hematite. The other types of iron ores are presented in Table 4 with information.

Table 4 – Iron ore types[16]

Mineral	Formula	Colour	Forms of Fe	%Fe	% Loss of ignition (LOI)
Hematite	Fe_2O_3	Red/Brown	Fe +3	69.94	0
Magnetite	Fe_3O_4	Black	2/3 Fe+3 1/3/Fe+2	72.35	-3.45
Limonite	$HfeO_2$-nH_2O FeO (OH)-nH_2O	Yellow/Brown	Fe+3	45-62	0-36
Goethite	$HfeO_2$	Brown/Black	Fe+3	62.85	10.14
Martite	Fe_2O_3 (Fe_2O_4 residual core)	Red/Brown	Fe+3 (Fe+2)	69.94-72.35	0 to -1
Ilmenite	$FeTiO_3$ FeO-TiO_2	Black	Fe+2	36.80	-5.27
Siderite	$FeCO_3$ FeO-CO_2	Range of colours	Fe+2	48.20	31.1
Pyrite	FeS_2	Metallic yellow	Fe+2	46.55	33.5

The essential characteristics of iron ore are:

- Reducibility – ease that the O_2 combined with Fe can be removed and higher reducibility results in lowered coke rate i.e., higher productivity in the blast furnace.
- Size and distribution – permit the uniform flow of gas through the charge bed and improves the utilisation of the chemical and thermal energies.
- Strength – the ability to maintain the size of the ore due to breakage that would result in choking in the furnace.
- Temperature and range of softening – the products have a range of melt temperatures, therefore, a smaller range of softening, the better the gas flow and higher the productivity.
- Iron, moisture, and gangue contents – moisture increases the thermal load and the fuel rate.

- Swelling and volume change – pellets tend to swell in a reducing atmosphere and consequently, have a loss of strength which resists the flow of gases.

Recycled materials are the lowest cost product and are high in C, Fe, MgO and Al_2O_3 from various on-site operations i.e., the blast furnace, BOS plant and the mills. Blast furnace dust is captured in two different abatements and the flue dust off the top of the furnace is captured in a water tank that settles in a slurry. It is a source of high Zn and alkali levels that limit its use and consist typically of 30-45% C and 20-30% Fe. Another recycled material called 'F scrap' produced by BOS slag needs to be processed magnetically, with a typical composition of 30-70% Fe, 15-30% CaO, 5-12% Si, 3-8% Al_2O_3, 3-8% MgO and 1-2% Mg. The other types of recycled materials utilised in the sintering process are "ravellings," which are contaminated spillages from conveyors that have been re-collected, and "mill scale," which is produced from mills that contain at least 80% Fe that is isolated from oil. Overall, there are various issues with the use of recycled materials, for example, blast furnace dust and ESP dust are rich in chlorides due to the chlorides deposited on high-voltage wires, decreasing the resistivity of the dust to capture lower levels of particulates, as shown by previous research by Lanzerstorfer *et al*.[17] Oil is an issue with the mill scale where above 0.1% can lead to glowing fires in the ESP. When anthracite coal is used as a fuel, which is <4mm diameter, with concerns on volatile material (VM) and ash content, the calorific value is key in selection as VM is driven off before it is possible to recover energy out of it and >3% VM causes issues in the ESP.[16] Burnt lime acts as a binder that allows the use of finer materials while maintaining particle size; without this when increasing the use of finer materials would decrease permeability and productivity, therefore, it functions as a binder for the adherent of finer materials to the coarser nuclei which increases permeability and productivity with the use of finer materials. Raw materials must be blended before the sintering operation which consists of laying the materials with the desired quantities, where ores, fluxes and recycled materials are added at various stages (Figure 2.8). This ensures the correct chemistry and fuel addition for optimum sintering conditions. A bed is laid in 60 hours, and consumed in 96 hours and the typical final bed composition by weight is shown below:

- 60-65% iron.
- 8-10%r recycled materials.

- 10-20% return sinter fines.
- 6-7% limestone.
- Lesser amounts of coke breeze, anthracite and burnt lime.

Key Processes	Sub-Processes
Planning Cycle of Fines Bed	Check Sufficient stocks of all required Raw materials are available.
	Check Current Sinter Specification
	Adjust Fines Bed Model on Area Computer in response to recent raw material analyses
	Construct spreadsheet for fines bed tonnage plan and data entry
	Construct bed laying order plan to complement tonnage plan above
Construction phase of Fines Bed	Lay materials to fines bed in accordance with tonnage plan and laying order
	Record information on shift log and tonnage entered into plan. Next shift updated until bed completion.
	Corrections / Trims made to tonnage plan by Quality Specialist
	East Bed end recycled on bed completion.
	Quality Specialist kept informed of any problems encountered during bed laying.
Recovery phase of Fines Bed	Re-run fines bed model with final bed data calculating theoretical blend and sinter chemistry
	Communicate to burdening / sinter production blend constituents and changes expected at SP from new blend
Monitoring of Sinter Chemistry	Differences between predicted and Actual chemistry monitored.
	Difference between amount laid to and recovered from fines bed trended
	Through-bed variation of sinter components checked and statistics generated for each bed.
Re-visiting fines bed during reclamation	If sinter analyses not meeting specification, checks made with customer on downstream effects.
	If Ok, continue to monitor as per normal operation.
	If not OK then, if possible, add further materials to adjust components via either addition or dilution

Figure 2.8 – Flow chart for preparations of fines bed[16]

Table 5 highlights the products used to make sinter in a sinter plant with details including optimum size ranges. Table 6 highlights the service level agreement between the sinter plant and blast furnace which includes vital chemical specifications for individual values. ISO (The International Organization for Standardisation) tumble measurements are used to measure the cold strength of sinter to analyse how much is broken down through abrasion (<5mm). Hot and cold strengths can be influenced by the amount of reductant added to the mix as a high reductant rate (high FeO, iron oxide) will lead to an enhanced RDI result but with an opposing effect on cold strength causing brittleness. Table 7 highlights the service level agreement between the sinter plant and the blast furnace. Sinter quality can have a dramatic effect on the fuel consumption within the blast furnace due to sinter with higher reducibility and a more efficient permeability reducing the amount of

coke required in the blast furnace. This makes the reduction and smelting process faster and more economical.

Table 5 – Products used to make sinter

Name	Details
Coarse iron ore	<6mm
Concentrate iron ore	<1mm
Ultra-fine iron ore	<10 microns
Limestone	Calcium carbonate (CaCO$_3$), optimum size 1.0 – 3.0mm
Burnt lime	Calcium oxide (CaO)
Magstone (basic flux)	Dolomite (Ca Mg) CO$_3$
Olivine (acidic flux)	Magnesium iron silicate (Mg, Fe)$_2$SiO$_4$
Recycled materials	Iron bearing by-products
Coke breeze	0.25-3mm
Coal	Bituminous and anthracite

Table 6 – Chemical specification (based on individual values for 2015-2016)[18]

Component	Minimum Limit (%)	Aim (%)	Maximum Limit (%)	Tolerance
Calcium Oxide/Silicon Dioxide	2.125	2.2	2.275	± 0.075
FeO	7.7	8.5	10	-0.8 / +1.5
Silicon Dioxide	4.9	5.1	5.3	±0.2 / ±0.2
Magnesium Oxide	1.55	1.75	1.95	±0.2
Aluminium Oxide	1.3	1.5	1.7	±0.2
Manganese	0.18	0.3	0.42	±0.12
Phosphorus			0.06	Maximum only
Potassium Oxide			0.06	Maximum only
Total Alkalis			0.15	Maximum only
Zinc			0.022	Maximum only

Table 7 – Physical specification (based on weekly average values 2015-2016)[18]

Component	Minimum (%)	Maximum (%)	Tolerance
-5mm	6	7	
ISO Tumble (6.3mm)		71.5	Maximum only

The main process steps in a sinter plant are distributed over several locations (Figure 2.9). Flux trim includes the addition of coke breeze, limestone (CaCO$_3$), burnt lime (GBL), and the recycling of internal returns fines and dust. After screening the size fractions, the water is added during the mixing and granulation stage to allow for the appropriate optimum moisture level. To control the lime excess, lesser amounts of calcium oxide (CaO) are

added to the final mixture or with another method where GBL is added directly which can improve the permeability of the sinter bed and granulation behaviour. After the product has been through the sinter strand and is screened, the fines are collected and reprocessed which has a positive effect on strand permeability but reduces the yield of the final product, along with the dust collected from the ESP abatement, as displayed in Figure 2.10. The use of burnt lime helps the binding process by holding the water as a hydroxide with the fines layer remaining stable up to a temperature of 500 °C, with the reaction shown in Equation 5.
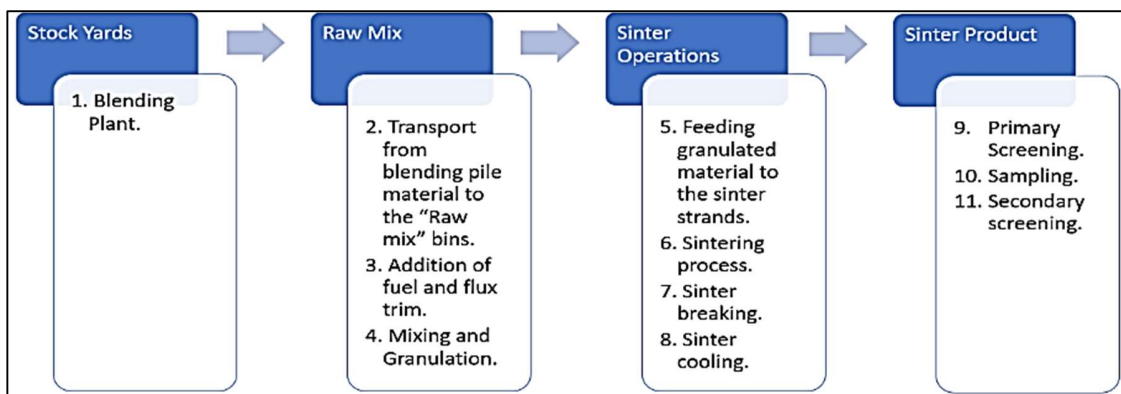
Figure 2.9 – The main process steps
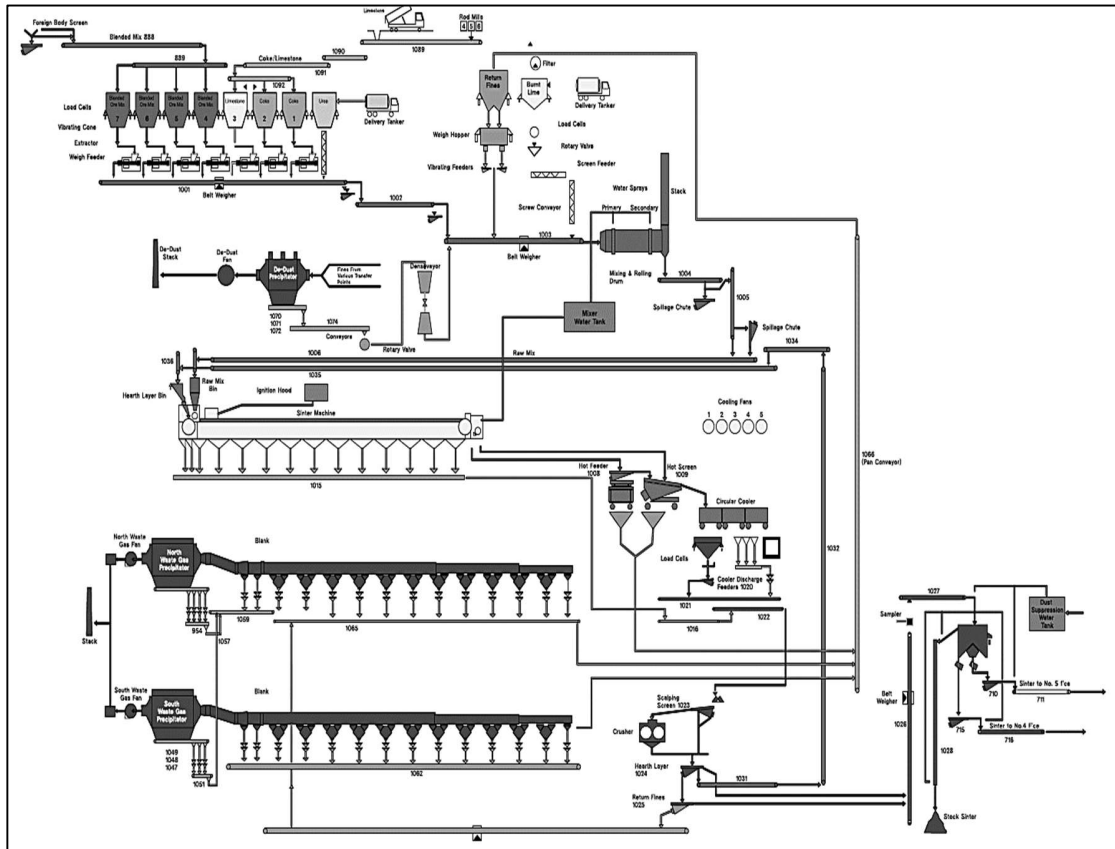
Figure 2.10 – Process flow diagram of the sintering process[19]

Equation 5 – GBL reaction with H₂O

$$CaO + H_2O \ = \ C(OH)^2$$
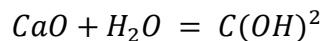
The thin calcined layers' rate of heating to coke combustion temperature is thought to be a key factor in determining the flame front speed. The voidage (effective particle diameter) and gas density are the two parameters for controlling the physical structure of the bed, which determines the ease at which the air can be drawn through the bed. The permeability of the flame front is influenced by its thickness, gas volume and physical structure of the flame front as shown in Figure 2.11 and due to the strong endothermic nature of limestone calcination, the T_f is typically in the range of 1300°C, while T_1 is much lower than T_f. Other heat-requiring reactions will also cause T_f to decrease. The time it takes for T_1 to achieve the temperature necessary for spontaneous coke combustion would grow as p increased. The time it takes for the layer to achieve coke combustion temperature and, consequently, the flame front speed, would both be affected in the same ways by reducing

the value of U.[20]The combustion rate of coke particles can influence the thickness of the flame front because of the increase in flame front temperature and gas velocity. Gas velocity in the flame front strongly depends on pre-ignition gas velocity due to the strong link between the physical structure of the pre and post-ignition beds and flame front temperature as shown in Figure 2.11.[20]
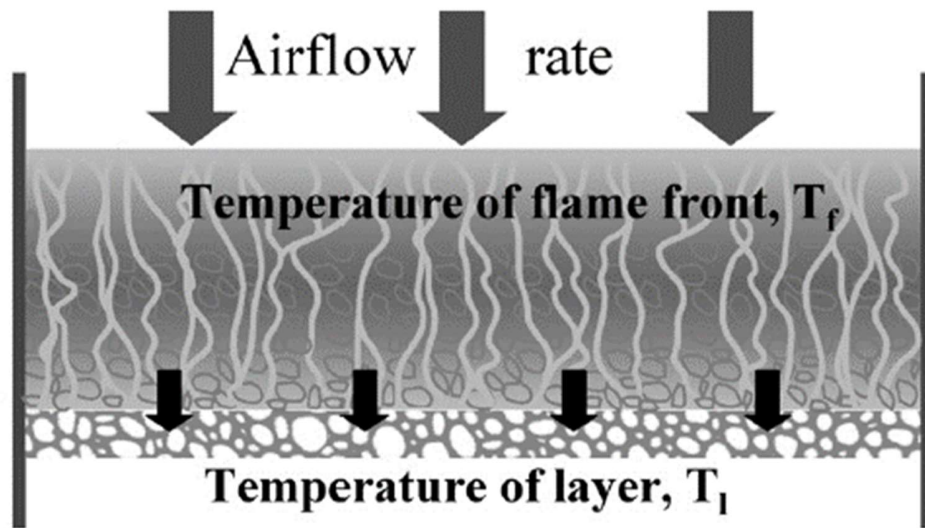
Figure 2.11 – Factors influencing the flame front speed and sintering time[20]
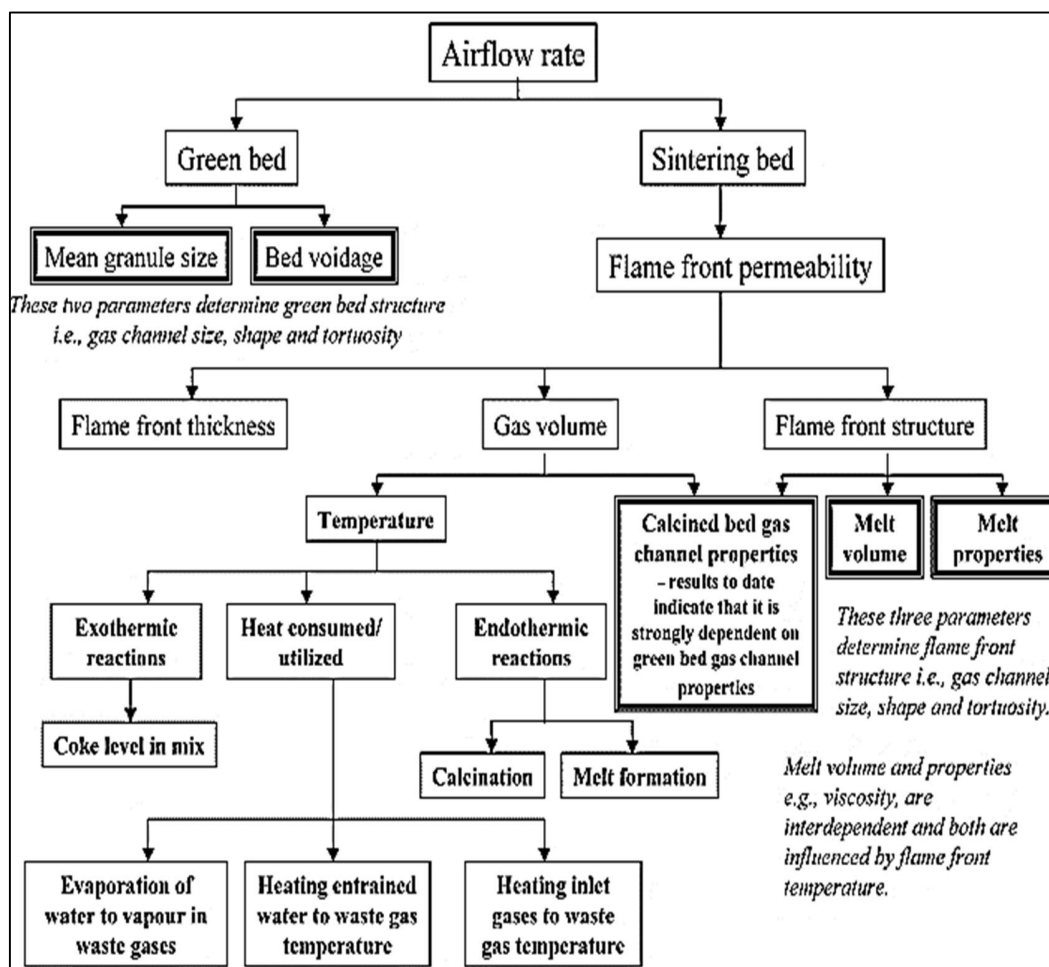
Figure 2.12 – Factors controlling airflow rate through a bed before and after ignition [20]

The raw mix is placed onto the hearth layer (recycled size fraction 10-16mm of sinter) and ignited by Natural Gas (NG) burners above the sinter strand (Figure 2.10) where the raw mix travels under the ignition hood and as the flame front is drawn vertically fuelled by coke breeze and gas flow by suction directed via two waste gas fans (wind boxes) to convert the raw mix to sinter. The main processes which take place in the sintering bed include conduction, heat transfer from other solid phases, convective heat transfer from the gas phase, radiation, heat of various reactions, heat loss by the release of gas produced by reactions, the volume fraction of each phase, pressure difference, heat, and mass transfer.[21] The two reactions take place, the first is the solid-gas reaction where coke combustion and lime decomposition take place and is heterogeneous (oxidisation and gasification). The most vital parameters for the sintering process are coke combustion rate, coke content in the material and air suction rate.[21] The preferred segregation of

materials across the strand width is finer particles at the edge and top and coarser particles at the centre and bottom of the bed to improve permeability. This ensures carbon distribution is more present at the top layers to have a beneficial effect on the ignition condition because less carbon is required in the lower section of the bed due to the preheating of the gas. A level bed top increases yield and productivity by minimising ignition time due to uniform sintering across the strand width. The particles become agglomerated in the zone of the highest temperature and the air is drawn through to provide the oxygen needed for combustion and oxidation reactions where the hot gasses from the combustion zone pass through the un-sintered section of the bed by preheating and removing the moisture in the mix prior. As the combustion zone descends it triggers sequence events:

1. Increasing temperature with the evaporation of water.
2. A rapid increase in temperature.
3. Partial liquefaction and solidification.
4. Cooling by the air pulled through the sintered material.

Melting begins at temperatures above 1100 °C as the coke breeze burns in the first layer with good fluidity of the gas flow through the bed and the process involves raising the temperature of the sinter mix to obtain partial fusion that causes crystallisation into various mineral phases which bond the structure together. Figure 2.13 illustrates how the gas in the hood can reach 1050 °C in the sintering zone and advances through where the raw mix pre-heats and the flame front propagates in a wave-like manner through the sinter bed. During sintering, the iron ore, and its component of silicon dioxide (SiO_2) reacts with the flux in the mix where a melt forms and solidifies which leads to the formation of numerous mineralogical phases such as Ca-Fe-rich minerals.
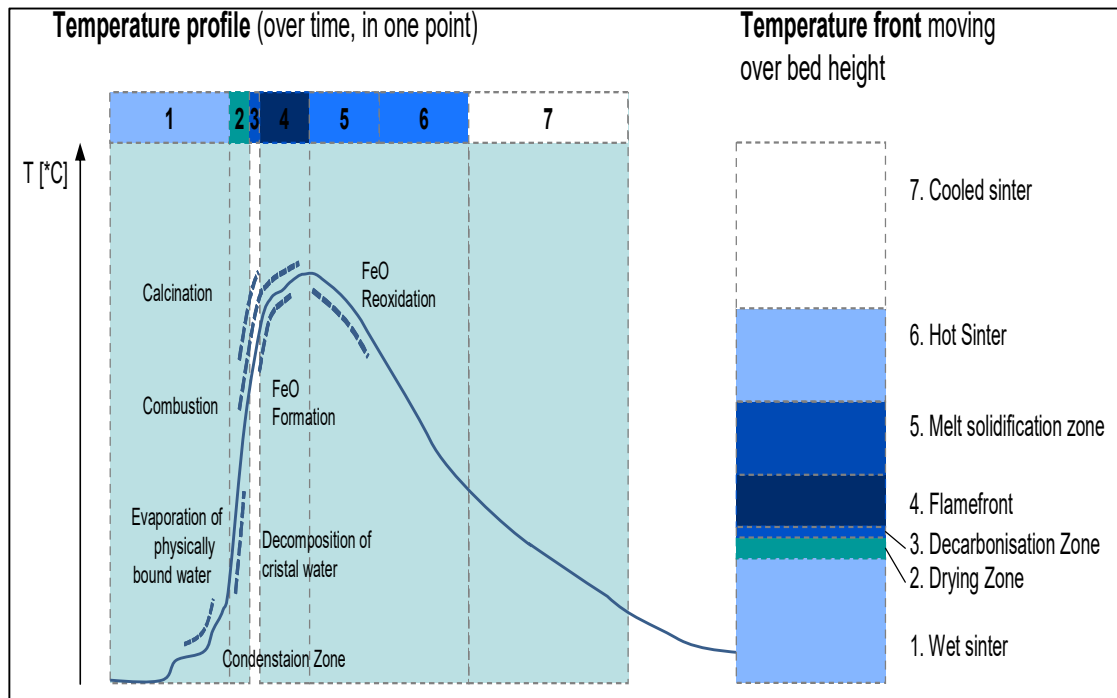
Figure 2.13 – Temperature profile of sintering in the sinter bed[18]

Before sintering, granulation takes place, and the purpose is to create a type of micropellets of the raw mix to produce a permeable sinter bed on the strand which outcomes in maximum voidage between particles with no fine particles filling the voids. Granulation requires coating the adherent fines to the nuclei and particles greater than 1mm are defined as nuclei and fines are up to 0.25mm, therefore, particles between 0.25mm to 1mm will not form micro pellets. Larger moisture additions improve the adherence of particles, but they can cause detachment when drying during sintering hence size range of 0.2-0.7mm should be minimised.[16] Haematite is deemed the most suitable nucleus rather than large coke due to any fine ore adhering to it inhibiting combustion, impacting minimal thermal efficiency, and reducing uniform and strong bonding. The adherence of fines to the nuclei is nearly 40% but this increases to 89-99% following pelletizing.[16] Moisture saturation measurement defines the capability of iron ore to hold water before dropping out and it indicates the porosity of iron ore (Figure 2.44), it is evident that ores with a greater moisture saturation value need further water to achieve good granulation efficiency due to the intraparticle pores require to be mainly filled before surface water becomes accessible for interparticle adhesion. Therefore, the moisture saturation value of iron ore provides a good indication of the amount of water required for

effective granulation.[22] The amount of moisture required for granulation was different with ore type (Figure 2.15) and the size distribution of an ore influences more on permeability, while the porosity of an ore decides the optimum mixture moisture content where the optimum permeability is attained.
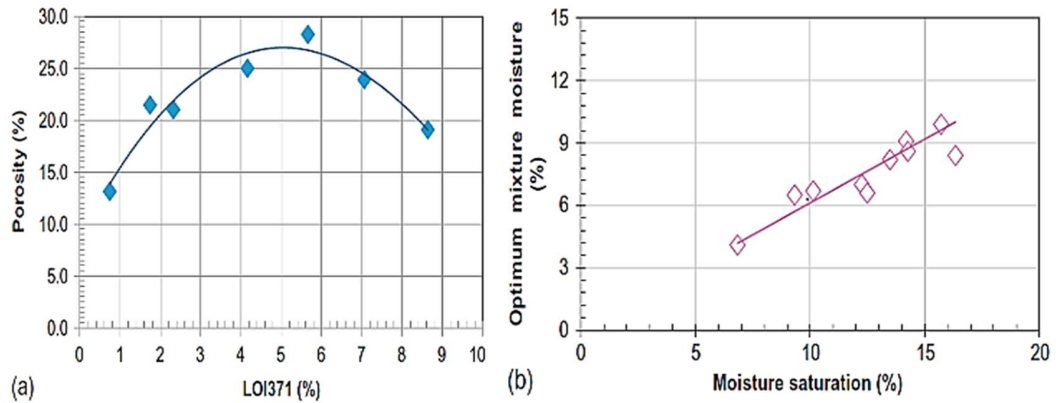
Figure 2.14 – Influence of ore mineralogy on (a) particle porosity and (b) optimum mix moisture content for effective granulation.[22]
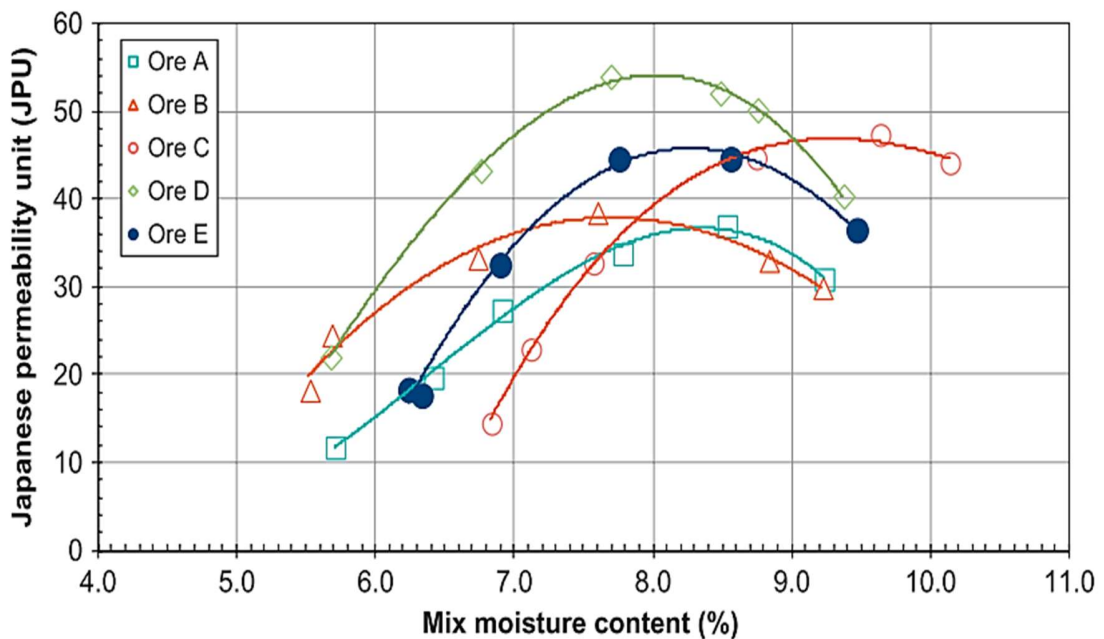
Figure 2.15 – JPU permeability vs. mixture moisture curves for different ores[22]

Optimum basicity, low gangue and high iron content are desired specifications for the sinter. In general, the reducibility and quality of the sinter improve with a higher level of hematite than magnetite, and the structure of the sinter improves with a higher level of

primary or residual hematite and ferrites as opposed to secondary or precipitated hematite. Table 8 sets out data on coke consumption, productivity, and sinter composition and quality of 36 sinter plants in Western European countries.[23] Parameters are used in a control function and are prioritised when defining sinter plant performance. From a blast furnace perspective, the key drivers are displayed in Table 9. To ensure a high-quality blast furnace operation, it is important to understand what quality indices in Table 10, impact the final sinter product, as the blast furnace demands a sinter with high cold strength, low RDI and high RI within a certain chemistry composition and optimum sizing (low fines and average size).

Table 8 – Data from the sinter plants of Western European countries[23]

	Minimum value	Maximum value
Coke consumed, kg t^{-1} of sinter	39	54
Productivity, t m^{-2} per 24h	26	43
Fe total %	51	61
FeO %	4.0	11
Al_2O_3 %	0.6	1.8
MgO %	0.7	2.2
RDI (>3 mm) %	27	33
Tumbler (>6.3 mm) %	63	79
Reducibility, R_{60} %	49	78

Table 9 – Key drivers from a blast furnace perspective

Key Drivers	Description
Metallurgical Quality	Maintaining burden permeability.
Chemical Consistency	Ensuring slag composition: Production needs to meet the defined sinter chemistry, primarily requiring stability in the raw sinter mix composition.
Production on Demand	Not underperforming on plan but in the case of overcapacity, it can also mean being able to follow the blast furnace demand.[18]

Table 10 – Quality indices[24]

Quality Indices	Type	Description
Chemical Composition	Fe phases	Sinter quality improves with a higher level of hematite than magnetite, and its structure improves with a higher level of primary or residual hematite and ferrites than with secondary or precipitated hematite.
	FeO	It is important to find an optimum FeO content to improve the RDI without altering other sinter properties. Higher FeO content negatively impacts reducibility.
	Al_2O_3	The strength and quality of the sinter deteriorate as the alumina content rises.

	MgO	The addition of MgO to the raw mix improves the RDI because MgO stabilises magnetite and thus decreases the hematite content, giving rise to less stress in the sinter during the hematite-to-magnetite reduction in the blast furnace stack. [24]
	CaO	CaO combines with iron oxides to form compounds with a low melting point that favour the formation of the primary melt.
	SiO_2	Silica combines with FeO and CaO to form compounds with a low melting point that favour the formation of the primary melt.
Granulometric distribution		The sinter is hot screened, and the 12-35 mm fraction is sent directly to the blast furnace, the larger fraction is crushed to obtain smaller-sized fractions, and the <5 mm fraction (return fines, RF) is recycled to the sinter plant. To keep a balance between the generation and recycling of return fines: B = RF generated / RF returned $0.95 \leq B \leq 1.05$.
Laboratory Testing	Low-Temperature Degradation (LTD)	The degradation of sinter in the blast furnace occurs during the reduction in the low-temperature zone, and harms the burden strength in the furnace, with the consequent loss of permeability to reducing gases and an increase in coke consumption. [23]
	Reducibility Index (RI)	Reducibility is an important characteristic of sinters which measures the ability to transfer oxygen during the reduction in the blast furnace stack, giving an idea of fuel consumption needs in the furnace. A heterogeneous structure is more reducible than a homogeneous structure. [25]
	Reduction Degradation Index (RDI)	Predicts the sinter's degradation behaviour in the lower part of the blast furnace stack. Secondary hematite, also known as skeletal rhombohedral hematite, is the main cause of a poor sinter RDI and is based on the frequent observation of cracks around the narrow neck regions of such hematite. [24]
	Tumbler Index (TI)	The cold strength of the sinter is determined by the tumbler test and depends on the strength of each ore component, the strength of the bonding matrix components and the ore composition. This test determines the size reduction due to impact and abrasion of the sinters during their handling, transportation, and in the blast furnace process.
Sinter Porosity		This impacts its properties and its reduction behaviour as the sinter experiences a strong increase in porosity after undergoing the reducibility test.
Sinter Structure		The raw mix is heterogeneous with a wide range of mineralogical components however it is formed by grains of iron oxide and calcium ferrites bonded by a gangue matrix.

The three internal laboratory tests that can determine a high-quality sinter product are the tumbler index (TI), reducing sinter reduction degradation index (RDI) and reducibility of sinter (RI). A TI of around 77%-80% is a good result and quantities of low-grade FeO are disadvantageous to sinter reduction as it makes the sinter larger/dense which harms sinter dynamics and is detrimental to reducing energy consumption. High-grade sinter will typically have a basicity of >1.80 with a Fe content higher than 58% and SiO_2 contents not exceeding 5%. This decrease in gangue content, increase in basicity and good iron content results in high-quality sinter grades with good blast furnace performance including good reduction properties. SiO_2 and Al_2O_3 contents impact the metallurgical property of the sinter involving degradation at low temperatures and soft melting at hot temperatures. RDI is important to ensure that the material maintains its integrity and does not break

down into fine powder allowing good gas permeability and is due to the crystalline transformation between primary hematite and secondary hematite where the primary haematite has a hexagonal lattice of a trigonal system and secondary has an isometric cubic lattice. The transformation creates torsion within the structure which generates large internal stresses leading to breakdown under mechanical action. Factors that can impact RDI are chemical composition, phase component and reducibility of iron ore. The quality of the sinter on blast furnace performance was dependent not only on the raw material selection and ore blending but also on the selection of reasonable process parameters including the optimisation of granulation, bed permeability, oxidising atmosphere, bed thickness and temperature and time at temperature. Sinter quality can have a dramatic impact on the fuel consumption within the blast furnace due to sinter with higher reducibility and a more efficient permeability reducing the amount of coke required in the blast furnace. This makes the reduction and smelting process faster and more economical.[26] The type of minerals produced in the sintered product depends on the chemical make-up of the ore, flux, fuel rate, and liquid temperatures of each component. Typically, the higher the amount of hematite and the lower of magnetite and wustite (Fe^{2+}), the greater the reducibility. The degree of oxidation is given by Equation 6 and the degrees of oxidation of the three iron oxides are FeO = 70%, Fe_2O_3 = 100% and Fe_2O_4 = 88.9%. During sintering, magnetite is formed due to the combustion gas slightly reducing it to hematite and the remaining amount of magnetite is oxidized to secondary hematite.[27]

Equation 6 - % Degree of oxidation

$$\% \, Degree \, of \, Oxidation = \frac{1 - Fe^{2+}}{3 \sum Fe} \times 100$$

The relationship between sinter mineralogy and strength and quality regarding the effect of the lime/silica ratio is shown in Figure 2.16 and Table 11. The sinter bond strength is achieved by:

- Slag or fusion bond – partial or complete embedding of the crystalline constitution in the matrix
- Diffusion bond – recrystallizing and crystal growth of hematite and magnetite
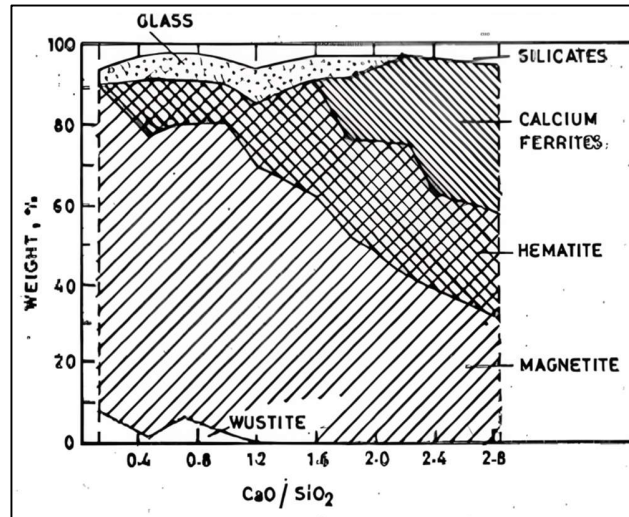
Figure 2.16 – Variation in the mineralogy of sinter of optimum strength with CaO/SiO₂ ratio at 0.5% magnesia and 1.5% alumina[28]

Table 11 – The importance of the CaO/SiO₂ ratio[27]

CaO/SiO₂ Ratio	Description	Product Characteristics
0	Fayalite forms from hematite and magnetite when there is no lime present. This forms a low-melting multi-component liquid whose viscosity increases with the Si content.	High Si and high fuel will form a strong product but with poor reducibility. For low Si and low fuel will form a weak but more reducible product.
0-0.8	By adding the lime, the crystalline silicates are replaced by the glass (less viscous) which requires less fuel due to a lower temperature.	Sinter strength decreases and the reducibility increases.
0.8-14	Increasing the lime causes the amount of glass to increase and the fuel rate to decrease. The basicity of minimum strength varies according to sinter composition.	Strength continues to decrease and the reducibility increases (or sometimes decreases depending on phase transformation)
1.4-2.8	The glassy matrix is now substituted for Calcium silicate and ferrites which improves bonding.	Increase in strength (needle-like ferrite precipitates to hold the ore grains together) and reducibility increases.

Regarding the chemical composition of the sintered product, the most key factors concerning the chemical composition of raw materials used are concentrations of Fe, compounds of Ca, Si, Mg, and Al and harmful compounds such as S, P, Z, and Pb. The raw mix is based on hematite ores and magnetite concentrates. All these raw materials differ significantly in terms of their chemical properties and grain size distribution which may lead to deterioration of the mixture sintering conditions and can cause negative environmental impact. [29] Most of the raw materials come from abroad and possess a higher content of elements such as Na, K, and Zn which are present in the forms of

oxides.[30] Besides the particle size of K_2O and Na_2O being less and their specific weight is also less, an increase in dust resistivity is likely to occur which is quite adverse to the performance of the ESP abatement.[31] Therefore the dust composition is of Fe_2O_3, SiO_2, Al_2O_3, CaO, MgO, MnO, P_4O_{10}, S, C, and other forms of K_2O, Na_2O and ZnO. The main phases occurring in iron ore sinter are iron ore particles, precipitated oxides of iron (magnetite and haematite), calcium-rich silicates, complex calcium ferrite phases and glass (Figure 2.17).
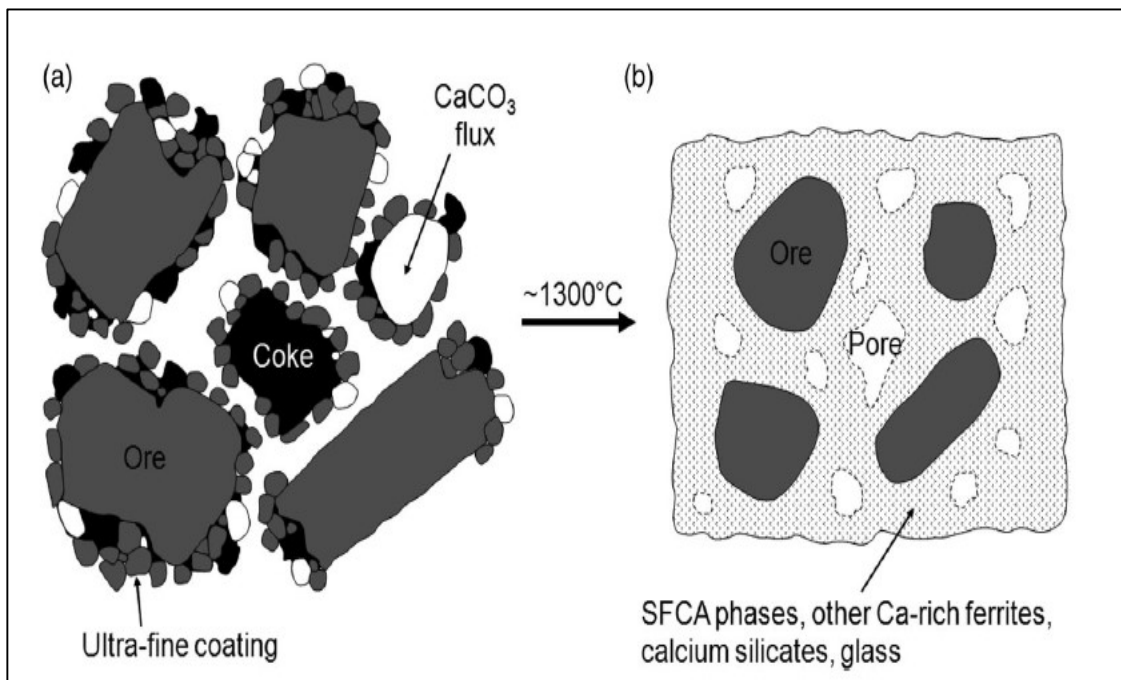
Figure 2.17 – Schematic of a typical mixture of iron ore fines, flux and coke, and b typical iron ore sinter product[32]

There are two types of SFCA (silicoferrite of calcium and aluminium) that have been recognised as the main types of fluxed sinter. One is a low Fe form, which is simply referred to as 'SFCA,' and the second is a high Fe, low Si form called SFCA-I. The SFCA-I is a higher-order homologue of SFCA that has a characteristic 'plate-like' morphology although it may sometimes appear needle-like or acicular in cross-section.[33] In contrast, SFCA tends to exhibit a prismatic form and its morphology has often been referred to as columnar, blocky or lath-shaped (Figure 2.18).[33] [34]
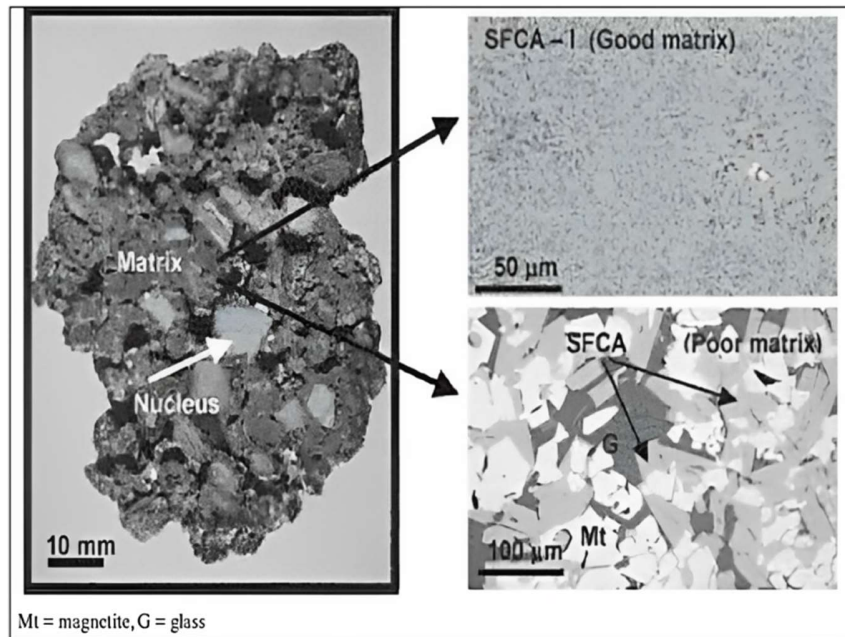
Figure 2.18 – Ideal Fe ore sinter composed of hematite nuclei and porous SFCA matrix (left), plus micrographs (right) showing typical SFCA-I and SFCA matrix textures.[35]

The fine (-1 mm) ore composition, particularly the Fe, SiO_2 and Al_2O_3 levels, directly constrain the high-temperature bonding phases that can form during sintering. Hence, it is the composition of the fine ore that controls the sinter and pellet quality. The chemical composition of typical hematite and goethite iron ores and sinter–pellet blends dictates that they will form a mixture of SFCA and SFCA-I bonding phases. The typical temperatures used in sintering (1270– 1300°C) encourage the formation of both SFCA and SFCA-I bonding phases up to 1300°C. Above 1300°C, SFCA only is favoured.[35] In-situ XRD measurements (Figure 2.19) show that typical temperatures (1270–1300°C) and compositions used in sintering favour the formation of both SFCA and SFCA-I bonding phases up to about 1250–1270°C (depending on bulk compositional parameters such as basicity and alumina content). Above these temperatures, only SFCA is favoured. Both low-iron prismatic SFCA and high-iron platy SFCA-I form from the reaction between solid iron oxide and calcium ferrite phases (C2F, CF and CFA) without the need to form by direct crystallisation from a high-temperature liquid (T>1300°C).
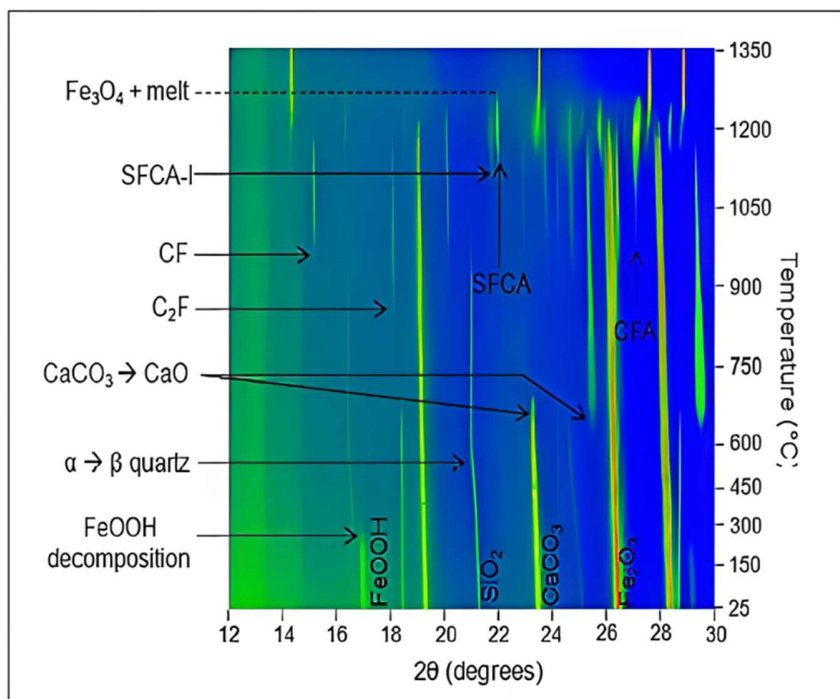
Figure 2.19 – In situ synchrotron XRD data collected for the natural sample viewed down the intensity axis over the range 25–1350°C. Annotated on the plot are: the major reflections for materials in the starting mixture; the low-temperature (<650°C) phase transformation (αβ-SiO2) and decomposition (e.g. CaCO3 → CaO) events; the formation events of C2F, CF/CFA, SFCA-I, SFCA, and the Fe3O4+melt phase [35]

Certain parameters were used to predict the tumbler index (26.3 mm) of the sinter. The variables to which the strength of the sinter was most sensitive were Al_2O_3/SiO_2, basicity, machine speed, and MgO, MnO and FeO. The TI (tumbler index) of the sinter was influenced by sinter porosity, which was determined by the firing temperature and green sinter mix carbon content. The predicted results were in good agreement with the actual data with a 3.5% error. [36] A neural network-based model has been developed and trained relating sinter strength with a set of nine process variables:

1. Basicity.
2. MgO.
3. MnO.
4. FeO.
5. Moisture.
6. Coke breeze.
7. Burn through temperature.
8. Machine speed.
9. Tumbler Index (26.3mm).

Al$_2$O$_3$/SiO$_2$, basicity (CaO/SiO2), MgO content of the sinter and machine speed have a significant effect on strength of the iron ore sinter. Sinter strength decreased with an increase in alumina content and to improve the sinter strength, the alumina content in the sinter mix should be minimised. Sinter strength increased with an increase in sinter basicity and MgO content and the sinter strength decreased with an increase in sinter MnO due to increasing in LOI (loss on ignition). Sinter strength increased with an increase in moisture addition from 6 to 8% due to the sharpening of flame front speed and an increase in coke breeze addition increases the FeO content of the sinter. Desired coke breeze addition supplied higher heat input to obtain the desired melt formation level to get proper bonding with other phases and increased the overall sinter strength. Sinter strength increased with an increase in burn-through temperature due to the formation of desired sinter phases.[36] The reduction properties of the mineral phases formed in the sinter influence the sinter reducibility. MgO has a varying effect on sinter reducibility at different silica contents. Pilot-scale sinter rig grate sintering experiments have been conducted to determine the influence of MgO addition on microstructure and reducibility of low and high silica sinter. MgO additions have been varied from 1.4% to 3.2% for low silica (4.5%), and high silica (6.3%) iron ore fines. Figure 2.20 highlights how the reducibility of both sinters decreased with an increase in Mg addition due to an increase in the magnetite/magnesia spinel phase and silicate/slag phase. High silica with high MgO sinter had lower reducibility compared to low silica with low MgO/high MgO and high silica with low MgO sinter.[37]
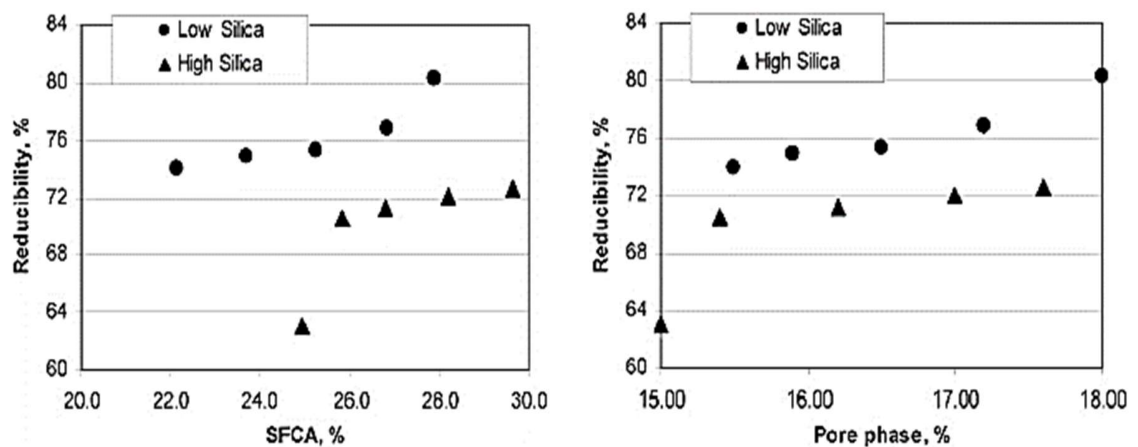
Figure 2.20 – Influence of SFCA phase on reducibility (left) and influence of pore phase on reducibility (right) [37]

The MgO in the blast furnace slag provides an optimum condition in terms of both good flowability and desulphurisation. The use of olivine/dunite/seroentine is being used as a source of MgO and SiO_2. MgO acts as a refractory phase during sintering as it increases the liquidus temperature of the melt resulting in higher energy and a decreased sintering rate.[38] The addition of MgO suppresses the formation of calcium ferrite that in turn forms a vitreous glass matrix but this can be corrected by the extra coke addition. MgO favours the formation of Fe_3O_4 ($FeO.Fe_2O_3$) rather than the preferred Fe_2O_3 and restricts melt formation that increases the porosity of the sinter (higher reducibility and RDI), (Figure 2.21) due to more surface area exposed to reducing gases. Overall, an increase in MgO has a direct negative correlation with the sintering rate, the fuel rate, sinter strength (Figure 2.22) and reducibility but high-temperature properties (RDI) and the softening-melting characterises of the product improve.[38]
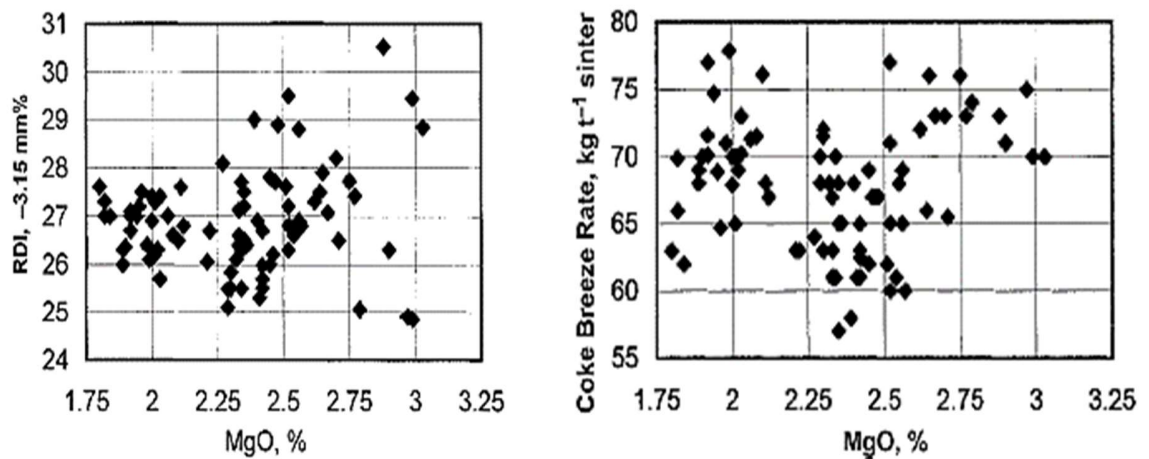
Figure 2.21 – Influence of MgO RDI -3.15mm% (left) and on coke breeze rate (right)[38]

a +6·3 mm; b −0·5 mm
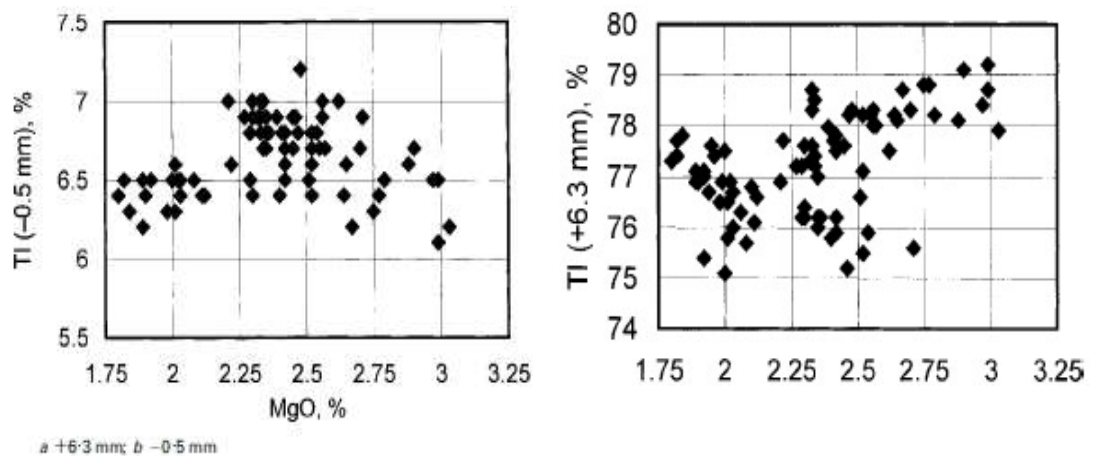
Figure 2.22 – Influence of MgO on TI -0.5mm% (left) and tumble index +6.3mm% (right)[38]

The mechanism of the influence of MgO and Al_2O_3 on softening properties of the sinter is different. Al_2O_3 has priority over MgO to enter the slag phase and forms the low melting-point phase while MgO remains in an un-slagged state and exists in wustite as FeO–MgO solid solution. When the sinter melts, the viscosity of the slag generated from the sinter containing high MgO and Al_2O_3 content is low, which would result in a low-pressure drop. As MgO and Al_2O_3 content increase, the main minerals of residual slag change from $2CaO•SiO_2$ to merwinte and melilite.[39] The primary phases of interest, including secondary hematite (H), magnetite (M), and SFCA (SF), are shown in a typical sinter region. Keeping in mind, the differences between the epoxy resin mount € and glass as well as the contrast between the glass (gl) and areas where larnite was present (L) as shown in Figure 2.23.[40]
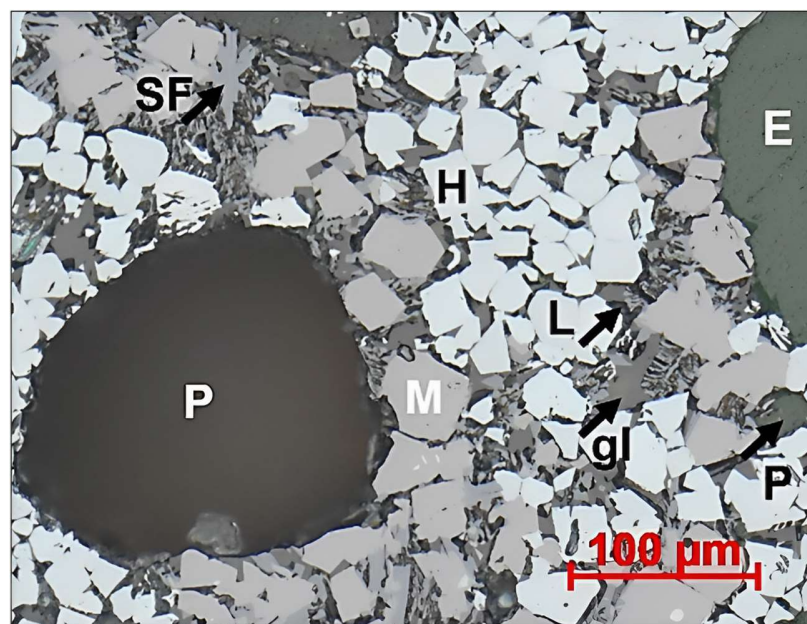
Figure 2.23 - Higher magnification reflected light photomicrograph of sinter prepared using the standard method. Secondary hematite (H), magnetite (M), SFCA (SF), epoxy resin mou€(E), glass (gl) and larnite (L)[40]

2.6.1   Emissions

At a typical sinter plant, the waste gas system is used to generate a flow of oxygen through the sinter strand to generate sinter. From this process, particulates are liberated from the strand and enter the vacuum-pressured wind main. The wind main is connected directly to the sinter plant main stack where waste products of sintering are emitted. The liberated

particulates are free to follow the flow of gasses out of the stack. In Figure 2.24, the red arrow represents combustion emissions, and the blue arrow represents process emissions. The operation of sinter plants produces emissions of air pollutants like nitrogen oxides, sulphur dioxides and volatile organic compounds from the combustion activities. Particulates are liberated from the strand and enter the vacuum-pressured wind main via a waste gas system that generates a flow of oxygen where the wind main is connected. This is in line with the sinter plant main stack where waste products of sintering are emitted. Typical pollutant emission levels for a sinter plant are displayed in Table 12 across 5 sinter plants in Europe and Table 13 displays typical upper limits for toxic species such as NOx, SO_2, PM and Dioxins across the rest of the world which highlights the pressures the governments are putting on the sinter plants in UK and Europe compared to the rest of the world.
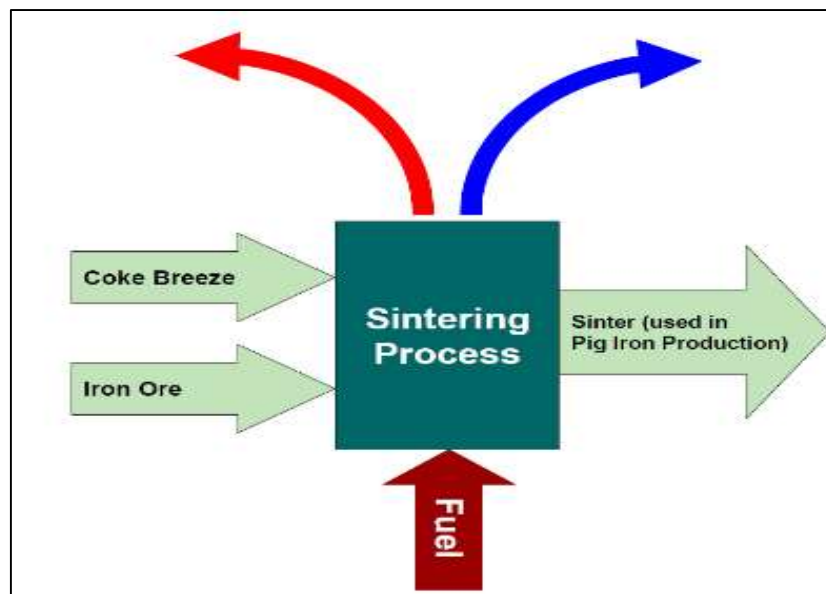
Figure 2.24 – Process scheme of the sinter plant production showing inputs and outputs[9]

Table 12 – Typical pollutant emission levels for sinter plant[12]

Sinter plant operation	Dust (g/t LS)	HF (g/t LS)	HCl (g/t LS)	SO_2 (g/t LS)	NOx (g/t LS)	CO (g/t LS)	CO_2 (kg/t LS)	VOC (gC/t LS)	PAH (mg/t LS)	PCDD /F (g/t LS)	PCB (mg/t LS)
Crushing/ blending	<5	n/a	n/a	n/a	n/a	n/a	n/a	n/a	n/a	n/a	n/a

Siner strand	100-400	0.4-53	23-95	480-3000	75-1600	7600-42500		50-150		1-30
Discharge	10-270	n/a	n/a	n/a	n/a	n/a	n/a	n/a	n/a	n/a
Sinter colling	40-150	n/a	n/a	n/a	n/a	n/a	n/a	n/a	n/a	n/a
Building atmosphere	n/a	n/a	n/a	n/a	n/a	n/a	n/a	n/a	n/a	n/a

Table 13 – Upper limits of toxic emissions from existing sinter plants required by different countries[41]

Toxic emissions	Unit	Japan	China	The United Kingdom
SO$_x$	mg/Nm^3	–	600	350–500 expressed as the SO$_2$ daily mean by way of limiting coke breeze, S in coke breeze, and S in iron fines, using activated carbon injection,
NO$_x$	mg/Nm^3	220ppm	500	500 expressed as NO$_2$ daily mean value using process-integrated measures.
PM	mg/Nm^3	100–150	130	40 for advanced ESP, and 15 for bag filters.
Dioxins	ng-TEQ (toxicity equivalent)/Nm^3	1.0	1.0	0.4 Polychlorinated dibenzo-p-dioxins and polychlorinated dibenzofurans (PCDD/Fs) <0.05–0.2 ng/Mm^3 for bag filter applications and < 0.2–0.4 ng/Mm^3 for electrostatic precipitator applications.

Only 20% of the material discharged from the sinter bed is below 300 μm in size and this implies that most of the material discharged from the sinter bed would not be entrained in the gas stream.[42]

2.6.2 Particulate Matter

The main reasons for conducting stack emission monitoring are:

- Authority permits.
- Collecting data for emissions-inventory compilation.
- Collecting data for environmental impact assessments.
- Collecting data to assess process efficiency and process control.
- Assessing the performance of a pollution-control device (abatement system).

A measurement campaign can be conducted at periodic intervals, such as once every three months. The sample is usually, but not always, withdrawn from the stack and analysed via extractive sampling. An instrumental/automatic technique may be used, where an online analyser conducts the sampling and analysis. Table 18 demonstrates the characteristics of an approved periodic monitoring sample campaign.

Table 14 – Characterises of periodic monitoring

Characteristic	Periodic monitoring
Sampling period	Snapshots of the long-term emissions profile.
Speed of results generation	Real-time results if instrumental analysers are used.
Averaging of results	Result from over typically 30 minutes to several hours.
Calibration and traceability	Standard reference methods can be used for periodic monitoring; also, instruments calibrated with certified reference gases can be used.
Operating cost	High because of labour intensive. The trained team is on-site for the whole duration of the monitoring campaign.
Certification of equipment	MCERTS certification in the UK for transportable stack-monitoring equipment is available.
Accreditation of monitoring	Accreditation to the MCERTS standard in the UK includes the requirement for individuals conducting monitoring to be certified under MCERTS as competent.

Whichever monitoring technique, method or equipment is chosen; the fundamental principle of sampling must be adhered to. This principle is that a small amount of collected material should be a representative sample of the overall character of the material. The number and locations of samples that need to be taken to make up a representative sample depend on how homogeneous the stack gas is. The sinter mix and the sinter itself function as a granular bed filter, but the contribution of the coarse pieces of the sinter will be negligible as <300μm will fall out of the gas stream.[43] The role of the flame front and the condensation front are unknown. For the filtering of dust in the sinter mix layer, it is assumed that the mix is a uniform granular bed filter. Theory and calculation methods known from granular bed filtering were applied to estimate the dust filtering of the sinter mix layer.[44]

Typical characteristics of the sinter plant layer are:
- Height of sinter mix layer – 0.48m
- Particle Diameter – 0.001m
- Bed Porosity – 0.45
- Flue gas velocity – 1.1 m/s

Four mechanisms of filtering in a granular bed are known:

1. Diffusional filtering: The dust particles drift to the filter granules by Brownian motion. This counts only for extremely fine particles < 0 .1 μm.

2. Inertial filtering: The dust particles fail to follow the lines of flow and collide with the filter granules. This counts for small particles > 1 μm.

3. Gravitational filtering: The dust particles are filtered by the force of gravity. This counts for particles > 10 μm.

4. Flow-line filtering: The dust particles collide with the filter granules while following the lines of flow. This counts for particles > 10 μm.[44]

The efficiency of a filter is the sum of the contributions of the four mechanisms. Dust particles in the range 0 .1 – 3 μm are difficult to filter as these particles are too small for inertial filtering or too large for diffusional filtering. Calculations are conducted with dimensionless numbers as follows:

- Diffusional Filtering – this is characterised by the Péclet number (Pe). This number describes the ratio of the mass transport by the mainstream and the transport by diffusion. Diffusional filtering is high for Pe < 1000.

- Inertial filtering – this is characterised by the Stokes number (St. This number describes the ratio of the momentum of a particle and the viscosity of the fluid. Inertial filtering is high for St > 0 .01.

- Flowline filtering – this depends on the ratio of the dust particle diameter and the diameter of the filter medium, d_{dust}/d_{filter}.

- Flowline filtering is negligibly small for $d_{dust}/d_{filter} < 0.01$. The filtering efficiency of the sinter mix was calculated for different diameters of flue dust particles. [44]

Table 15 shows that flue dust particles > 5 μm will be filtered by the sinter mix and the smaller particles are only partially filtered.[44]

Table 15 – Filter efficiency of sinter mix for different diameters of flue dust particles

	Diffusional Filtering		Inertial Filtering		Flow-line filtering		Filter Efficiency	
Dust Diameter	Péclet Number	Yes/No	Stockes Number	Yes/No	d_{Dust}/d_{Filter}	Yes/No	Estimate	Scale
0.1	1.6×10^6	No	4.7×10^{-4}	No	1.0×10^{-5}	No	0.30	Low
0.5	1.8×10^7	No	5×10^{-3}	No	5.0×10^{-4}	No	0.36	Low

1	4.0×10^7	No	0.02	Yes	1.0×10^{-3}	No	0.59	Medium
5	2.4×10^8	No	0.41	Yes	5.0×10^{-3}	No	0.99	High
10	4.6×10^8	No	1.63	Yes	10×10^{-3}	Yes	1.00	High

In Figure 2.25, the cumulative mass distribution of dust emitted from various sinter plants in Western Europe is shown. Most particle size measurements have been analysed by particle impactors. Therefore, the particle size is based on the aerodynamic diameter (dae). Assuming an average density of the particles (ρP) of 2500 kg/m³, the calculated Stokes diameters (dSt) will be about 1/3 smaller than the aerodynamic diameters ($\rho 0 = 1000$ kg/m³) which are displayed in Equation 10. At sinter plant 6, the particle size determination was performed using electron microscope images of short-time exposed filters, thus the particle diameters are equivalent to Stokes diameters.[87]
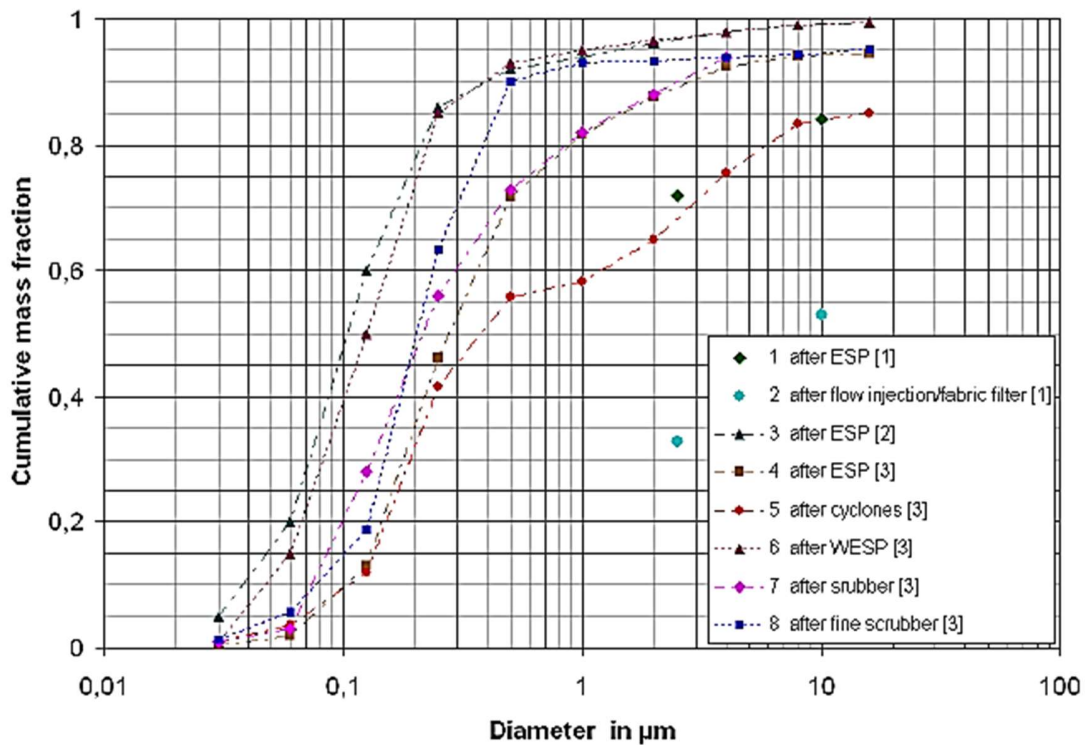
Figure 2.25 – Cumulative mass distribution of dust emitted from sinter plants (sinter plant 1-5),7,8: particle size measurements by impactor – aerodynamics diameter of particles; sinter plant 6:partcilte size determination by SEM – Stokes diameter of particles)[17]

Equation 7 – Calculating stokes diameters

$$d_{St} = d_{ae_-} \sqrt{\frac{\rho_0}{\rho_P}}$$

It is important to understand how the ESP abatement works to understand how the historical data from the pilot-scale sinter rig can be discussed. The ESP abatement uses high-voltage electrodes to give the catalyst particles suspended in the flue gas a negative charge. These negatively charged particles are subsequently drawn to a positively charged grounded collecting surface (collection plates). On the collecting plates, the particles collect. The plates are "rapped" at regular intervals, which causes the particles to fall into the hoppers. The PM emissions from a sinter plant's main stacks of the sintering process account for 45% of the total PM emissions.[2] This has led to an increase in stringent demands for lower emissions. Various species contain the availability of relevant data from sources of internal process information (PI) databases. The PI database collates all real-time and historical data therefore that each recorded process point (called a "Tag") is stored online. Table 16 highlights the main species of interest in sinter emissions and their effects on the environment and health of the local community.

Table 16 – Information on species

Species	Description	Effects on the environment and health
Particulates and gaseous forms: PM_{10}, $PM_{2.5}$, NO_x, SO_2, CO	The main PM emissions sources in a sinter plant are gases from the wind boxes – these contain considerable amounts of entrained PM, some of which is released into the air via the main stack, after passing through the particulate air pollution control equipment.[45]	Exposure to such particles can impact the lungs and heart which can lead to chronic injuries or potential death. Consequential effects of gaseous forms have on the environment, such as global warming, ozone, smog, and acid rain.
Urea	Addition of a small quantity of urea directly as a solid to the raw sinter mix for dioxin emissions control.	Urea has a direct effect on the increase in the number of public complaints regarding the visibility of the sinter plant plume. [46]
Dioxins	The iron ore sintering process has been recognized as one of the major industrial emission sources of polychlorinated dibenzo-p-dioxins and dibenzofurans (PCDD/Fs). [47]	Environmental concerns worldwide about dioxins, the sources and fates of these compounds and their effects on animal and human health. (Anderson and Fisher, 2002)

2.7 Air Pollutants

The World Health Organisation (WHO) has linked ambient air pollution to an estimated 4.2 million premature deaths globally,[49] cardiovascular diseases account for 60-80% of air pollution-related deaths[50] from stroke, heart disease, pulmonary disease, lung cancer and acute respiratory infections in children. Furthermore, short, and long-term air pollution exposure is linked to reduced life expectancy and mortality. Major sources of air pollution consist of fuel combustion, industrial facilities, power generation, waste incineration and polluting fuels. In response to the link between high particulate matter

concentrations and health problems, the Expert Panel on Air Quality Standards (EPAQS) has established a limit of 50 μg/m^3 of PM_{10} (all particles passing through an inlet which allows 50% of 10-μm aerodynamic diameter particles) a day for the UK, although this mass limit is commonly exceeded in urban and industrial areas.[51]

2.7.1 Particulate Pollutants

Particulates can be particles can be of any shape, structure or density dispersed in the gas phase and can be measured by the concentration of particles that was less than or equal to 10 μm in diameter named PM_{10}. Similarly, the concentration of particles that were less than or equal to 2.5 μm in diameter named $PM_{2.5}$ or the total of all sizes of concentrations of particles named TPM (total particulate matter) and the health effects of particulates can aggravate asthma and other lung diseases. The concentration of particles in the air at any given time is also dependent on weather conditions, notably temperature and rainfall (with the highest concentrations occurring during cold and dry days), wind strength and direction.[51] This correlates with the change of seasons from winter to summer phenomenon that increases particulates when in the summer season. Sub-micrometre-sized particles can be produced by organic compounds that were vaporised in high-temperature combustion processes and by the condensation of gases that have been converted in atmospheric reactions to low vapour-pressure substances. The particles produced by the intermediate reactions of gases in the atmosphere are called secondary particles. Secondary sulphate and nitrate particles were usually the dominant components of fine particles. For example, sulphur dioxide (SO_2) is oxidised in the atmosphere to form sulphuric acid (H_2SO_4), which can be neutralised by ammonia (NH_3) to form ammonium sulphate. Nitrogen dioxide (NO_2) is oxidised to nitric acid (HNO_3), which in turn can react with NH_3 to form ammonium nitrate (NH_4NO_3)[52]. In 2013 a comprehensive report by the World Health Organisation (WHO) on PM phenomenology in Europe was compiled. It stated that sulphate and organic matter were the two main contributors to the annual average PM_{10} and $PM_{2.5}$ mass concentrations, except at kerbside sites where mineral dust (including trace elements) is also the main contributor to PM_{10}[53] PM consists of both primary components, which was released directly from the source into the atmosphere and secondary components, which was formed in the atmosphere by chemical reactions. PM

comes from both manufactured and natural sources. It contains a range of chemical compounds, and the identity of these compounds provides clues to the origin as shown in Table 17.

Table 17 – Primary and secondary sources of PM

Primary Components	Sources
Sodium chloride	Sea salt
Element carbon	Black carbon is formed by the combustion of fossil fuels
Trace metals	Generated by metallurgical processes, such as steelmaking, or by impurities found in or additives mixed into fuels used by industry.
Mineral components	Coarse dust from construction and wind-driven dust.
Secondary components	**Sources**
Sulphate	Formed by the oxidation of SO_2.
Nitrate	Formed by the oxidation of NOx.
Water	Components of the aerosol form PM.
Primary and secondary components	**Sources**
Organic carbon	Primary organic carbon comes from traffic and industrial combustion sources. Secondary organic carbon comes from the oxidation of volatile organic compounds.

The main health concern concerning PM_{10}, smaller fractions is the potential effect due to inhalation and the spherical particles below 10μm in diameter may penetrate the lungs, where damage is caused. Since the late 1980s, numerous epidemiological studies have inferred a statistical link between the concentration of PM_{10} in ambient air and health effects.[54] These effects include mortality, decreased lung function, increased respiratory symptoms, and increased incidence of pneumonia. Although the statistical link is significant, there is little consensus on the actual mode of action of PM_{10} to cause these health effects. Several modes of action have been suggested.[54] and these include the following:

- An inert size/mass effect – smaller particles can travel deeper into the lungs and may become lodged in the lung tissue and cause inflammation and local immunological cell responses.
- An acidity effect – acidic species such as sulphates and nitrates may be carried deep into the lungs via PM.
- A toxicity effect – the large surface area of PM_{10} can carry significant amounts of toxic species deep into the lungs.

2.7.2 Inorganic Gaseous Pollutants

There are various inorganic gaseous pollutants which influence the variation of atmospheric composition that can be caused by the fossil fuel combustion process: NOx (nitrous oxides), CO (carbon monoxide) and SO_2 (sulphur dioxide) are produced from S-based fossil fuel combustion and CO_2 are produced from inefficient partial fossil fuel combustion. Nitrogen oxides react with Ozone (O_3) or radicals in the atmosphere forming NO_2. These inorganic gaseous pollutants can impact the respiratory system as well as instigate haematological problems and cancer.[55]

2.7.3 Persistent Organic Pollutants

There are thousands of chemicals which may be classified as persistent organic pollutants (POPs), this is a group of organic compounds that include pesticides (Dichlorodiphenyltrichloroethane, DDT) and dioxins (Polychlorinated Dibenzofurans, PCDD/PCDF), furans, and polychlorinated biphenyls, PCBs). POPs are a major global issue due to their persistence, long-range transportability, ability to bioaccumulate in fatty tissue, and are highly toxic even at low concentrations.[56]
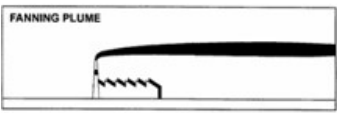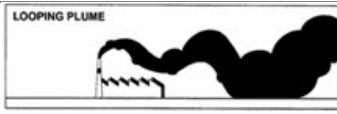
2.7.4 Heavy Metals

Definition of heavy metal is a metallic element with a density greater than five and examples are lead (Pb), mercury (Hg), cadmium (Cd), nickel (Ni), silver (Ag), copper (Cu), chromium (Cr), manganese (Mn), selenium (Se) and vanadium (V) which neither can be degraded nor destroyed. The most common products/processes of heavy metals are heavy industry processes, batteries, fertilizers, mining, industrial waste, and vehicle emissions. These chemicals are bioaccumulation since the compounds are taken and stored quicker in an organism than they metabolize. Heavy metals impact nuclei, lysosomes, cell membranes, mitochondrial and enzymes responsible for detoxification, metabolism, and maintenance.[55]

2.7.5 Plume Behaviour

A typical tall stack located on flat terrain with a plume exhibits a character's shape depending on the stability of the atmosphere and Table 18 shows the variety of different plume behaviours with a description of corresponding temperature and condition profiles. Increasing the height of stacks results in the emission of pollutants higher up in the atmosphere. In theory, this means that the pollutants will be more diluted by the atmosphere when they return to the ground and hence the effect on those closest to the stack is decreased compared to if the emission occurred at a lower height or ground level. Whilst this is true it also means that the pollutants are spread over a much greater area with taller stacks, and more individuals may be impacted. In general, higher stacks allow the emission of higher levels of pollutants.[57]

Table 18 – Different types of plume behaviour that are exhibited from stacks [57]

Plume Behaviour	Description
FANNING PLUME	Inversion condition (fanning) displays normal air movement and temperature inversion. A layer of warm air limits the rise of the plume into the upper atmosphere and creates an increase in the concentration of polluted air at lower levels in which the plume exists for several hours.
LOOPING PLUME	Strong lapse condition (looping) in windy conditions can swirl up and down and is common in the afternoon. Moderate and strong winds are formed on sunny days creating unstable conditions and existing for several hours.
CONING PLUME	Weak lapse condition (coning) is a type of fanning plume that developed overnight under stable operations. As the day heats up, unstable air is produced causing the plume to move vertically up and down.
LOFTING PLUME	Inversion, lapse aloft (lofting) is where the plume is above the inversion layer and with normal wind direction/speed, it will disperse the plume into the atmosphere without effect from ground warming or cooling.

Previous research by Davis ML *et al* and Cornwell DA *et al* has shown that the way the dispersion parameters vary with downwind distance from a point source depends on the state of the atmospheric boundary layer (height h), the height of the source (z_s) and the height of the plume as it grows downwind.[57][58] The broad criteria that were considered in devising the plume spread formulas included the maximum mean concentration at ground level (C_{glmx}) should be at least within a factor of two of the maximum of (agreed) field measurements, and the position of maximum (x_{max}) should be within ±50% of the

measurements, and the position $x_{1/2}$, where the ground level concentration ($C_{gl} = \frac{1}{2}C_{glmx}$) should be within ±50% of the measurements.[58] The distribution of the concentration profile within the boundary layer is a Gaussian plume with reflections at the ground and the inversion layer (Equation 1).[59] Where Q_s is the source emission rate in mass units per second and σ_y (Equation 2).[59]

Equation 8 - Gaussian distribution

$$C = \frac{Q_s}{2\pi\sigma_y\sigma_z U} \exp\left(\frac{-y^2}{2\sigma_{\overline{z}}^{\frac{2}{z}}}\right)\left\{\exp\left(\frac{-(z-z_s)^2}{2\sigma_z^2}\right) + \exp\left(\frac{-(z+z_s)^2}{2\sigma_z^2}\right)\right.$$

$$+ \exp\left(\frac{-(z-2h+z_s)^2}{2\sigma_z^2}\right) + \exp\left(\frac{-(z+2h-z_s)^2}{2\sigma_z^2}\right)$$

$$+ \left.\exp\left(\frac{-(z-2h-z_s)^2}{2\sigma_z^2}\right)\right)$$

Equation 9 - Source emission rate

$$\sigma_y^2 = \frac{\int_{-\infty}^{\infty}\int_0^{\infty} y^2 C\,dz\,dy}{\int_{-\infty}^{\infty}\int_0^{\infty} C\,dz\,dy}$$

The dispersion model used for the impact assessment reported here was the commercially available ADMS (Atmospheric Dispersion Modelling System), version 5, released in November 2012. A recommendation is that a wind monitoring station should be installed near the coast to improve the certainty of wind data when the wind blows from the sea towards the town, which is the direction of principal concern.[60] For dispersion modelling, additional meteorological parameters were also required. Solar radiation, rainfall and relative humidity are recorded. The default value for mixed urban/industrial areas of 30 metres was selected.[61] All other meteorological parameters were left at the default values. Figure 2.26 displays that the most frequent and highest wind speeds

continually come off the local sea, dispersing the PM emissions emitted from stacks towards the local community.
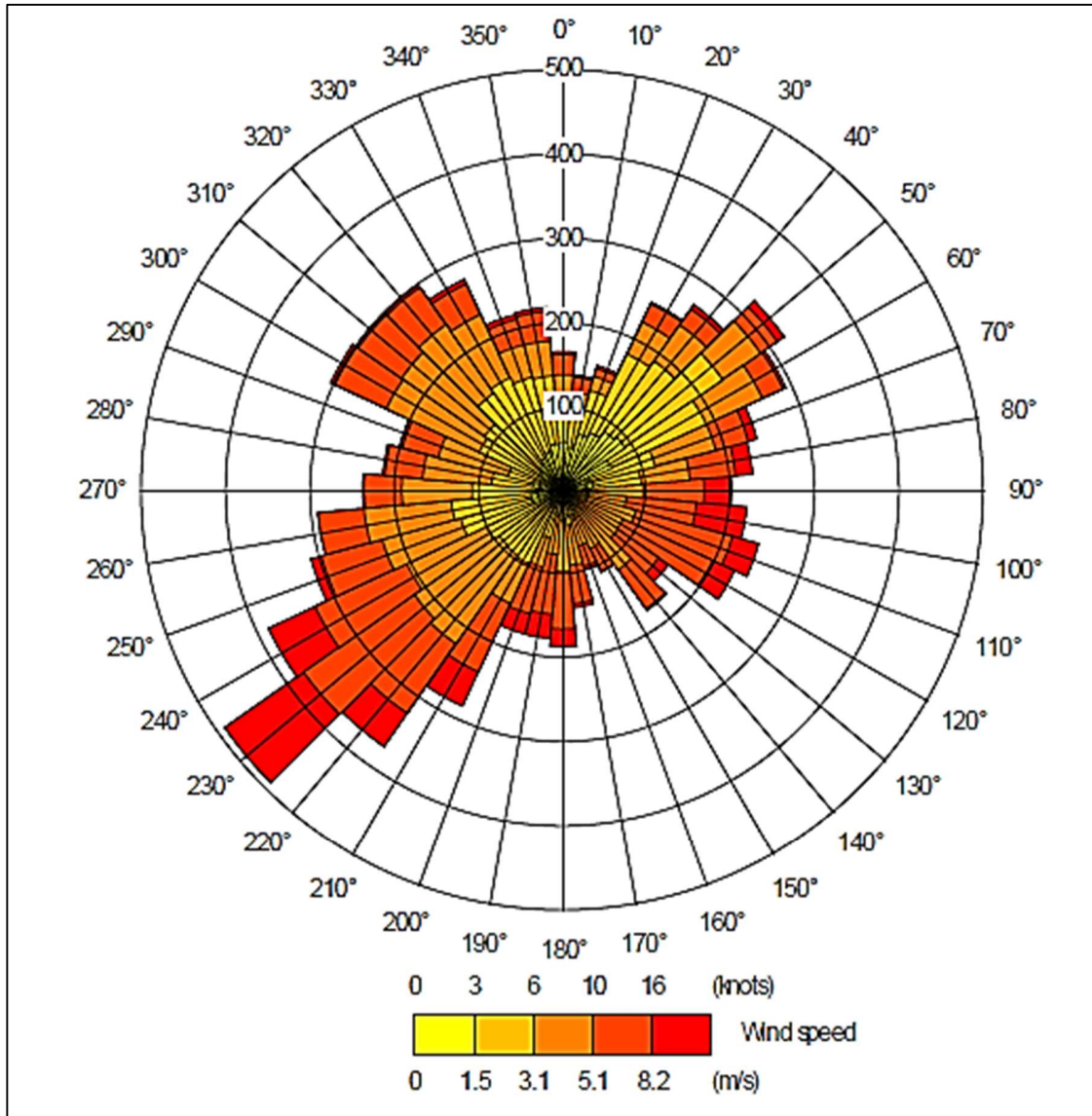
Figure 2.26 - Typical Wind Rose used for viewing trajectories to gauge impact [61]

2.8   Abatements

In 2010, the Industrial Emission Directive (IED) was enforced.[4] Article 3 defines the Best Available Technique (BAT) as the most effective and advanced stage in the development of activities and their methods of operation which indicates the suitability of techniques for providing the basis for emission limit values and preventing where that is

not practicable, to reduce emissions and the impact on the environment.[62] The meaning of each of these three words is important to understand the concept of BAT:

- Best - The technique considered is the most effective for achieving a high general level of protection of the environment.
- Availability - developed on a scale which allows implementation in the industrial sector, under economically and technically viable conditions.
- Technique - technology used and how the installation is designed, built, maintained, operated, and decommissioned.

2.8.1 Scrubbers

Scrubbers are used throughout large industrial plants and impaction is the primary capture mechanism. Figure 2.27 shows how it can be utilised as when the waste gas approaches a water droplet, it flows along streamlines around the droplet. Particles with enough inertial force maintain their forward trajectory and impact the droplet. Due to their mass, particles with diameters greater than 10 µm was collected using impaction[63]. However, particles that pass sufficiently close to a water droplet were captured by interception and the capture due to the surface tension of the water droplet.[64]
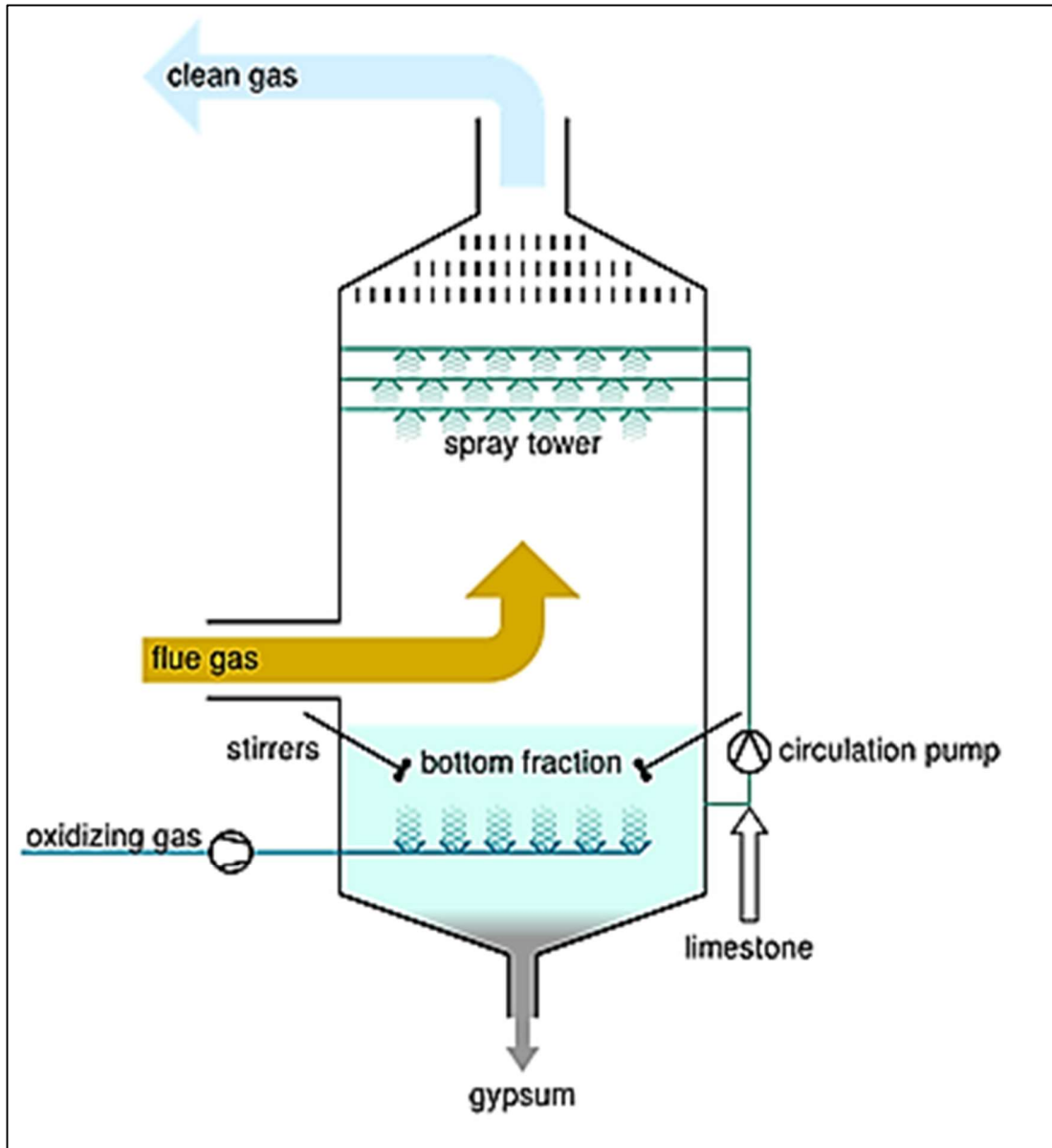
Figure 2.27 - Wet scrubber diagram[65]

2.8.2 Centrifugal Separators

A cyclone separator (Figure 2.28) is composed of four parts: the inlet part, the body, the conical part, and the outlet port. The gas and solid flow enter the cyclone inlet at remarkably high velocities, best practices of which have been reported as between 6 and 15 m/s.[66] Most inlet structures are designed so that the gas flow starts its swirling motion with a minimal pressure drop at the inlet side.[67] The purpose of the conical part is to divert the gas flow toward the vortex finder and the particles are collected in the dust bin.

[68] The performance of a cyclone separator is expressed by collection efficiency and pressure drop. These two performance criteria are intimately related to each other. Usually, collection efficiency increases with increasing pressure drop. Therefore, the prediction of pressure drop is an essential step in cyclone design.[69]
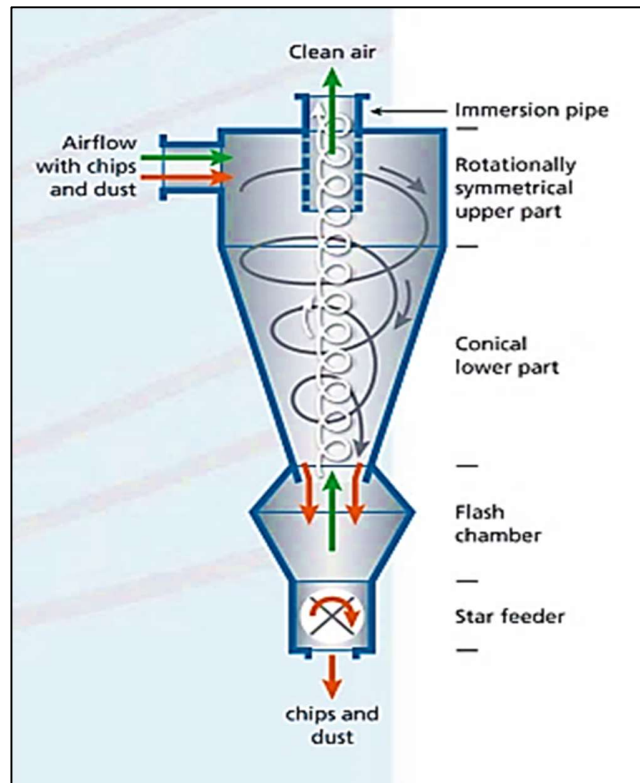
Figure 2.28 - Centrifugal separator diagram[70]

2.8.3   Fabric and Ceramic Filter

A diagram of a fabric filter (Figure 2.29) displays the bags in mechanical shaker-type filters that are anchored to a bottom tube plate and the bottoms of the bags are open. The dirty air enters the hopper and travels up the inside of the bags depositing dust on the inside. Depending on whether the dust is collected on the inside or outside of the bag, the air either pressurises the compartment being cleaned and partially collapses the bags or pressurises the bags. In either case, the dust cake cracks and falls off the bags. Ceramic catalyst filters (Figure 2.30) are composed of fibrous ceramic materials mixed with nano-bits of proprietary catalysts. This new generation of lightweight, ductile ceramic filters is very efficient in removing NOx and other pollutants, including submicron particulate, to

extremely low levels. Ceramic catalyst filters typically capture particulate to levels less than 2 mg/Nm^3 and the unique structure of the filters keeps the collected particles on the surface.[71]
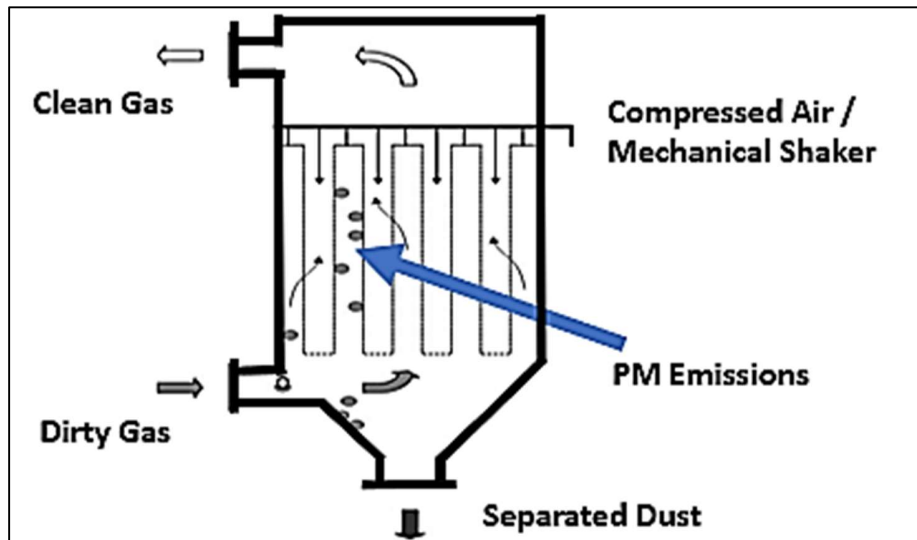
Figure 2.29 – Fabric bag filter diagram
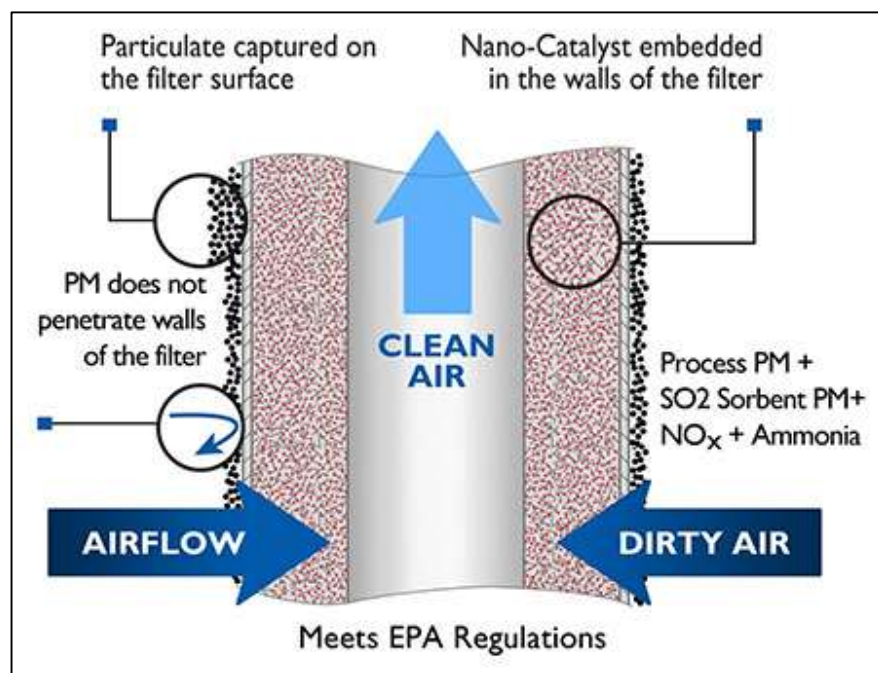
Figure 2.30 – Ceramic fibre filter tube with embedded nano-catalysts diagram[71]

2.8.4 Electrostatic Precipitator

All sinter plants typically employ modern dry ESP (Figure 2.31) to control the air releases of PM emissions and the ESP abatement is the BAT for sinter plants in the current edition of the EU BAT reference document due to its ability to remove PM emissions at high temperatures with high removal efficiency.[72] The precipitator contains numerous parallel gas passages containing a high-voltage electrode system at the centre line of each gas passage. ESP abatements have two advantages over fabric filters: they do not need to be bypassed during start-up, shutdown, and failures. ELVs are exempted for these periods, therefore this advantage has not been factored in during the development of regulations and when determining the best available air pollution control technologies. ESP abatement also uses much less electric power than fabric filters which is the more environmentally friendly option currently. The material design of the high voltage electrode usually varies from mild steel to high alloy and stainless. Other types of corona-emitting surfaces may be comprised of sharp-edged metal stampings that are fastened into a rigid steel frame which is supported by the high-voltage insulator assembly. [72] The overall structure (Figure 2.31) is enclosed in a steel housing or shell built around structural steel that also supports the collection hoppers, and the hoppers periodically collect the material which is removed from the electrode surfaces by rapper or vibrator apparatus. There are often 12 to 20 transformer rectifiers located on the roof of the precipitator to power the fields.[73]
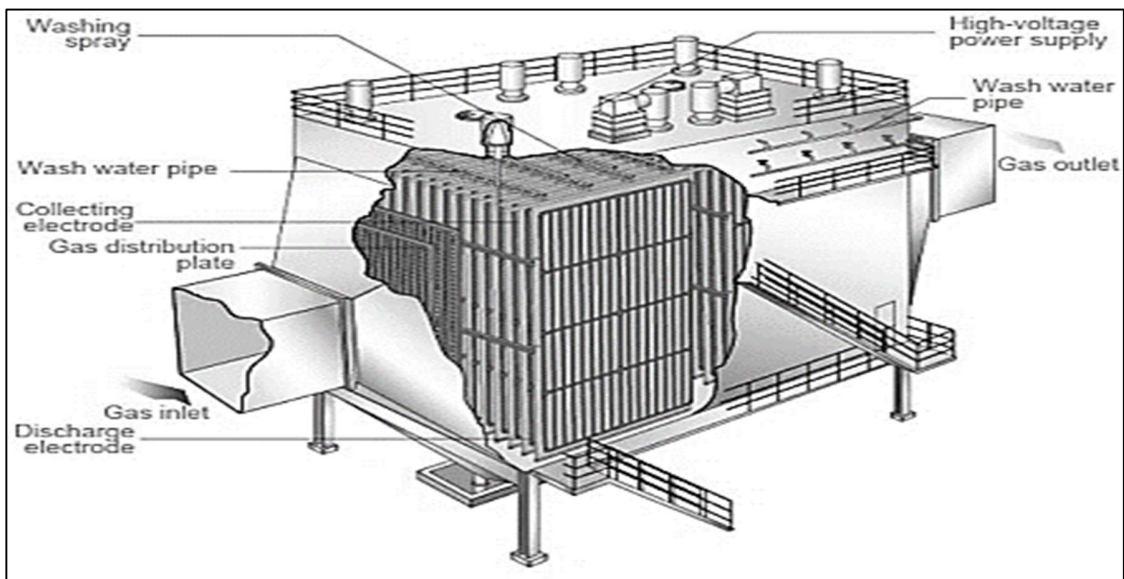
Figure 2.31 - Electrostatic precipitator design[74]

When current was applied in Figure 2.32 and Figure 2.33 to the discharge electrode this forces corona discharge (Equation 3) that takes place and the ions and electrons are produced at the corona point and ionic current flows through space. These ions attach to suspended solid particles and are attracted towards the collecting electrode by a coulomb force and the coulomb law indicates that the force was inversely proportional to the square of the distance between two points charged.[73]
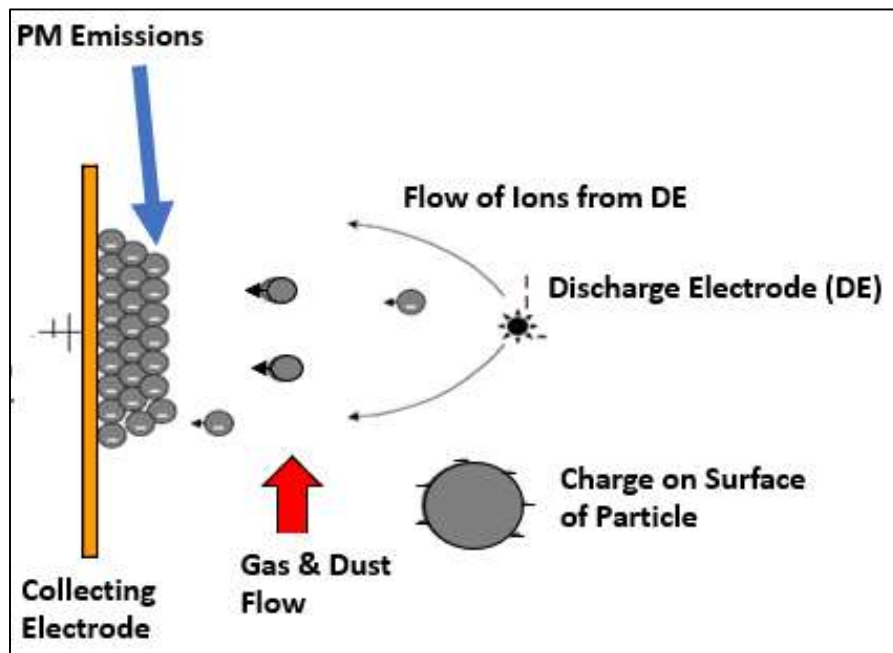
Figure 2.32 – PM emissions attraction to electrostatic precipitator plate within the abatement
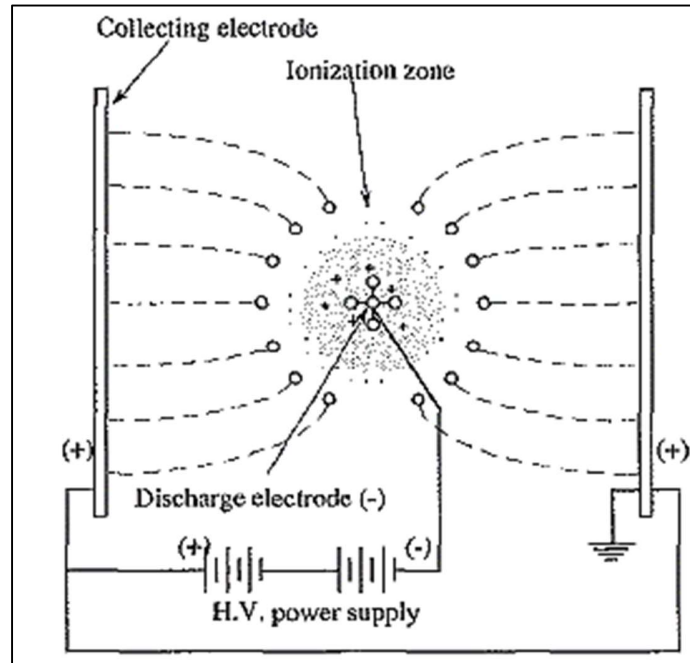
Figure 2.33 - Schematic Diagram of an electrostatic precipitator [73]

The voltage-current characteristics of corona discharge are expressed as:

Equation 10 - Corona discharge

$$I = AV(V - Vc)$$

Where A is a constant, V, *is* the corona starting voltage, I *is* the electric current and V_c is the applied voltage. Typical efficiency of an electrostatic precipitator as a function of the corona power ratio, which is the power consumed (in Watts) divided by the airflow in cubic feet per minute. Figure 2.34 shows the typical efficiency of an electrostatic precipitator and shows the relationship between collection efficiency and the corona power ratio. A positive correlation is shown when you increase the corona power ratio the collection efficiency increases at the same time. During the cleaning of the PM emissions, the electrostatic precipitator is kept at a low velocity of <1.5m/s to allow particle migration. This velocity is enough to carry it to the hopper for particles to exit and the electrostatic precipitator efficiency equation is shown in Equation 11 and Equation 12.
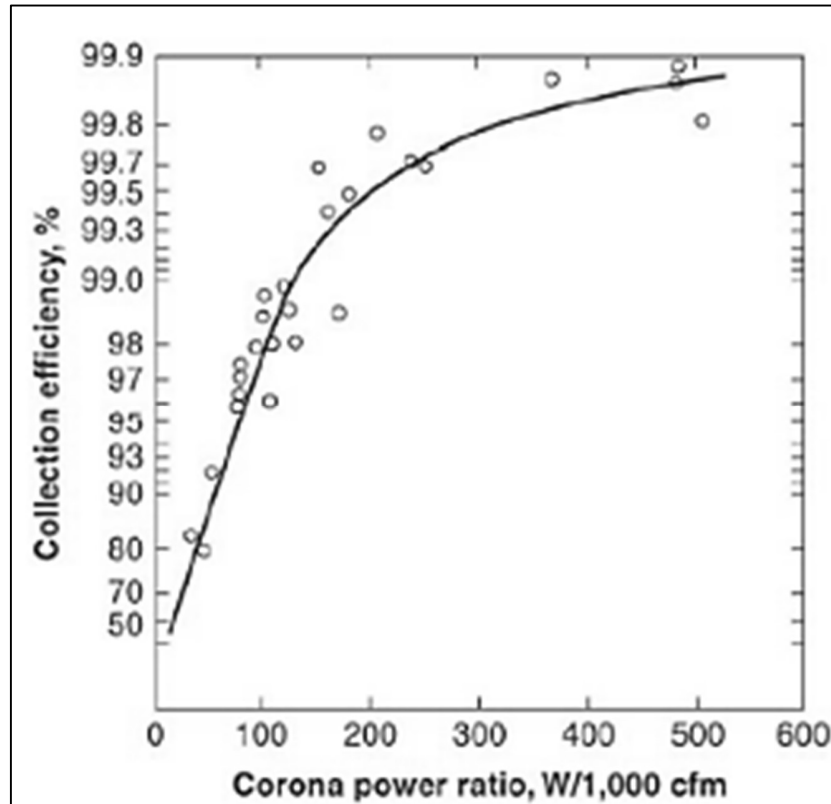
Figure 2.34 - Typical efficiency of an electrostatic precipitator[73]

Equation 11 - ESP abatement efficiency (1)

$$\eta = \left(-\frac{Aw}{Q_g}\right) 1 - esp$$

A = collection area of plate (m^2)

w = migration velocity of particles (m/s)

Q_g = gas flow rate (m^3/s)

Where w is:

Equation 12 - ESP abatement efficiency (2)

$$w = \frac{qE_pC}{6\pi \; \mu}$$

q = charge (C)

E_p = collection field intensity (volts/m)

R = particle radius (m)

μ = dynamic velocity of gas (Pa .s)

C = Cunningham correction factor (Cc = 1 + λ/d [2.514 + 0.8 exp(-0.55 d/λ)] Cc = 1 + (0.167 / d[μm]))

A dry ESP abatement design is used to filter the exhaust gas to a concentration <40mg/Nm³ with a flow rate of approximately 1,245,000 Nm³/hr. This normalised flow rate should be achieved under the following operating conditions of an optimum gas temperature of 120°C - 160°C, -145 mbar dP with two fans with a rotational speed of 1,000 rpm The main advantages of hot ESP are that it can treat large volumes of waste gases at a low-pressure drop, have a relatively low maintenance requirement, can easily recover dust that is easy to manage and can recycle through the repeatable process. Particle resistivity, the ability to accept a charge, plays a key role in the collection efficiency of the ESP. If a particle is resistant to receiving an adequate charge, the particle resistivity needs to be modified or the ESP treatment time needs to be increased. Some of the key factors that would directionally lower the catalyst's resistivity are:[75]

- Higher inlet temperature
- Higher rare earth concentration in the catalyst
- Ammonia injection
- Moisture content

The design and performance of an ESP also depend on numerous criteria shown below[75]

- Inlet catalyst loading
- Superficial flue gas velocity inside the ESP
- The number of gas passages per chamber
- Collecting electrode spacing
- Total treatment length
- Treatment of time
- Discharge electrode type, quantity, and spacing
- Electrical sectionalisation (number of fields in series)
- Hopper volume, heater capacity, and level detection

Figure 2.35(a) shows a combination of ESP and a fabric filter where particles are pre-charged and thus polarised by the electric field, and enter the dust collection part, consisting of the fabric filter. High performance can be achieved with a low-pressure drop

and with a combination of a pulsed discharge plasma with a catalyst. Pulse energisation avoids the deleterious effects of back corona for dust in the range of 1011−1013 ohm cm. The technology has been accepted as a viable, dependable, and effective method for significantly improving the performance of existing electrostatic precipitators and reducing the size and cost of new ESP designs treating difficult high-resistivity dust.[76] A plate-to-wire electrode is used, and a pulsed voltage superimposed on a DC voltage is applied, as displayed in Figure 2.35(b). The electrode is followed by a ground mesh coated with a TiO_2 (titanium dioxide) catalyst, known as a photo-catalyst.[73] The particles are collected at the grounded electrode. The catalyst surface can be activated by ozone, and the gaseous pollutants adsorbed on the catalyst can be oxidised. Active charcoal or other catalysts also can be used for the simultaneous removal of dust particles and gaseous pollutants.[73]
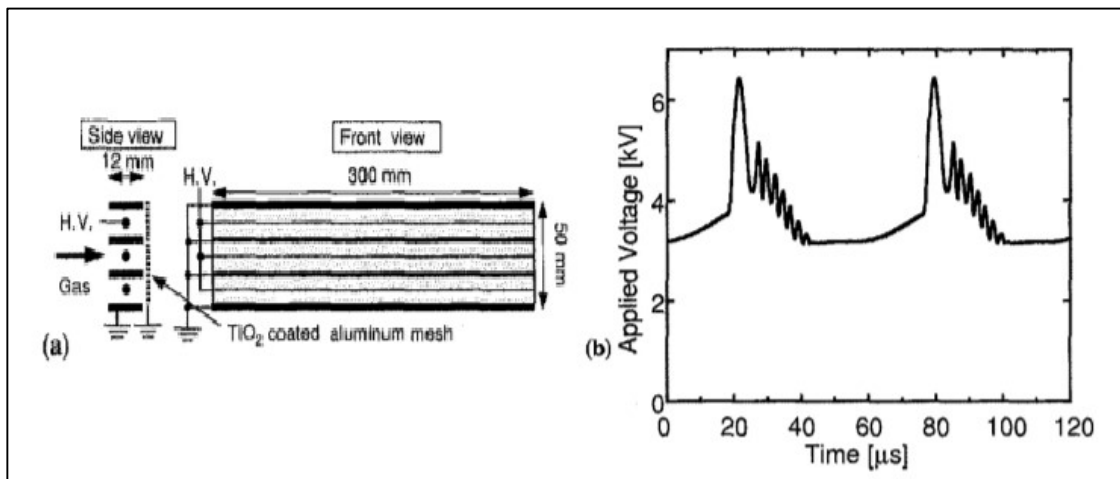
Figure 2.35 – Improved ESP (a) shows a combination of ESP and a fabric filter. (b) The waveform of pulse voltage. [73]

Summary

Table 19 displays that ceramic filters are the best abatement and this is due to the ability to remove the smallest particle sizes, and these have an achievable emission of $<1mg/Nm^3$ but are prone to major frequent failure in larger plants due to cracking from vibrations. Fabric filters (baghouses) are the second-best abatement with >99.5% collection efficiency but only have a maximum operating temperature of 220°C. This will be a challenge as currently; the gas temperatures can range above the fabric filter's maximum operating temperature. The ESP has low maintenance, easy cleaning and can handle a large volume of gases. Therefore, the BAT for the sinter plant is the hot ESP as it is

designed for elevated temperatures with a high collection efficiency of >99% and improving this abatement may be a more viable option. Table 20 displays the process features of the individual features of each abatement including the ESP and the fabric bag filter abatements which underlines why there is a demand for a fabric bag filter along with extra expenditure to be spent on another system that involves the cooling of waste stream gas to make it feasible for a sinter plant.

Table 19 - Abatement systems and their effects on monitoring[4]

Technique	Particle size (um)	% Collection efficiency at 1μm	Maximum operation temperature (ºC)	Range of emissions mg/Nm^3	Comments
Hot ESP	<0.1	>99 Depending on the design	450	<5 - 15 (pre-abatement>50)	4 or 5 zones.
Wet ESP	0.01	<++	90	<1 – 5	2 zones in the series.
Cyclone	10	40	1100	100 – 300	Coarse particles – used to assist other methods
Fabric Filter	0.01	?99.5	220	<1 – 5	Very good performance with suitable dust type
Cermaic Filter	0.001	99.5	900	0.1 – 1	Very good performance with suitable dust type
Wet Scrubber	1 – 3	>80 – 99	Inlet 1000 Outlet 80	<4 – 50	Good performance with suitable dust. Acid gas reduction.

Table 20 - Summary of the abatements processes features

Abatement technique	Features
Scrubber	• Capable of removing gases • Removes vapours • Produce effluent • Can produce a plume • Low capital cost • Small space requirement • High-pressure drops
Centrifugal	• Low efficiency • No moving parts • Low cost • Subject to erosion • Leakage can impact performance • Can be used as pre-collectors
Fabric Filter	• Collects particles only • Excellent collection efficiency • Dry dust • Low-pressure drops

	• Not sensitive to changes in the composition
	• High maintenance
Ceramic Filter	• Collects particles only
	• Excellent collection efficiency
	• Dry dust
	• Low-pressure drops
	• High maintenance
ESP	• High collection efficiency
	• Low maintenance
	• Manages a large volume of gases
	• Negligible pressure drops
	• Easy cleaning

2.9   Understanding PM Emissions

2.9.1   PM Emissions Profile

Gan *et al* demonstrated via experiments using a pilot-scale sinter rig that the flue gas temperature (FGT) curve in Figure 2.36a is vital to understand the PM emissions properties from the sintering process and six typical sintering stages have been divided according to the FGT curve:[77]

1. Ignition period.
2. The gradually stabilising process of FGT.
3. The stable process of FGT.
4. The short period before the rise of FGT.
5. 1st half of the FGT rising process.
6. 2nd half of the FGT rising process.
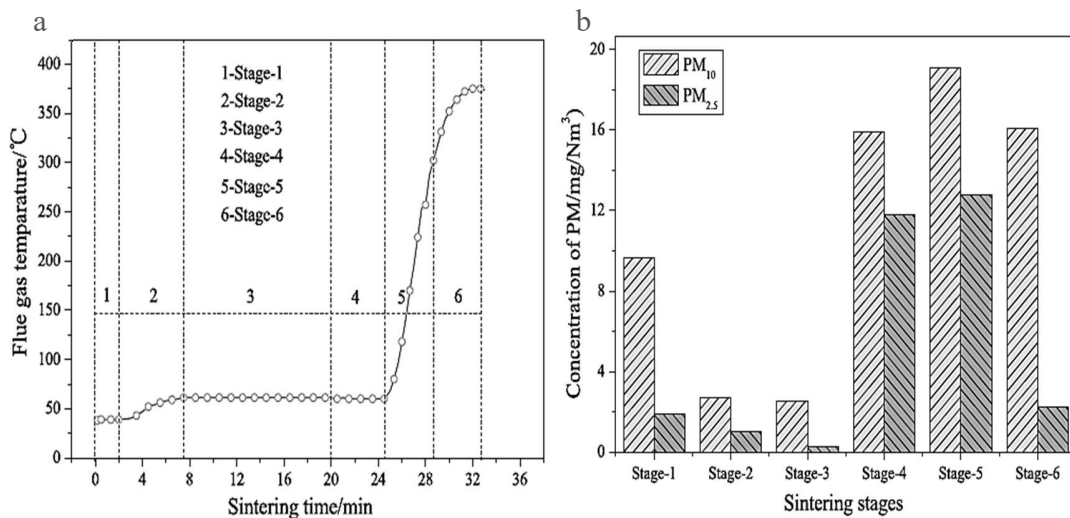
Figure 2.36 – a) Typical trends of flue gas temperature in the sintering process and b) emission properties of PM in different sintering stages[78]

The concentration of PM_{10} emitted from stage-4 to stage-6 is higher than that of stage-2 to stage-3 (Especially for stage-2 and stage-3, the concentration of PM_{10} from these stages is even lower. Therefore, stage-4 to stage-6 are the most important emitting stages of PM_{10} during an integrated sintering process due to the temperature. (Figure 2.36b). During sintering, the raw mix is converted into several zones (Figure 2.37).

The state of PM in each zone is:

- Sintered zone – unlikely, minimal free particles.
- Dried zone – highly likely, the strong capillary forces holding granules together are no longer there,
- Calcination zone – high calcination can result in the decrepitation of particles and the formation of fines.
- Flame-front zone – elevated temperatures can cause the formation of substances such as KCl fume
- Wet zone – unlikely, acts as a wet scrubber for the flowing gas.[79]

During the sintering process described in this study, the sintering stages started from the gradual disappearing of the over-wetted layer to the burn-through point for the main area for PM_{10} emission (Figure 2.38) and this is detrimental due to the over-wetted layer and

the raw mixture layer which enables the scrubbing of PM_{10} from flue gas. PM_{10} and $PM_{2.5}$ have been characterised as having high emission concentrations in sintering stages-4 to stage-6 and sintering stage-4 to stage 5 (Figure 2.39a and b). The emission load of PM_{10} and $PM_{2.5}$ in those specified areas accounted for about 63.5 and 47.0% of the total PM emissions.[80]
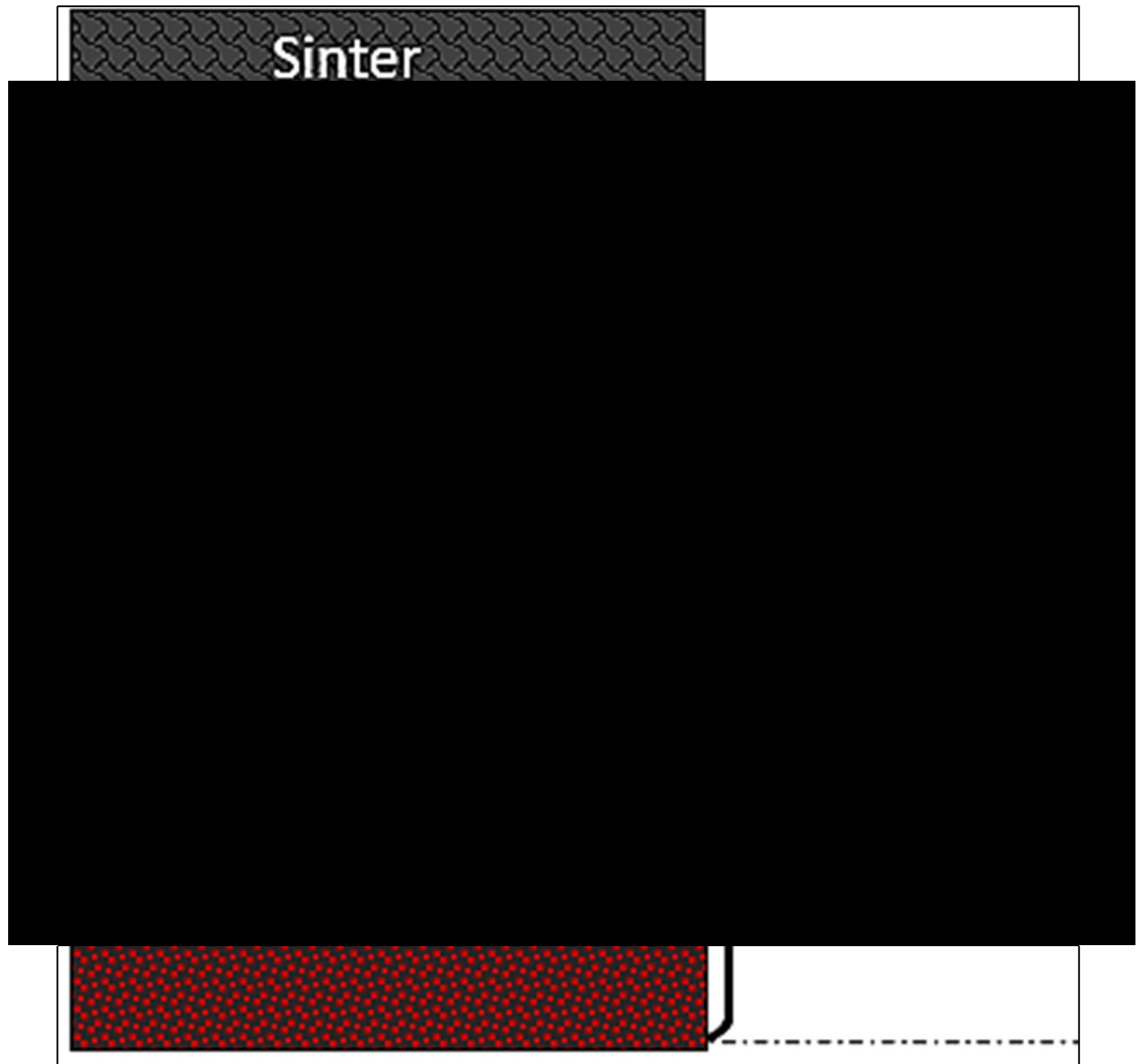
Figure 2.37 – Schematic diagram showing different zones present in a sinter bed and where the source of PM emissions is located
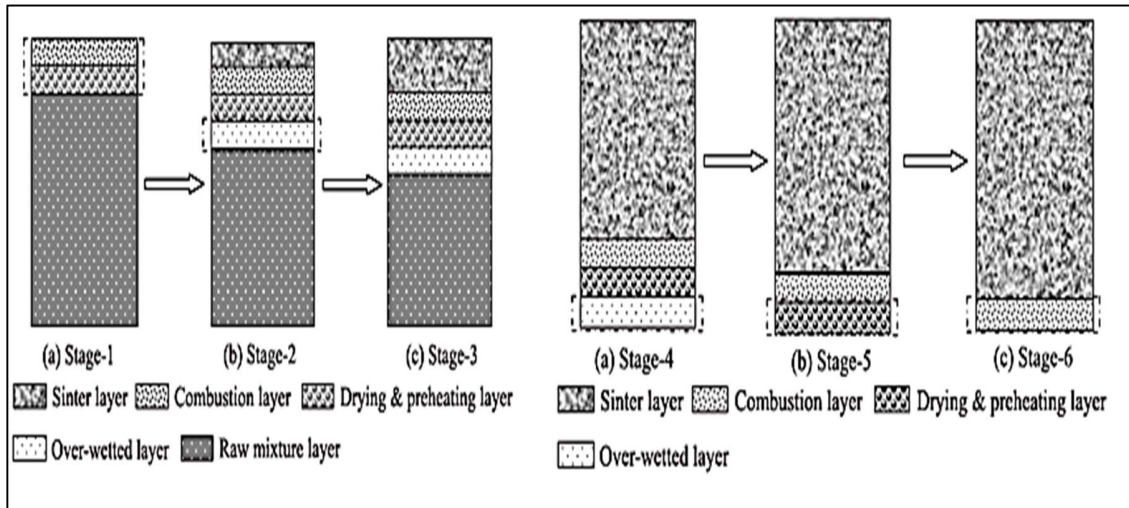
Figure 2.38 – Characteristics of the sintering layers in the sintering process[78]
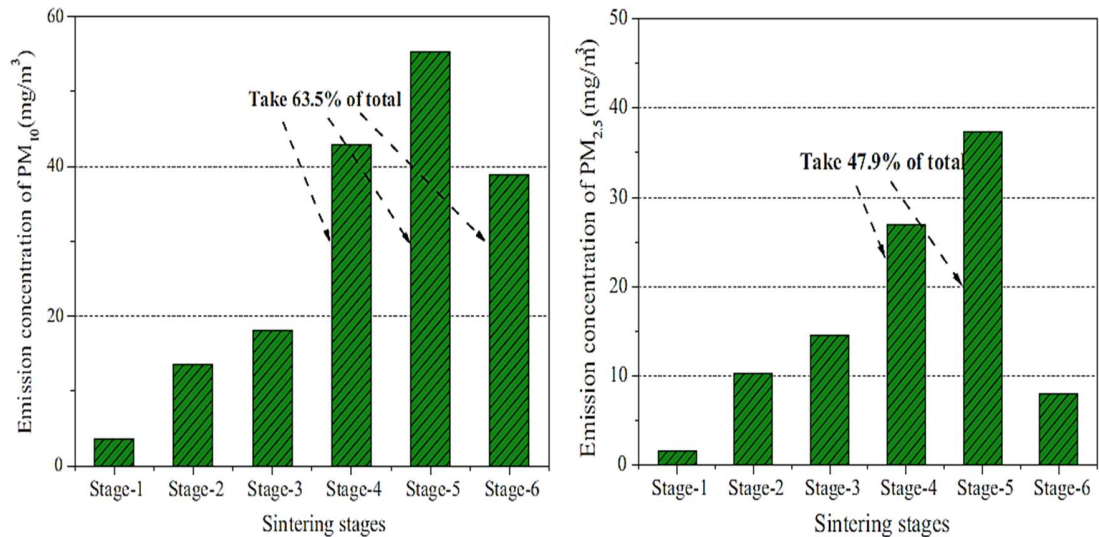
Figure 2.39 – Emission properties during sintering of a) PM$_{10}$ and b) PM$_{2.5}$ [80]

As flue gas with entrained PM flows through the over-wetted layer and raw mixture layer, the gas flow is easily changed from its previous moving direction along with the channel formed in the sintering bed. This is due to the lower emission concentration of PM in stages 2 to 3, as well as a potential mechanism involving these layers. (Figure 2.40) However, when the direction of the gas flow changes abruptly, the particles, especially the coarser ones, have a higher likelihood of colliding to form granules. This can be the reason most of the PM measured from stages 1 to 3 is small-grained spherical. Condensed water from flue gas blocks or narrows some channels in the overwetted layer, allowing

the gas flow velocity to be increased. Therefore, it is not only the coarser particles but the finer particles are also captured by the sinter layers due to the inertia effect.[78]
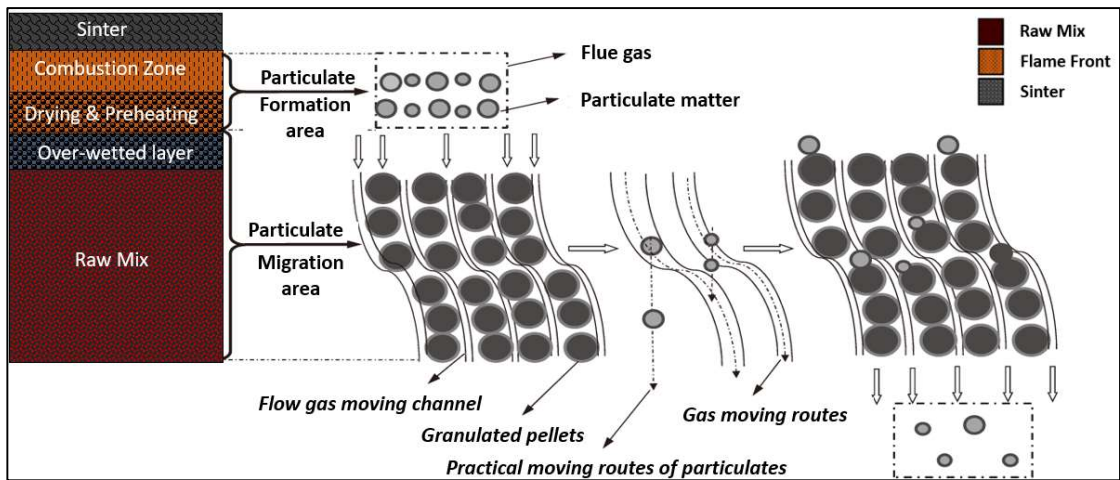
Figure 2.40 - The proposed mechanism for the interceptive role of the sintering bed for PM emissions[78]

The detachment force needs to exceed the adhesion force for PM release from the sinter bed. Adhesion forces, excluding the wet zone, include:

1. Solid bridges are formed as moisture is dried from the granules *e.g.*, clays present.
2. Frictional forces are dependent on the number of inter-particle contact points.
3. Short-range forces, such as van der Waals.[43]

Based on the particle's inertia and drag force, an entrained particle can either deposit further into the wet zone of the bed or leave the bed with the gas stream because the breakdown of particles caused by thermal shock or calcination is likely to weaken interparticle adhesion and lead to their entrainment in the gas stream.[43] In sintering zones, 1-3, the majority of PM emissions were characterised by discrete spheres under <1μm in diameter (Figure 2.41a), small part flake-like particles and other irregular particles. However, the morphology of particles from stage 4 starts to change. Spherical particles (<1 μm) from this stage only assume a small proportion of the total particles, and coarser PM emissions appeared, which were characterised by flake-like shapes angular shapes with a smooth surface. PM emissions emitted from stages 5-6 exhibited greater shape-related irregularities with fewer spherical particles, but the surface of the particles tends to be sticky. A large number of fine particles sticks to the surface of coarser particles or several fine particles aggregated to form a coarser particle.[78] The main chemical

composition of PM$_{2.5}$ emitted (Figure 2.41b) from the ignition period to the rising point of FGT characterises high contents of Fe and low contents of trace elements; PM from the rise of FGT process is characterised by high contents of K, Pb, Cl and S, and low content of Fe for the first half, while high contents of Al, Si, and low content of Fe for the second half.[78] Gan *et al* highlighted in the research that the components of PM$_{2.5}$ existed primarily as Fe$_2$O$_3$– CaO, xAl$_2$O$_3$-ySiO$_2$, K(Pb/Na)Clx, and K$_2$(Ca/Pb)SO$_4$.[78] Figure 2.42 encapsulated the key transformation paths for these specifications which consist of minerals melting, escaped fine fuel fly ash, chlorination reactions and forming sulphate.
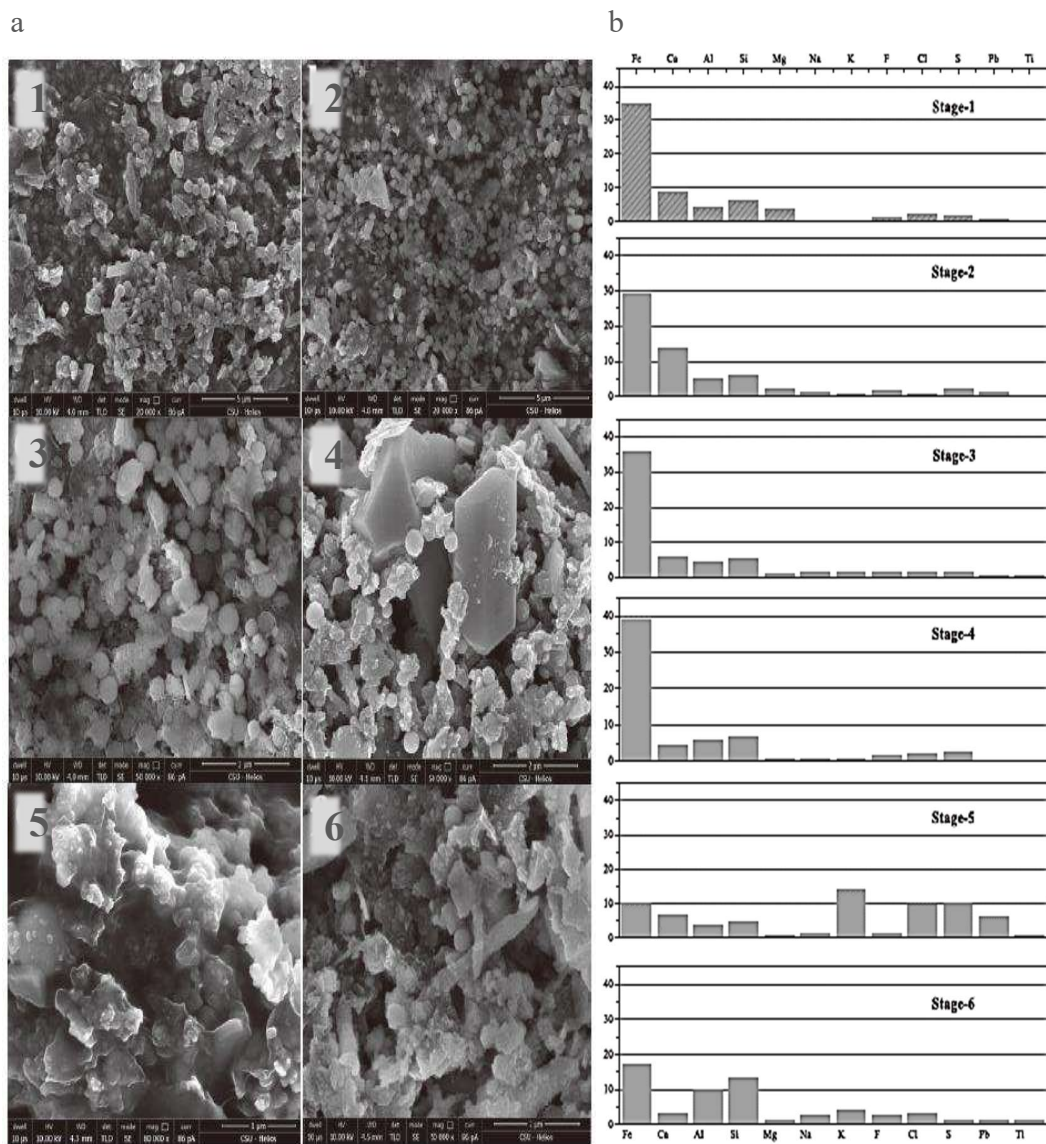
Figure 2.41 – a) SEM images from different sinter stages and b) major components from PM$_{2.5}$ from different sintering stages (mass%)[78]
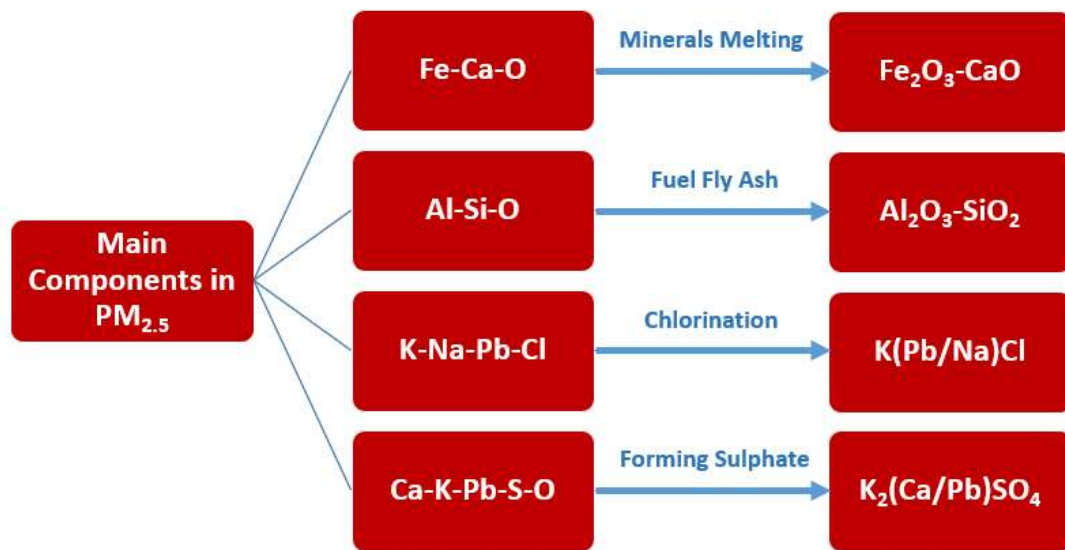
Figure 2.42 - Summary of the main speciation in PM2.5 and main transformation paths[81]

2.9.2 Control Techniques

Using the knowledge previously mentioned, different control techniques can be implemented with the potential to minimise PM emissions. In terms of control techniques. Gan *et al* experimented with a pilot-scale sinter pot rig and this showed that most PM emissions had a size of <1.18 mm indicating that it comes mostly from the adhering fines layer of granules. [77] This highlights the importance of understanding the nuclei-to-layer ratio (NTLR) concerning the particle size distribution used. By controlling the NTLR, it may be possible to control the release of PM emissions by regulating the amount of large and smaller particles in the sinter bed. Another issue to consider is the correlation between burn-through flow and PM emissions was observed when green mix moisture was varied, while weak correlations existed between green mix and sintering flow with PM emissions (Figure 2.43). The formation of thicker layers of adhering fines on nuclei particles decreases the interfacial contact area between the flowing gas and particles. A higher moisture level would also help to form stronger bridges between particles by dispersing the clays present over a wider area. This result suggests that the increased burn-through flow and, hence, the increased detachment force was outweighed by the increased adhesion force as moisture was increased. Decreasing the burn-through flow decreases the detachment forces which remove PM from the sintering bed, and it may be possible to

reduce PM emission on the plant by reducing the pressure drop across the wind boxes where burn-through occurs but due to a slower frame front it may decline productivity.[43]
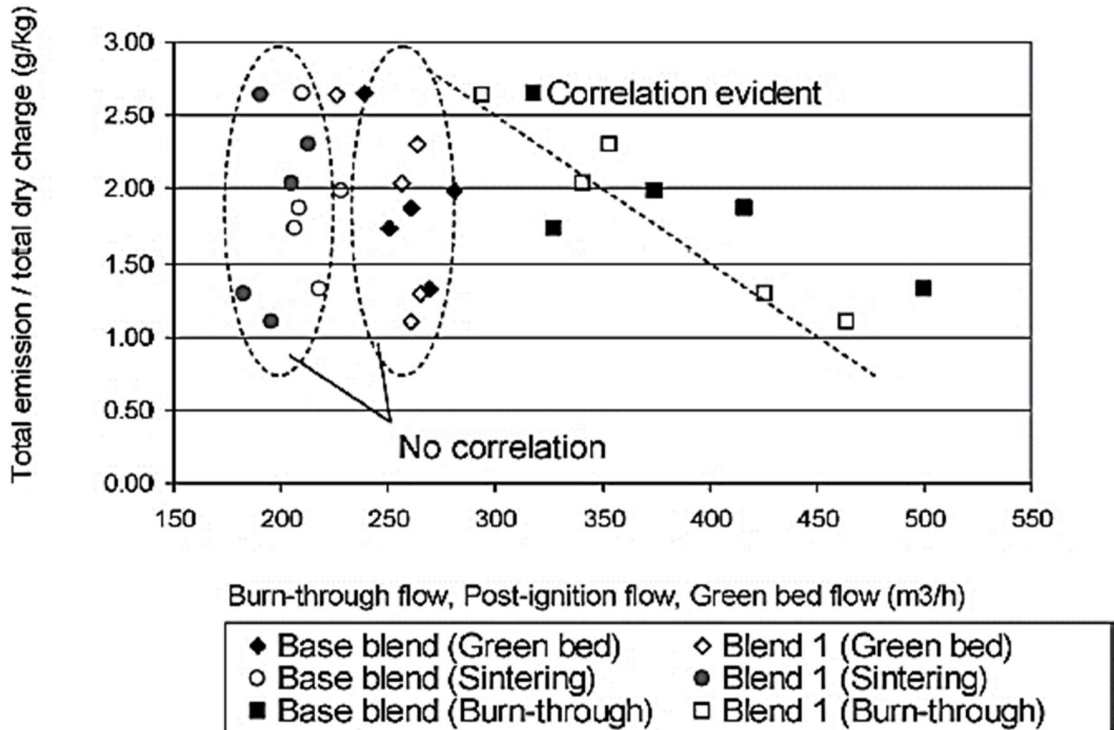
Figure 2.43 - Variation of total PM emissions/total dry charge plotted against the burn-through flow, sintering flow and green bed flow for a constant coke rate of 6.5 mass% dry ore basis while varying moisture[43]

The overwetted area refers to the region where the moisture content in the sinter bed is higher than the base level and would increase in size if the raw mixture's moisture content were increased. A larger overwetted area means a stronger scrubbing effect of the PM emissions (Figure 2.44).[82]Sinter productivity increases with a rising moisture content which is consistent with findings by Chen *et al*, who revealed that the increase of waste content in raw mixtures would increase the permeability of the sintering bed and combustion efficiency due to the abundant of coke breeze and limestone fines coating on the surface of particles.[83][43]
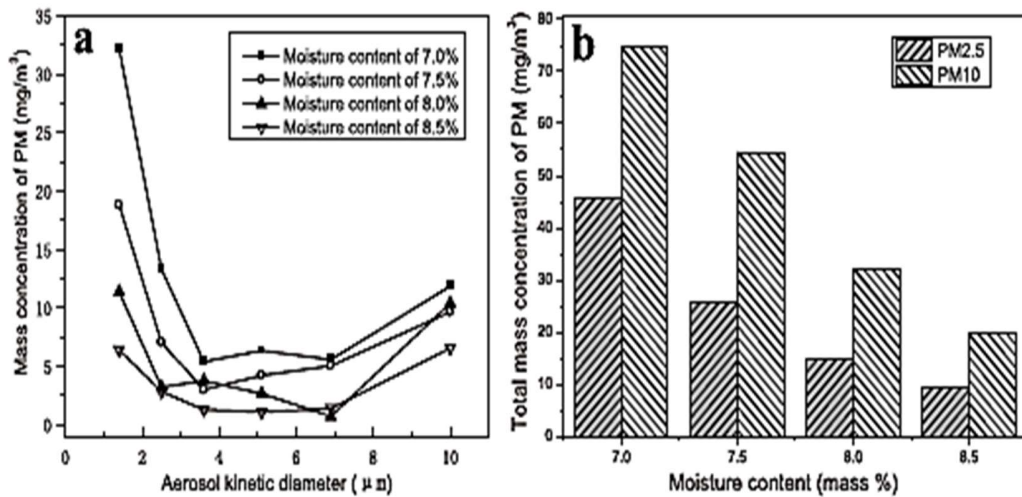
Figure 2.44 Influences of moisture content on the emission property of PM$_{10/2.5}$. (a) Influences on emission concentration of PM emissions with different diameters; (b) Influences on total emission concentration of PM emissions[82]

Coke rate is the amount of fuel used in the sinter bed limiting the use will decrease costs related to the sinter plant. However, in terms of PM emissions, increasing the coke rate while keeping moisture constant, decreases sintering flow (determined at the ambient condition) because of higher drag forces in the flame front zone. Increasing the coke rate will decrease gas density but it is not clear what will happen to velocity since the expanded gas is accompanied by reduced mass flow through the bed. By increasing the coke rate, the drying zone will become broader which will increase the time available for particles to detach from the drying zone.[43] Increasing the coke breeze rate tends to increase the emission concentration of PM as shown in Figure 2.45. The rate of coke breeze has a direct impact on the temperature and atmosphere during the sintering process (Figure 2.46a). Increasing bed temperature has the function to increase the volatile of trace elements like K, Na, Pb, and Sn (Figure 2.46b) which is also detrimental to the ESP efficiency.[82]
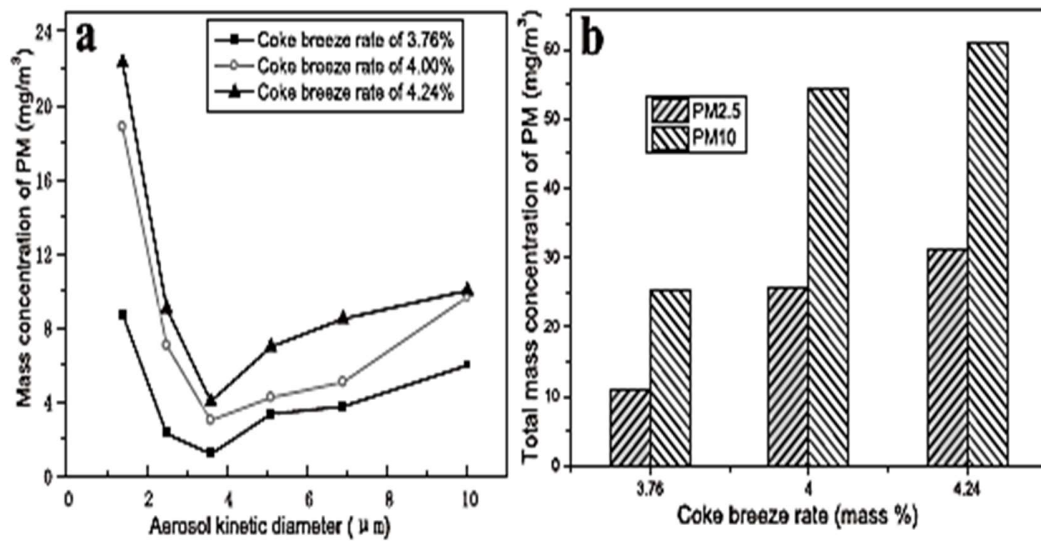
Figure 2.45 - Influences of Coke breeze rate on the emission property of PM10/2.5. (a) Influences on emission concentration of PM emissions with different diameters; (b) Influences on total emission concentration of PM emissions [82]
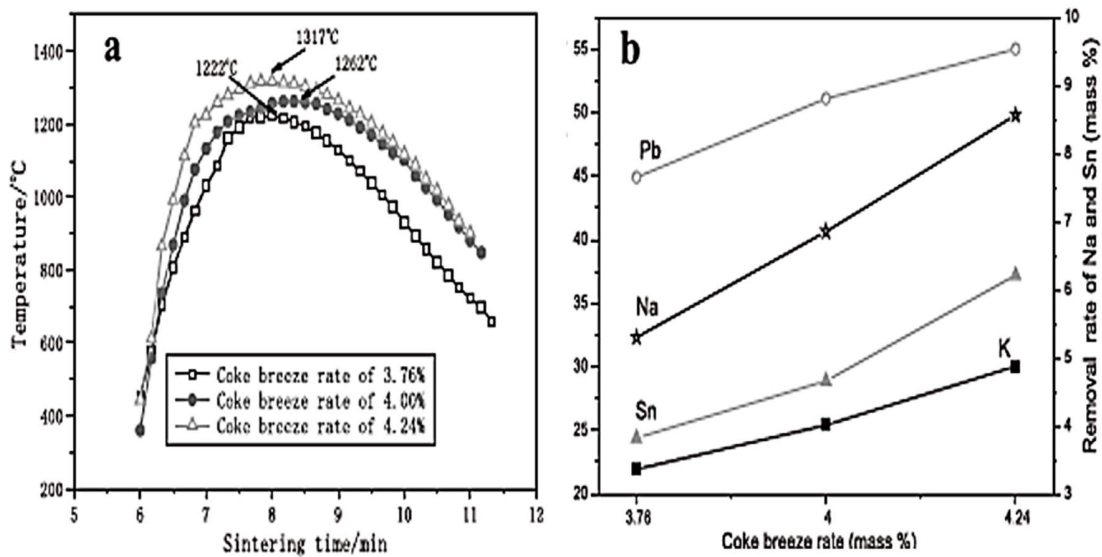
Figure 2.46 – (a) Influences of coke breeze rate on the temperature of sinter bed; (b) Influences of coke breeze rate on removal rates of K, Na, Pb and Sn [93]

Biomass is becoming an attractive alternative source of energy to traditional fossil fuels such as coal for environmental purposes. Due to the soft, fibrous nature of the alternative carbon source, biomass from a cutting mill was used. It was discovered that the peak temperature for the biomass reaches a maximum for the material in the size range that is smaller than the optimum carbon breeze size. The data indicates that the biomass needs to

be finer than the coke breeze that it replaced, but no PM emissions were measured when conducting this experiment. Gaseous emissions were recorded when researching lignin (wood sawdust), this has a calorific value that corresponds to 80% of the calorific value of coke and its reactivity is higher.[84] The lower emissions of sulphur and nitrogen oxides as well as the reduction of carbon footprint in the agglomeration process due to zero CO_2 balance in the formation of the biomass correspond to its positive aspects. Up to a 50% substitution of coke powder with this type of biomass can be predicted for the technology of agglomerate production in real operation.[85] Another influencing factor is extending granulation time which can enhance the mechanical strength of granules and makes adhesive fines tightly adhered and decreases the ability to drop from the surface during the sintering process (Figure 2.47a and b). Ball *et al* found this effect of granulation time and enhanced mechanical strength, with a focus aimed at the formation of total dust.[86] Effects of the removal of volatile trace elements to flue gas also decreased due to the linkage between fine particles constraining the drop of PM and minimising the mass transfer of K, Na, Pb, and Sn to flue gas.[82]
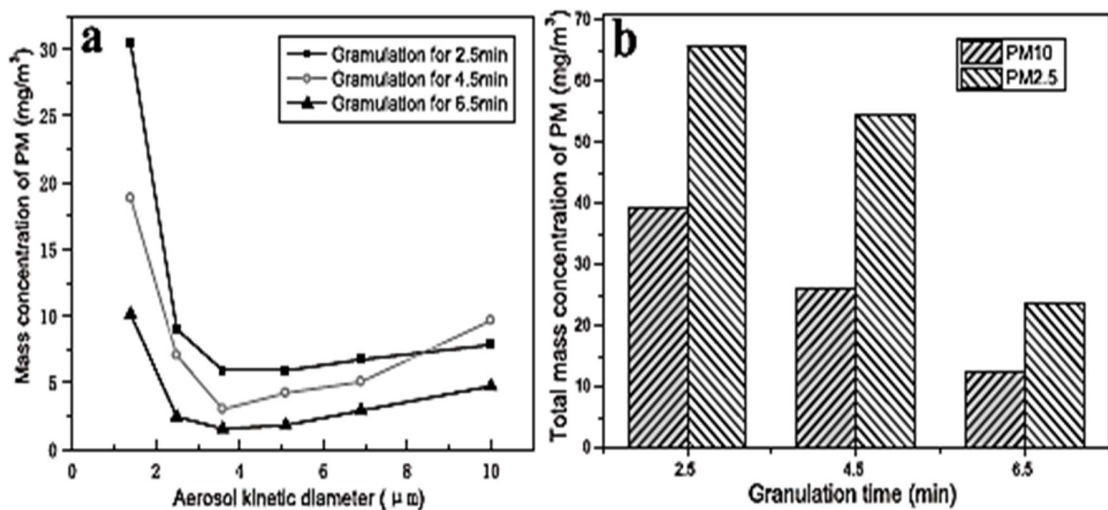
Figure 2.47 - Influences of Granulation time on emission property of PM10/2.5. (a) Influences on emission concentration of PM emissions with different diameters; (b) Influences on total emission concentration of PM emissions[82]

2.9.3 Raw Materials

The utilisation of recycled materials in sinter production is challenging, considering the physical and chemical characteristics of undesirable by-products of the steel-making process. Gao-yuan *et al* studied the relationship among sinter feed, dust components and dust emissions from the sinter plant main stack.[87] Among the chemical components of sinter feed, alkali metal such as K, and Na exerts a negative effect on ESP efficiency. The effective way to improve ESP efficiency is to decrease the content of alkali metal.[87] Fan *et al* researched those trace elements and S was shown to be a significant component of $PM_{2.5}$ emitted from the sintering process for the $PM_{2.5}$ collected from stage 2, contributing to the formation of Fe-rich and Fe–Al–Si-rich particles through a heterogeneous pattern;[88] S can homogeneously participate in forming $CaSO_4$ particles in sintering stage-1 and stage-2; Pb, K, Na and Cl would homogeneously participate in the formation of hybrid $PbCl_2$– KCl, KCl and NaCl particles only in stage-2.[88] Increasing recycled materials from the steel industry (such as flue dust or ESP dust) can drastically increase the PM (Figure 2.48a) and the structure of granules, the finer particles distribute on the surface of granules which can escape from granules to flue gas. An additional source of PM is the transformation of trace elements from recycling materials (Figure 2.48b) and the particles formed from the volatile-condensation process of K, Na and Pb typically have a diameter of less than 2.5µm. Hence, increased volatile elements have a considerable influence on the emission of $PM_{2.5}$ while influencing the formation of particles.[82]
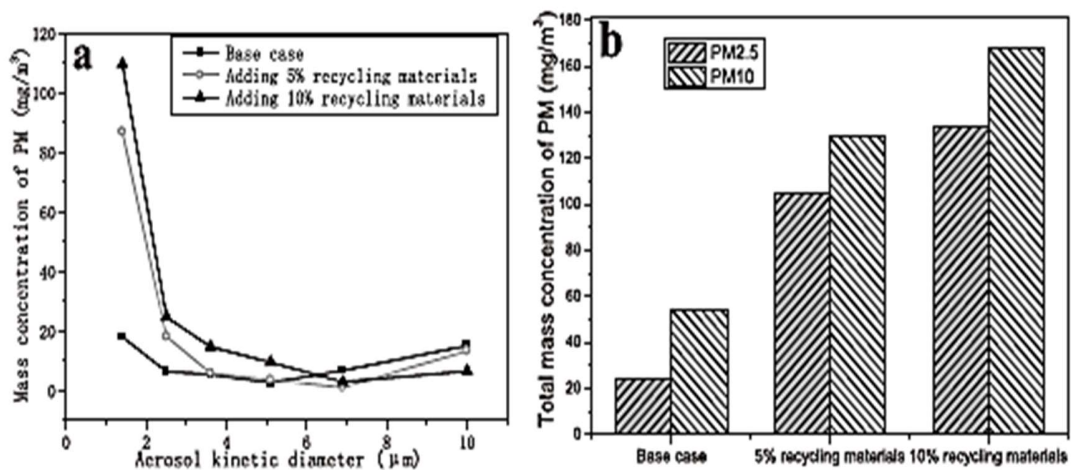
Figure 2.48 - Influences of adding recycling materials on the emission property of PM10/2.5. (a) Influences on emission concentration of PM emissions with different diameters; (b) Influences on total emission concentration of PM emissions[82]

Lanzerstorfer *et al* and Harp *et al* researched recycled materials such as mill scale and BF flue dust and found it has a positive impact on sinter quality, strength and grain size distribution and returns fines, but these effects differ on a variety of influences which shows the complexity of the process.[17][89] Limitations for utilisation of recycled materials in sinter plants were often due to high emissions, which can be overcome by highly efficient waste gas cleaning systems.[89] Therefore the apparent next step would be to measure emissions when experimenting with ESP dust, millscale and BF flue dust. Removal properties of hazardous elements during sintering were clarified by a novel approach developed by Gan *et al* regulating its distribution with different layers and PM$_{2.5}$.[17] Figure 2.49 displays the distributions of recycled materials in the sinter bed. (a) uniformly distributed in the sinter bed; (b) disturbed in the top layer; (c) distributed in the middle layer; (d) distributed in the bottom layer; (e) disturbed in the bottom layer with higher contents of coke breeze. Separate layers revealed that distributing recycled materials in the bottom layer with higher contents of CaO and coke breeze enhanced the removal rates of hazardous elements with PM$_{2.5}$ released into flue gas during temperature rising.[90]
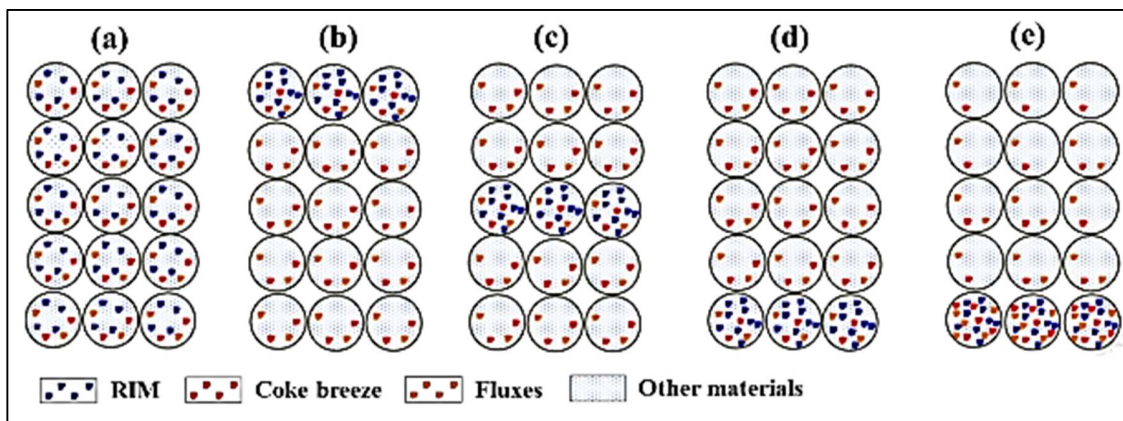
Figure 2.49 – Distribution of recycled materials in the sinter bed[90]

2.9.4   *Additives*

A polymer agglomerate solution can be adsorbed and polymerized with flue gas fine particles to produce flocculated aggregates, which are easily trapped by subsequent

electrostatic precipitators. Thus, the effective emission reduction of PM_{10} and $PM_{2.5}$ in sintering flue gas can be realised (Figure 2.50). Spraying polymer organic binder solution on the surface of granules helps to improve the absorption efficiency of the wet mixture layer to PM_{10} and $PM_{2.5}$ (Figure 2.51).[80]

particulate matter　　Agglomeration agent　　aggregate
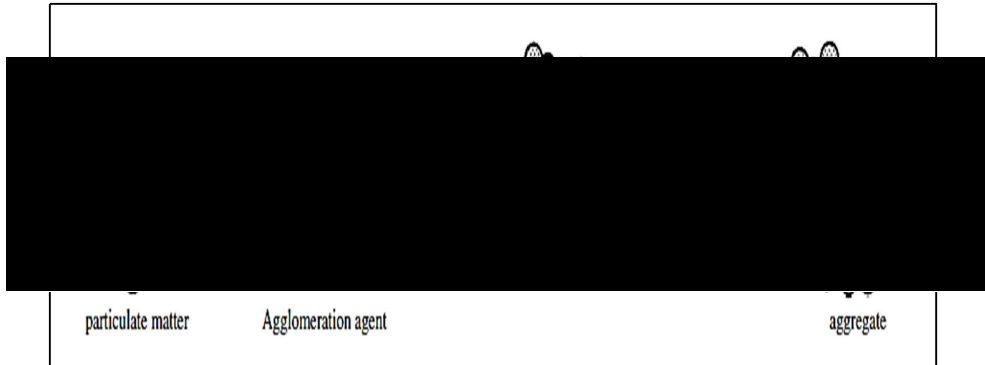
Figure 2.50 - Schematic diagram of polymer agglomeration agent solution agglomerated PM
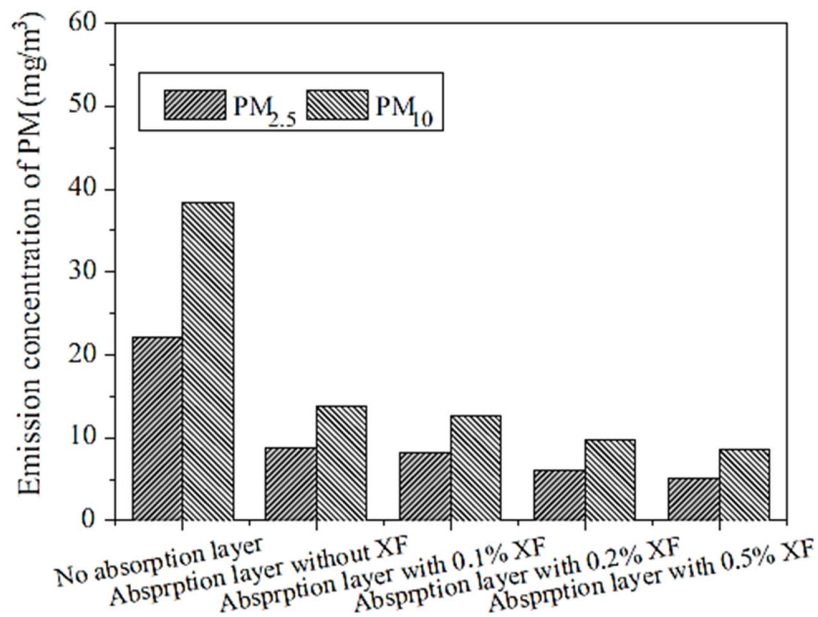
Figure 2.51 - Influences of organic binder solution concentration on the emission of PM[80]

Summary

Most of the recent literature focuses on the formation, morphology, and characterisation of PM emissions from the iron ore sintering process. It is evident that enhancing the major detachment forces required, lowering undesirable volatile materials, and improving the wet layer and combustion zone all play crucial roles in minimising PM emissions. This

literature reviews show that it is possible to develop novel methods for minimising PM emissions during iron ore sintering operations and to drive scientific improvement including the sintering efficiency and by looking into how to use raw materials most effectively, including recycled materials to create a circular economy, and optimising processing without degrading or compromising sinter quality at the sinter plant.

3   Materials and Methods

This chapter covers the materials and samples that were used throughout the project including the chemical composition, processing, and handling. In addition, an overview of the experimental methodologies and analysis techniques that were utilised throughout is also provided here.

3.1   Raw Materials

The iron ores listed were used as high-iron content raw materials in the pilot-scale sinter rig blend throughout the experiments (Table 21). Other raw materials used in the sinter rig blend included sinter fines, fuel, (coke breeze) and fluxes (limestone and magstone), which are high in carbon and calcium, respectively. The recycled materials (BOS slurry and ESP flue dust) were produced at the steel works on-site (Table 22) from their corresponding processes. These blends included materials that are reused as much as possible during the process to promote a circular economy within the steel industry and remove the expense associated with landfilling these materials, which is a key performance indicator for steelmaking driven by environmental and economical demand.

Table 21 - Chemical composition of iron ores

Component (mass %)	iron ore A	iron ore B	iron ore C	iron ore D	iron ore E	iron ore F	iron ore G
*TFE	62.37	65.58	65.38	61.28	66.56	63.53	63.22
CaO	0.01	0.44	0.12	0.01	1.08	0.06	0.13
SiO_2	7.66	4.34	2.37	6.76	3.21	5.62	6.51
MgO	0.015	0.42	0.12	0.02	0.02	.17	0.06
Al_2O_3	0.67	0.03	0.23	1.99	0.89	0.56	1.51
P	0.035	0.007	0.00	0.094	0.049	0.012	0.06
Mn	0.14	0.14	1.87	0.106	0.09	0.07	0.28
S	0.006	0.004	0	0.025	0.02	0.004	0.01
FeO	0.7	12.76	0.96	3.2	37.58	0.30	1.72
Na_2O	0.001	0.016	0.028	0.01	0.04	0.012	0.001
K_2O	0.007	0.01	0.032	0.01	0.03	0.019	0.009
Zn	0.001	0.004	0.005	0.002	0.01	0.005	0.003
TiO_2	0.08	0.04	0.01	0.044	0.07	0.05	0.08
LOI	1.75	0.38	0.22	3.18	0.71	4.22	2.86
H_2O	6.29	3.22	3.5	9.3	5	7.23	10.1

[a]TFe: Total iron content; [b]LOI: loss on ignition at 950°C in air

Table 22 - Chemical composition of fluxes, coke breeze and other

	Sinter Fines	Limestone	Magstone	Coke Breeze	BOS Slurry	Flue Dust	Si Addition (Gilfach)
*TFE	55.56	0	0	0	56.39	5.93	3.62
CaO	10.14	54.13	30.36	0.92	8.9	1.48	0.31
SiO_2	5.86	1.15	2.07	5.66	1.7	3.77	80.25
MgO	2.36	1.65	18.52	0.25	0.97	0.48	0.55
Al_2O_3	1.26	0.12	0.62	2.94	0.19	2.49	8.80
P	0.055	0	0	0.090	0.043	0.02	0.03
Mn	0.24	0	0	0	0.44	0.04	0.06
S	0.003	0.002	0.004	0.71	0.002	0.418	0.00
FeO	9.16	0	0	0	57.43	4.08	1.05
Na_2O	0.060	0.003	0.052	0.070	0.268	0.078	0.330
K_2O	0.065	0.013	0.111	0.164	0.128	0.257	1.510
Zn	0.026	0.003	0.002	0.004	0.8	0.187	0.001
TiO_2	0.126	0	0	0.164	0.08	0.13	0.44
LOI	0	43.55	45.11	85.85	2	43.55	2.77
H_2O	1.42	1.29	4.48	16.31	19.	1.29	6

For processing all the raw materials 'BS EN 932-1: 1997 tests for general properties of aggregates' were followed for all tests and a 500g scoop was used. Scooping was performed from the surface of each layer of the stockpile of the desired raw material, making sure to provide equal space between sample sites. From the top third of the pile, one scoop was collected. Around the middle part of the pile, two equal-sized scoops were taken. Five scoops were finally collected from the stockpile's bottom third. All materials were oven dried for at least 24 hours at 105 °C before the screening. Ores and fluxes were sieved to < 5 mm and fuel to < 3.15 mm and were subjected to chemical analysis via x-ray fluorescence (XRF) and inductively coupled plasma (ICP) before facilitating the blend model to maintain sinter quality levels in all blends. Minebea Intec Signum 1 scales were used to weigh raw materials to masses specified in the blend model. Each blend was mixed using an Altrad Belle Maxi 140 cement mixer for 2 minutes, and the moisture content of mixed blends was recorded using a Mettler Toledo HB43 Halogen Moisture Analyser. The moisture content was considered when granulating with the Gladstone Engineering G94 Special Granulator, to ensure all blends had the same moisture content. After 5 minutes of granulation, the granulated sample was split using a Gilson SP-1 Universal Splitter riffle box to obtain two equal samples for testing.

3.2   The Pilot-scale Sinter Rig

All experimental studies were carried out using the following method. To simulate a full-scale sintering process, a pilot-scale sinter rig was developed with a raw sinter mix capacity of 7.0 kg, a bed diameter of 100mm and a height of 150mm as displayed in Figure 3.1.[84] The sintering mixture is charged into the pilot-scale sinter rig and ignited by an ignition burner above the bed and the hood supplying simulated flue gas was lowered simultaneously after the two-minute ignition. A suction fan is used to draw the flue gas through the sinter as the flame front is propagated simultaneously where emissions was entered into the waste gas stream (Figure 3.2). When the temperature of the exhaust gas reaches the set temperature, the hood is moved aside, and fresh air is drawn through the bed. The remaining sintering and cooling process is completed with fresh air. Typically, the sintering time for each rig test is about 35 min.[91] 400 g of hearth layer is added to the base of the pilot-scale sinter rig, to avoid the granulated blend fusing to the base rate during sintering. The granulated blend is carefully added to the pilot-scale sinter rig chamber, rotating the direction of charging by 90° each time to avoid preferential consolidation. A cold permeability test is run using a VP FlowScope flowmeter at ~ 100 mbar pressure. The top of the granulated blend is ignited at approximately 1300 °C for 1 minute, after this flowmeter is restored to monitor airflow during sintering. Temperatures during sintering were recorded from 5 thermocouples which were supplied by TC Ltd. Once all temperatures were recorded as < 100 °C, the finished sinter can be discharged from the rig. The process is monitored via a computer panel and the data are recorded in five-second intervals. After discharge of the pilot-scale sinter rig, the sinter cake is subjected to the desired post-analysis testing. The laboratory configuration and equipment can be seen in detail in Tariq Al-Haji *et al.*[92]
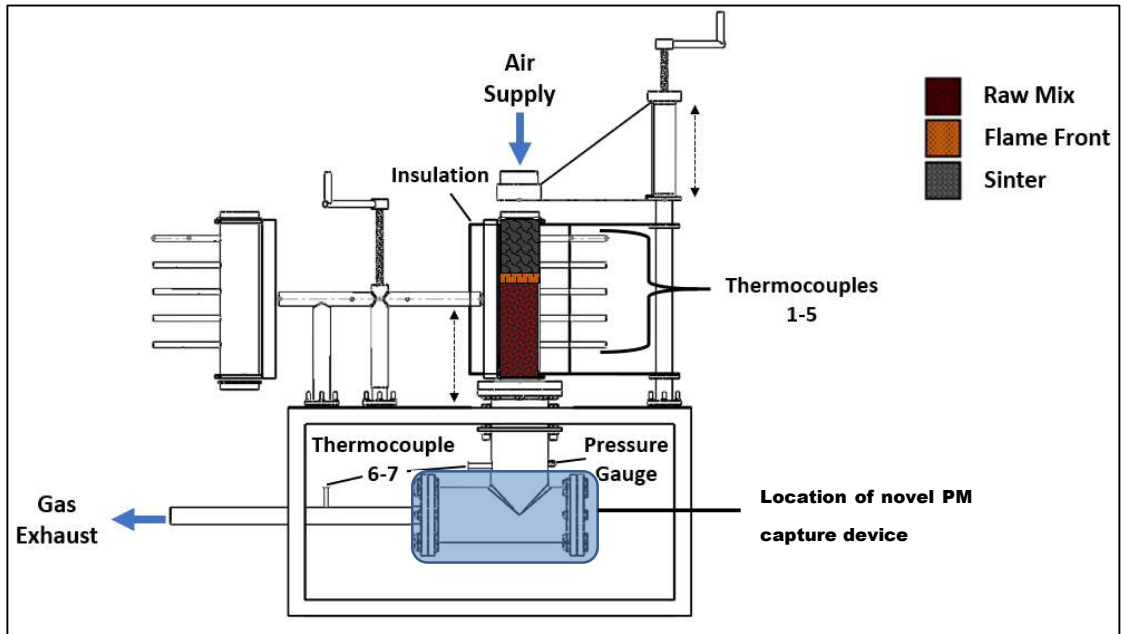
Figure 3.1 – Schematic of the pilots-cale sinter rig
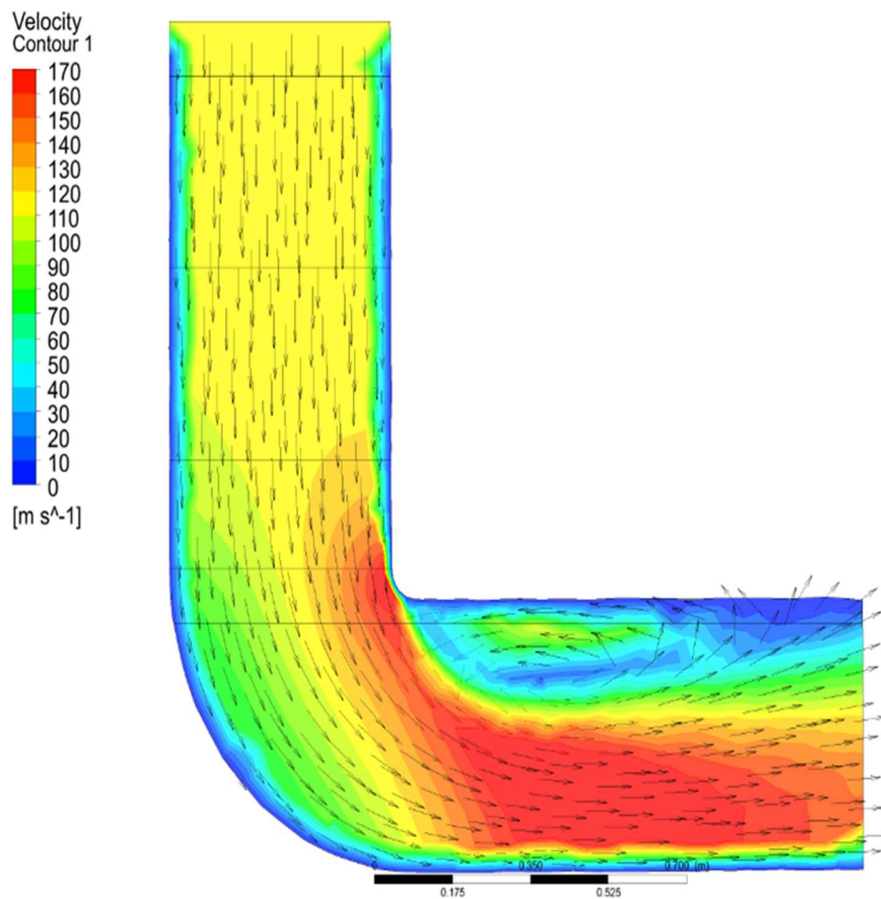
Figure 3.2 – Velocity of the gas stream inside a pilot-scale sinter rig[93]

A formula sheet has been implanted when using the pilot-scale sinter rig :

- Sintering time: the time taken from the 1st thermocouple reaches 40 °C until the maximum off-gas thermocouple is reached
- Cold flow - measurements were recorded five minutes before ignition when the appropriate pressure drop is obtained
- Hot flow - measurements were recorded from the point at which the maximum value of thermocouple 2 is reached until the maximum value of thermocouple 4 is reached
- Sintered airflow - measurements recorded and averaged throughout a 5-minute burn
- Flame front speed - calculated by the time taken for each thermocouple to reach peak temperature between each thermocouple concerning time and distance
- Flame front thickness - calculated using an established flame at 1100 °C and the midpoint of the flame front concerning time and distance
- Cooling rate - measured from the maximum sintering temperature to 600 °C

Every sinter rig test for all the experiments and all post-analysis performed had a repeat. In addition, the base blend for each experiment had four repeats which were used to calculate the standard error for each test and post-analysis completed. All samples were stored in Fisherbrand Acrylic Desiccator Cabinets which were dust and moisture-free storage and hold solid desiccant.

The current setup of the pilot-scale sinter rig has no PM emissions monitoring system therefore different techniques were evaluated. Two known existing test techniques are typically used for monitoring PM emissions, and these are shown below:

1. Light scattering analyser - an in-situ light scattering system can be configured to classify particulate numbers into size ranges. Gives a measure of particulate concentration but after calibration with the SRM
2. Particle impactor - batch results (no live data) and can measure particle size on different filters but must be external and the device needs to be heated (above dew point)

The evaluation of each test method was analysed against the feasibility of representative sampling, ease of collection and cost. A light scattering instrument was not a feasible option due to the diameter of the ducting being less than 4" and the smallest instrument probe possible being 6". Most of the previous research by Lanzerstorfer *et al*, Ji *et al*, and Gan *et al*, as previously discussed in the literature review used the particle impactor but this was not financially feasible.[17][77][90] A new approach was considered, that satisfied the project objectives of capturing PM emissions and return fines and thus an in-situ filter and tray-capturing device was designed.

The design specifications included a typical working temperature between 300-550 °C and working pressure between 70-130 mbar and situated in an area above the dew point (100 °C) to avoid potential condensation issues. The filter type selected was a glass fibre filter (GF/A), weight 85 g/m², thickness 0.43 mm, particle retention 99.998 %, with a maximum of temperature 550 °C. The pilot-scale sinter rig was modified to include the emission collection system designed in the off-gas pipe as shown in (Figure 3.3). Whatman® 110mm [Ø] borosilicate glass filters were specifically selected to collect the emitted PM emissions between each test. The filter can collect particles down to 1.6µm, which meant that alkali chloride fume would also be collected and return fine particulates were collected from the tray at the bottom of the wind box, which retained the deposited dust particles.
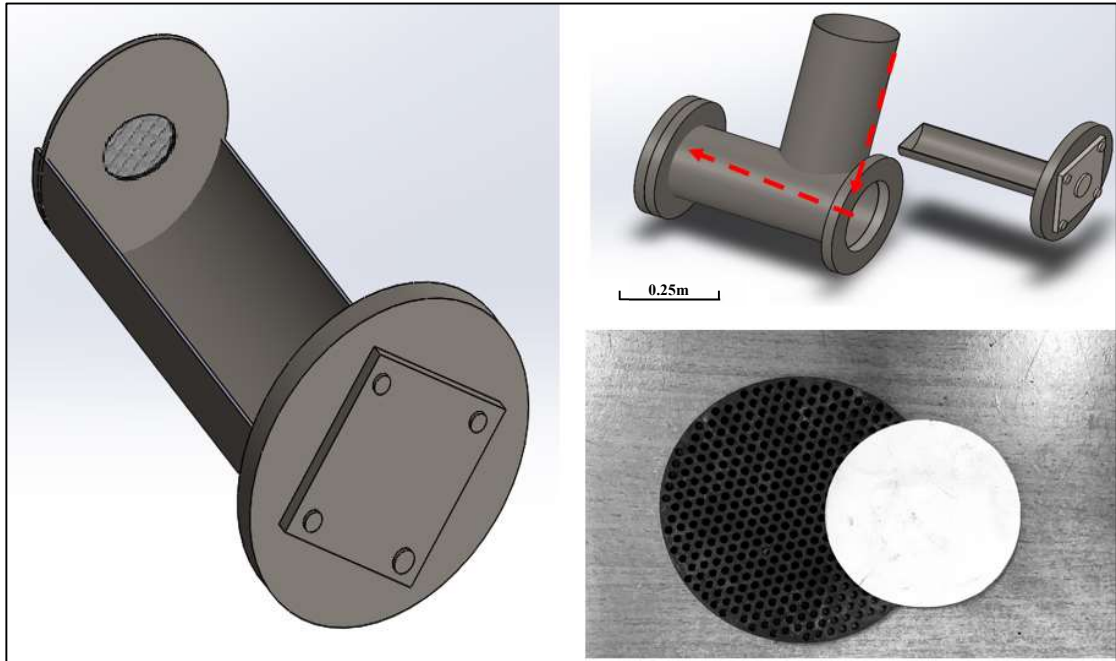
Figure 3.3 – Design of novel PM emissions capture device and modification of a pilot-scale sinter rig

Following BSEN 13284:2002 for measuring PM emissions by using Whatman® 110 mm [Ø] borosilicate glass filters. Pre-sampling conditions include drying the filter in an oven for at least 1 hour, at a minimum of 180 °C and cooling in a desiccator for at least 4 hours to reach ambient temperature. Post-sampling conditions include drying the filter in an oven for at least 1 hour at 160 °C and afterwards will be equilibrated as previously mentioned. Before each weighing series, the balance is checked against the standard weight of 20 mg (within ±0.2). The mass concentration of PM emissions was calculated by Equation 13.

Equation 13 – Mass concentration of PM emissions

$$Cp = \frac{mt - mo}{Qt}$$

Where Cp is the mass concentration of PM, mg/m^3; mt is the mass of the fibre filter after sampling, in mg; m0 is the mass of the fibre filter before sampling in, mg; Qt is the total volume of flue gas during the whole sampling process, in m^3.

The commissioning includes numerous risk analyses and a safe working procedure (SWP) for using the pilot-scale sinter rig (Appendix 1) and how to use the novel dust capture device (Appendix 2).

3.3 Post Analysis Techniques

After completion of the pilot-scale sinter experiments, the sintered product was screened to determine the sinter yield and various size fractions for the sinter cake product and the cold strength. The sintered product from 16-20mm was subjected to reduction degradation index testing which is a standard and established technique which is used to understand how it would react and reduce in a blast furnace environment and chemical analysis (XRF and ICP) was conducted to determine the chemical composition. To determine if the PM emissions on the filter would be harmful to the effectiveness of the abatement, the emissions were submitted to a chloride and sulphate analysis by inductively coupled plasma-optical emission spectroscopy (ICP-OES).

To understand the chemical composition produced by the return fines particulates collected on the dust tray submitted to particle size distribution analysis, XRF and ICP, Scanning Electron Microscopy with Energy Dispersive Spectroscopy (SEM-EDS) and X-Ray Photoelectron Spectroscopy (XPS). Each blend performed post-analysis tests to identify any relationships between the sintering process, the sintered product (quality), and PM emissions. Figure 3.4 shows the hierarchy of order that is followed to ensure continuity for each experiment from start to finish of the thesis. This includes starting from pre-processing of raw materials, process parameters, quality testing, post-analysis of the sintered product and emission collection to ensure all experiments were treated equally.
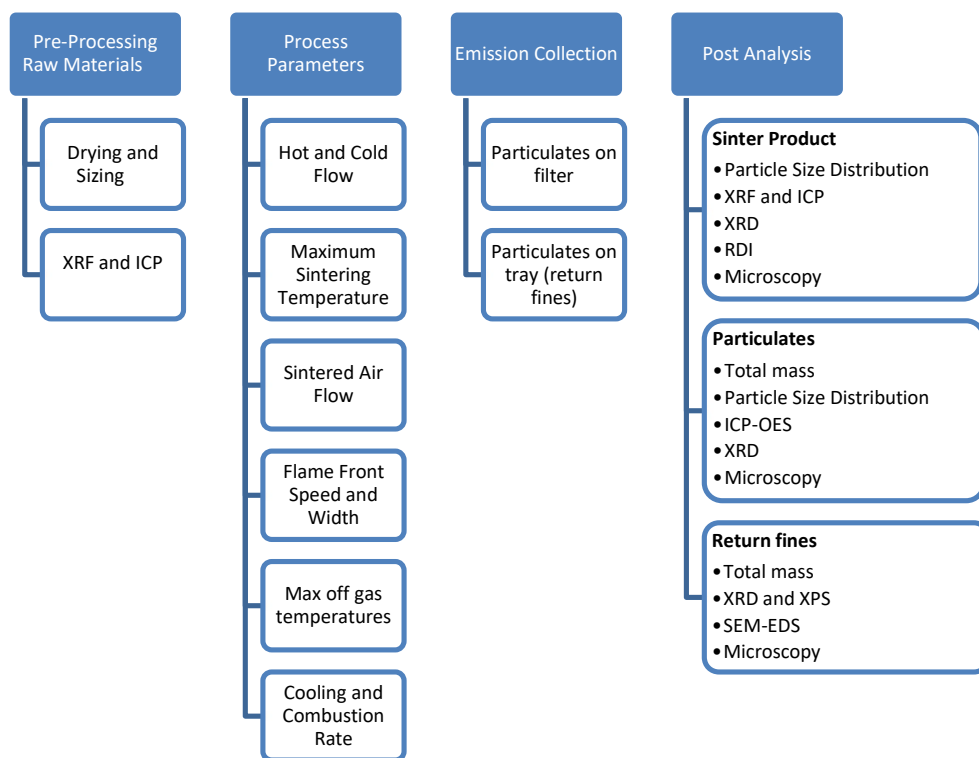
Figure 3.4 – Flow chart of order from start to finish for each experiment

It was determined that post-analysis was important to determine the impact of each experiment and to help understand and characterise the raw materials, sintered product, PM emissions and deposited particulates. All post-analysis was kept the same for each experiment for every sample. The order presented is in order of the post-analysis testing procedure that was followed. All the techniques were applied to every experiment, but only key findings have been shown.

Thermogravimetric Analysis

Thermogravimetric analysis (TGA) was carried out using a SETARAM Labsys EVO instrument. The specimen of raw materials was analysed in the air at 5 °C increments per minute up to 1000 °C, and the mass of the sample was recorded over time as the temperature varies. This measurement gives insight into chemical reactions including thermal breakdown and solid-gas reactions. These include phase transitions, absorption, adsorption, desorption, oxidation and/or reduction and are measured by DT (differential thermal) and DTG (derivative thermogravimetric) which is a useful technique for understanding how raw materials react before use.

Total Moisture Determination of Raw Materials

A portion of crushed, homogenous material was weighed before being air dried in an oven at 1050 °C GallenKamp oven until a constant mass is recorded as a minimum overnight. The moisture was calculated from the loss in mass using a Minebea Intec Signum 1 scale following Equation 14 this enabled a constant sinter blend for more accurate results.

Equation 14 – Total moisture of raw materials

$$\% \, Moisture = \frac{Loss \, wt}{Net \, wt} \times 100$$

Determination of Particle Size Distribution

Between a set of tests and a yield indication, the determination of PSD provides a qualitative cold strength of the sintered product produced. The required round sieves (smaller) sizes were assembled in a stack with a receiver at the bottom, and the stack was placed on a Pascal sieve shaker for ten minutes. By measuring the contents of each test sieve separately on a calibrated Soenle Top Pan Balance, weights can be recorded. The required square test sieves (bigger) size was assembled in a stack with a receiver at the bottom, and the stack was placed on a Siebtechnik sieve shaker for 10 minutes. Using a calibrated Minebea Intec Signum 1 scale, weigh the contents of each test sieve independently to record weights.

Determination of Heavy Metals

The ICP-OES Agilent 5110 was used to determine the metal concentrations in liquid samples designed to ascertain Cu, Na, K, and Zn which are the hazardous elements used in the sinter blends. These are volatile and semi-volatile substances that can persist as gases or concentrate in smaller particles, making it challenging to eliminate them using standard methods for reducing PM emissions. A sample of 0.5 g was dissolved in an acid mixture on a hotplate. The solution is diluted to a fixed volume and the concentration of sodium and potassium is determined by Atomic Absorption Spectrometry and ICP analysis.

Determination of Elements

Axios X-ray fluorescence (XRF) was utilised and is the emission of characteristic "secondary" (or fluorescent) X-rays from a material that has been excited by high-energy X-rays or gamma rays. For chemical and elemental analysis, before being converted into glass beads suitable for analysis using a 0.6 g to 6 g of flux ratio, samples were crushed and dried which was used on raw materials and the sintered product to understand element composition.

Determination of Chlorides and Sulphates

The Metrochm ICP– MS (Inductively coupled plasma mass spectrometry) was used to measure chlorides and sulphates. A nebuliser creates a fine mist from prepared solutions, which is driven into the ICP's plasma flame. The spectrometer receives and records the light emissions produced by the various elements present in the solutions and was a chosen technique to understand how chloride quantities impact PM emissions.

Quantification of Powder Diffraction

Powder characterisation is needed to understand in more detail what phases were present which will provide a clear conclusion with the experiments' Bruker D8 Discover with a copper source (1.54), between 20-80 coupled 2Theta in Bragg/Brantano set-up with a step size of 0.035 is an advanced X-ray Diffraction (XRD) system for powder applications in the industrial process which was used in these experiments. Additionally, in sinter plants or during the direct reduction of iron, mineralogical phase characterisation by XRD was used to establish crucial process parameters. These criteria include basicity, total iron, metallic iron, and FeO concentration, among others.

Determination of Carbon and Sulphur Using Combustion Analysis

Using the Eltra CS500 which is a combustion technique, the samples were combusted in an oxygen environment to oxidise carbon to carbon dioxide and sulphur to sulphur dioxide. After removing moisture and dust, an infrared detector measures the gases such as carbon dioxide and sulphur dioxide and this was to ensure that the sinter blend which was produced was consistent throughout.

Calculation of Basicity, B3 and Glass ratio

After quantifying the XRF results for each test, Equation 15 displays the equations for calculating the requirement of flux to the blast furnace and serves as one of the levers used to adjust FeO and ISO/RDI. Equation 16 also displays the equation for calculating the customer requirement to flux the blast furnace and this is important due to the promotion of fluidity and to remove the impurities in the form of slag. The sinter plant does not typically control B3, which is a unique way to measure basicity $(MgO + CaO)/(SiO_2)$, but it can be used as a good indicator for the blast furnace. Equation 17 shows how much of the matrix is made up of glassy phases made of silica, which means the sintered product is typically more brittle which has a determinate impact on the blast furnace. These 3 equations are unitless.

Equation 15 - Basicity

$$Basicity = \frac{CaO}{SiO_2}$$

Equation 16 – B3

$$B3 = \frac{MgO + TiO_2}{SiO_2}$$

Equation 17 – Glass ratio

$$Glass\ Ratio = \frac{SiO_2}{SiO_2 + Al_2O_3 + CaO + MgO}$$

Determination Of Low-Temperature Reduction Disintegration Indices

The reduction disintegration indices (RDI) as previously mentioned in the literature review, were analysed using an RB Automazione Control Panel, Reactivity Furnace, and RB Tumbler (TB 3000). The analysis complies with ISO 4696-2:2015 - Iron ores for blast furnace feedstocks. RDI specifies a method to provide a relative measure for evaluating the level of size degradation of iron ores when reduced with carbon monoxide and nitrogen, under circumstances like those present in the low-temperature reduction zone of a blast furnace. Also, the analysis complies with ISO 7215:2015 - Iron ores for blast furnace feedstocks to calculate the RDR index using a 500 g sample, which involves isothermally reducing a test piece in a fixed bed at 900 °C for 180 minutes using a reducing

gas made of carbon monoxide and nitrogen. The degree of reduction is calculated from the oxygen mass loss after 180 min.

Particle Mapping

Specimens were examined using a scanning electron microscope (SEM), a Zeiss Evo LS25. P pin stubs with carbon stickies attached were carefully pressed after mixing the sample on a petri dish for a representative sample. The carbon stickies were placed into a sample holder and removed any loose particles by compressed air. The Everhart-Thornley Secondary Electron Detector (SE) and HD Backscattered Electron Detector (BDS) guns were used to capture micrographs of the dust. Energy Dispersive Spectroscopy (EDS) was used to provide chemical compositional maps of the samples.

Determining Average Particle Size

The average particulate size of each dust sample was determined by ImageJ analysis of SEM images; a Java-based image processing application. This was accomplished by obtaining the perimeter of each particle by highlighting each visual particulate. Dividing the perimeter by π gives an approximate value for the diameter, and from this, the PM emissions can be categorised.

Hot and Cold Mounting with Polishing

Cold mounting was conducted by placing the specimen in a 40mm mounting cup. In a disposable paper cup, the resin and hardener were combined in a 7:1 ratio and stirred with a wooden stirrer. The paper cup was placed for two minutes inside a glass vacuum chamber to degas, preventing frothing. In the glass vacuum chamber for two minutes, the mixture was poured over the specimen in the 40 mm mounting cup. The final micro is removed from the mounting cup after curing overnight. Hot mounting was placed with the specimen in the Citopress and Prontopress ram chamber with its face down. On top of the sample in the ram chamber, pour the necessary amount of resin. Struers polishing equipment was used for each specimen and silicon carbide 120 grit (coarse) and 800 grit (fine) grinding pads were used. Water phase diamond suspension solutions with 6 microns and 1-micron particle sizes were used for polishing. The possibility of scratching and other unwelcome sample preparation artefacts, which would compromise final image quality,

is reduced by washing with soapy water and industrial methylated spirits and drying with compressed air in between phases.

Microscopy

Leica DM4M microscope was used for higher magnification images and the microscope automatically recognises the selected contrast technique and objective in use, accurately opens and closes the aperture and field diaphragms, and adapts the light intensity. For lower magnification images a wireless digital microscope, YINAMA Handheld Microscope Camera was used. For all microscopes including SEM images, three were taken per sample from the centre of the specimen and either side of the centre at 500 microns (x50) and 20 microns (1000x) magnifications.

X-ray Photoelectron Spectroscopy

Axis Supra XPS is a tool for examining the chemistry of a material's surface and employs a conventional concentric hemispherical analyser and is outfitted with monochromated Al, K and achromatic Mg, K, the X-ray source and used a 0.5 g sample. Industrially, this top 10 nm's chemistry is essential for a quantitative understanding of processes like cleaning, wetting, adhesion, and curing, or monitoring failure brought on by surface degradation.

ZEN Intellesis

ZEN Intellesis software uses machine learning to segment multi-dimensional images, including datasets from three-dimensional (3D models). By learning ZEN Intellesis to segment the images, images that formerly required manual processing can be processed automatically by machine learning. Image learning by artificial intelligence was used following research by *Donskoi et al* as previously mentioned in the literature review to understand particles from emissions.[40]

4   Experimental Studies

4.1   Advanced Analytics of Sinter Plant Operations to Minimise Particulate Emissions

Introduction

Since electrostatic precipitator (ESP) and bag filter abatements are end-of-system approaches, they require additional investment for equipment modification and operation. As a result, reducing the particulate matter (PM) emission from sintering is of utmost importance. Recent research has shown that these approaches were prospective means of realising efficient removal rates.[3] [77] Techniques for controlling operations before or during sintering within the sinter bed, such as choosing appropriate materials and operating conditions, appear to be more competitive. To determine which key levers, have the biggest impact on the rise in PM emissions, this study analyses PM emissions output from the sinter plant with process parameters and raw materials used. When a correlation is established between parameters and output, it will be possible to control or modify input variables to reduce PM emissions. Using the pilot-scale sinter rig to understand the various factors impacting the predicted sinter quality with known sinter plant blends, and processing parameters, it will be possible to relate this information with PM emissions. The main emission sources in a sinter plant are displayed in Table 23.

Table 23 - The main emission sources at the sinter plant[94]

Emission type	Sources	Description
PM	Gases from the wind boxes	Considerable quantities of trapped PM are released into the air via the main stack.
PM	Crushing, raw material handling, belt charging, discharging from the breaker and hot screens	Generation of considerable amounts of PM and where the potential emissions are ducted to a separate dust removal system and discharged through a stack.
PM	Handling and transportation of the raw materials	Discharge of collected dust from the abatement hoppers and of the cooled sinter.
NOx	The nitrogen content of raw materials	Formation of gaseous species and secondary contribution to PM emissions.
SO_2	The sulphur content of raw materials	Formation of gaseous species and secondary contribution to PM emissions.
CO2	Results from the fuel used for the burning process	Contributes from the bonding agent consumption.
CO	Incomplete combustion	Incomplete combustion of carbon content.

To conduct sinter plant data analytics, over 200 data parameters were compiled from 2011 to 2020 from the integrated steelworks internal Pi database (Figure 4.1) The parameters can be categorised and summarised below:

- Production – number of fans, ESP fields, strand speed, production output and continuous emission monitors (CEMS)

- Process – temperatures, suction, and moisture level

- Raw materials – iron ores, fluxes, fuels, and recycled materials used

- Standard reference method (SRM) – PM concentration, flow rate, pressure, and gaseous species

- Chemical composition – Predicted chemistry and actual chemical composition

- Post-analysis sizing – ranging from +6.3mm to -0.25mm

Process Information (40 data tags over 9 years)
- Fan information, ESP fields, temperatures, strand data, production output and continuous emission monitors (CEMs).

Sampling Data (114 days with 14 parameters)
- PM concentration, velocity, flowrate, pressure and numerous gaseous concentrations.

Raw Materials (168 parameters)
- Predicted chemistry composition, screen sizing's, and the raw materials including amount of reverts used

Figure 4.1– Data collection of historical infromation from the sinter plant which includes process information, sampling data and raw materials

Isokinetic Sampling

Each data parameter was compared to PM emissions results which were taken by SRM at the sinter plant main stack. The SRM followed the standard ISO:13284S stationary source emissions – Determination of low-range mass concentration of dust. This included the importance of sampling isokinetically and how to calculate each PM result. Concentration measurements are reported to a standard set of conditions, and this enables the results can be comparable with ELVs and other similar processes. Isokinetic sampling is achieved

when the gas enters the sampling nozzle at the same velocity and direction as the gas travelling in the stack or duct.[95] The principle of isokinetic sampling is that a sharp-edged nozzle is positioned in the stack facing into the moving gas stream and a sample of the gas is extracted through it, at the same velocity as the gas in the stack, for a measured period. To allow for non-uniformity of particulate distribution, samples were taken at a pre-selected number of points across the sample plane of the stack. The PM emissions collected in the sampler are later weighed, which calculates the concentration of particulate. The mass flow rate in the stack can be calculated from the concentration and the velocity of the gas in the stack. Due to the wide range of particle sizes normally present in process emission streams, it is necessary to sample isokinetically to ensure that a representative sample of the PM emissions is obtained. To perform isokinetic sampling, it is necessary to calculate the required sampling flow rate to ensure that the velocity of the gas entering the nozzle is the same as the velocity of the stack gas at the sampling plane (Equation 18). This considers the velocity of the gas in the stack at the sampling point and the effective diameter of the sampling nozzle (Equation 19). It is also possible to check for isokinetic sampling compliance by comparing the required sampling flow rate to the actual sampling flow rate performed during the monitoring (Equation 20).

Equation 18 – Theoretical sampling flow rate

$$Theoretical\ Sampling\ Flow\ Rate$$
$$= Area\ of\ Nozzle\ x\ Velocity\ of\ Gas\ Entering\ Nozzle$$

Equation 19 – Actual sampling flow rate

$$Acutal\ Sampling\ Flow\ Rate = \frac{Volume}{Time}$$

Equation 20 – Isokinetic ratio (%)

$$Isokinetic\ Ratio\ (\%) = \frac{Actual\ Sampling\ Flow\ Rate}{Theoretical\ Samping\ Flow\ Rate} \times 100$$

BS EN 13284-1:2004 stationary source emissions – determination of low-range mass the concentration of dust states that if the mean actual isokinetic ratio during the sampling at the sampling plane differs by more than -5 to +15% the measurement is not valid. If the

sampling velocity is less than the isokinetic rate, at first sight, the emission will be underestimated. However, because the sampling rate is too low, there is a divergence inflow around the sampling inlet. Small particles can follow the flow and a percentage of them will not be sampled. Larger particles, on the other hand, are not able to follow the flow because of their greater inertia and more of these particles will enter the sampler. Consequently, a sub-isokinetic sampling rate will lead to a bias in the sampled particle size distribution towards the larger particles. This would lead to an overestimate of the particulate concentration depending on the original size distribution. The sample line composition is needed to measure PM emissions using the SRM at the sinter plant main stack and is displayed in Figure 4.2 which includes the following:

1. Interchangeable Nozzles
2. S Pitot Tube
3. Filter Holder
4. Probe
5. Locking Device
6. Impingers (Water Condensation)
7. Supporting Box
8. Silica Gel Trap
9. Unbiblical Cord
10. Automatic Isokinetic Sampler – ST5 EVO Dado lab
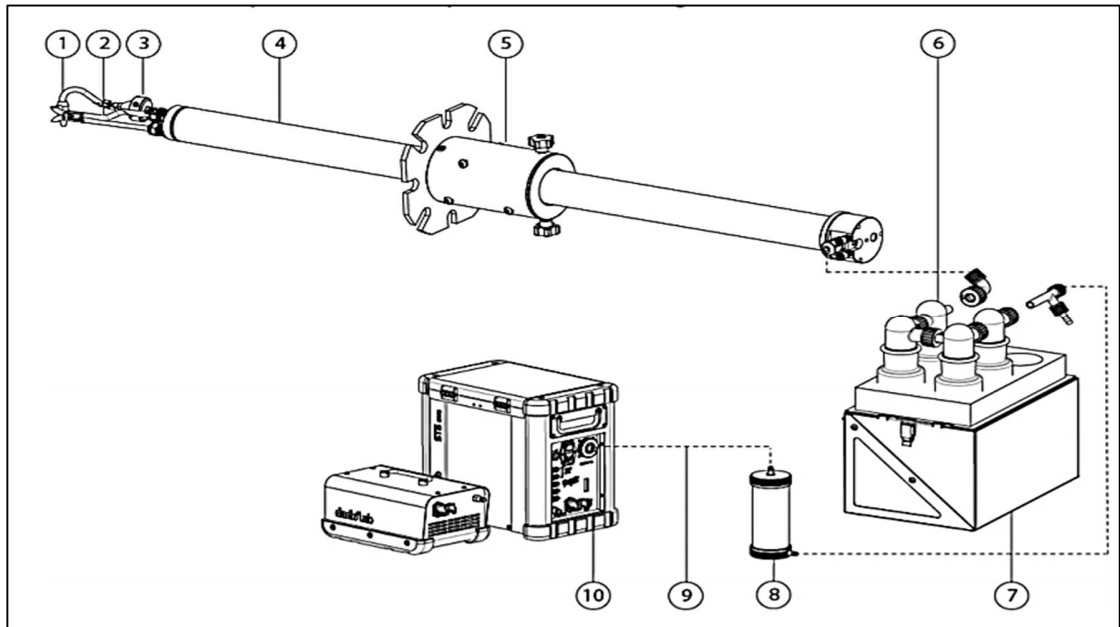
Figure 4.2 – In-stack sampling system 1.Interchangeable Nozzles, 2.S Pitot Tube, 3.Filter Holder, 4.Probe, 5. Locking Device, 6. Impingers (Water Condensation), 7.Supporting Box, 8.Silica Gel Trap, 9.Unbiblical Cord, 10.Automatic Isokinetic Sampler – ST5 EVO Dado lab [96]

The expected particulate concentration and flow characteristics of the stack gas must be known such that an appropriate sample duration and location can be selected. When selecting a sample location, it is important to be aware that the automatic isokinetic sampler requires a set flow rate, which means adjustments to maintain isokinetic conditions during the test is possible. An in-stack sampling system (Figure 4.2) is used to extract the PM from the stack onto a filter. Pitot tubes and thermocouples were used to calculate the pressure and temperature, respectively. Following the BSEN 13284:2004 at low particulate concentrations standard was used the equations below were used:

The example used: Sample 91

Using Equation 14 – Theoretical sampling flow rate

$$\frac{\pi 0.004^2}{4} \times 14.6 = 0.000184 \ m^3/s$$

$$0.000184 \times 1000 \ x \ 60 = 11.04 \ L/min$$

Corrected for H_2O, Temperature and Pressure:

$$11.04 \times \frac{(100\text{-}5) \ x \ 273.15 \ x \ 101.6}{(100\text{-} \ 0) \ x \ 404.9 \ x \ 101.3} = 7.11 \ L/min$$

Using Equation 15 – Actual sampling flow rate

$$\frac{211}{30} = 7.03\ L/min$$

Using Equation 16 - Isokinetic ratio (%)

$$\frac{7.03}{7.11} \times 100 = 99\%$$

The isokinetic ratio is within tolerance (between +115% and -95%)

Isokinetic Calculations

To calculate a concentration, the mass of the substance collected during sampling is divided by the volume of stack gas sampled (Equation 17). To convert a concentration to a mass emission (Equation 18), it is necessary to know the volume flow rate of gas discharged from the stack. However, the volume flow rate and concentration must be at the same reference conditions.

Equation 21 - Concentration

$$Concentraion\ = \frac{Mass\ of\ Substance}{Sample\ Volume}$$

Equation 22 – Mass emission

$$Mass\ Emission = Concentraion \times Volume\ Flow\ Rate$$

Using Equation 21 -

$$\frac{6.6}{211 \times 1000} = 31.3\ mg/Nm^3$$

Corrected back to wet for H_2O as needed to report the result as specified in the permit:

Equation 25 – Moisture correction

$$31.3 \times \frac{(100\text{-}5)}{(100\text{-}0)} = 29.8\ mg/Nm^3$$

Using Equation 22 – Mass emission

$$29.8 \times \frac{1111332}{(1000000)} = 33.1\ Kg/hr$$

Concentration measurements were reported to be 273 Kelvin (K) and 101.3 kilopascals (kPa). Since it is most unlikely that the concentrations will be at these conditions, correction factors Ft and Fp. To convert the concentration as measured at a temperature of T K to the concentration at 273 K, it is required to multiply by Ft (Equation 23). To convert the concentration as measured at a pressure of P kPa to the concentration at 101.3 kPa, multiply by Fp (Equation 24). For concentration measurements, P will be the pressure at the point where the sample volume is metered.

Equation 23 - Normalising with temperature

$$Ft = \frac{T}{273}$$

Equation 24 - Normalising with pressure

$$Fp = \frac{101.3}{P}$$

Emissions of stack gases were often expressed on a dry gas basis as stated in the EPR/BL7108IM - Integrated Iron and Steel Works Permit. To convert a concentration from wet gas to dry gas by Equation 25.

Equation 25 – Moisture correction

$$Dry\ Gas\ Concentration = \frac{Wet\ Gas\ Concentraion}{(100 - H_2O\%)} \times 100$$

Measurement uncertainty quantifies the dispersion around the true value inherent in a measurement result. The uncertainty assigned to a result represents the range of values about the result in which the true value is expected to lie. All measurements have associated uncertainty; the goal was to quantify this uncertainty such that the results could be properly interpreted. Table 24 shows how different quantification types of uncertainties and how they were sourced.[95]

Table 24 - Quantification of different types of uncertainties

Types of Uncertainty	Quantification archived by
Corrected Volume [Nm^3]	UKAS certificate
Gas Temperature [K]	UKAS certificate
Pressure [kPa]	UKAS certificate
Gas Humidity	Dry gas meter = 0
Oxygen Content [%]	Internal repeatability of UKAS certificate gas test
Mass Particulate [mg]	Internal repeatability of filters test on balance

The measurement uncertainty defines the size of the region in which the true value is expected to lie, and the confidence interval defines how likely this is. The list below describes how this is possible:

- Review the measurement method and identify potential sources of uncertainty
- Quantify the significant sources of uncertainty
- Combine the uncertainty components and expand to give the required level of confidence
- Report the measurement uncertainty with the measurement result

The collected mass Qx (Equation 26) is obtained from weighing the filter from the probe before and after sampling and weighing the residue from the probe washings. Four balance readings were involved with uncertainties associated with the calibration of the balance, repeatability of the reading and drift.

Equation 26 – Weighing and volume uncertainty

$$C_x = \frac{Q_x}{Vstd}$$

$$V_{std} = V_{T.p} \times \frac{Tstd}{T} \times \frac{p}{p_{std}}$$

T and p are the actual temperatures and absolute pressure at the gas meter and VT; V is the actual measured volume. T_{std} = 273.1K, p_{std} = 101.3KPa and both were assumed to have negligible uncertainty. T, p_{atm} and VT, p have uncertainties due to the calibration of measuring instruments, repeatability of the readings, the resolution or readability of the device and drift. The final reported concentration needs to be corrected to a reference oxygen concentration (Equation 27).

Equation 27 – Oxygen reference

$$C_{x,O2ref} = C_\% \times \frac{(21 - O_{2ref})}{(21 - O_{2meas})}$$

If calculating the component, standard uncertainties are related to each of the 6 input quantities: u(QX), u(VT,p), u(p_{rel}), u(P_{atm}), u(T) and u(O2$_{meas}$). Calculation of the standard uncertainty of CX by summing the squares of the component uncertainties multiplied in

each case by the sensitivity coefficients. Using the principle that when dealing with products or quotients we sum the fractional (or percentage) quantities and when dealing with the addition we sum the absolute quantities (Equation 28). The addition of the uncertainty is due to the oxygen uncertainty in the correction factor (Equation 29).

Equation 28 - Sum of uncertainties

$$\frac{u^2(C_x)}{C_x^2} = \frac{u^2(Q_x)}{Q_x^2} + \frac{u^2(V_{T.p})}{V_{T.p}^2} + \frac{u^2(T)}{T^2} + \frac{u^2(P_{rel})}{(p_{rel} + p_{atm})^2} + \frac{u^2(p_{atm})}{(p_{rel} + p_{atm})^2}$$

Equation 29 – Combined uncertainty

$$\frac{u^2(C_{x,O2re})}{C_{x,O2ref}^2} = \frac{u^2(C_x)}{C_x^2} + \frac{u^2(O_{2mea})}{(21 - O_{2meas})^2}$$

Uncertainties were calculated with the guidance from the National Physical Laboratory (NPL) which is the UK's National Measurement Institute and is a world-leading centre of excellence in developing and applying the most accurate measurement standards. Table 25 displays the data needed to calculate the uncertainty for the SRM for sample 90. Sample 91 was taken from a sinter main stack in 2021 and examples of the calculations used with this sample are given below.

Table 25 – Uncertainty data from SRM sample 91

ELV (mg/Nm³)	40					
Measured mg/Nm³ STP	31.1652					
Ref O2	17.0					
	Value	**Std U**	**S Factor**	**u (fs)**	**U as %**	**Required**
Corrected Volume [Nm³]	0.249	0.0001	---	---	0.0402	<=2%
Gas Temperature [K]	287.2	2	0.003	0.0067	0.6964	<=1%
Pressure [Kpa]	101.9	0.00029	0.009	0.0000	0.0003	<=1%
Gas Humidity (DGM = 0)	0	0	0.010	0.0000	0.0000	<=1%
Oxygen Content [%]	16.4	0.2	0.189	---	1.2195	<=5%
Mass Particulate [mg]	8.6	0.20	---	---	2.3256	<=5% LV

STP Factor	0.9562	O₂ Correction Factor	0.9
STP Uncertainty (fs)	0.0067	O₂ Factor Uncertainty	0.193237
Volume Uncertainty (fs) [m³]	0.0017	O₂ u	0.038647

	Value	**S Factor**	**U Contribution**	**U as %**

Collected Volume STP [m³]	0.249	125.368	0.21	0.667
Mass Particulate [mg]	8.600	3.624	0.72	2.326
O₂ Correction Factor	0.870	35.840	1.39	4.4
Combined Uncertainty			1.58	mg/m³
As % of a measured value			10.1	%
In units of measurement			3.15	mg/m³
As % of Limit Value			7.9	% ELV

Using Equation 28 - Sum of uncertainties

$$Volume\ u\ Contribution = \frac{Concentration}{Collected\ Volume} \times Volume\ Uncertainty$$

$$\frac{31.1652}{0.249}\ x\ 0.0017 = 0.21$$

$$Mass\ u\ Contribution = \frac{Concentration}{Mass\ Particulate} \times Mass\ Uncertainty$$

$$\frac{31.1652}{8.600}\ x\ 0.2 = 0.72$$

$$O2\ u\ Contribution = \frac{Concentration}{Mass\ Particulate} \times O2\ u$$

$$\frac{31.1652}{0.870}\ x\ 0.038647 = 1.39$$

Using Equation 29 – Combined uncertainty

$$Combined\ Uncertainty = (\sqrt{0.21^2 + 0.72^2 + 1.39^2}) \times 2$$
$$Uncertainty = 3.2\ +/-\ mg/Nm^3$$

The commissioning and validation of the pilot-scale sinter rig and the dust capture device are the main topics of this part, it also included a variety of tests that involved processing a sinter plant blend in the pilot-scale sinter rig and contrasting the quality of the sinter produced and PM emissions with that of the sinter plant. It also includes the experiments that will be performed to examine potential relationships by manipulating one or more independent variables and evaluating their impact on one or more dependent variables. Developing a set of procedures to methodically evaluate a hypothesis is what this experimental design entails. The key design processes involve taking the factors and potential relationships into account. To influence the independent variable, write a precise and testable hypothesis and establish experimental procedures. Choosing a representative

sample and controlling any external variables that can impact the results was essential for drawing a valid conclusion. Planning how to measure the dependent variable is also important.

4.2 Validation of Pilot-Scale Sinter Rig, Novel Capture Device and Utilisation of Sinter Plant Beds

Six pilot-scale sinter rig tests were used to validate the pilot-scale sinter rig and post-analysis (validation 1) along with validation of the dust capture device for repeatability (validation 2). The blend's composition, process parameters and the methods used for analysis remained constant. The raw material contents of the blend stayed the same (Table 26).

Process parameters:

- Fuel rate – 5%
- Moisture content – 8%
- Granulation time – 5 minutes
- Ignition period – 1 minute
- Pressure drops a set point – 100 mbar

Table 26 – Raw material contents of the blend for validation (1) and (2)

Component (mass % dry ore basis)	Base blend 1
ORES	
iron ore B	20.42
iron ore A	8.17
iron ore G	16.34
iron ore E	8.17
iron ore F	28.59
FLUXES, BREEZE and OTHER	
Sinter fines	18
Limestone	11
Magstone	7
Coke breeze	5

A full-scale plant trial at the sinter plant was conducted which included three different sinter plant beds taken from the sinter plant strand over one week, to be used in the experimental pilot-scale sinter rig (validation 3) to compare the pilot-scale sinter rig directly to a sinter plant. Samples were collected before the materials were dropped onto the sinter plant strand, just before ignition. Table 27 and Figure 4.3 shows each sinter plant bed was similar in raw material composition. The primary variations between each sinter plant bed sample were an increase in nucleus particles and a decrease in adhering particles, while the non-adhering remained constant, increasing the nuclei to layer ratio (NTLR) for each sinter plant bed from 1.5, 1.6, and 1.7 NTLR as shown in Figure 4.4 and Figure 4.5. For the full-scale plant trial, the results from the pilot-scale sinter rig were compared to plant data on the sintering process, quality, and continuous emission monitors (CEMs) provided data on the plant's PM emissions for a direct comparison. As this had never been studied before, more research was done with the compilation of pilot-scale sinter rig return fines particulates by chemical analysis at different size fractions to understand what is being continuously returned into the sinter plant system for potential optimisation.

Process parameters:

- Fuel rate – 5%
- Moisture content – 8%
- Granulation time – n/a
- Ignition period – 1 minute
- Pressure drops set point – 130 mbar
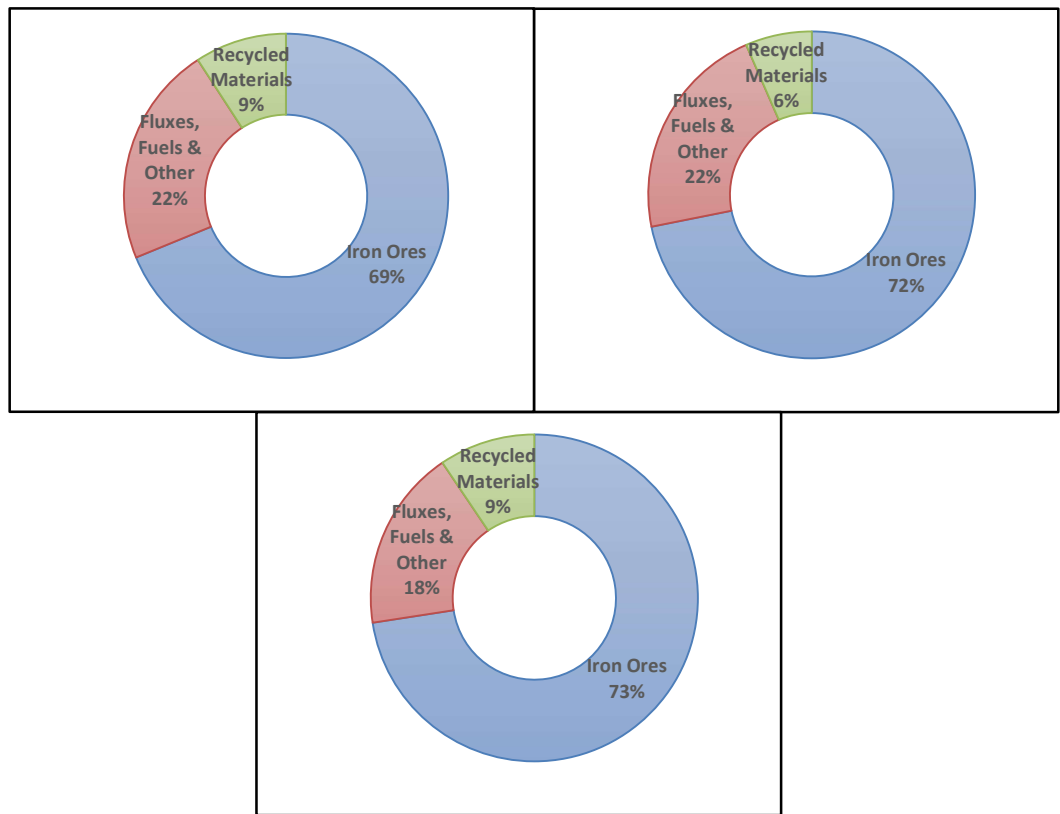
Figure 4.3 – Raw material composition of the sinter plant beds (left to right: beds 1, 2 and 3) for validation (3)
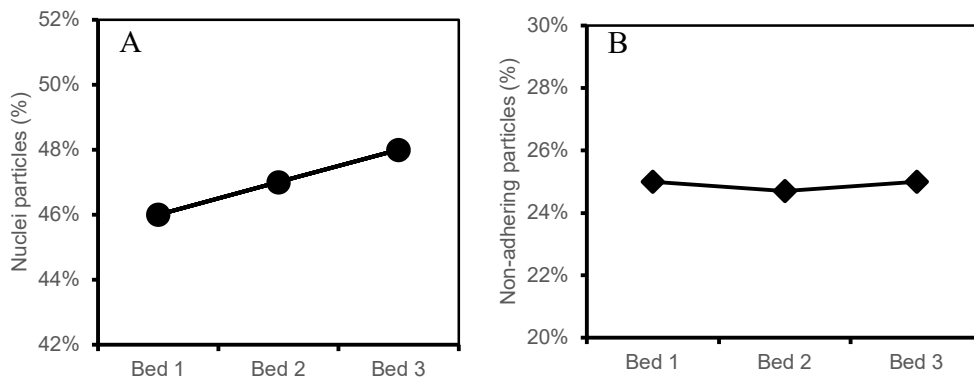
Figure 4.4 – Particle size distribution of the sinter plant beds a) nuclei particles b) non-adhering particles for validation (3)
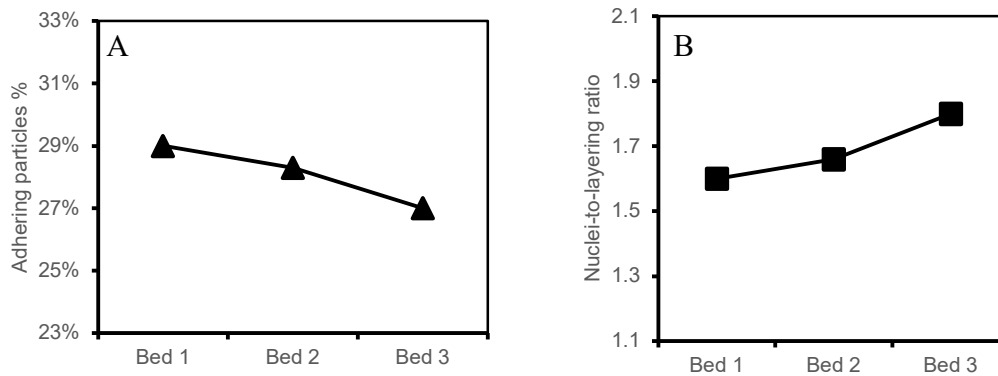
Figure 4.5 - Particle size distribution of the sinter plant beds a) adhering particles (%) b) NTLR of particles for validation (unitless) (3)

Table 27 – Bed component from the sinter plant

Bed Component %	Bed 1	Bed 2	Bed 3
iron ore H	10.0%	10.2%	9.2%
Sinter Fines	10.3%	9.3%	5.5%
iron ore F (Vessel 1)	10.0%	10.3%	12.0%
iron ore D	7.0%	11.2%	7.4%
iron ore F (Vessel 2)	4.0%	0.7%	0.0%
Limestone	5.2%	6.2%	6.3%
Magstone	5.1%	4.7%	4.6%
BOS Plant Scrap	2.1%	1.2%	3.2%
iron ore F (Vessel 3)	1.9%	0.0%	0.0%
iron ore H	10.0%	7.5%	7.4%
Mixed Ore	2.0%	1.9%	2.3%
BOS Grit	0.0%	0.3%	0.3%
BOS Slurry	1.5%	1.0%	1.0%
Flue Dust	0.5%	0.6%	0.7%
Blast Furnace Sludge	0.3%	0.2%	0.2%
Fine Ravelling's	3.0%	2.1%	2.8%
iron ore F (Vessel 4)	6.0%	4.4%	5.5%
iron ore E	6.0%	7.4%	8.8%
Anthracite	0.2%	0.2%	0.2%
iron ore F (Vessel 5)	11.3%	18.0%	19.4%
Screenings	0.5%	0.4%	0.6%
Millscale	1.4%	0.9%	1.0%
Coke Breeze	0.3%	0.3%	0.3%
Anthracite (2)	1.2%	1.3%	1.3%

The hypothesis for the validation is the results will be within the expected variation and will be repeatable due to the chosen technical specifications of the new dust capture device. Validating the expected findings requires repeatability. As a result, it will be possible to produce the same result in an experiment using identical setups, processes, and conditions. For the full-scale plant trial, the hypothesis is that PM emissions will decrease as the NTLR is increasing as the introduction of more nuclei particles and fewer adhering particles was used in the three sinter plant beds.

4.3   Investigation and Optimising the Use of Micropellets in Sintering

Recent studies have shown that effective particle removal rates may be achieved by using physical abatements such as high-quality filter bags and hybrid particulate collectors.[3,4] These require substantial investment and do not directly address the *production* of particulate matter at the source. Through a fundamental approach, it is hypothesised that a reduction in emissions can be achieved through process parameter optimisation, as opposed to the implementation of a physical abatement. As supplies of high-grade lump ores continue to decline, it is becoming more common to use fine iron ore concentrates and micropellets in their place. Pelletisation of by-products during the integrated steelmaking process has been previously explored to improve the cold handling of fine materials. When sintered, the quality of the resultant product is comparable to that of conventional blast furnace sinter.[97] When using the same proportion of fines and micropellets in separate sintering tests, results showed that although both additions decreased bed permeability, the micropellets showed a better permeability response compared to the finer concentrates [98,99]. This experiment aims to explore the use of micropellets during sintering from an environmental perspective for the first time. The use of micropellets thus far has shown to be beneficial from an operational point of view, but their impact on PM emissions is yet to be understood. This study aims to quantify the PM emissions output as a result of micropellets substitution during sintering through laboratory simulation and advanced characterisation while exploring the limitations of use and any effects on the sintering process and the resultant product. Table 28 shows the raw material contents of each blend used in these micropellets experiments.

Process parameters:
- Fuel rate – 7%
- Moisture content – 8%
- Granulation time – 5 minutes
- Ignition period – 1 minute
- Pressure drops set point - 100mbar

Table 28 – Raw material contents of blends for micropellets study

Component (mass % dry ore basis)	Base Blend 7 (0% MP)	Blend 1 (3.63% Initial MP)	Blend 2 (7.27% Initial MP)	Blend 3 (3.63% Recycled MP)	Blend 4 (3.63% Iron ore A MP)	Blend 5 (3.63% Iron ore B MP)
ORES						
Iron ore B	17.2	19.4	18.2	19.4	19.4	19.4
Iron ore A	24.1	24.8	20.4	24.8	24.8	24.8
Iron ore D	17.2	19.4	18.2	19.4	19.4	19.4
Iron ore E	10.3	11.6	10.9	11.6	11.6	11.6
FLUXES, BREEZE and OTHER						
Sinter fines	18.0	18.0	18.0	18.0	18.0	18.0
Limestone	10.7	12.7	11.7	12.7	12.7	12.7
Magstone	7	7	7	7	7	7
Coke breeze	7	7	7	7	7	7

The hypothesis is that mircopelletising will improve the sintering process by increasing the permeability of the bed and thus potentially improving sinter quality. By binding the finer materials as pellets, it can reduce the amount of free finer materials in the sinter bed, making it more difficult for those materials to escape as PM emissions into the exhaust waste gas stream. Additionally, the micropellets may retain unwanted volatile substances rather than releasing them as PM emissions, which would increase the sinter plant's efficiency in the ESP abatement.

All non-pelletised materials used for sintering were pre-dried at 100 °C in a muffle furnace for 24 hours before the screening. The base blend consisted of a 0% micropellets substitution where the ESP dust, flue dust and BOS Slurry were incorporated into the blend, representing a typical sinter plant blend, thus allowing for baseline comparisons to be made. Subsequent blends incorporated the following additions of micropellets; Blend 1 - 3.63%, Blend 2 - 7.27%. Blends 3,4 and 5 consisted of 3.63% micropellets additions that were optimised following the results of the first three experiments. The materials to be pelletised were mixed with a cement-based binder, with the binder making up between 8 – 10 % of the overall content. This mixture was added to a rotating drum for 6 minutes at 12 rpm with 0.5 litres of water to take the shape of micropellets. The pellets were allowed to cure in ambient conditions for 48 hours. The size fraction of the micropellets was at a ratio of 2:1:1 of 5-7mm, 3-5mm, and 1-3mm. Figure 4.6 shows the material content of all the micropellets. The initial micropellets study consisted of 0%, 3.6% and

7.27% of iron ore A but was variable in shape. The initial micropellets of the first batch varied in shape, ranging from spherical to sub-angular as shown in Figure 4.7 and the second batch method is optimised to achieve consistency by using what was learned from the first batch. The 2nd batch of optimised micropellets showed a noticeable improvement in the bigger size fractions. After optimisation of the micro pelletising process to improve the shape, three micropellets types were generated; iron ore A, iron ore B and recycled MP, Micropellets material content highlighted in displays micropellets size fraction (Table 29) and chemical composition (Figure 2.14).
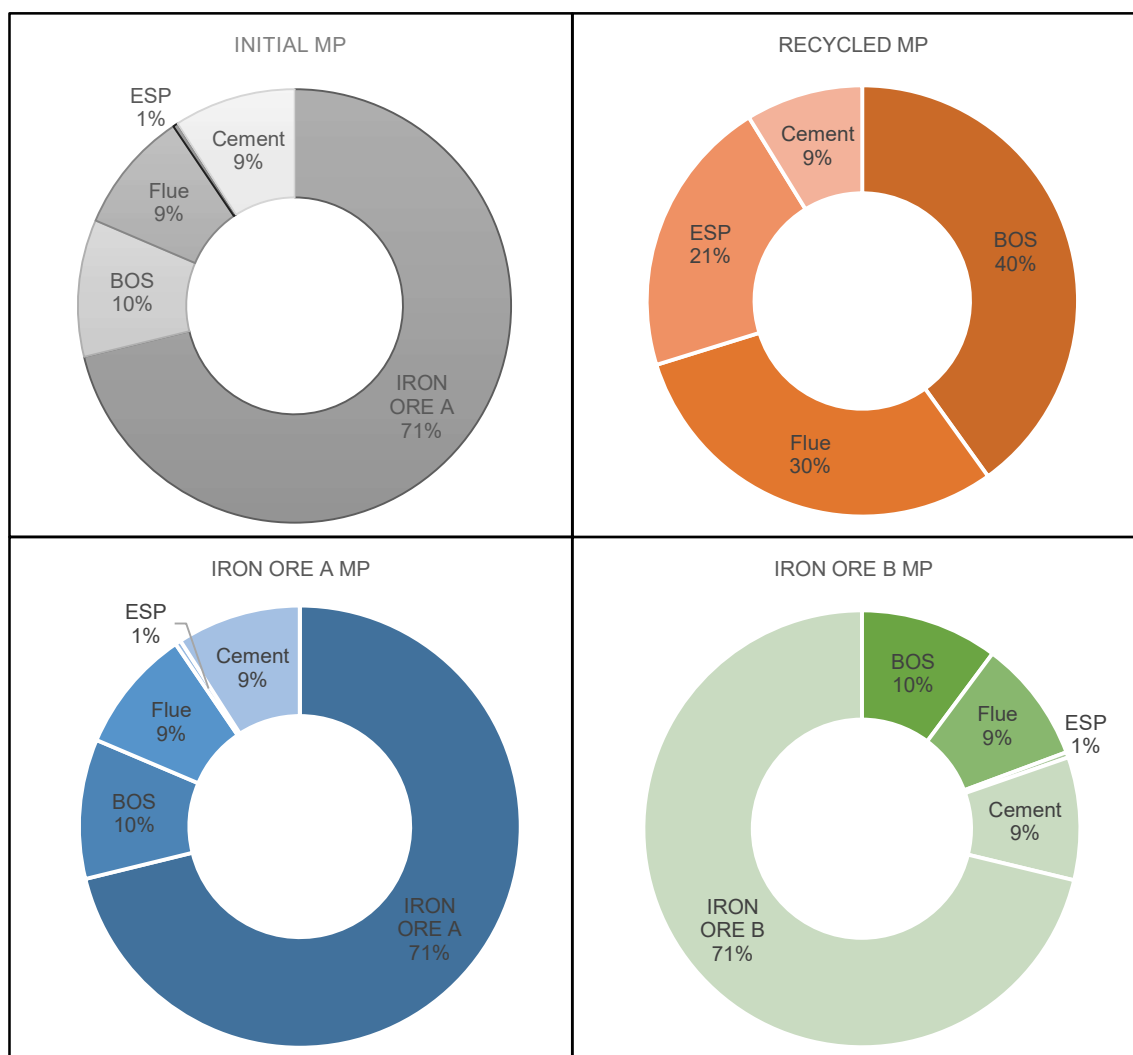
Figure 4.6 – Material content of four different micropellets that were used

Figure 4.7 – a) Initial Micropellets b) Optimised iron ore A, recycled and iron ore B micropellets (left to right)

Table 29 - Size fraction of micropellets

Size fraction (%)	Initial MP	Recycled MP	Iron Ore A MP	Iron Ore B MP
8 – 5 mm	30	51	49	53
5 – 3.35 mm	33	24	23	26
3.35 – 1 mm	37	26	29	22

Table 30 - Chemical composition of micropellets

Chemical Composition %	Initial MP	Recycled MP	Iron Ore A MP	Iron Ore B MP
*TFE	53.36	56.2	54.9	56.94
CaO	4.59	3.51	4.09	6.47
SiO_2	6.37	3.52	5.8	5.71
MgO	0.46	0.55	0.26	0.54
Al_2O_3	1.04	1.14	1.52	0.8
P	0.04	0.018	0.05	0.006
Mn	0.19	0.09	0.09	0.12
FeO	3.98	21.97	4.94	8.79
Na_2O	0.05	0.062	0.019	0.032
K_2O	0.173	0.219	0.057	0.136
Zn	0.009	0.013	0.006	0.008
TiO_2	0.11	0.09	0.06	0.09
LOI	3.72	6.2	6.12	4.56
H_2O	12.1	9.46	11.34	8.4

4.4 Investigating the Effect of Chloride and Removal of Chloride by the Washing of a Revert Material

The chloride-focused tests were designed to evaluate the premise that, because of the high volatility of the element, adding chloride can harm the process and/or sinter quality. It will be interesting to see how much of the additional chloride added is released as PM emissions because it is already known to impact the effectiveness of the ESP abatement. It is anticipated that removing a significant proportion of chloride from the ESP dust through washing[100] will improve the sintering process and sinter quality while also reducing the PM emissions and enhancing the effectiveness of the ESP abatement at the sinter plant. The ESPs are efficient at removing the larger particles, but often smaller PM escape and are unable to cope with the high resistivity of emissions. However, it is unknown how they may impact the sintering process, the sintered product, and the PM emissions which are physically released. The four tests used the pilot-scale sinter rig where the addition of pure KCl (97% concentration) was added as trim at increased increments of 0, 200, 400 and 600 Cl mg/kg and was determined using Equation 30. Further experimental work investigated the effect of the removal of chloride by washing. ESP dust is the predominant source of chloride in the sinter blend; therefore, this material was chosen to be washed. The ESP dust was collected from the supply conveyor belt from the sinter. The ESP dust which was washed was supplied was mechanically stirred, washing at 400 rpm for 10 minutes, before being filtered and dried at 105 °C for 24 hours. The seven pilot-scale sinter rig tests used ESP dust at concentrations of 0%, 0.35%, 2.5%, and 5% as well as washed ESP dust (WESP) dust at the same concentrations. All the blend's composition, process parameters and methods used for analysis remained constant. The raw material contents of the blend stayed the same (Table 31). This experiment was conducted in collaboration with others which is in a journal which is yet to be submitted.

Process parameters:
- Fuel rate – 5%
- Moisture content – 8%
- Granulation time – 5 minutes
- Ignition period – 1 minute
- Pressure drops set point - 100mbar

Table 31 – Raw material contents of blends for chloride study

Component (mass % dry ore basis)	Base Blend 1 (0 Cl)	Blend 6 (200 Cl)	Blend 7 (400 Cl)	Blend 8 (D (600 Cl)	Base Blend 7 (0% ESP/W ESP)	Blend 10 (0.35% ESP)	Blend 11 (2.5% ESP)	Blend 12 (5% ESP)	Blend 13 (0.35% WESP)	Blend 14 (2.5% WESP)	Blend 15 (5% WESP)
ORES											
iron ore B	20.4	20.4	20.4	20.4	17.2	17.1	16.6	16.0	17.1	16.6	15.95
iron ore D	8.2	8.2	8.2	8.2	17.2	17.1	16.6	16.0	17.1	16.6	15.95
iron ore E	8.2	8.2	8.2	8.2	10.3	10.3	9.9	9.6	10.3	9.9	9.57
iron ore G	16.3	16.3	16.3	16.3							
iron ore F	28.6	28.6	28.6	28.6							
iron ore A					24.1	24.0	23.2	22.3	24.0	23.2	22.33
FLUXES, BREEZE and OTHER											
Sinter Fines	18	18	18	18	18	18	18	18	18	18	18
Limestone	11.1	11.1	11.1	11.1	10.7	10.7	10.5	10.6	10.7	10.5	10.5
Magstone	6.8	6.8	6.8	6.8	6.7	6.7	6.5	6.5	6.6	6.6	6.4
Coke Breeze	5	5	5	5	7	7	7	7	7	7	7
SiO_2 Addition	0.3	0.3	0.3	0.3							
Potassium Chloride	0g	6.73g	13.46g	20.19g							
BOS Slurry					7	7	7	7	7	7	7
Flue Dust					6.2	6.2	6.2	6.2	6.2	6.2	6.2
ESP Dust Raw					0	0.4	2.5	5	0	0	0
ESP Dust Washed					0	0	0	0	0.4	2.5	5

Technical details:

Potassium chloride ≥97%,

Formula: KCl

Molecular weight: 74.56 g/mol

Boiling Point: 1420 °C (1013 hPa)

Melting Point: 773 °C

Density: 1.98 g/cm³ (20 °C)

The molecular weight of Cl: 35.46 g/mol

Equation 30 – Calculation of KCl trim

$$KCl\ Trim\ = (Amount\ of\ Blend\ Material \times KCl\ Trim\ Desired)$$
$$\times \left(\frac{Molecular\ Weight\ of\ KCl}{Molecular\ Weight\ of\ Cl}\right) \div 1000$$

4.5 Investigation of the Particle Size Distribution of Ultra-fines Iron Ores

This experiment was to investigate sinter process stability, sinter quality of sinter ore blends and its environmental effects by incorporating iron ore concentrate called iron ore C concentrate with a trim of SiO_2 addition while replacing iron ore B with a plant representative blend. It is hypothesised that the full or partial replacement of iron ore with another more cost-effective iron ore may well improve sintering processing and sintering quality as the addition of more nuclei particles may improve the permeability and decrease the number of PM emissions due to the improvement of detachment forces required. The more optimum ratio between the two iron ores may be a more suitable choice if the sinter bed becomes too coarse with nuclei particles. Theoretically, by increasing NTLR while varying individual size fractions in further experimental investigation, it may be possible to determine the optimal ratio of nuclei, non-adhering, and adhering particles. The base blends 1 and blends 16,17,18,19,20 was replacements of iron ore B for 5% iron ore C, up to 25% iron ore C, and 0% iron ore B as presented in Figure 4.8. Iron ore C has the advantages of being more commercially feasible and having lower costs over iron ore B whether replacing it entirely or in part. Further investigation by maintaining nuclei-to-layer ratio (NTLR) whilst varying absolute levels of individual size fractions of nuclei, non-adhering and adhering particles while analysing sinter process stability, sinter quality of a sinter ore blends and its environmental effects. The size fractions used were % nuclei (>1 mm), non-adhering (1-0.25 mm) and adhering (<0.25 mm). Table 32 shows the raw material connections of the blends used. For ultra-fines study 2 (blends 21 to 25), the pressure drop set point was adjusted from 100 mbar to 130 mbar. This was done to help the pilot-scale sinter rig simulate sinter plant conditions for a more direct comparison for this study. Table 33 displays that for blends 1, 16,17,18,19 the NTLR and particle size fractions were kept constant throughout the experiment. For blends 21,22,23,24 and 25, the NTLR was kept as constant as possible but the absolute values for particle size distribution varied for nuclei, non-adhering and adhering by sizing using a 1 mm sieve,

0.25 mm sieve and a receiver (<0.25 mm) as displayed in Table 32 for iron ore E which is segregated into the size fractions for the pilot-scale sinter rig tests.
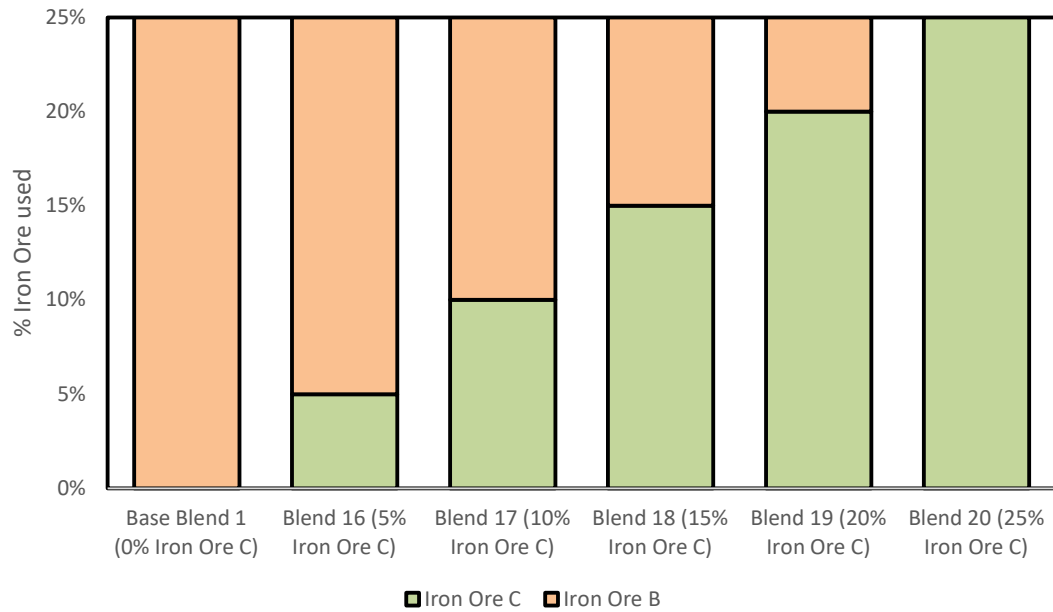
Figure 4.8 – Replacement of iron ore B with iron ore C for the displacement of two ultra-fines iron ores

Process parameters:

- Fuel rate – 5%

- Moisture content – 8%

- Granulation time – 5 minutes

- Ignition period – 1 minute

- Pressure drops set point – 100 mbar and 130 mbar

Table 32 - Raw material contents of blends for investigation of the particle size distribution of ultra-fines iron ores

Component (mass % dry ore basis)	Base blend 1 (0% iron ore C)	Blend 16 (5% iron ore C)	Blend 17 (10% iron ore C)	Blend 18 (15% iron ore C)	Blend 19 (20% iron ore C)	Blend 20 (25% iron ore C)	Blend 21 (35% Nuclei)	Blend 22 (40% Nuclei)	Blend 23 (45% Nuclei)	Blend 24 (50% Nuclei)	Blend 25 (55% Nuclei)
ORES											
iron ore B	20.4	16.3	12.2	8.1	4.1	0					
iron ore D	8	8	8	8	8	8					
iron ore E	8	8	8	8	8	8					
iron ore G	16.3	16.3	16.3	16.3	16.2	16.2					

|											
iron ore F	28.5	28.5	28.5	28.5	28.5	28.5	41	41	41	41	41
iron ore C	0	4.1	8.1	12.2	16.2	20.3					
iron ore E (Non-adhering)							32.8	20.5	13.1	0.4	0
iron ore E (Adhering)							16.4	20.5	23.0	27.1	26.2
iron ore E (Nuclei)							0	0	4.9	9.8	14.8
FLUXES, BREEZE AND OTHER											
Sinter Fines	18	18	18	18	18	18	18	18	18	18	18
Limestone	11	11	11	11	11	11	6	6	6	6	6
Magstone	7	7	7	7	7	7	8.5	8.5	8.5	8.5	8.5
Coke Breeze	5	5	5	5	5	5	5	5	5	5	5
SiO₂ Addition	0.3	0.5	0.6	0.7	0.8	0.9					

Table 33 – Size fraction used in blends of raw material contents of blends for investigation of the particle size distribution of ultra-fines iron ores

| Particle Size Distribution %	Base blend 1 (0% iron ore C)	Blend 16 (5% iron ore C)	Blend 17 (10% iron ore C)	Blend 18 (15% iron ore C)	Blend 19 (20% iron ore C)	Blend 20 (25% iron ore C)	Blend 21 (35% Nuclei)	Blend 22 (40% Nuclei)	Blend 23 (45% Nuclei)	Blend 24 (50% Nuclei)	Blend 25 (55% Nuclei)
Nuclei			*Not applicable*				35	40	45	50	55
Non-Adhering			*Not applicable*				41	30	23	14	10
Adhering			*Not applicable*				23	29	32	36	35
NTLR	1.3	1.3	1.3	1.3	1.3	1.3	1.5	1.4	1.4	1.4	1.5

Two ultra-fines iron ores were used and displaced at 5% increments from 0% to 25% in the sinter blend in the pilot-scale sinter rig. Initial particle size distribution analyses of iron ore C and iron ore B were conducted using the standard sizing method. In Figure 4.9, iron ore B and iron ore C concentrates have more adhering particles (0.25mm) and fewer non-adhering particles. The key factor contributing to the granulation of a sinter ore mix is the adhering particles of iron ore concentrates. Therefore, it makes it plausible that adding more adhering particles to iron ore C can increase permeability. Iron ore C's like-for-like displacement of iron ore B delivers a permeability benefit, as the initial particle size distribution analysis initially proposed. The composite blend (10% iron ore B, 15%

iron ore C) provided a higher cold permeability. It was concluded from Figure 4.10 that iron ore C when exchanged for iron ore D, offers a permeability benefit.
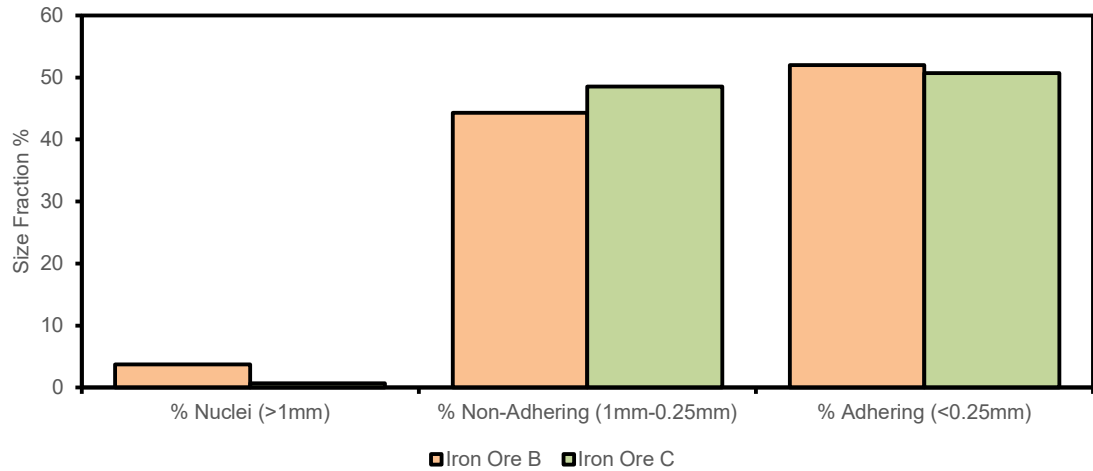
Figure 4.9 – Size fraction of iron ore C and D for ultra-fines study for the displacement of two ultra-fines iron ores
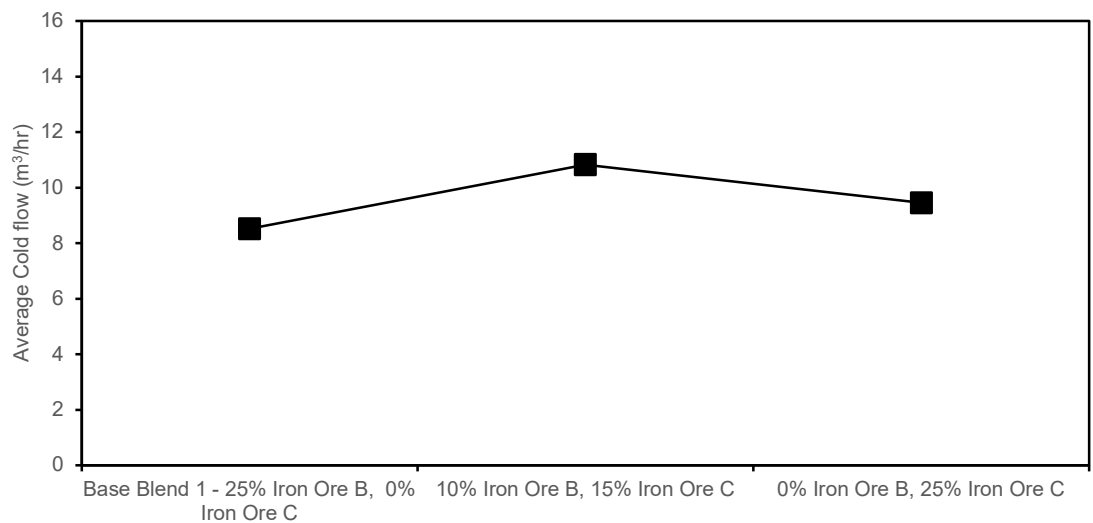

Figure 4.10 – Cold flow permeability test for ultra-fines study for the displacement of two ultra-fines iron ores

A representative sample of 1.3 kg of iron ore E was taken, and the desired size fractions were separated using sieves of 1 mm, 0.25 mm, and a receiver as indicated in Figure 4.11. Figure 4.12 shows the PSD of iron ore E consists of 48% of iron ore E composed of nuclei-sized particles, of which 35% adhering and 17% were non-adhering particles. Figure 4.13

and Figure 4.14 highlight that SiO_2, Al_2O_3, CaO and Na_2O decrease as particle size increases, this was to be further investigated in this thesis.


Figure 4.11 – Iron ore E (left to right; size fraction of nuclei, non-adhering and adhering) for varying absolute levels of individual size fractions
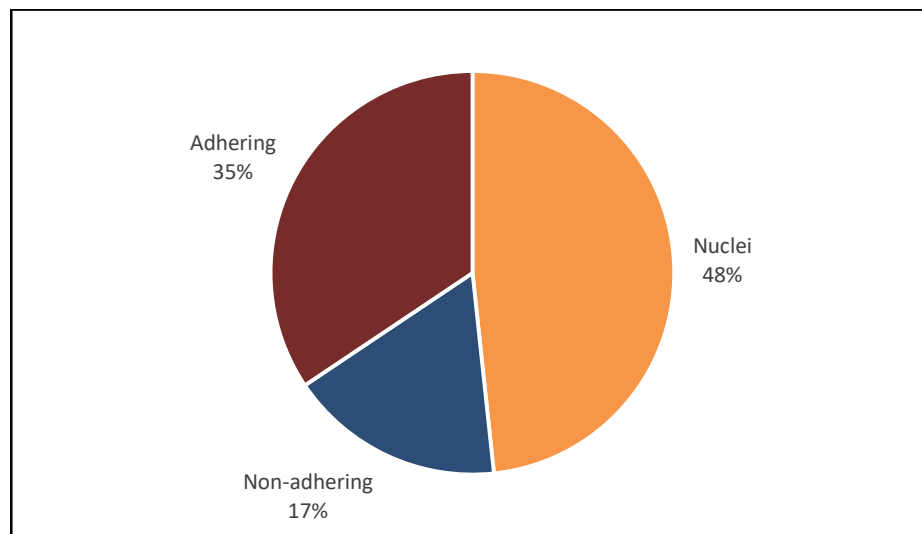
Figure 4.12 – Percentage of size fractions of iron ore E for varying absolute levels of individual size fractions
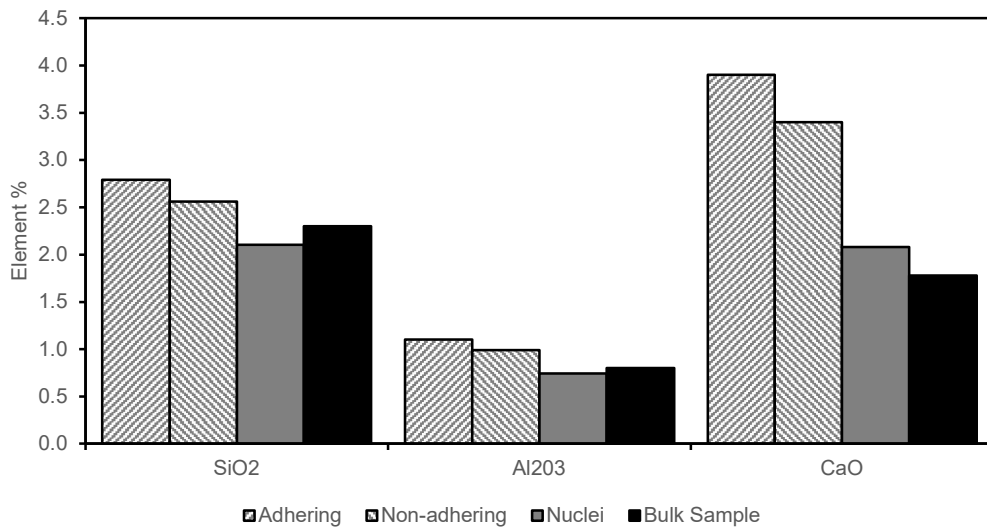
Figure 4.13 - Elements of SiO$_2$, Al$_2$O$_3$ and CaO of iron ore E for adhering, and non-adhering. nuclei and bulk samples for varying absolute levels of individual size fractions
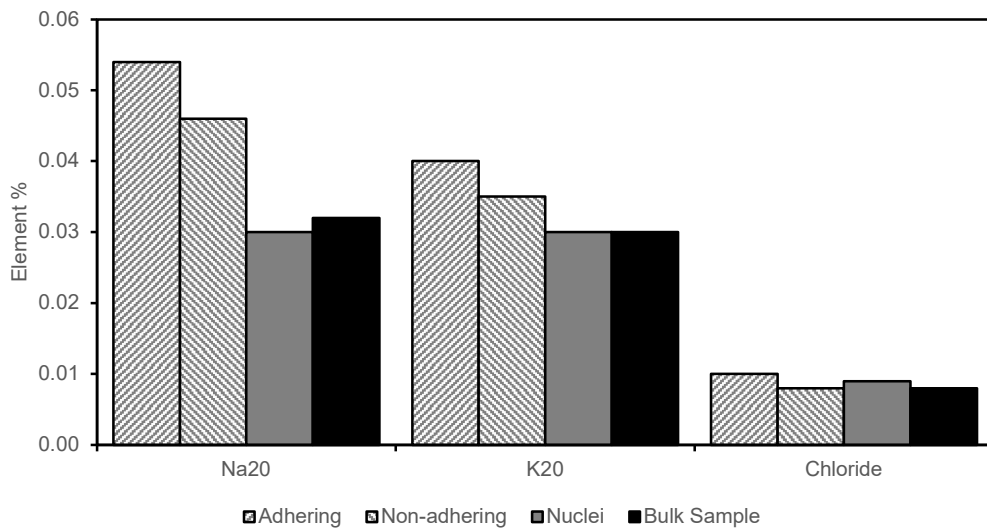
Figure 4.14 - Elements of Na$_2$O, K$_2$O and chloride of iron ore E for adhering, and non-adhering. nuclei and bulk samples for varying absolute levels of individual size fractions

5 Results and Discussion

5.1 Advanced Analytics of Sinter Plant Operations to Minimise Particulate Emissions

This section will aim to analyse particulate matter (PM) emissions output from the sinter plant with process parameters and raw materials utilised to identify the major levers that have the greatest influence on the increase in PM emissions. The ability to regulate or alter input factors to lower PM emissions will be achievable after a correlation between parameters and output has been established. Monitors deployed strategically throughout the plant to examine conditions and operations provide process information (PI) data. To account for any residence time of the dust or gas within the process, the information was obtained at intervals of 5 seconds during the testing period, including 30 minutes before the testing. Due to the commercial sensitivity of the content, some of the process data has been normalised. For this study, a total of 141 samples were analysed due to their main parameters being comparable. The full dataset is provided in Appendix 3 and further analysed and discussed below.

A general overview of the data suggests when the fan operation is decreased, it highlights the overloading of waste gas volume on the south side which is the electrostatic precipitator (ESP) abatement at the sinter plant which creates unstable operations due to the flowrate increase as only 50% of ESP abatement was available. Fan operations have a major effect on PM emissions from the continuous emission monitors (CEMs) as a standard reference method (SRM) results when switching from 2 to 1 fan operations as displayed in Figure 5.1. Large extreme spikes in the data that were above 100 mg/Nm^3 were highlighted and shown in Figure 5.2. The main cause of this was a large inlet temperature increase of 19%. The average inlet temperature for all samples was 137.1 °C but the average inlet temperature for the spikes samples was 162.7 °C. It required more investigation to comprehend this development. The ability of a particle to receive a charge, or resistivity, is crucial to the ESP's collection effectiveness. The particle resistivity needs to be changed or the ESP treatment time needs to be extended if a particle is resistant to acquiring an appropriate charge. Figure 5.3 displays a trend of increasing inlet temperatures (orange line on the right axis of the figure mentioned) from 2014 to 2020 but from 2018 to the current year there was a high increase in average inlet temperatures from 134.3 °C to 151.1 °C. Sample numbers 95 to 100 had no data for inlet temperature

due to the connection being offline due to the upgrading of hardware which was resolved later. Figure 5.4 illustrates the key levers for PM emissions from the sinter plant production and operations and displays that changing from 1 to 2 fan operations causes the greatest influence with a -31% decrease in SRM results. Suction from the north and south wind-box which was situated on either side of the ESP and when below the sinter plant's target of 75 mbar decreases the SRM result by 26% and 27%. Another key lever was moisture and when above the average of 6.1% the SRM results decrease by -9% since 2018 when the average inlet temperature was below the average of 149.9 °C resulting in a 21% decrease in particulate matter (PM) emissions. The suction average was 75 mbar, the moisture average was 6.1% and the inlet temperature (since 2018) was 150 °C.
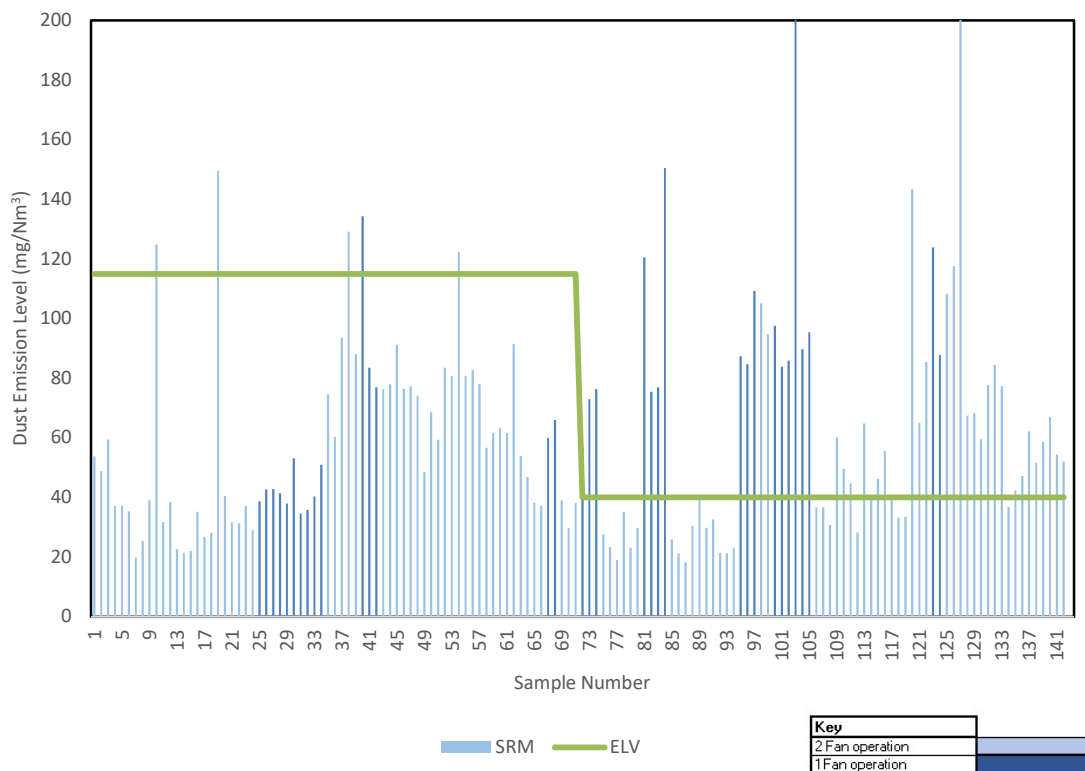

Figure 5.1 – Data analytics of fan operations using historical sinter plant data
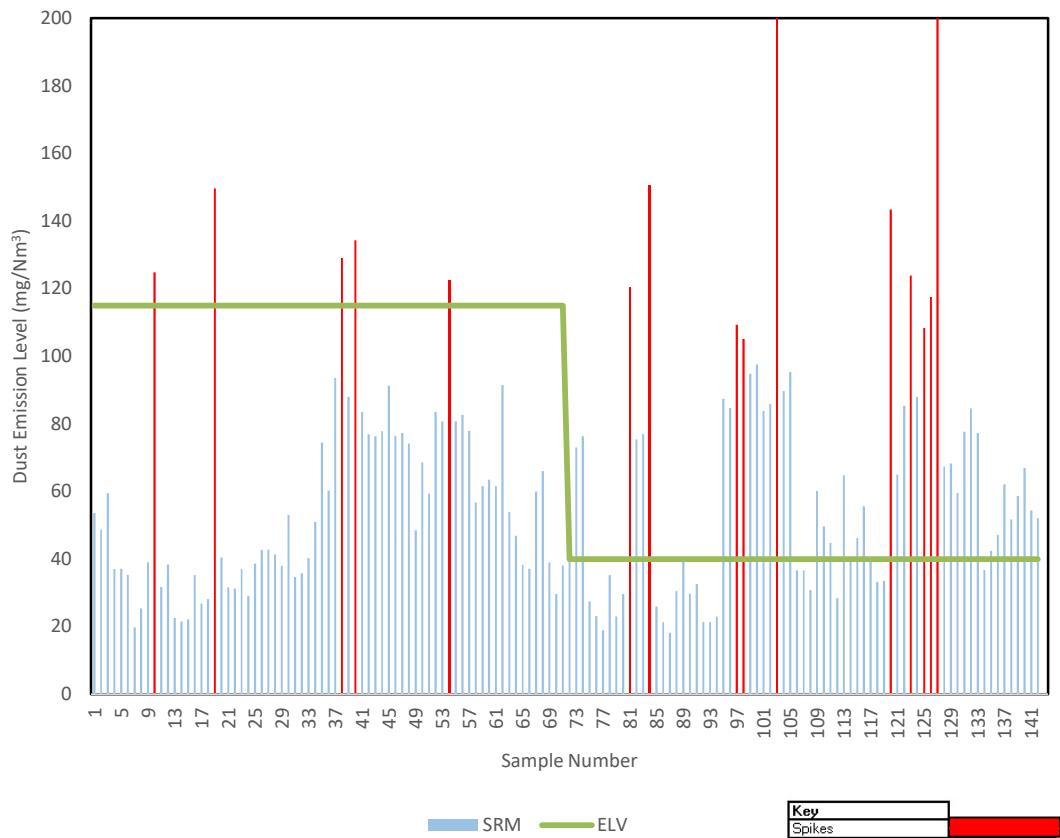
Figure 5.2 – Data analytics of highlighted spikes above 100mg/Nm³ using historical sinter plant data
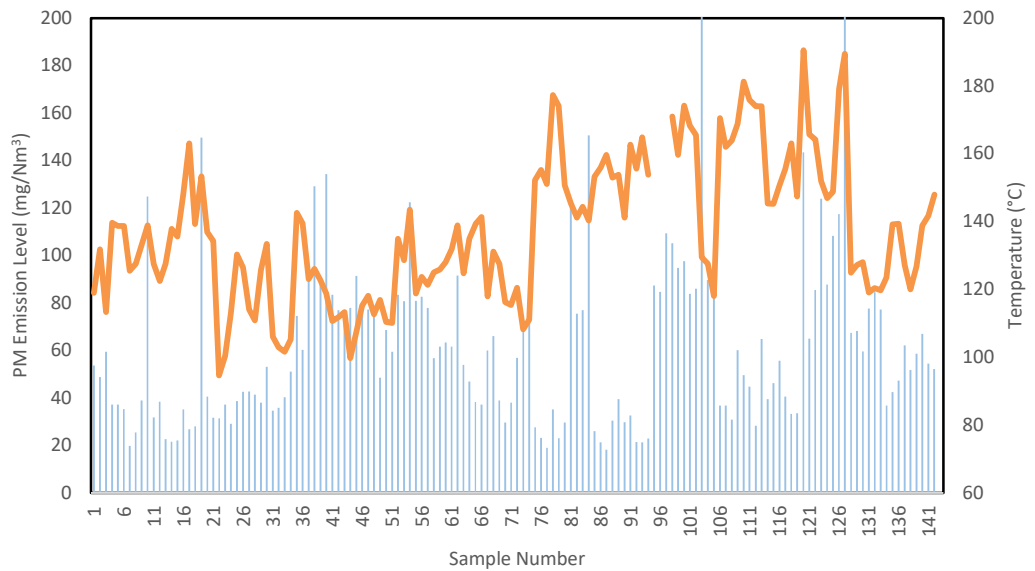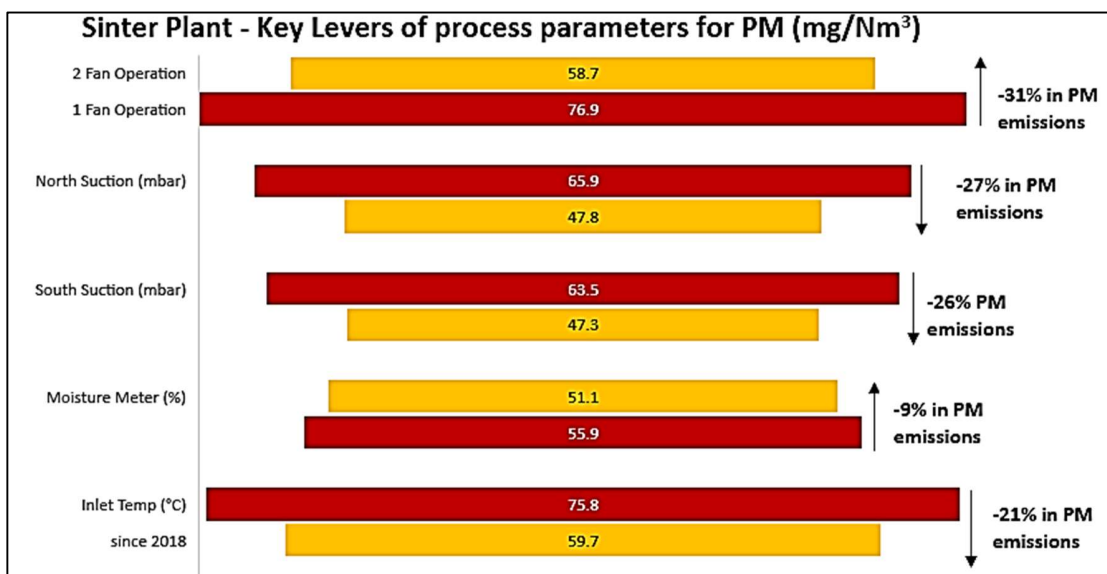

Figure 5.3 – – Data analytics of outlet temperature effect on standard reference method (SRM) results using historical sinter plant data

Figure 5.4 – Key levers for PM emissions from the sinter plant production and process information using historical sinter plant data

The next step was to understand the raw material's effect on PM emissions, it was required to remove production and process key levers from the data from this point. Following the criteria below, sample selection was therefore performed on the data collected, of which 30 of 142 samples were down-selected:

1. 2 fan operations
2. Spikes emitted ($>100mg/Nm^3$)
3. >80% of fields in use
4. The average output of 489 t/hr ±25%
5. Average strand speed of 2.7mtr/min ±25%
6. The suction target of 75mbar ±25%
7. Ave Inlet Temp: 147.8°C ±25%
8. No data for raw materials used before 2017

Figure 5.5 displays the major correlation results from raw materials of the blend on SRM results and the raw data can be seen in Appendix 3. The fluxes have a negative correlation with the SRM result. Type A, B and C iron ores are typically fine ores that have a positive correlation. Also, the addition of recycled materials such as basic oxygen steelmaking (BOS plant) slags and scrap has a positive correlation with SRM results. K_2O which was essentially chloride has a high affinity to be attached to potassium. In sintering, this has a

positive correlation because it has a detrimental effect on the ESP abatement collection efficiency. Figure 5.6 displays the results of the major correlation from raw materials of the blend to inlet temperatures. The fluxes (magstone and limestone) have amounts of MgO that all have a negative correlation with the inlet temperature. The increase of fuels (coke breeze and duff anthracite) may lead to over-fuelling with carbon which can cause poor combustion efficiencies. Across the sinter strand at the sinter plant, the wind box temperatures vary depending on the process and raw materials in use. Figure 5.7 highlights that temperature increases across the sinter strand as the sinter reaches burn through the point (maximum temperature), this was an indication that most PM emissions may be held in the wind boxes near the end of the strand, and this would be a potential opportunity to control the PM emissions.
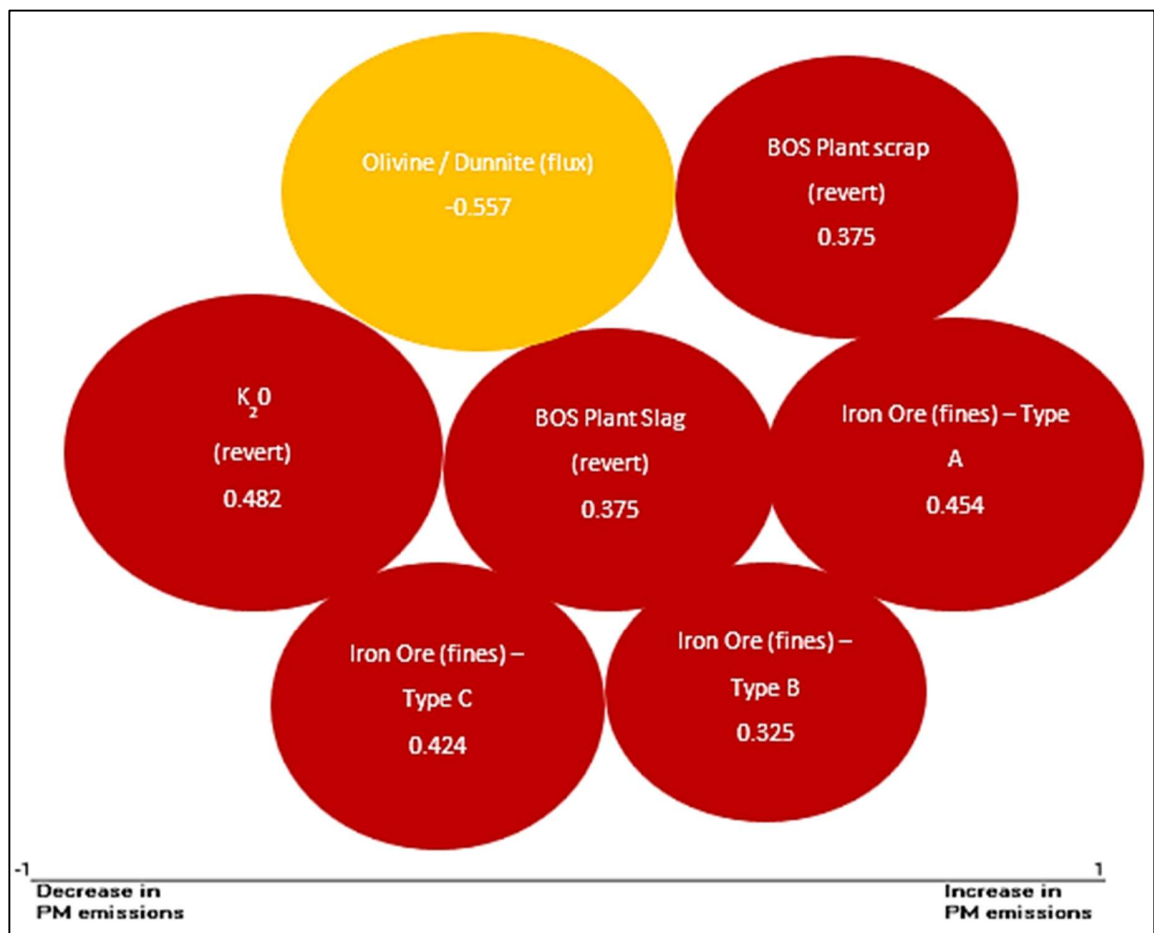

Figure 5.5 – Key levers of raw materials on SRM at the sinter plant main stack using historical sinter plant data
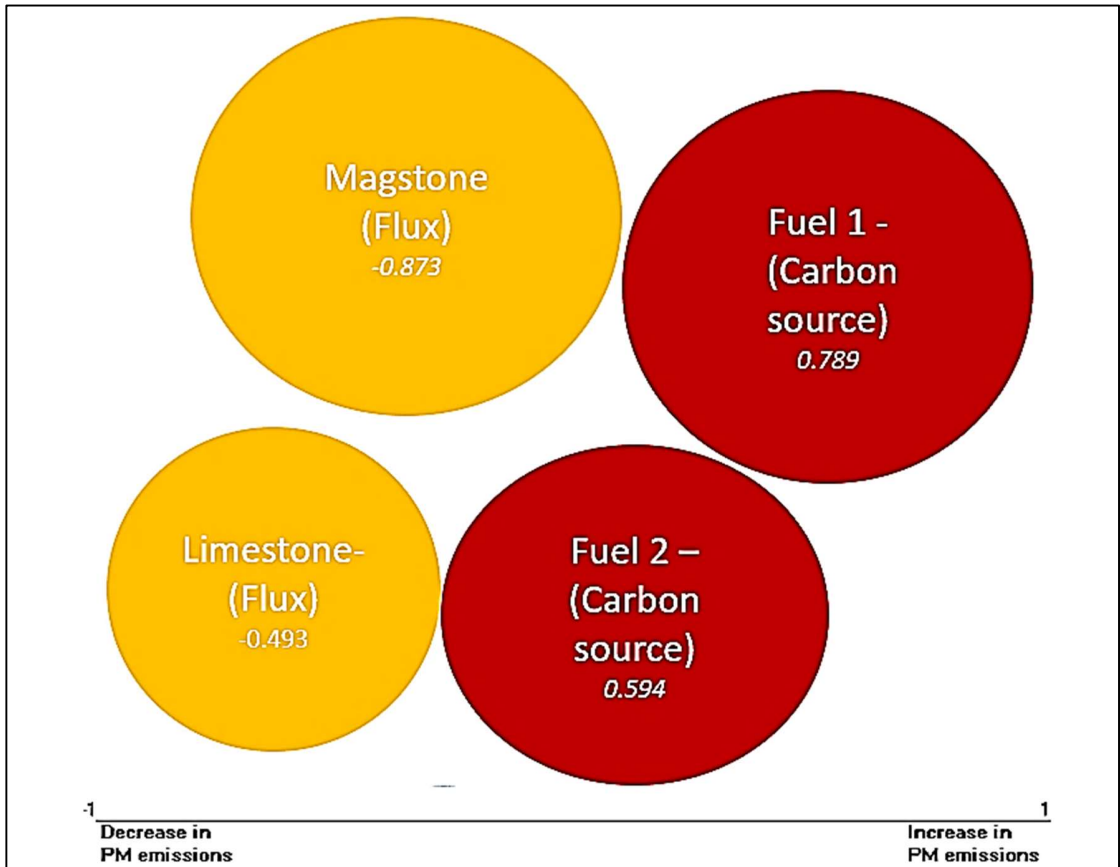
Figure 5.6 – Key levers of raw materials on the inlet temperature at the sinter plant main stack using historical sinter plant data
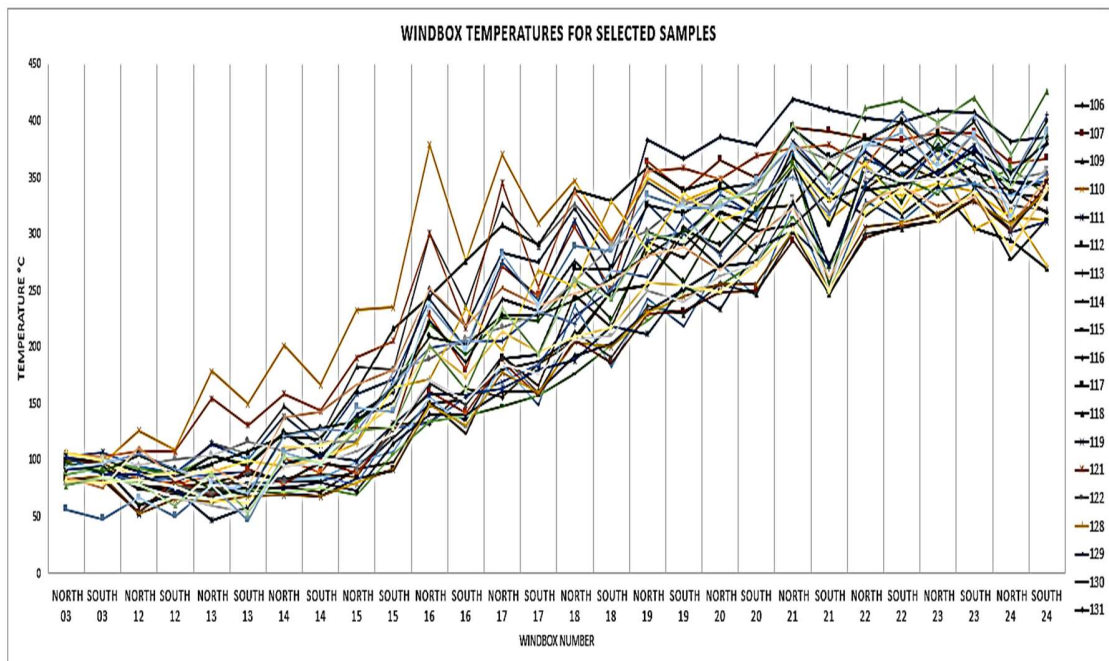

Figure 5.7 – Windbox Temperatures for selected samples at the sinter plant main stack

Summary

The number of fan operations being used, the suction pressure of the fans, the moisture of the bed, and the inlet temperature of the ESP abatement all have an impact on the rise in PM emissions. Despite sintering being an extremely complicated and constantly changing process, distinct relationships were observed in the data. With the use of this information, data scrubbing was conducted which was able to produce a stable sintering process for analysis. To reduce PM emissions, it was found that an increase in PM emissions with fine iron ores, an increase in fuel, the amount of recycled material employed, and the amount of K_2O which was chloride in sintering which was in the sinter blend were the main levers that impacted the effectiveness of the ESP collecting system. The use of fuel and the use of finer[90] and more trace metals tend to have the biggest effects on the raw materials. Along with pilot-scale sinter rig testing of these findings, further research can examine whether there was a mix of different parameters that may impact each of these individual important levers.

5.2 Validation of Pilot-Scale Sinter Rig, Novel Capture Device and Utilisation of Sinter Plant Beds

This section aims to validate the sinter pot and a newly built and installed dust capture device, as well as the sinter pot with a sinter plant while using three different beds. To understand what is continuously being returned into the sinter plant system and to identify areas for potential optimisation, a compilation of pilot-scale sinter rig return fines particles will need to be chemically analysed at various size fractions to potentially minimise particulate matter (PM) emissions.

5.2.1 Validation 1 – Pilot-scale Sinter Rig

Validation 1 included the repeatability and deviation of the pilot-scale sinter rig's sintering process, product and PM emissions. The analysis was repeated to determine how much variation there was between tests and aimed to impose a standard deviation per test parameter. For the base blend (BB) composition chosen, an optimal moisture study had to be conducted. Maximum cold permeability for the base blend was observed to be 11.07m^3/hr at 8% moisture (Figure 5.8). Subsequent granulations for each blend were conducted at 8% moisture. This was crucial because an insufficient bed permeability caused by too much moisture in the green mix would lead to an unstable flame front. It will take more energy and it will reduce the sintering temperature, both of which will be important to the sintering process if there is too much moisture to evaporate. The airflow for each blend fluctuated between 10-12 m^3/hr which indicated a stable moisture level (Figure 5.9). Each element exhibited a variation of less than 15%, indicating good accuracy and repeatability of the analysis performed before sintering. (Table 34). This was to confirm that the mixes were made correctly, including the selection of the right raw materials and the appropriate quantity.
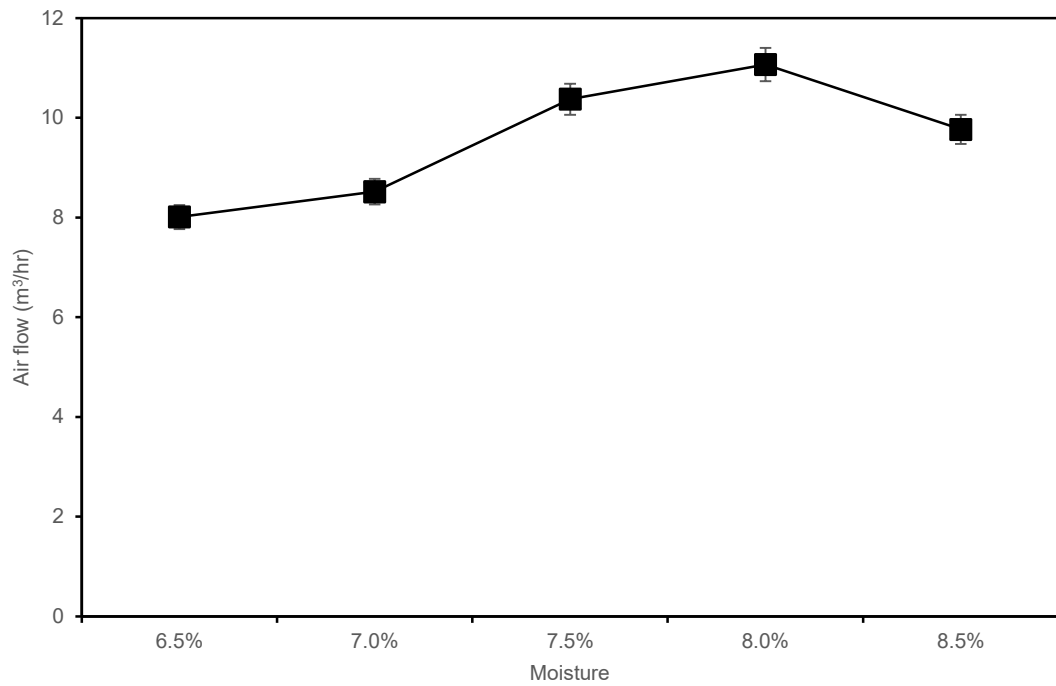
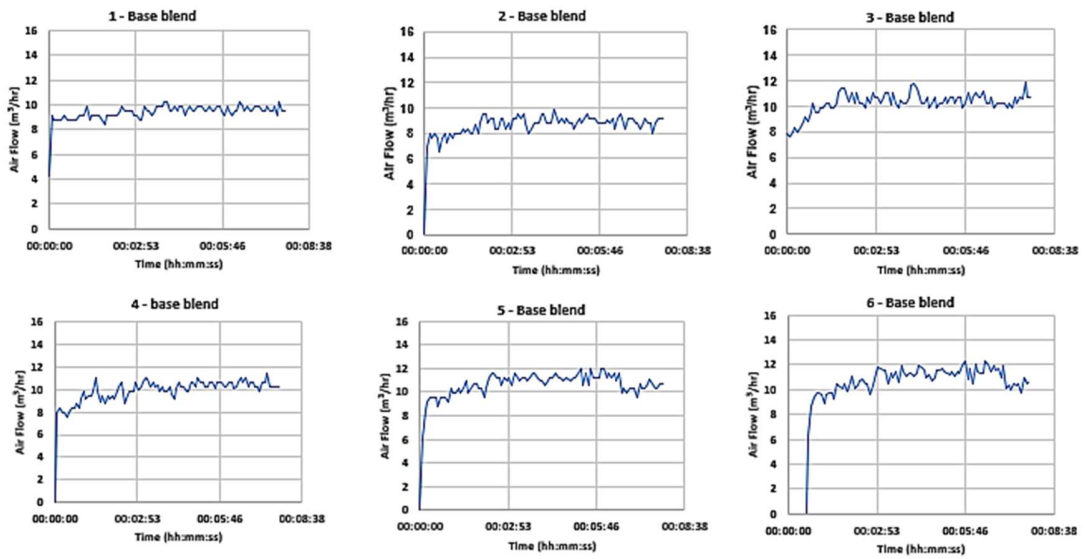**Figure 5.8 – Optimal moisture study for validation (1) shows the effect of moisture on a sinter blend**

Figure 5.9 – Cold flow for validation shows a consistent result (1)

Table 34 – Green mix for validation (1)

Element (%)	1 - Base blend	2 - Base blend	3 - Base blend	4 - Base blend	Standard Deviation	Deviation
SiO_2	10.91	12.98	11.56	11.15	0.80	7%
Al_2O_3	4.83	5.23	5.05	4.75	0.19	4%

TiO$_2$	1.08	0.88	1.02	1.09	0.08	8%
CaO	0.097	0.100	0.099	0.100	0.00	1%
MgO	7.62	7.28	8.56	9.24	0.77	9%
Fe	1.46	1.22	1.55	1.72	0.18	12%
Fe$_2$O$_3$	50.44	50.67	49.71	45.84	1.95	4%
FeO	68.9	70.87	69.74	63.9	2.66	4%
P	1.49	1.43	1.21	1.48	0.11	8%
Mn	0.021	0.016	0.02	0.02	0.00	10%
Na$_2$O	0.15	0.13	0.15	0.14	0.01	6%
K$_2$O	0.054	0.051	0.065	0.055	0.01	9%
Zn	0.051	0.041	0.05	0.042	0.00	10%
Cu	0.012	0.014	0.01	0.013	0.00	12%
Cl	0.001	0.001	0.001	0.001	0.00	0%

Understanding that each thermocouple peaked one after the other in the temperature profiles (Figure 5.10) shows a stable process for the base blend since the flame front steadily passed each thermocouple without any issues such as re-ignition (Figure 5.11). The fact that the off-gas temperatures rose and peaked after the thermocouples achieved their maximum temperature, indicating that the flame front had burned through entirely and had now entered the waste gas system, was another stable process indicator. For all upcoming tests, all standard deviations were calculated and were included (Appendix 4) as error bars. The average cold flow rates for each test had a standard deviation of 0.78, ranging between 8.9 and 11.1 m^3/hr. The average heat flow rate ranged from 6.7–7 m^3/hr, with a standard deviation of 0.36. The thermocouples were positioned into the blend on the pilot-scale sinter ranging from number 1 at the top of the blend to number 5 at the bottom of the blend. The off-gas temperature 1 ranged from 399 to 325 °C, with a standard deviation of 26 °C. Off-gas temperature 2 had a standard deviation of 5.76 and ranged from 101 to 84 °C. PM emissions on the filter ranged from 19.3 to 14.8 mg/m^3, with a standard variation of 1.79 mg/m^3. The return fines particulates that were gathered on the tray ranged from 18.3 to 29.8 g, with a standard deviation of 4.72g. These were appropriate variations and showed very few fluctuations. Results are shown in Appendix 4.
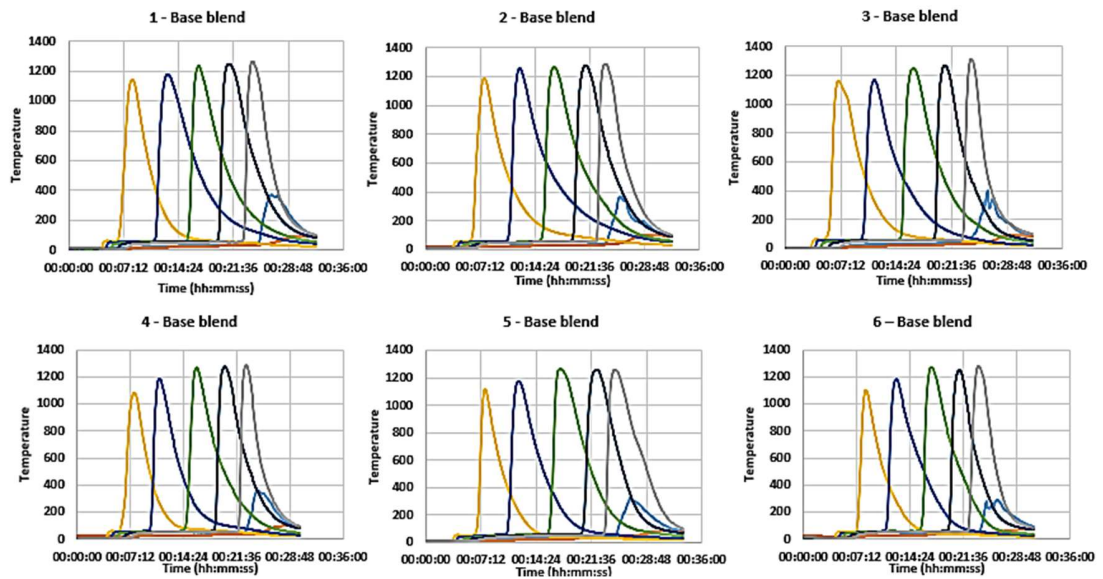
── TC1	── TC2	── TC3	── TC4	── TC5

Figure 5.10 – Temperature profiles for validation that show minimal variation (1)
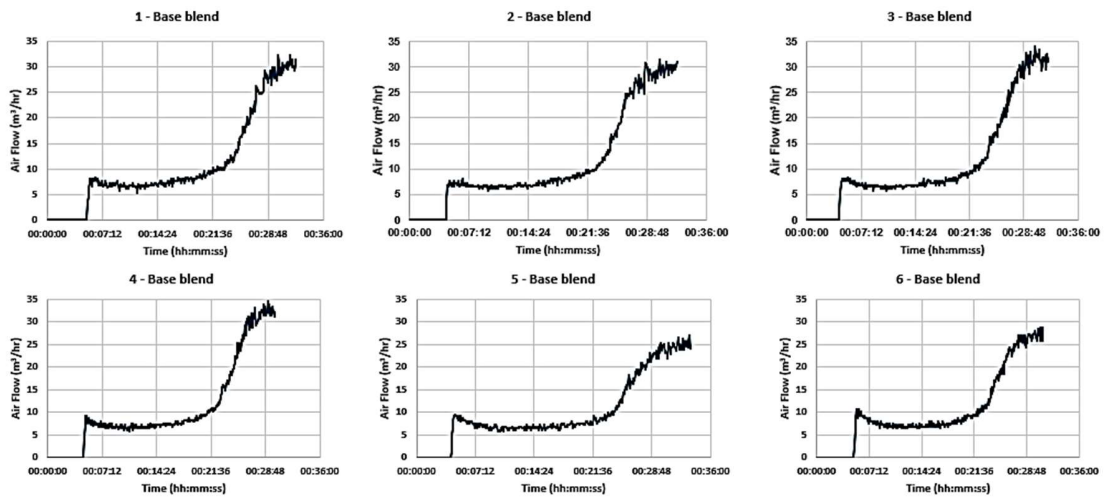

Figure 5.11 – Hot flow for validation that shows a minimal variation (1)

After discharge, three samples of sinter were extracted from the same position as the thermocouple which was subjected to XRF and ICP. The main constituents for sinter product chemistry were SiO_2 which had a maximum of 5.95 % and a minimum of 5.72 % with a standard deviation of 0.1 %. Fe had a maximum of 57.07 % and a minimum of 56.33 % with a standard deviation of 0.3 %. Fe_2O_3 had a maximum of 77.94 and a minimum of 75.06 % with a standard deviation of 1.21 %. Additionally, understanding where the chloride was for future experiments, was important to analyse as well: Na_2O had a maximum of 0.62 % and a minimum of 0.48 % with a standard deviation of 0.1 %.

K$_2$O had a maximum of 0.34 %. and a minimum of 0.31 % with a standard deviation of 0.00 %. Cl had a maximum of 0.003 % and a minimum of 0.002 % with a standard deviation of 0.00 %. Overall, all sinter product chemistry has a deviation of <20%. It was important to mention that all other elements were within a range of normal sinter plant operation. After the sintered product was subjected to a mechanical shaker for particle size distribution (PSD), the <5 mm size fraction had a maximum of 53 % and a minimum of 51 % with a standard deviation of 0.69 %. When comparing the four tests conducted as part of an experiment series, the low variance in size fractions for the sintered product would give a good indication of cold strength (Figure 5.12). The 5–16 mm size fraction had a maximum of 27 % and a minimum of 24 % with a standard deviation of 0.82. The >16 mm size fraction had a maximum of 23 and a minimum of 24 % with a standard deviation of 0.34. Chemical analysis and reduction degradation index (RDI) tests were carried out to provide a more precise indicator of sinter quality. RDI analysis was completed on a sample of sinter that was between 16 and 20 mm in size. The < 6.3 mm RDI values maximum was 78.8 % and a minimum of 74.8 % with a standard deviation of 2.11 %.

Table 35 – Sinter product chemistry for validation (1) that shows minimal variation

| Compound / Element (%)	1 - Base blend	2 - Base blend	3 - Base blend	4 - Base blend	Standard Deviation	Deviation
SiO$_2$	5.95	5.72	5.93	5.95	0.10	2%
Al$_2$O$_3$	0.99	1.08	1.01	0.99	0.04	4%
TiO$_2$	0.080	0.100	0.08	0.08	0.01	10%
CaO	9.1	8.68	9.08	9.1	0.18	2%
MgO	1.65	1.8	1.67	1.65	0.06	4%
Fe	56.33	57.07	56.54	56.33	0.30	1%
Fe$_2$O$_3$	75.06	77.94	75.39	75.06	1.21	2%
FeO	4.32	4.29	4.91	4.94	0.31	7%
P	0.022	0.028	0.028	0.022	0.00	12%
Mn	0.17	0.20	0.17	0.17	0.01	7%
Na$_2$O	0.049	0.063	0.048	0.049	0.01	12%
K$_2$O	0.031	0.034	0.032	0.031	0.00	4%
Zn	0.009	0.008	0.006	0.009	0.00	15%
Cl	0.002	0.002	0.003	0.002	0.00	19%
Basicity	1.53	1.52	1.53	1.53	0.01	*0%*
B3	1.81	1.83	1.81	1.81	0.01	*1%*
Glass Ratio	0.25	0.24	0.24	0.24	0.00	*1%*
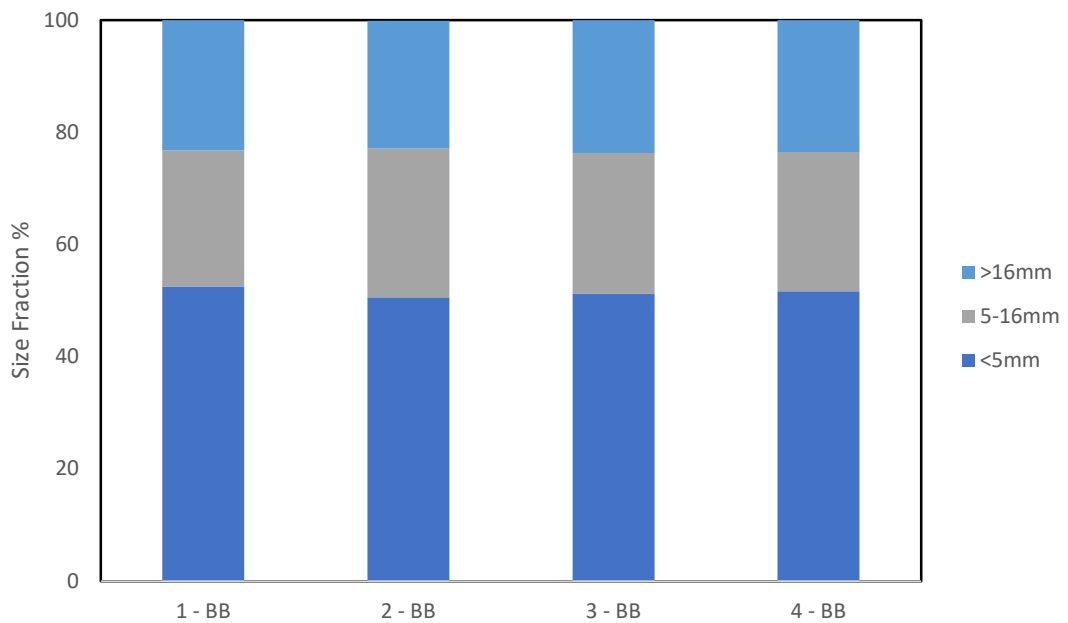
Figure 5.12 – PSD of product for validation (1)

5.2.2 *Validation 2 – Novel Dust Capture Device*

Validation 2 included a novel technique using a dust capture device that was installed to capture the PM emissions and particulates which were deposited on the tray. To demonstrate that no particles passed through the filter and that all PM emissions were collected, visual and optical analysis was conducted and recorded as images, (Figure 5.13). It was demonstrated that the quartz filter had withstood the dynamic pressures and high temperatures produced during sintering on the pilot-scale sinter rig. After the PM emissions were collected on the quartz filter, the mass was recorded. The mass concentration of PM had a maximum of 19.3 and a minimum of 14.8 mg/m^3 with a standard deviation of 1.79 (Appendix 4) which was displayed in Figure 5.14. Additionally, the quartz filter was submitted for Inductively Coupled Plasma Optical Emission spectroscopy (ICP-OES) for total Fe (maximum of 2861 µg/filter, minimum of 2224 µg/filter with a standard deviation of 237.85 µg/filter), total water-soluble sulphate (maximum of 422 µg/filter, minimum of 327 µg/filter with a standard deviation of 35.41 µg/filter), total water-soluble chloride (maximum of 59 µg/filter, minimum of 50 µg/filter with a standard deviation of 3.54 µg/filter) which was calculated to chloride content to consider the mass concentration of PM emissions (Table 36).
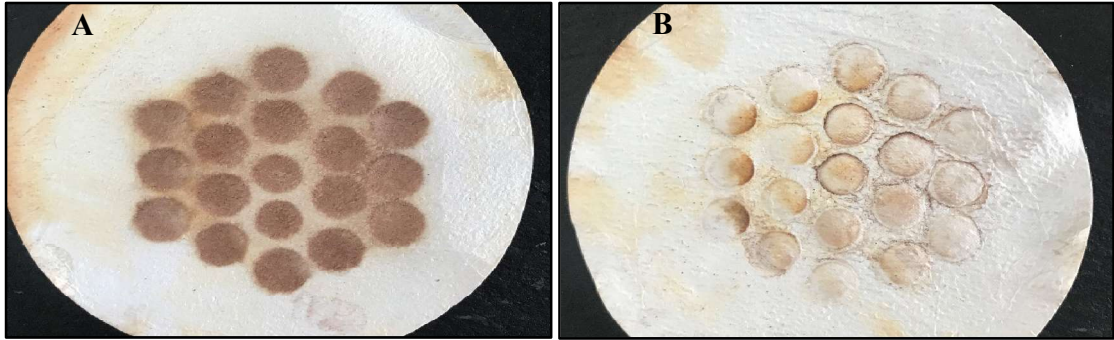
Figure 5.13 – Filter view of front (a) and back (b) for validation (2) and demonstrates all PM emissions have been captured and are unable to escape into the exhaust to be released into the air
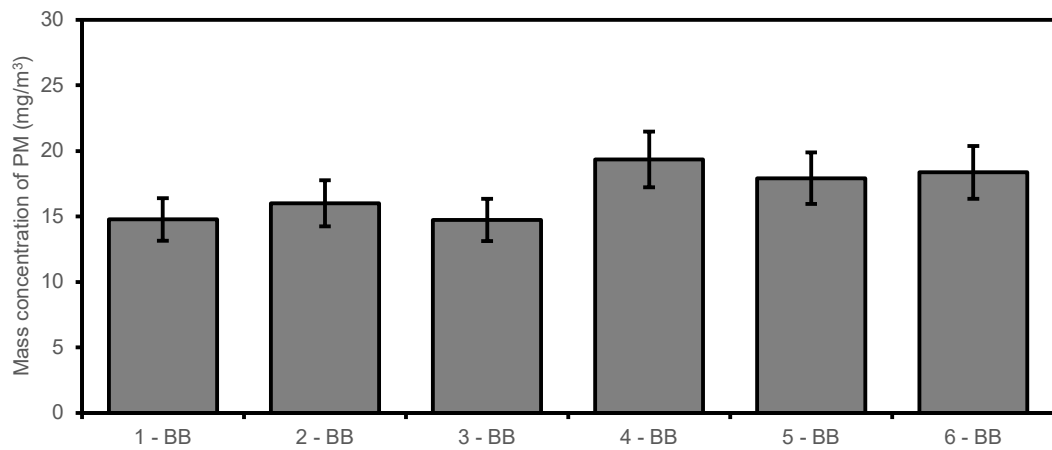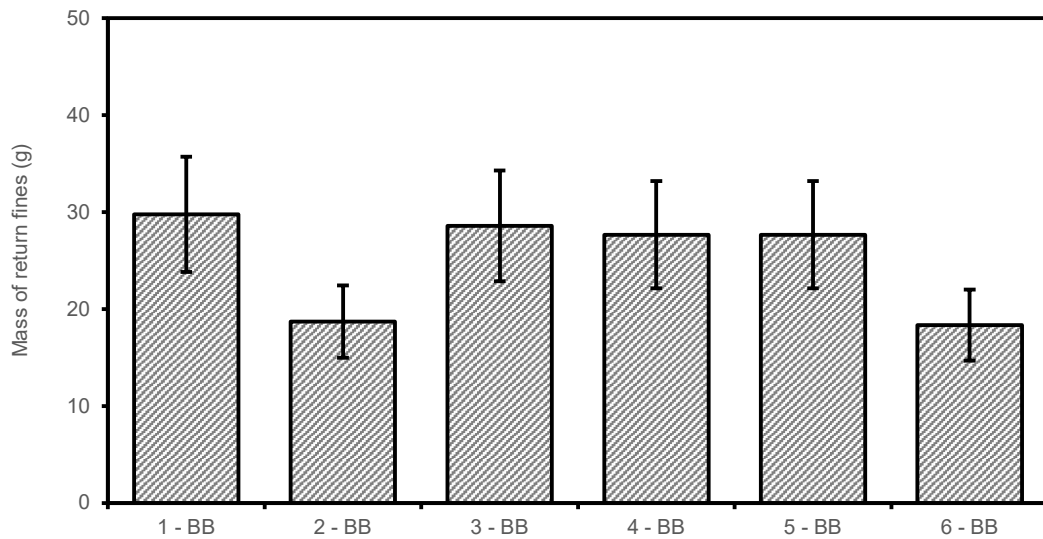

Figure 5.14 – PM emissions for validation that displays minimal variation (2)

Table 36 – PM emissions on the filter: post analysis for validation that demonstrates minimal variation (2)

PM emissions on Filter Analysis	1 - Base blend	2 - Base blend	3 - Base blend	4 - Base blend	Standard Deviation	% Deviation
Total Fe (µg/filter)	2224	2861	2497	2356	237.85	*10%*
Total Water-Soluble Chloride (µg/filter)	50	51	52	59	3.54	*7%*
Total Water-Soluble Sulfate (µg/filter)	399	422	371	327	35.41	*9%*
Chloride content (mgCl/kg)	3383	3463	2900	3213	215.82	*7%*

At the same time, the PM emissions were collected on the quartz filter and were also collected from the tray underneath the pilot-scale sinter rig (return fines particulates) where the mass was recorded for both. The return fines particulates had a maximum of 29.8 and a minimum of 18.3 mg/m^3 with a standard deviation of 4.72 (Appendix 4) which

is displayed in Figure 5.15. Descriptive statistics analysis was conducted (Table 37) and with confidence, it can be stated that the percentage deviation of the filter of the dust capture device was 11 % and the return fines particulates of the tray from the capture device were 19 %. The return fines particulates were further subjected to XRF and ICP for elemental analysis (Table 38). Since this has never been done before, it was impossible to compare it to typical sinter plant operations, although it was reasonable to assume that either sinter or green mix would be involved. SiO_2 (maximum of 4.96 %, minimum of 4.65 % with a standard deviation of 0.17), CaO (maximum of 3.51 %, minimum of 3.24 % with a standard deviation of 0.11), Fe (maximum of 58.2 %, minimum of 54.81 % with a standard deviation of 1.29), Fe_2O_3 (maximum of 79.27 %, minimum of 73.62 % with a standard deviation of 2.20). Heavy metals and chlorides need to be taken into consideration in understanding how these return fines particulates may impact sinter plant operations when re-circulated. Na_2O (maximum of 0.019 % and a minimum of 0.016 % with a standard deviation of 0.00 %), K_2O had a maximum of 0.031 %. and a minimum of 0.026 % with a standard deviation of 0.00 %. Cl had a maximum of 0.029 % and a minimum of 0.024 % with a standard deviation of 0.00 %. After the return fines particulates were collected, PM emissions were subjected to different size sieves to determine the PSD. The >1 mm size fraction had a maximum of 3 % and a minimum of 1 % with a standard deviation of 0.27 % (Table 39). When comparing the tests conducted as part of an experiment series, the low variance in size fractions for the return fines particulates gave a good indication of what size material was being re-circulated at the sinter plant (Figure 5.16).

Figure 5.15 – Return fines particulates for validation that shows a minimal variation (2)

Table 37 – Descriptive summary for validation (2)

Descriptive Summary	PM emissions	Return Fines
Mean	16.9	25.0
Standard Error	0.8	2.1
Median	17.0	27.4
Standard Deviation	1.72	4.72
Sample Variance	3.8	25.7
Kurtosis	-2.2	-1.8
Skewness	0.0	-0.8
Range	4.6	11.4
Minimum	14.7	18.3
Maximum	19.3	29.8
Sum	101.1	149.7
Count	6	6
% Deviation (+/-)	**11%**	**19%**

Table 38 – Return fines particulates chemical analysis for validation that shows a minimal variation (2)

Compound / Element (%)	1 - Base blend	2 - Base blend	3 - Base blend	4 - Base blend	Standard Deviation	Deviation
SiO_2	4.96	4.94	4.57	4.65	0.17	4%
Al_2O_3	0.5	0.56	0.53	0.53	0.02	4%
TiO_2	0.07	0.07	0.06	0.06	0.01	8%
CaO	3.24	3.49	3.5	3.51	0.11	3%
MgO	0.6	0.68	0.61	0.6	0.03	5%
Fe	54.81	56.37	57.57	58.2	1.29	2%

Fe$_2$O$_3$	73.62	75.63	79.27	78.13	2.20	3%
FeO	2.59	2.71	2.75	2.77	0.07	3%
P	0.01	0.01	0.009	0.01	0.00	14%
Mn	0.160	0.150	0.13	0.13	0.01	9%
Na$_2$O	0.016	0.017	0.013	0.019	0.00	13%
K$_2$O	0.026	0.030	0.023	0.031	0.00	12%
Zn	0.112	0.116	0.12	0.124	0.00	4%
Cl	0.024	0.026	0.024	0.029	0.00	8%

Table 39 – PSD Data of return fines particulates for validation that shows a minimal variation (2)

Size fraction (%)	1 – Base blend	2 – Base blend	3 – Base blend	4 – Base blend	Standard Deviation	% Deviation
>1mm	2	2	2	1	0.27	*15%*
0.5mm	21	22	17	24	2.49	*12%*
0.25mm	43	42	41	39	1.59	*4%*
0.15mm	22	21	22	22	0.54	*2%*
0.063mm	9	10	14	11	1.83	*17%*
<0.063mm	3	3	4	4	0.33	*10%*
Total mass (g)	**29.8**	**28.6**	**27.7**	**18.3**	**4.54**	***17%***
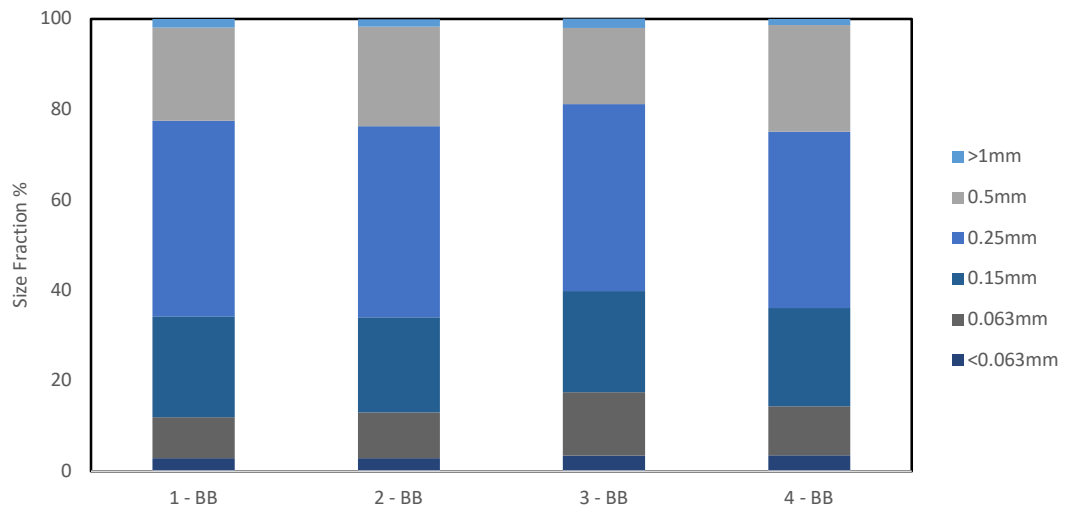
Figure 5.16 – PSD of return fines particulates for validation that shows a minimal variation (2)

5.2.3 Validation 3 – Utilisation of Sinter Plant Beds in a Pilot-scale Sinter Rig

Validation 3 included three sinter plant beds which were used in the pilot-scale sinter rig for direct comparison to the sinter plant. Focusing on sinter stability, process, sinter quality and PM emissions as the nuclei-to-layering ratio (NTLR) increases from 1.5 to 1.7. Further investigation included the return fines particulates, which have not been previously analysed. Currently, at the sinter plant, the return fines were being re-circulated

with the assumption that it was a green mix which has fallen through the sinter bed. Before the testing, the analysis revealed that the cold flow had increased as the NTLR of the sinter bed increased, with the increase of more nuclei particles. The use of larger particles and at higher quantities increases the oxidising reactions after ignition and makes the sinter bed more porous, allowing for more oxygen to enter. Figure 5.17 b) displays an increasing hot flow rate while Figure 5.18 displays decreasing sinter times, illustrating a relationship between the two types of flow rates for each sinter plant bed. The hot flow rate was shown to trend with the cold flow rate by increasing and decreasing sinter times with the sinter plant bed 3 sample achieving the most desirable results concerning productivity. For blend process stability all beds have a stable flame front however the maximum sintering temperature for sinter bed 3 has the higher and sinter bed 2 has the lowest as shown in Figure 5.19 and Appendix 5 which was interesting as fuel rate stays the same throughout the beds which shows the impact that particle size distribution can have on the sintering ability of the bed.
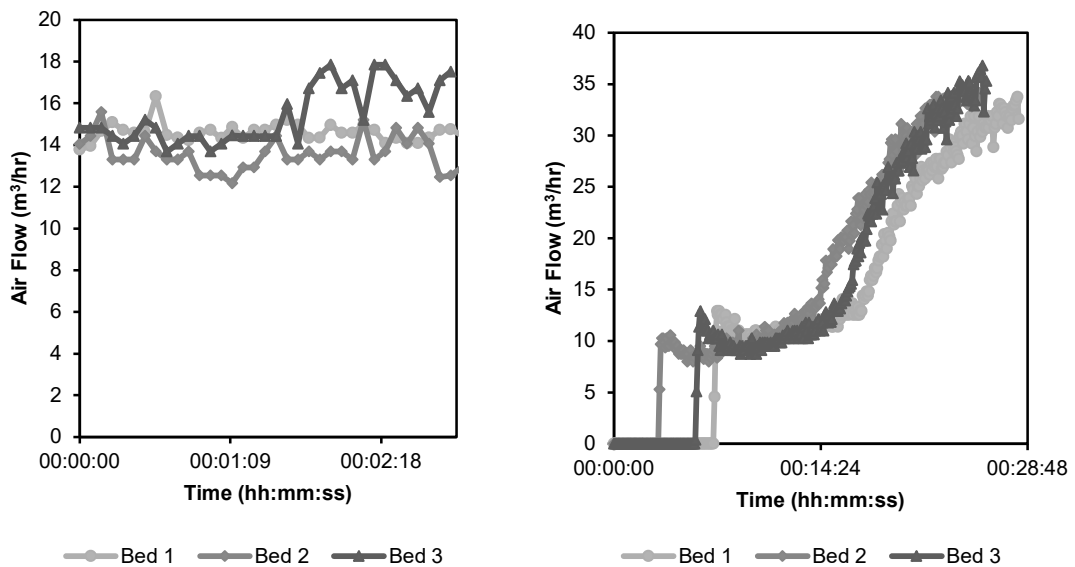
Figure 5.17 - Air flow during Sintering Process a) cold b) hot for validation that shows the variability between three different sinter plant beds (3)
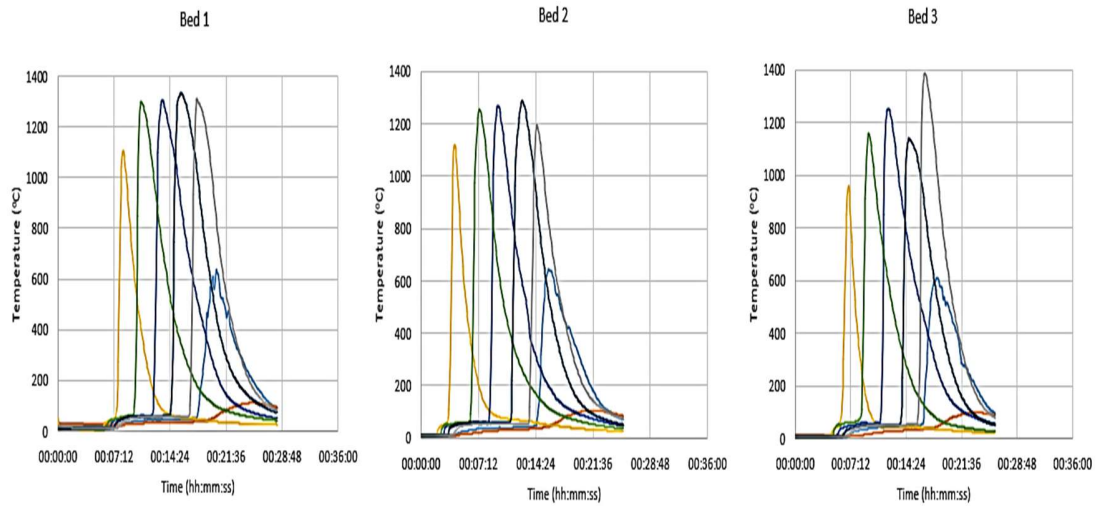
Figure 5.18 - Thermocouple temperature profile during the sintering process for validation (3)
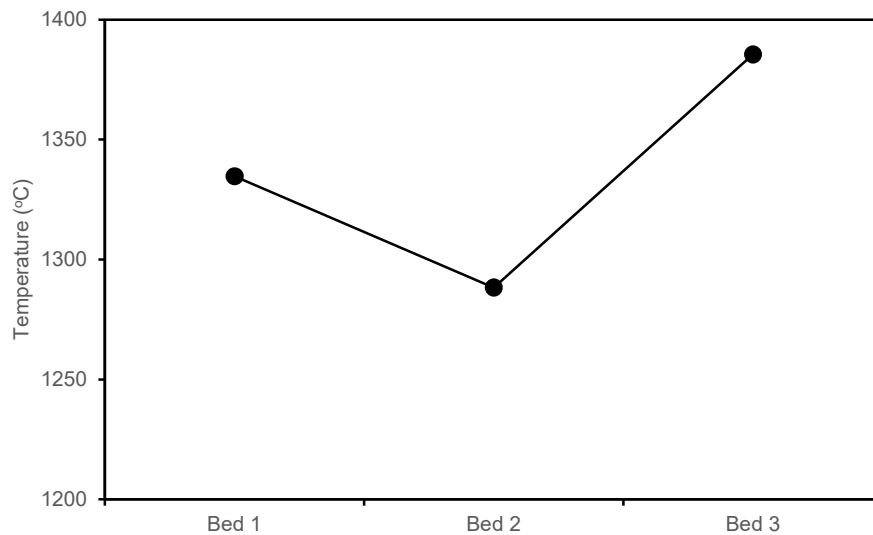
Figure 5.19 – Maximum sintering temperature for validation that shows the variability between three different sinter plant beds (3)

Figure 5.20 shows that the sinter produced during testing was similar after the initial observation and similar-sized sinter fractions and overall yield was obtained for all the sinter plant beds. The sinter generated was of similar chemistry, according to further XRF analysis of the sintered product. However, RDI analysis showed a modest rise in results for sinter plant bed 2 which exhibits the sinter quality produced. Figure 5.21 illustrates how the sinter product properties, including basicity, B3, glass ratio, and RDI results for the sinter plant and pilot-scale sinter rig follow the same trend and change for each bed simultaneously when increasing and decreasing.
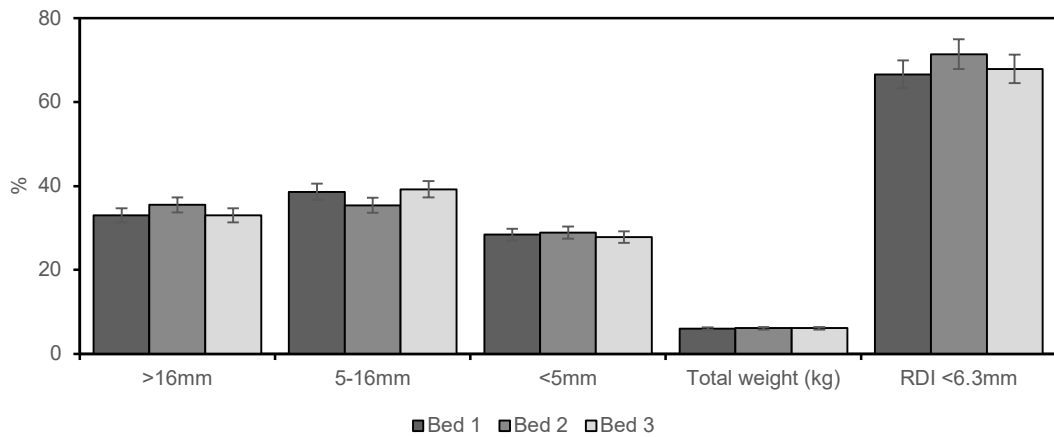
Figure 5.20 - Particle size distribution and RDI for validation for three different sinter plant beds (3)
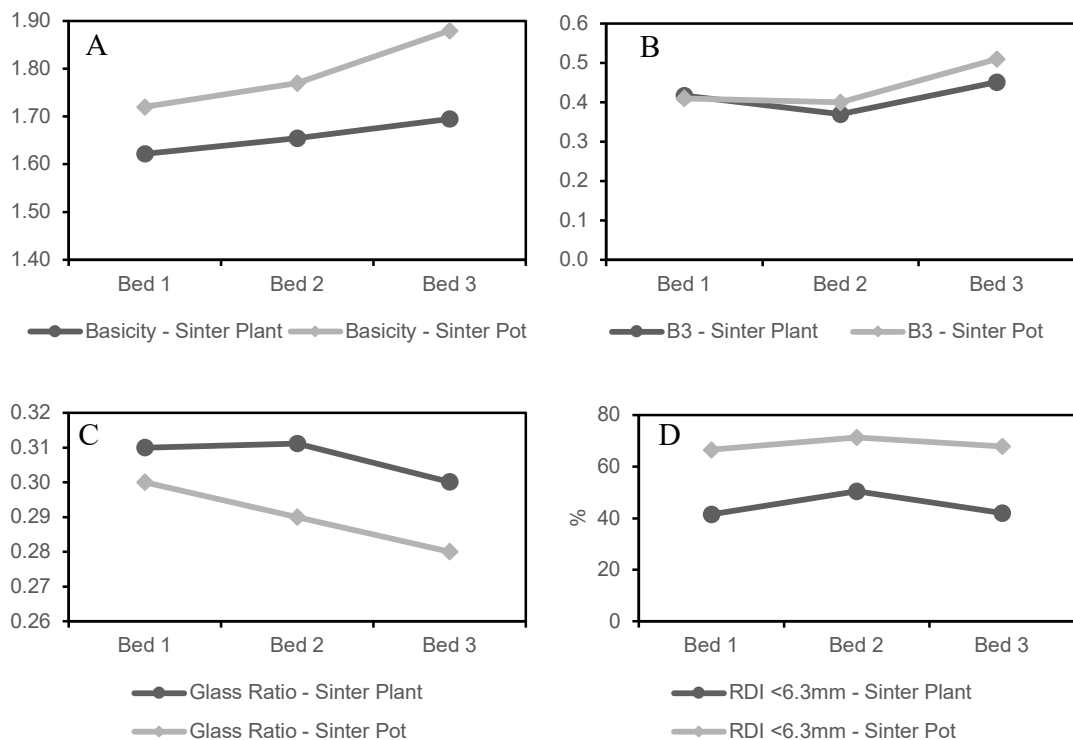
Figure 5.21 - Sinter product properties for sinter plant and pilot-scale sinter rig for each bed (top left to bottom right: a) basicity, b) B3, c) glass ratio and d) RDI for validation (3)

Figure 5.22 (a) indicates that Bed 2 has the highest total emission concentration compared to Bed 1 and 3, and Figure 5.22 (b) shows that bed 1 has the lowest chloride content and Bed 3 has the highest chloride content. This was intriguing because the number of recycled materials used in bed 2, which typically contains smaller particles and chloride, decreased by 3% but this highlights the importance of considering this during sinter plant bed making

as the NTLR was controlled at 1.6, 1.7 and 1.8 for each bed for this reason. When the NTLR increased due to the usage of more nuclei particles and fewer adhering particles in the sinter bed, the chloride content with the PM emissions across the beds was reduced. This was to be expected since each bed's predicted chemistry, which was based on the total number of raw materials particle sizes employed in the whole sinter bed, Na_2O reduced from 0.092, 0.082, and 0.069 %. To allow for a direct comparison of the PM emissions from the pilot-scale sinter rig to the sinter plant, the data from the south inlet CEMs are used which are located before ESP abatement on the sinter plant as the pilot-scale sinter rig is a non-abatement system, which explains why this CEM was chosen instead of post-abatement CEMs. Figure 5.23 demonstrates a distinct relationship trend between the PM emissions for the pilot-scale sinter rig and inlet CEMs and this can be a great tool for predicting future PM emissions from the sinter plant for each bed before it is used. Figure 5.24 demonstrates that the maximum off-gas temperature from the pilot-scale sinter rig has a similar relationship trend to the sinter plant's ESP abatement inlet temperature.
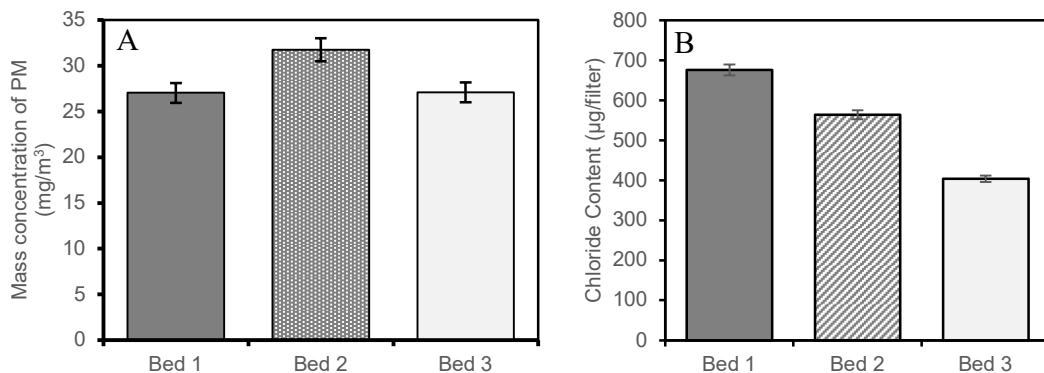
Figure 5.22 - PM emissions collected: (a) total emission concentration and (b) chloride content for validation (3) for three different sinter plant beds
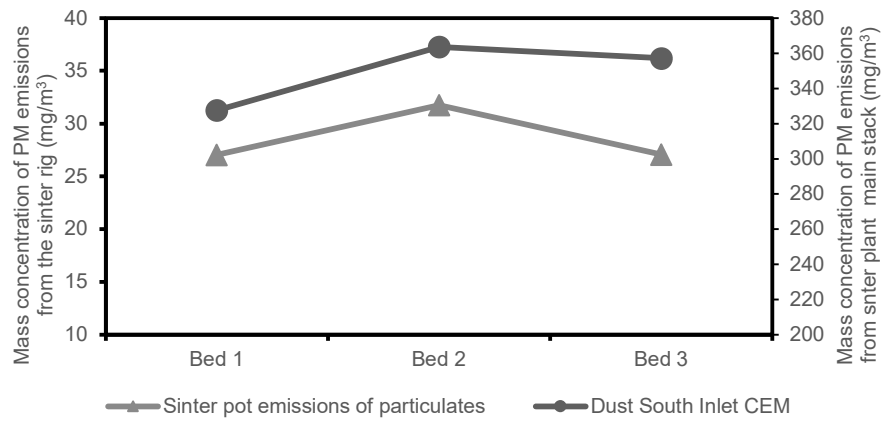
Figure 5.23 – PM emissions collected: relationship from the pilot-scale sinter rig PM emissions result with sinter plant main stack CEMs for PM emissions for three different sinter plant beds
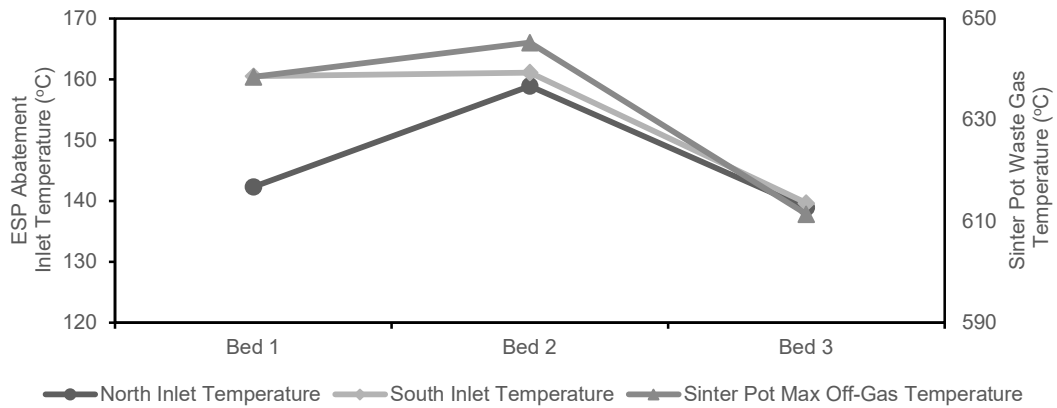
Figure 5.24 – Relationship between ESP abatement temperature with pilot-scale sinter rig wage gas temperature for validation (3) for three different sinter plant beds

Since it has never been feasible to quantify or analyse the return fines particulates before using a real sinter bed from the sinter plant on the pilot-scale sinter rig. Since it was commonly assumed by sinter experts that the return fines particulates consist of a raw mix that has fallen through and is repeatedly recirculated into the sinter plant, further research was done to determine the constitutes of the return fines particulates. As a result, it was possible to size and perform chemical analysis on each unique size fraction using a sample made from repeats of pilot-scale sinter rig bed 1. Figure 5.25 shows that bed 2 had a slight increase in return fines particulates of the sinter plant beds along with the highest PM emissions as previously shown. However, in terms of return fines particles, all sinter plant beds were comparable and similar. Figure 5.26 shows the composition of sinter bed 1 return fines particulates to be greater than 0.25 mm in particle size with over 83.5% (34%

0.25 mm, 30% 0.5mm and 19.3 >1mm). Figure 5.27 shows the chemical analysis of each size fraction and revealed that Na_2O, K_2O, and Zn increase as particle size decreases. This can prove to be useful in the future to remove unwanted smaller-size particles from the return fines particulates before they were recirculated back into the sinter plant. Contradicting evidence was seen as to what large pieces of sinter present in the return fines particulates was in Figure 5.28, demonstrating that sinter particles as well as raw mix were being recirculated back in the sinter plant. As a result of this finding, it has been found that return fines particulates were primarily sinter particles with a diameter of 0.25 to 1 mm shown also in Figure 5.26 previously, while smaller particles less than 0.25 mm were often raw mix with a high concentration of Na_2O, K_2O, and Zn and the effectiveness of the ESP abatement at the sinter plant would suffer as a result.
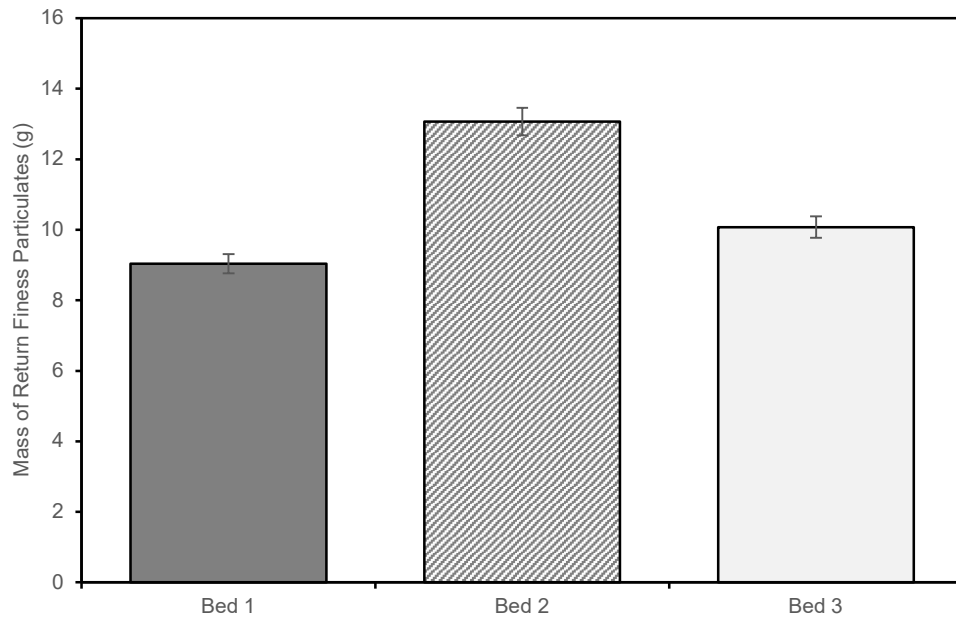
Figure 5.25 - Return fines particulates for validation (3) for three different sinter plant beds
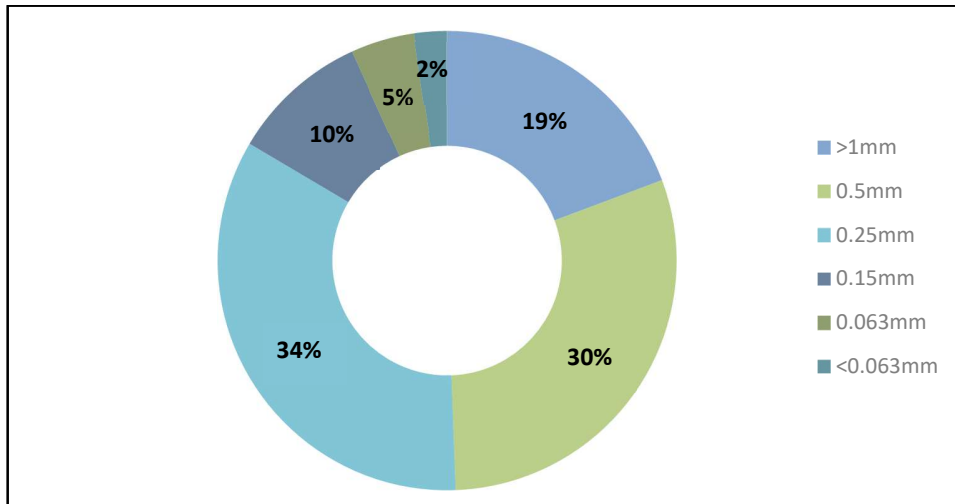
Figure 5.26 – Particle size fraction of composite of return fines particulates for pilot-scale sinter rig bed 1
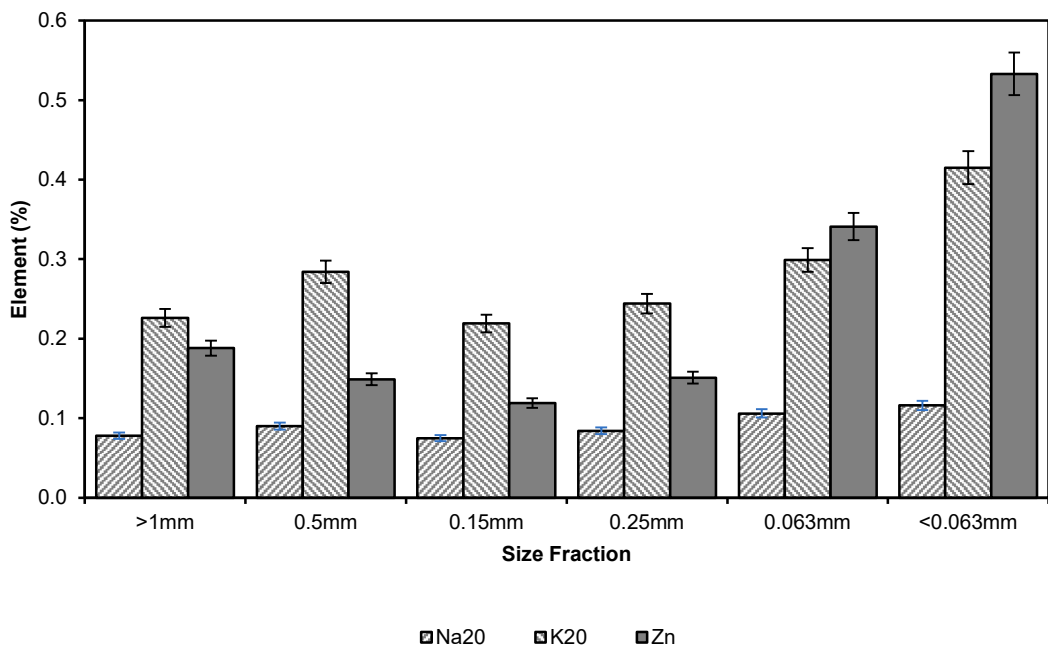
Figure 5.27 – Chemical analysis Na₂O, K₂O and Zn of the composite of return fines particulates for pilot-scale sinter rig bed 1
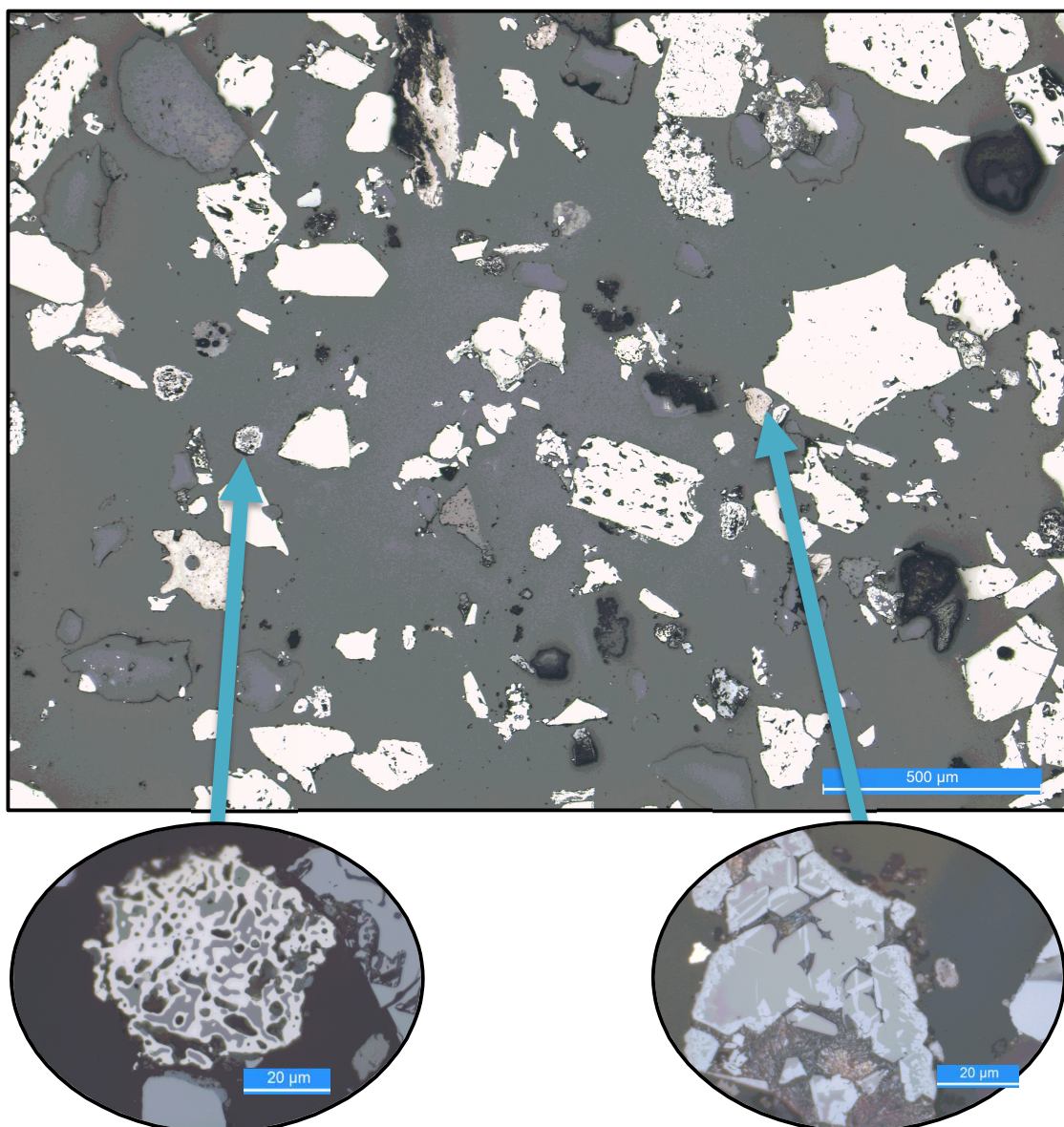
Figure 5.28 – Microscopy at x50 and x1000 magnification of return fines particulates from bed 1 for validation (3)

Summary

This validation study findings and discussions focused on the variance of the pilot-scale sinter rig with six identical tests. The variations were analysed with the raw mix, sintering process, product (quality), particulates (PM emissions and return fines from tray), and various post-analyses (including elemental and particle size distribution). This validates the pilot-scale sinter rig as an excellent tool to compare directly to the sinter plant A full-scale plant trial was successful and had an expected relationship between the PM

emissions collected from the pilot-scale sinter rig and an online pre-ESP abatement online CEMs from the sinter plant.

- The pilot-scale sinter rig can be successfully used as a tool to mimic the sintering operations of that of the sinter plant.
- To maintain a constant moisture level for each base mix, an ideal moisture study was required. To determine the blend's permeability with the least amount of variation, cold and hot permeability tests were conducted.
- Before each test, a green mix elemental analysis will be performed to make sure that all base blends were identical and have a small degree of variation.
- The flame front was stable, as there was little volatility in the sintering process, temperature profiles, sintered airflow, cooling rate, and combustion rate and has little deviation.
- The sintered product, PM emissions and return fines particles underwent post-analysis testing for elemental and PSD, and there was little variance.
- The use of the novel dust capture device was advised since it was suitable and appropriate due to the resulting minimum standard deviation from the validation experiment.
- When comparing the pilot-scale sinter rig to the sinter plant, process parameters and sinter quality followed the same trends.
- It has been demonstrated that it was possible to compare pilot-scale sinter rig PM emissions to the sinter plant's pre-abatement online CEMs as proven in this experiment.
- The NTLR was useful to consider along with the number of nuclei, adhering and non-adhering particles used in the sinter bed to minimise PM emissions along with the number of unwanted elements in the sinter bed.
- For the first time, the chemistry and size of the return fines particulates that were circulated at the sinter plant can now be studied and it was proven that the majority were larger particles that were sinter and with a small quantity of smaller particles that were raw mix which had unwanted elements attached.

5.3   Investigation and Optimising the Use of Micropellets in Sintering

From an operational perspective, micropellets have so far shown to be useful, although it is unclear how they will affect particulate matter (PM) emissions. Using a pilot-scale sinter rig and advanced characterisation, this study intends to measure the PM emissions output because of substituting micropellets during sintering while also investigating any usage restrictions and potential implications on the sintering process and the finished product.

Figure 5.29 shows the results of the Thermogravimetric analysis (TGA), where the Thermogravimetric and differential thermal analyses (TG DT) testing ends at 900 °C since nothing reacts after this temperature. Iron ore A and B micropellets were similar and more stable throughout the test. Figure 5.30 shows the X-Ray Diffraction (XRD) results where iron ore A and iron ore B micropellets were similar due to their hematite, quartz low and calcite materials. Recycled micropellets were different as K has been found which would be from electrostatic precipitator (ESP) dust and hydrocarbon which would be from flue dust. The x-ray fluorescence (XRF) analysis of the green mix showed that the blends were the same as the predicted blend model chemistry (Table 40) which was as anticipated, with blend 3 having the highest amount of K_2O as these micropellets were predominantly made from recycled materials with higher volatile elements due the higher chloride materials used the recycled micropellets.
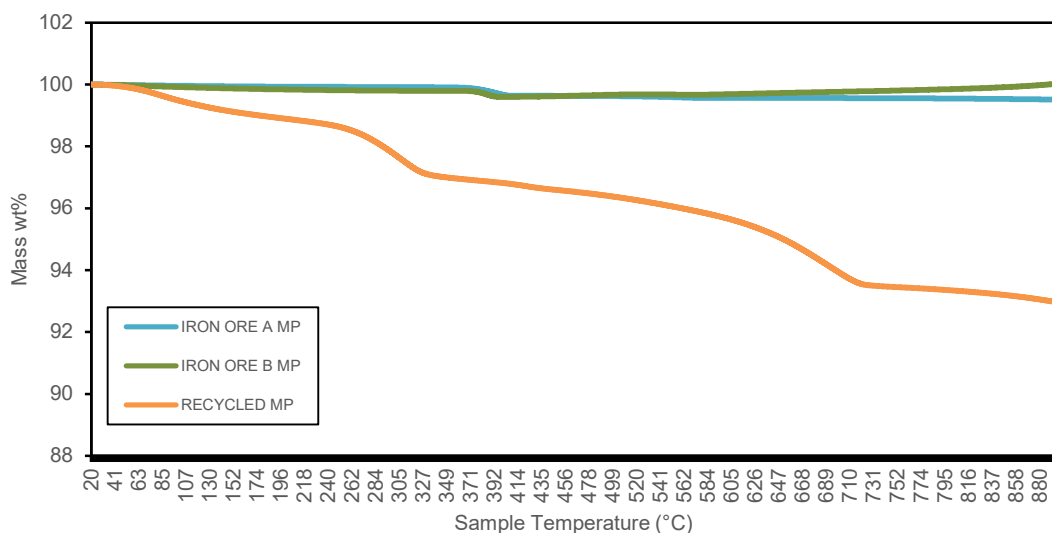
Figure 5.29 – TGA DT of iron ore A, iron ore B and recycled micropellets that highlights how numerous iron ores can react differently at various times
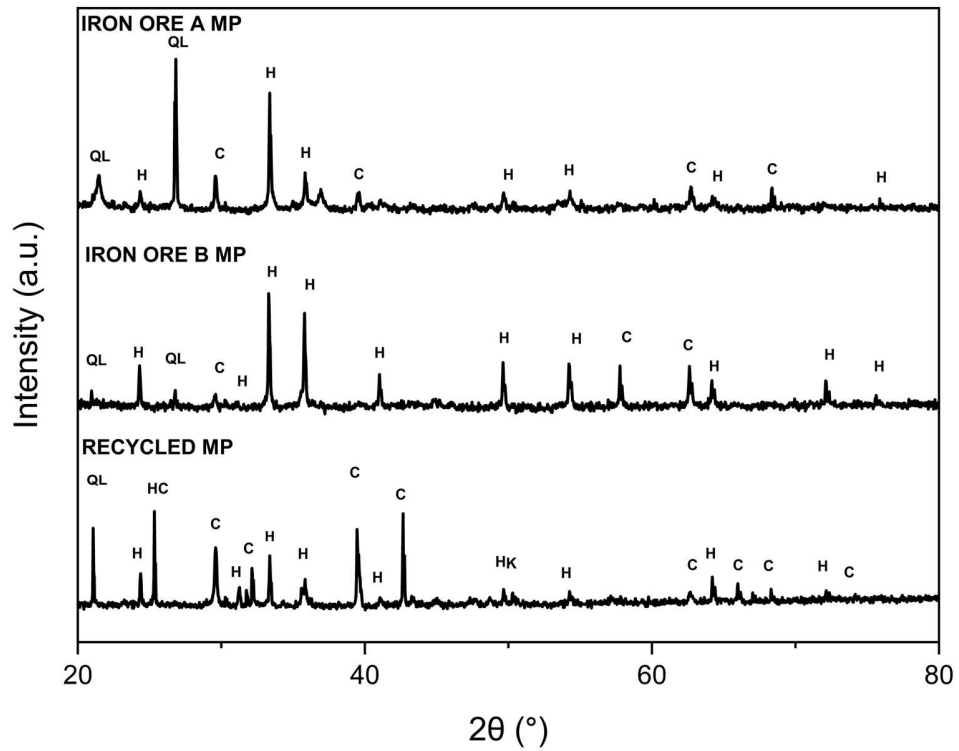
Figure 5.30 – XRD of micropellets QL = Quartz Low, H = Hematite, HC is a Hydrocarbon , C = Calcite with Mg, K = K or KCL, Ho = Holdenite

Table 40 - Green mix

Element (%)	Base blend (0% MP)	Blend 1 (3.63% Initial MP)	Blend 2 (7.27% Initial MP)	Blend 3 (3.63% Recycled MP)	Blend 4 (3.63% Iron Ore A MP)	Blend 5 (3.63% Iron Ore B MP)
SiO_2	5.44	5.37	5.42	5.53	5.94	5.78
Al_2O_3	1.12	0.6	0.63	0.83	1.05	0.89
TiO_2	0.060	0.08	0.08	0.090	0.134	0.089
CaO	6.69	7.89	6.17	8.06	9.75	8.05
MgO	1.16	1.44	0.83	1.41	2	1.39
Fe	46.36	45.1	49.14	49.83	46.39	47.54
Fe_2O_3	61.91	54.15	59.83	65.33	60.07	60.68
FeO	3.94	9.3	9.4	5.33	5.64	6.57
P	0.024	0.021	0.031	0.03	0.03	0.02
Mn	0.1	0.09	0.1	0.1	0.14	0.13
Na_2O	0.03	0.033	0.027	0.021	0.019	0.021
K_2O	0.06	0.039	0.024	0.041	0.028	0.031
Zn	0.006	0.009	0.006	0.001	0.001	0.002
Cu	0.001	0.001	0.001	0.001	0.001	0.001
Cl	0.008	0.013	0.011	0.009	0.008	0.005

The cold flow results, carried out before testing, show that the analysis of the cold flow through the sinter bed was carried out before testing shown in Figure 5.31 and the results showed that both the cold had increased, as would be expected given the increased use of micropellets. The use of larger particles and their quantity, which makes the sinter bed more permeable and allows for more oxygen to enter and can be attributed to the increasing oxidising reactions after ignition. The hot flow rate trends with the cold flow rate by increasing and decreasing sinter times. Figure 5.33 displays decreasing sinter times and Figure 5.32 shows an increasing hot flow rate, which illustrates a relationship between the two types of flow rates for base blend, blends 1 and blend 2. Blend 3 had the lowest cold flow rate when compared to blends 4 and 5 which can be explained by the increase of recycled materials that were typically hard to process which leads to smaller size particles within the micropellets due to difficulty when processing these recycled materials.
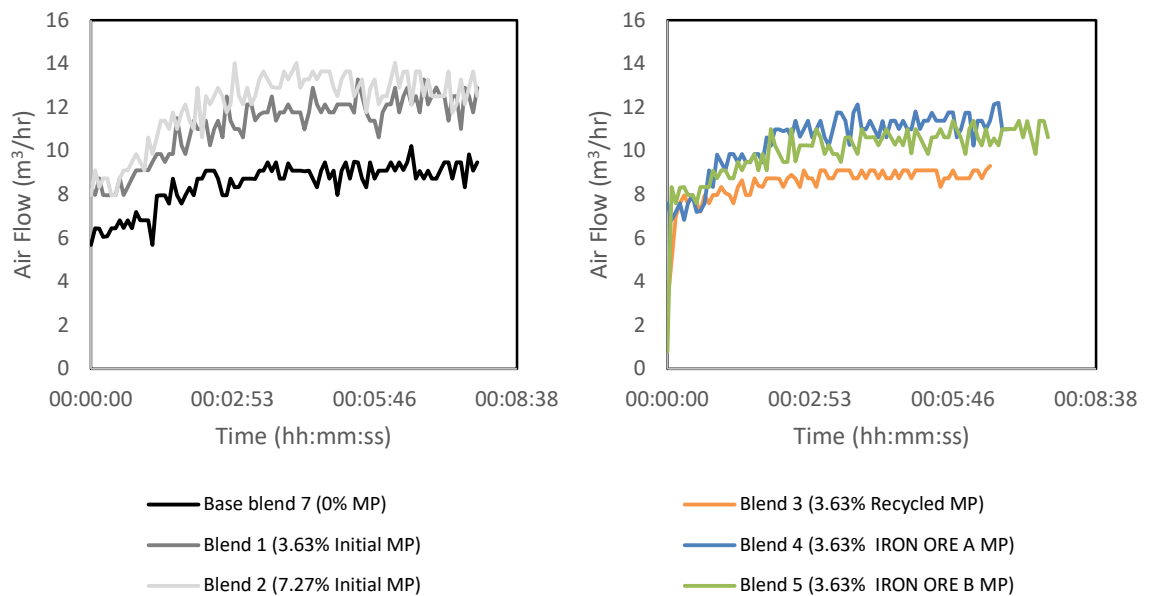
Figure 5.31 – Cold flow through the sinter bed for micropellets experiment for all blends
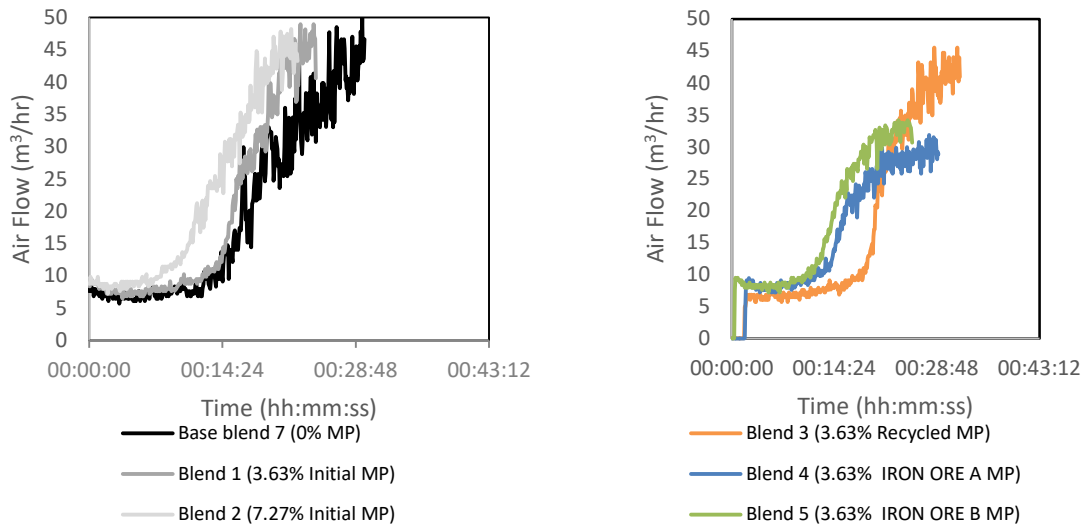
Figure 5.32 – Hot flow through the sinter bed for micropellets experiment for all blends
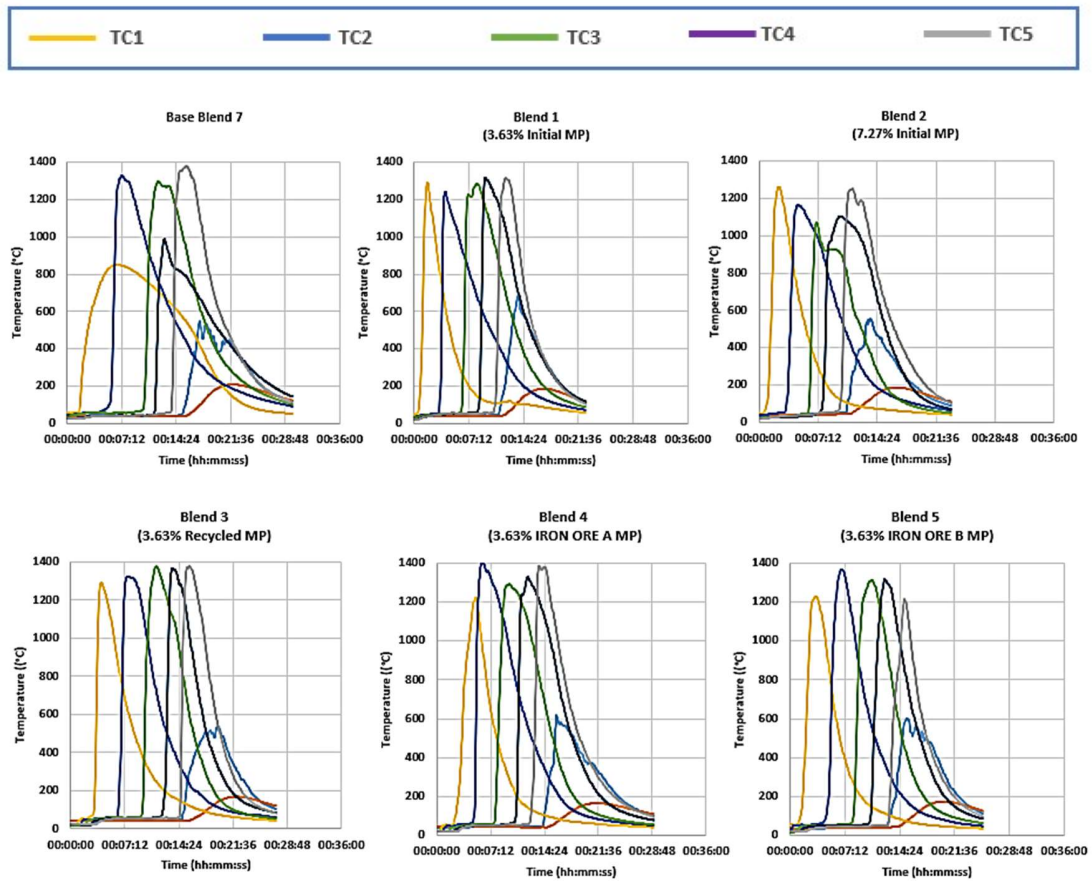
Figure 5.33 – Thermocouple temperature profile during the sintering process for micropellets for all tests

The addition of micropellets, in all variations and concentrations, decreased the overall test duration (excluding blend 3), stabilised the thermal profiles, and produced greater average and peak temperatures. This was evident in Figure 5.33 which displays the sintering profile and Appendix 6 which displays the process results. The blend 1 profile was far more stable throughout the test and exhibits more constant temperatures. The base blend tests typically took 30 minutes, whereas the other blends took less than 23 minutes (apart from recycled micropellets). With cold permeability air flows of about 13 m³/hr and 10 m³/hr, respectively, in blend 2 compared to the base blend, the increased airflow was about 33% higher in that test. Blend 3 did seem to be less consistent and steady, which would suggest that there was a limit for micropellets incorporation that, when crossed, negatively impacts the process or/and was not economically viable. The base blends thermocouple 4 test profile continues to take the longest time to sinter. In blend 2, thermocouple 4 had before now peaked and had cooled to < 1000 °C before the base blend had peaked. It is also worth noticing that the base blend had the lowest peak temperature of all tests at thermocouple 4.

Figure 5.34 – Observation of sinter product strength for micropellets from the pilot-scale sinter rig for 0%, 3.63% and 7.27% blends

After initial observations were made, the sinter produced during testing was analysed and noted to vary substantially. The base blend was discharged from the pilot-scale sinter rig chamber with a noticeably smaller particle size, as shown in Figure 5.34 by mechanical screening. The base blend exhibited the highest proportion of 5mm, which was close to twice the quantity observed in blends 1 and 2, indicating enhanced strength (Figure 5.35). Blends 3, 4 and 5 had a 10% increase in yield produced which would be highly beneficial

to the sinter plant due to an increase in productivity. Further analysis of the sintered product by XRF indicated it was clear that the two sintered products' chemistry barely differed from one another, as displayed in Table 41. When using any micropellets, RDI increased significantly when compared to the base blend, which may have contributed to the earlier observation of an increase in sinter strength.
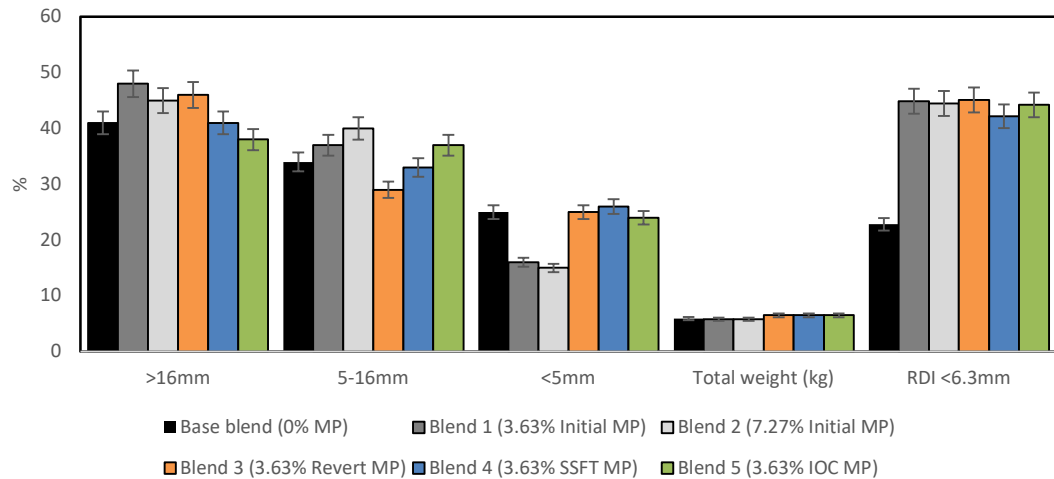
Figure 5.35 – Particle size distribution and RDI for micropellets for all blends

Table 41 - Sinter product chemistry for micropellets

Compound / Element (%)	Base blend (0% MP)	Blend 1 (3.63% Initial MP)	Blend 2 (7.27% Initial MP)	Blend 3 (3.63% Recycled MP)	Blend 4 (3.63% iron ore A MP)	Blend 5 (3.63% iron ore B MP)
SiO_2	6.19	5.91	6.32	5.84	6.42	6.39
Al_2O_3	1.16	1.1	1.06	0.95	0.96	1
TiO_2	0.170	0.1	0.08	0.080	0.11	0.11
CaO	10.09	10.66	10.22	10.02	10.35	10.09
MgO	2.04	2.05	1.92	1.8	1.76	1.8
Fe	55.13	59.27	53.16	55.61	53.24	59.44
Fe_2O_3	52.7	64.16	65.29	65.08	61.12	71.55
FeO	23.5	18.52	9.651	12.99	13.5	12.09
P	0.034	0.03	0.03	0.031	0.031	0.042
Mn	0.17	0.15	0.14	0.12	0.11	0.14
Na_2O	0.040	0.029	0.032	0.039	0.043	0.048
K_2O	0.065	0.028	0.041	0.037	0.036	0.034
Zn	0.011	0.005	0.008	0.005	0.004	0.005
Cu	0	0	0	0.001	0.001	0.001
Cl	0.003	0.002	0.001	0.001	0.001	0.001
Basicity	1.63	1.80	1.62	1.72	1.61	1.58
B3	0.36	0.36	0.32	0.32	0.29	0.30
Glass Ratio	0.32	0.30	0.32	0.31	0.33	0.33

Figure 5.36 is a LEICA microscope image of the sintered product for base blend, blend 1 and blend 2 and there were more SFCAs present within blend 2 compared to the base blend with an increase of 50 % to 69 %, also a decrease in primary hematite, and an increase of 5 to 16 % in magnetite when following the methodology previously mentioned in this thesis. It must be noted that these various phases have not been conclusively identified. This would account for the reason the RDI and sinter strength improved as the number of micropellets increased. When using micropellets in increasing increments, the PM emissions were reduced by more than half in Figure 5.37(a). This was reduced further when using optimised micropellets with the same composition in blend E. This agrees with previous research by *Ball et al* who showed by granulating for longer to create a more pellet-shaped blend, resulted in reduced dust emissions due to the increase in detachment forces needed to exceed the adhesion forces and this was also evidenced by *Debrincat et al*.[86] [43] Micropellets with greater recycled content in blend 3 have a slightly higher chloride content in PM emissions, as shown in Figure 5.37(b). Therefore, a rise in chloride levels would be linked to a rise in PM emissions. This follows previous research conducted by Gan *et al* where it was shown that it was possible to minimise PM emissions by controlling the distribution of recycled materials which enhances the removal rates of volatile elements.[90]
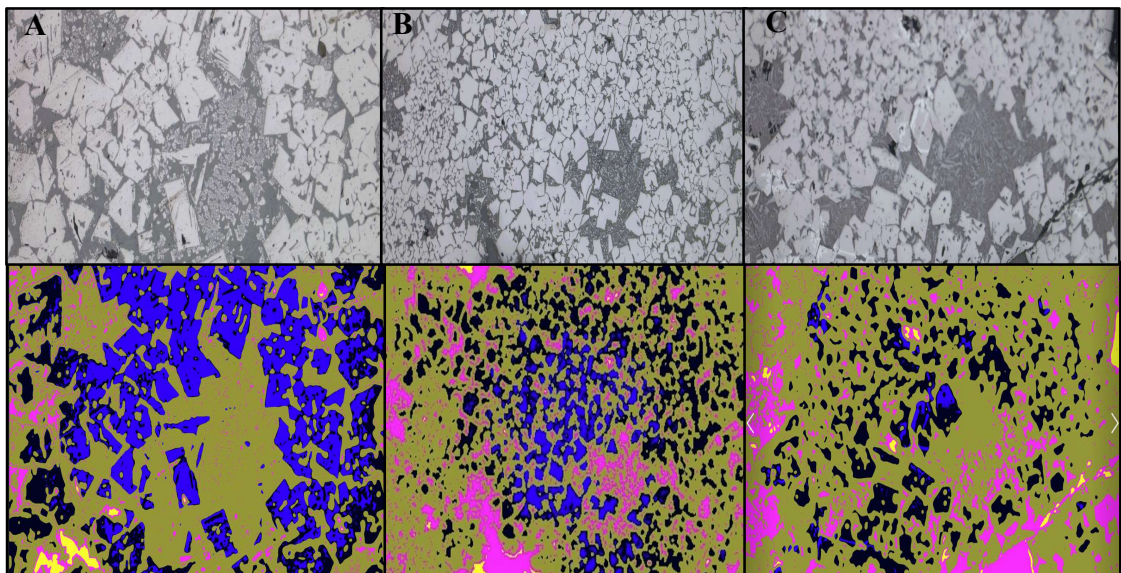
Figure 5.36 – Microscope images of sinter product at 1000x resolution (left to right, A - base blend, B - blend 1, C - blend 2) for micropellets. Colour scale: Purple-SCFAs, Blue-Primary haematite, Yellow-magnetite.
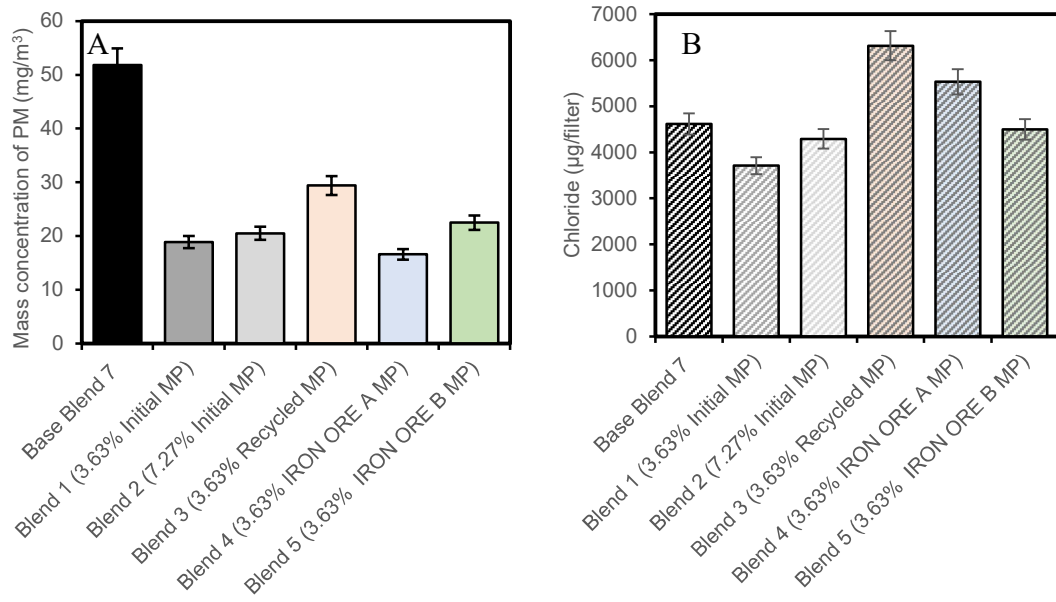
Figure 5.37 - PM emissions collected (a) total emission concentration (b) chloride content for micropellets for all blends

The filter has a specified particle retention of 1.6μm, suggesting that the dust in the PM_{10} and $PM_{2.5}$ categories was present. The electrostatic precipitator currently installed in the sinter plant was not an efficient capture method for such small PM emissions and literature states up to 80% of $PM_{10/2.5}$ was released from them.[77] $PM_{2.5}$ released from sinter plants has been found to consist of O, Fe, K and Cl, element, with trace amounts of Ca, Si and Al. [101] and heavy metals are naturally occurring elements that have a high atomic weight and a density at least five times greater than water [102]. The optimised micropellets in blends 4, 5, and 6 recovered more return fines (Figure 5.38a), resulting in a reduction in PM emissions that would otherwise be returned to the sintering process. Blend 1 and blend 4 have the highest quantities of trace metals and chlorides in the return fines, indicating that the chloride has been retained rather than released as PM emissions into the waste gas stream (Figure 5.38b).
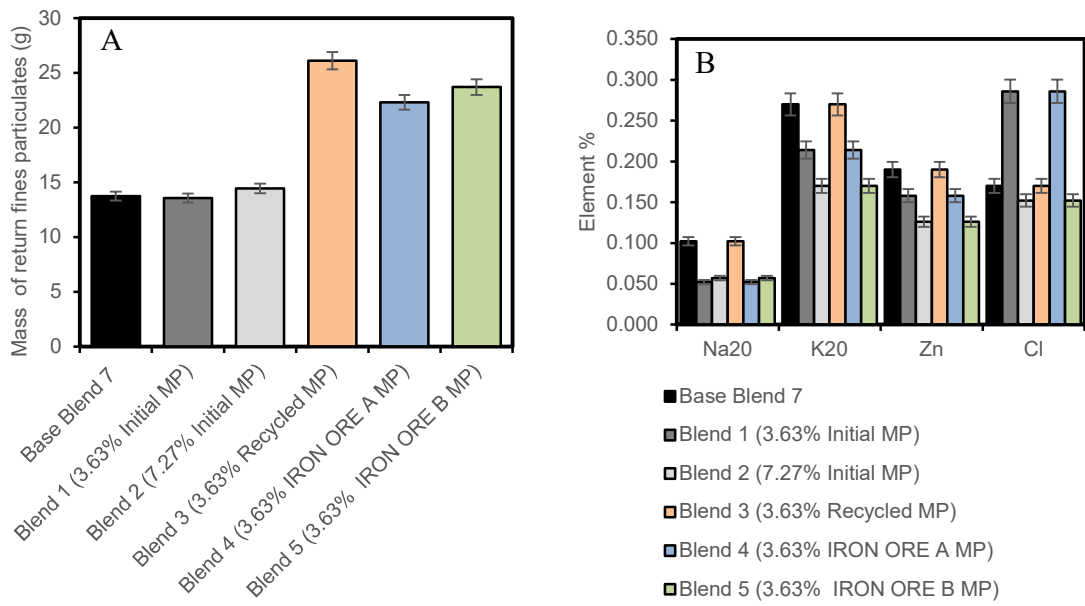
Figure 5.38 - Return fines particulates collected (a) total mass collected (b) trace metals and chloride content for micropellets for all blends

For the return fines particulates that were collected, the XRD results shown in Figure 5.39 the amorphous region from flue dust and BOS slurry were not present when using micropellets, as it was preserved in the sinter as revealed by an increase in Fe_2O_3 in the sintered product and this was demonstrated by the changing amount and peak height of hematite in the XRD. Layering or stacking (crystal orientation) may have contributed to this, but the XRF disproved this as the QL intensity was increasing which means the concentration was likely increasing.
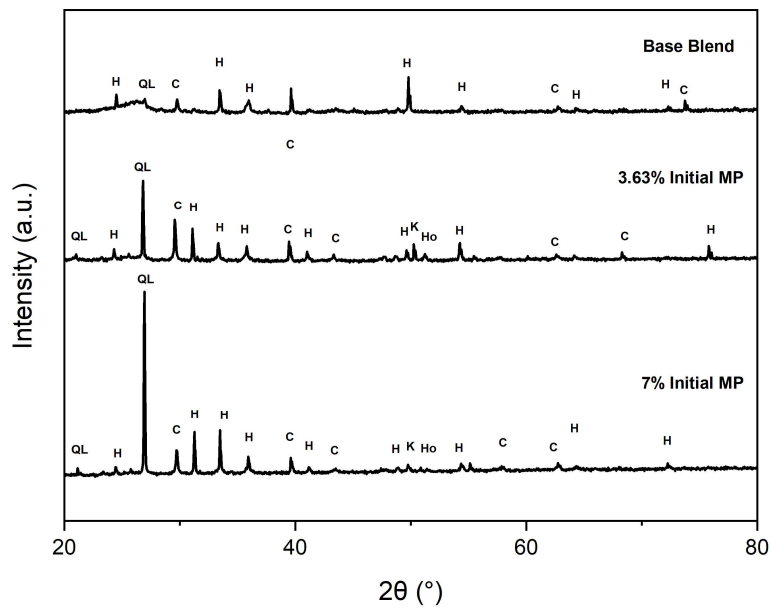
Figure 5.39 - Diffraction pattern of initial MP return fines (QL = Quartz Low, H = Hematite, HC is a Hydrocarbon C, Calcite with Mg, K = K or KCL, Ho = Holdenite) for micropellets

Figure 5.40 demonstrates a difference in the morphology of the return fines particulates, which may be caused by the inclusion of blend 3's finer recycled materials. When recycling the return fines particles back into the sinter plant, this contains the larger amount of K illustrated in Figure 5.38 and would have a significant impact on the sinter plant process and efficiency of the ESP abatement. According to these findings, the sinter plant's permeability was improved by the addition of micropellets, allowing heat to move through the sinter bed more quickly and in turn, can improve productivity due to this. Increased use of micropellets causes a distinct change in the morphology of particle sizes, as seen in Using another technique in SEM which is shown in Figure 5.41, this highlights that particle sizes increased, indicating that smaller particles were trapped in the sinter bed and were unable to escape into the flue gas to be emitted as PM emissions. These micropellets blends have drawbacks despite enhancing small fine output and lowering PM emissions, as they were expensive to produce. Iron ore concentrate, an ultrafine form of iron ore, can be used instead of iron ore micropellets since it has a cheaper production cost and generates fewer PM emissions. Overall, the micropellets containing iron ore B, (instead of iron ore A) produced from an iron ore concentrate, appear to be the most advantageous choice for a sinter plant due to the cost associated with inexpensive iron ore concentrates.
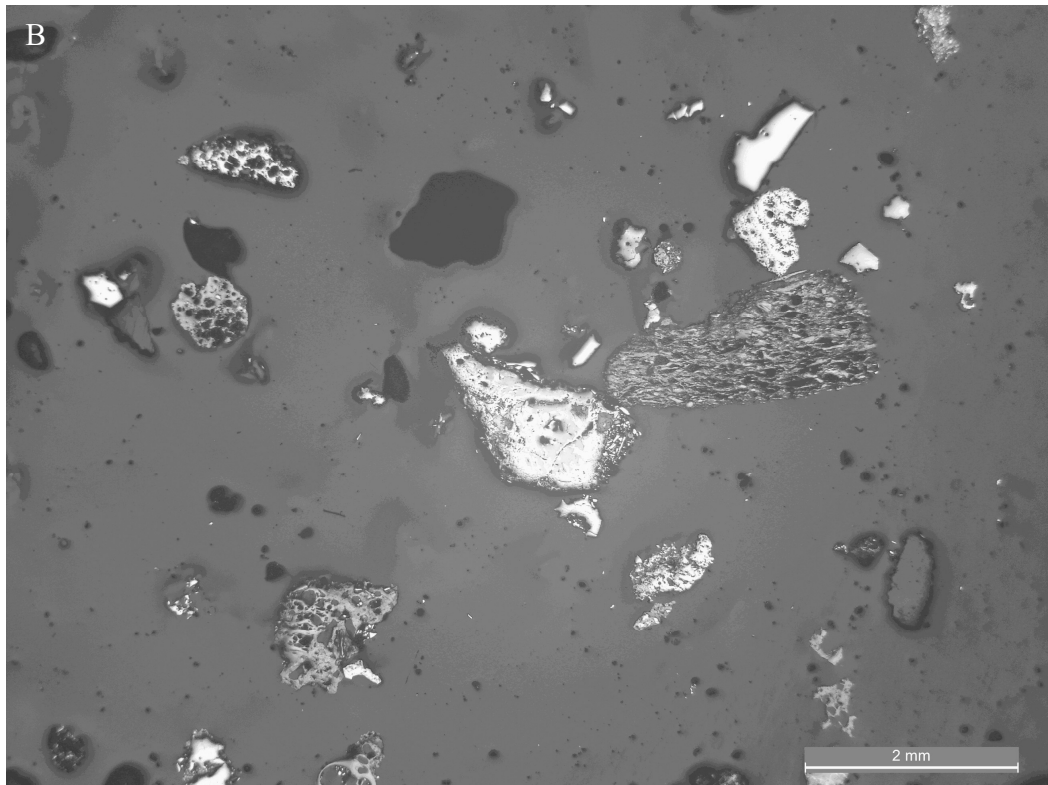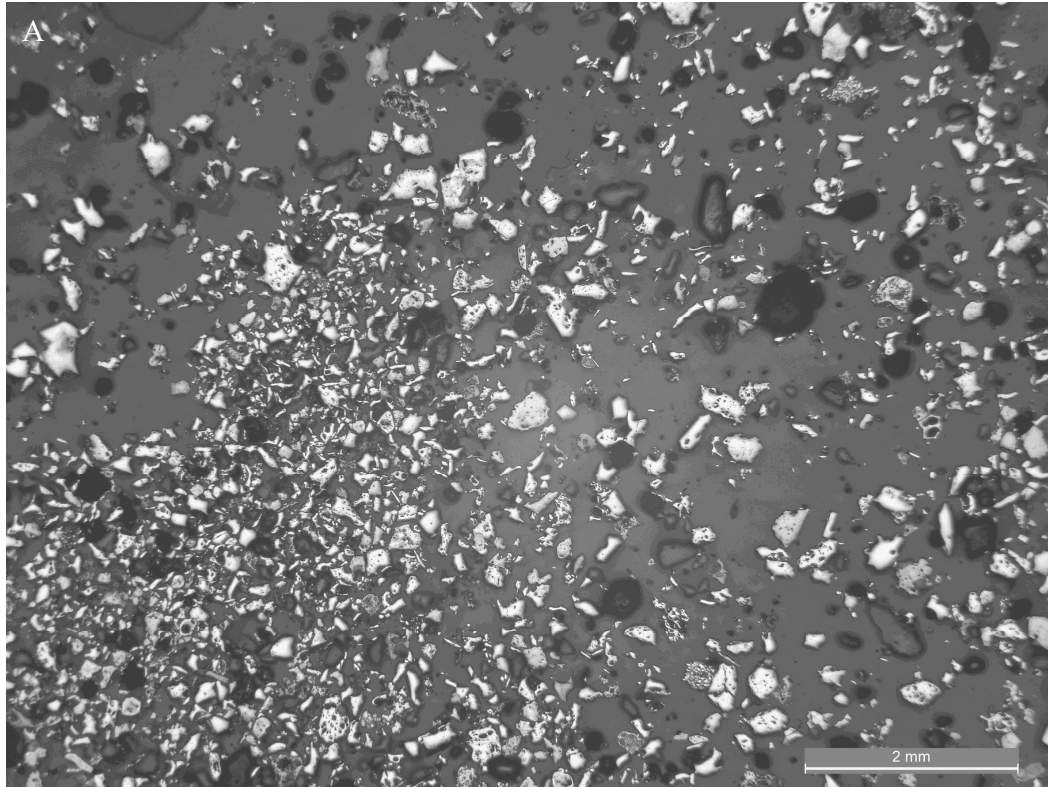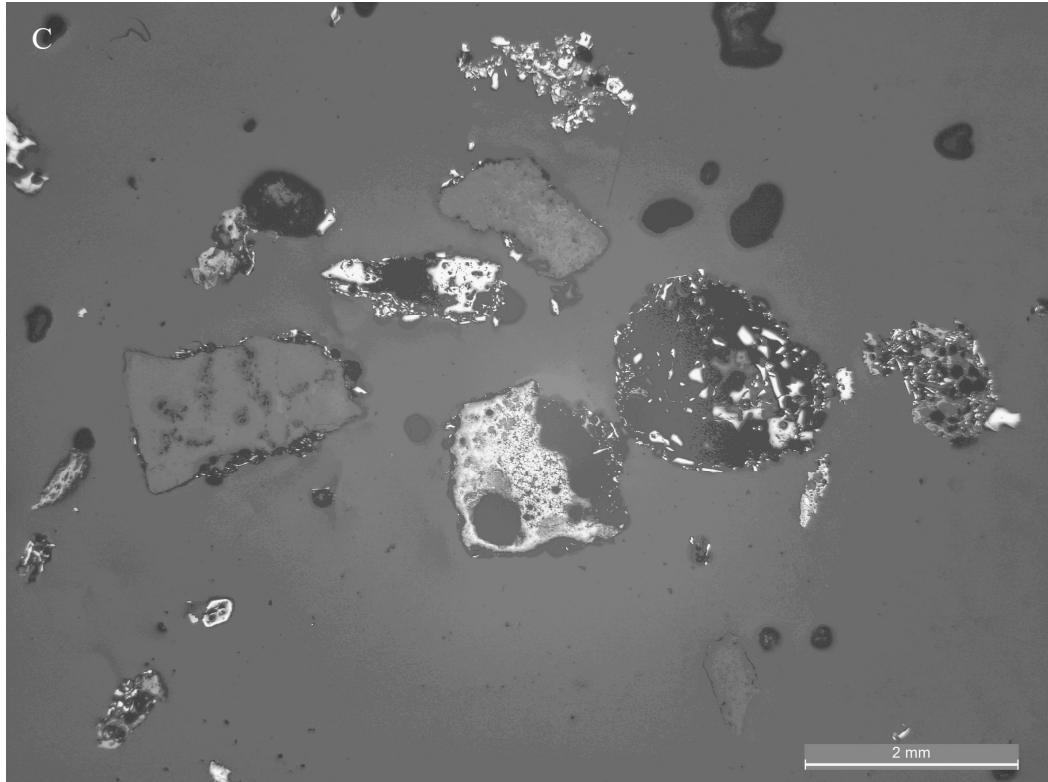
Figure 5.40 - Leica microscope images of return fines particulates 2x 200 500x (top to bottom: A - blend 3, B - blend 4, C - blend 5) for micropellets
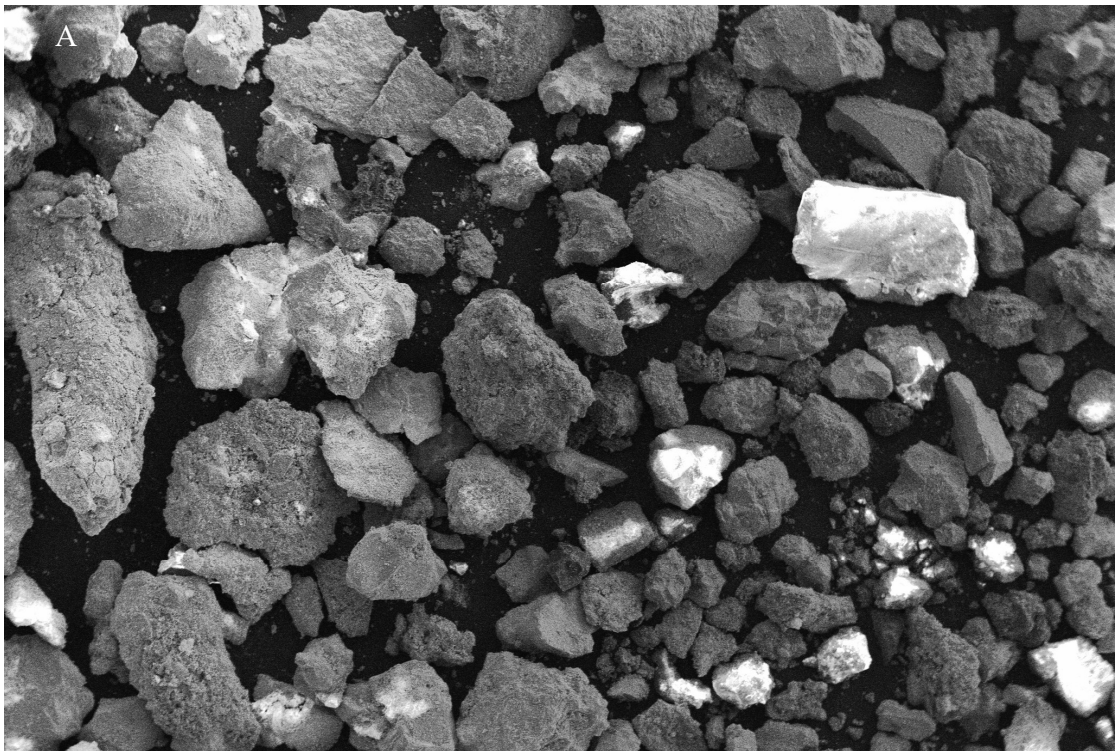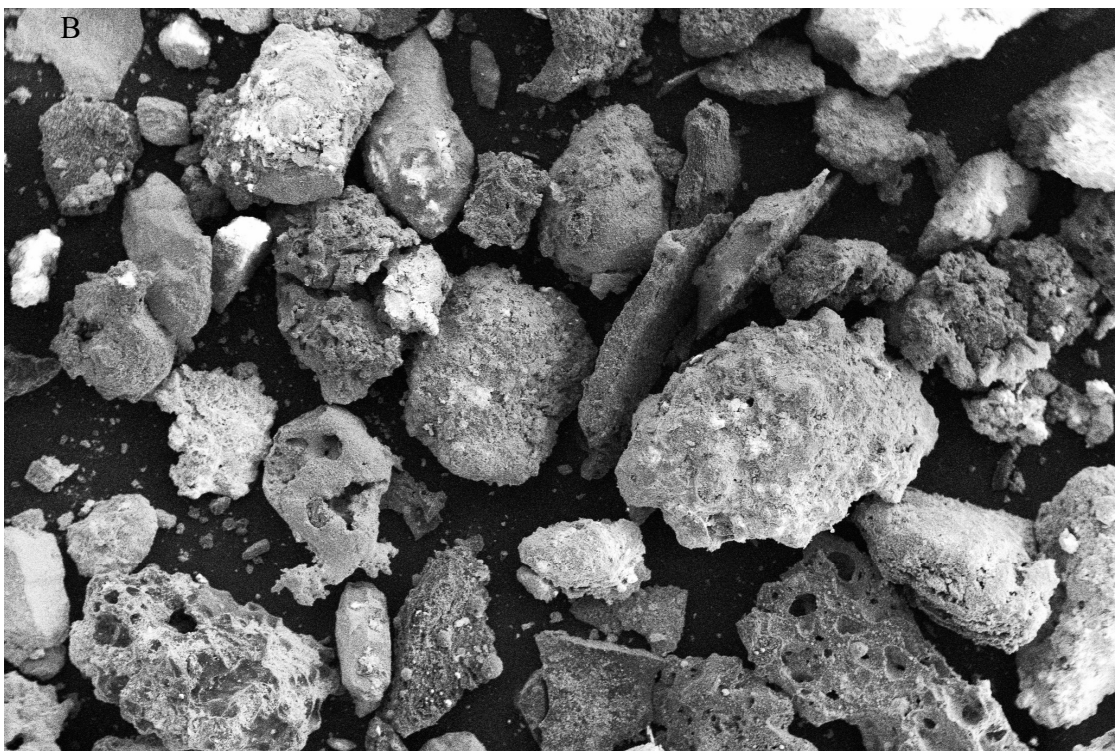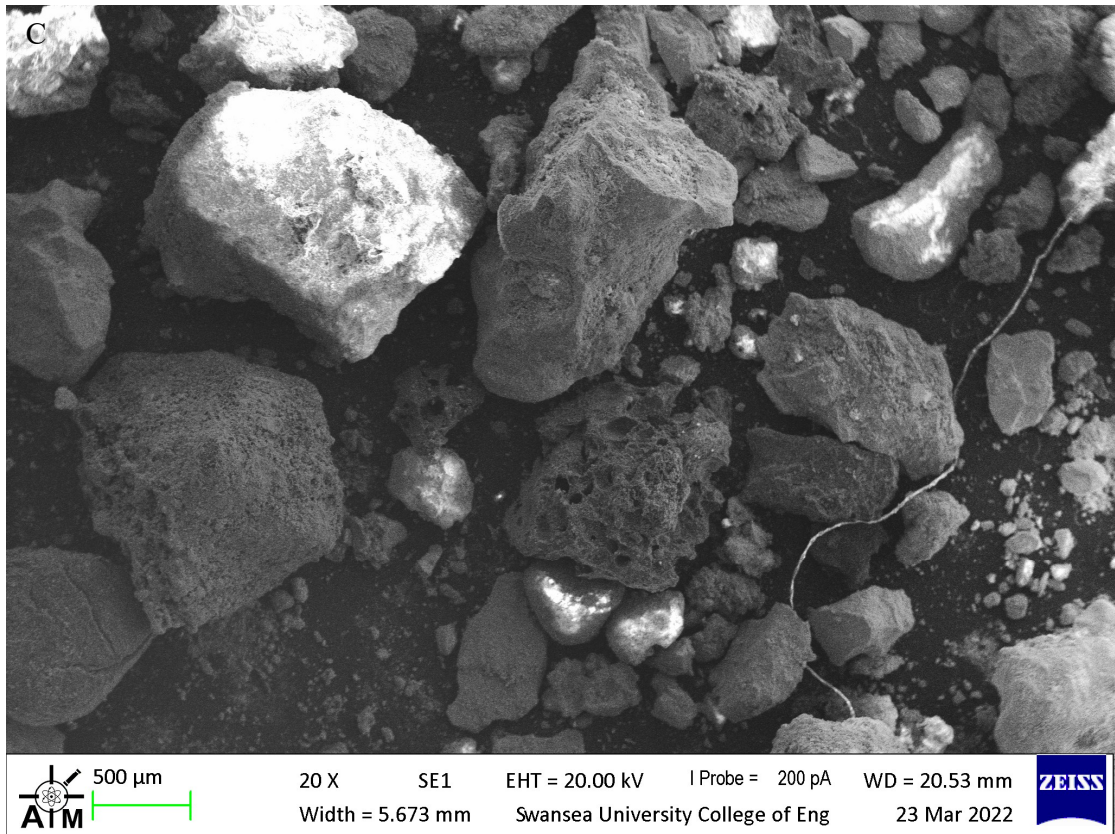
Figure 5.41 – SEM images of return fines particulates (top to bottom: A - base blend, B - blend 1 and C - blend 2) for micropellets

Summary

- The addition of micropellets improved the stability of sintering thermal profiles.

- Improvement in micropellets processing produced more homogeneous micropellets.

- The sintered product indicated that the addition of micropellets in the blend increased strength. This was evident before particle size distribution (PSD) testing as the sinter had larger pieces after discharging from the pilot-scale sinter rig. After mechanical sieving, the quantified PSD data again supported this, with fewer fine particles when compared to the base blend.

- All micropellets additions dramatically reduced PM emissions. However, applying recycled materials wisely can increase the particle release and the detachment force needed as less volatile trace elements were entrained into particulate matter.

- The return fines particulates from blends 1 and 4 have the highest concentrations of trace metals and chlorides, but they also have the lowest particle emissions, suggesting that the chloride has been held rather than emitted as PM emissions.

- It was found that increased micro-pellet content in sinter blends decreased the average particulate size and reduced the amount of fine PM emitted to the air due to them being held in the micro-pellet and the return fines.

5.4 Investigating the Effect of Chloride and Removal of Chloride by the washing of a Revert Material

The aim is to evaluate the hypothesis that introducing chloride can impair the process and/or sinter quality due to the element's high volatility using chloride-focused tests that were created for this purpose because it is already known to affect the efficiency of the electrostatic precipitator (ESP) abatement and to examine how much of the additional chloride added is released as particulate emissions (PM) emissions. The sintering process and sinter quality are expected to improve as well as the PM emissions and the efficiency of the ESP abatement at the sinter plant to minimise PM emissions if a considerable amount of the chloride from the ESP dust is removed through washing[100].

5.4.1 Addition of Potassium Chloride at Controlled Increments Study

Figure 5.42 shows the cold flow rate results which were similar for all test blends (base blend 1, blend 6, blend 7 and blend 8). The average cold flow rates ranged from 11 to 11.9 m^3/hr which indicates a homogeneous and stable blend and that the addition of KCl trim had no effects on cold permeability. The temperature profiles from the tests performed in increments of 0, 200, 400, and 600 Cl mg/kg was shown in Figure 5.43. It was clear that every thermal profile was uniform across all blends. The thermocouple traces began to rise and peak one after the other gradually. The off-gas thermocouples also began to rise and peak one after another. This demonstrated that, for all experiments performed, the flame front spread steadily down the rig until it finally diminished into the gas stream at the bottom of the rig. This demonstrates that the sintering process was unimpacted by the addition of a KCl trim at all increments. Appendix 7 displays a further indication that the blends were uniform and similar as the sintering maximum temperatures and sintered air flow were identical and were within the standard deviation of the repeatability.
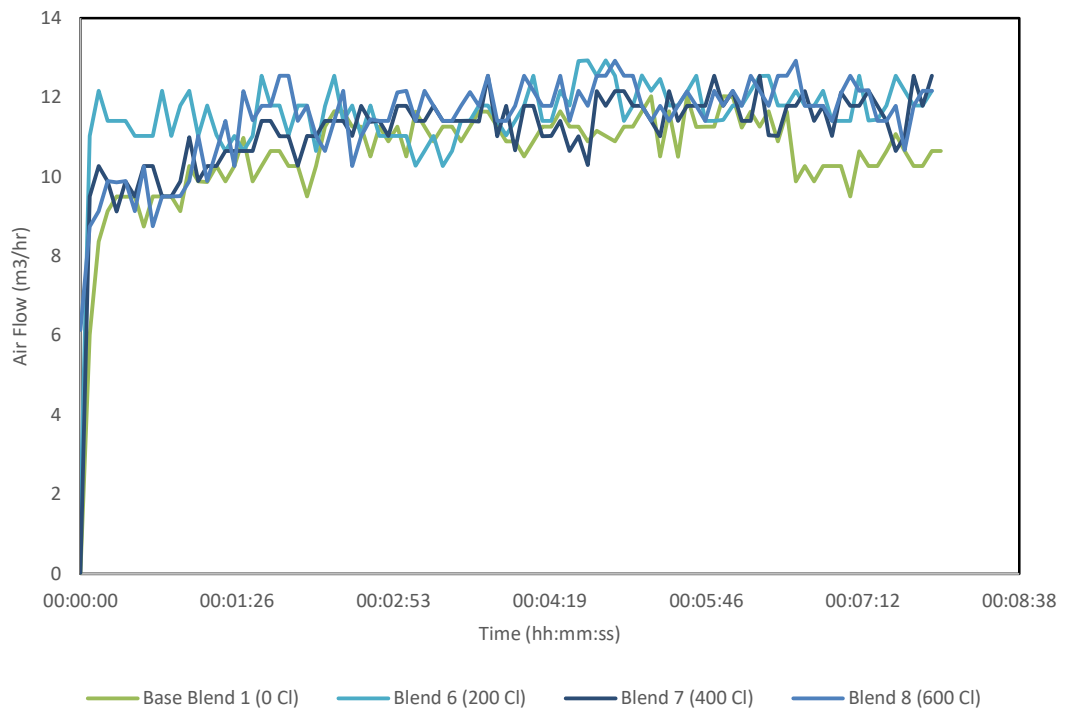
Figure 5.42 – Cold airflow through the sinter bed for the addition of KCl for each blend ranging from 0, 200, 400 and 600 mgC/kg
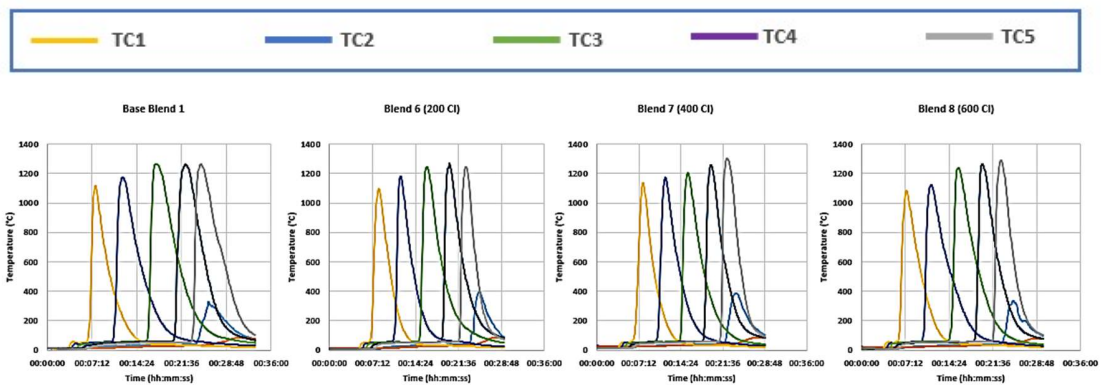
Figure 5.43 - Thermocouple temperature profile during the sintering process for the addition of KCl for each blend ranging from 0, 200, 400 and 600 mgC/kg

It became clear from analysing the XRF data that there was little chemical variation in the sintered product as indicated by the consistency of the properties of B2 basicity, B3 and glass ratio results (Figure 5.44). This was as expected as the KCl trim in theory does impact the iron oxide formation as it is highly dependent on the thermal conditions. The total yield of the sintered product was 6 kg for all the test blends shown in Figure 5.45 and

this was expected as suitable sintering temperatures were attained. as Figure 5.46 shows an increase in K_2O as the KCl trim was added across all the blends for the sintered product. However, this was minuscule and only a trace amount concerning the quantity of KCl retrained in the sintered blend.
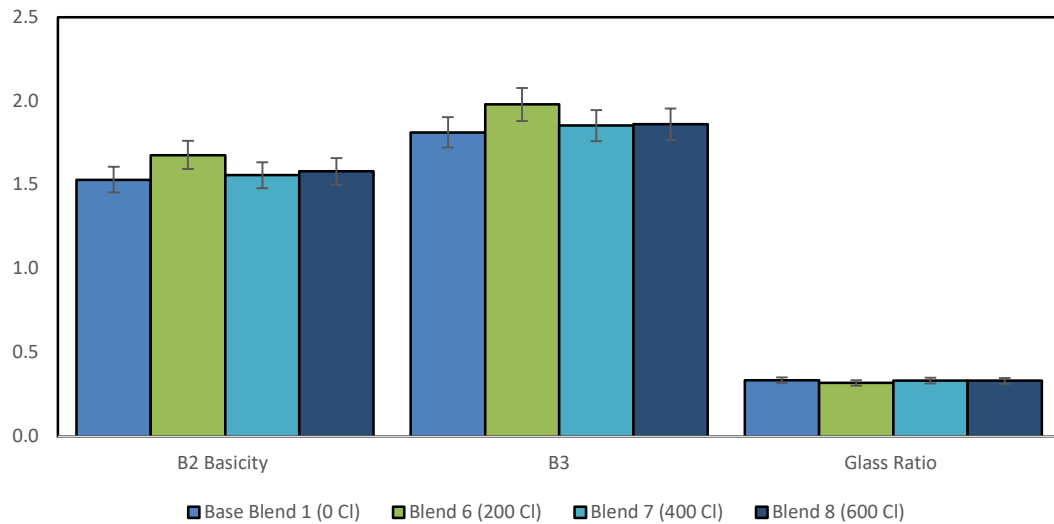
Figure 5.44 – Sinter product properties for the addition of KCl (unitless)
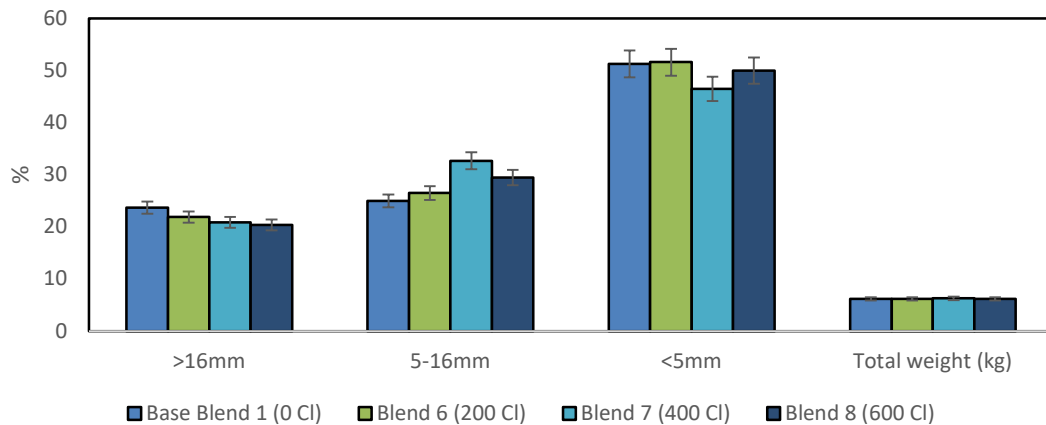
Figure 5.45 – Size fraction and total yield for the addition of KCl for each blend ranging from 0, 200, 400 and 600 mgC/kg
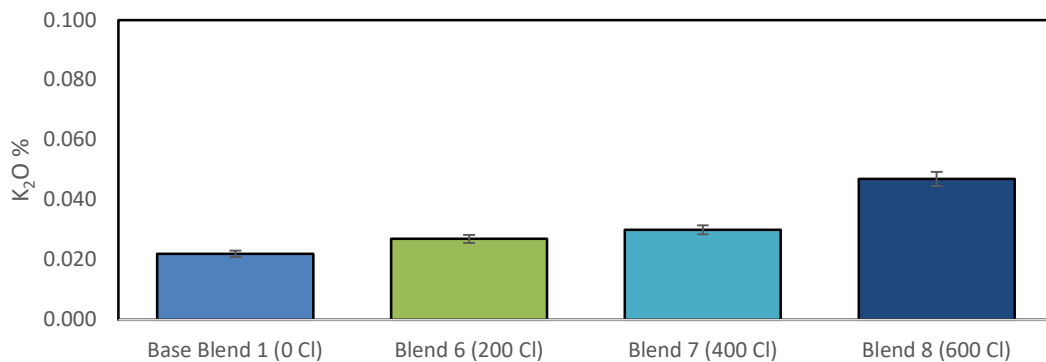
Figure 5.46 – K₂O content of sinter product for the addition of KCl for each blend ranging from 0, 200, 400 and 600 mgC/kg that shows a steady increase

The filters displayed in Figure 5.47 revealed an increase in the discolouring of the PM emissions on the filter after each test and visually looks fewer PM emissions on the filter but this was not the case and this was proven to be chloride particles as indicated in Figure 5.48 (b) which influenced this discolouring effect, and this would be due to smaller size particles of KCl which were more easily released in the waste gas stream. Total PM emissions are shown in Figure 5.48 (a) as the increments of KCl trim were increased, the PM emissions increased showing a clear exponential correlation relationship highlighted in Figure 5.49 with an R^2 of 0.988. This proves there was a clear chloride transformation path where the chloride particles can be easily released during sintering which in turn increases PM emissions. This was observed in previous research by Debrincat *et al* which during experimental sintering on a pilot-scale rig showed that most PM emissions had a size of <1.18 mm, indicating that it comes mostly from the adhering fines layer of particles, in which the KCl particles were present.[43] The chloride transformation path was fully saturated at 400mg/kg as the chloride content in total emission concentration of PM emissions significantly increases with 400 and 600 mg/kg of KCl addition in Figure 5.48 (b). This follows the research by *Peng et al*, who determined that K was the second most abundant element in sintering dust on a pilot-scale sintering rig and showed by chemical analysis that increasing KCl will have a significant impact on PM emissions.[100]

Figure 5.47 – Discolouring of filter (left to right: base blend 1, blend 6, blend 7 and blend 8) for the addition of KCl
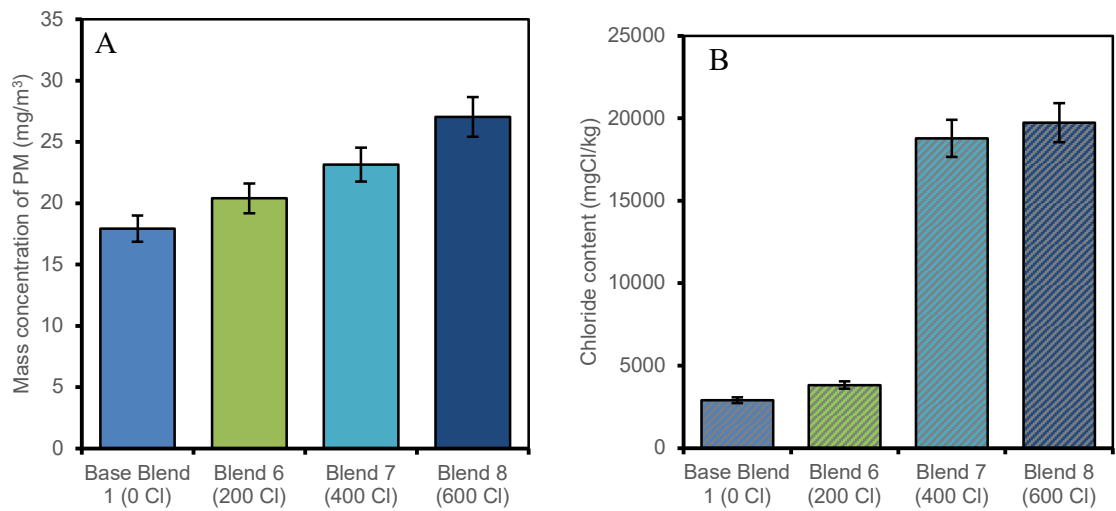
Figure 5.48 - PM emissions collected: (a) total emission concentration and (b) chloride content for the addition of KCl for each blend ranging from 0, 200, 400 and 600 mgC/kg and shows an increase of PM emissions with each addition of KCl.
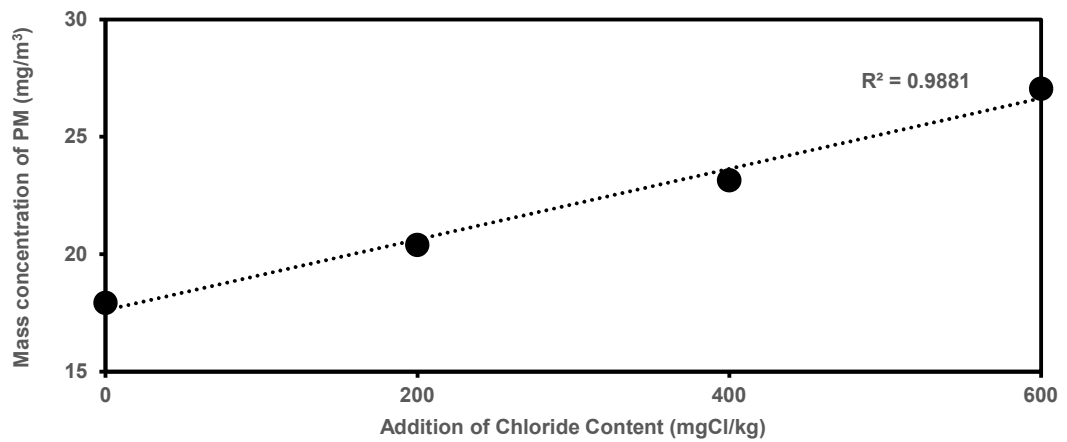
With the addition of KCl trim, PM emissions rise; nevertheless, the return fines particulates total mass collected decreases, as shown in Figure 5.50. This demonstrates that the chloride is emitting PM emissions into the waste gas stream rather than being trapped inside the moist layer of mix or bound to any other larger particles to be deposited in the tray as return fines particulates. Figure 5.51 highlights that as the return fines particulates decrease with the addition of KCl trim, a larger size fraction of the return fines particulates was produced. This demonstrates that the smaller particles (<0.63mm) were being emitted into the waste gas as PM emissions through the chloride transformation path. Figure 5.52 (a) shows that heavy metals and chloride content also increase within the return fines particulates, where Fe decreased, Figure 5.52 (b). However, it was vital to keep in mind that this was in proportion to a lesser quantity of return fines particulates of the total mass collected decreased. Chlorides enter the waste gas system as alkaline metal chlorides that were volatilised and react together at the end of the sintering process where the fines of iron ores were less prone to be volatilised and therefore fall through return fines particulates. The chemistry was distinct because KCl and Na, for example, were driven out as vapours and condensate with particle sizes ranging from 2.5 to 0.01 microns, whereas other finer particles were coarser, ranging from 2.5 to 10 microns, with a different mechanism to the waste gas system.
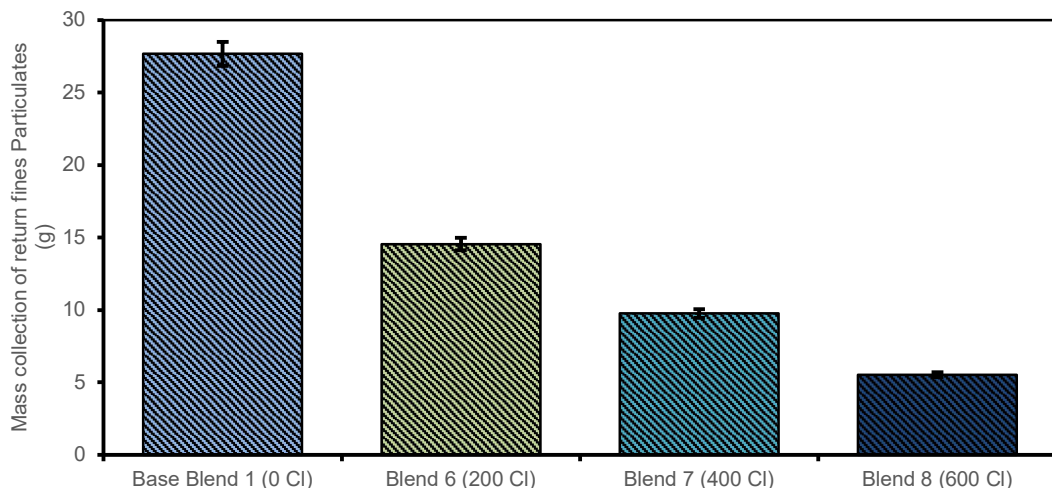
Figure 5.50 - Return fines particulates of the total mass collected for the addition of KCl for each blend ranging from 0, 200, 400 and 600 mgC/kg and shows a decrease of KCl in the return fines particulates.
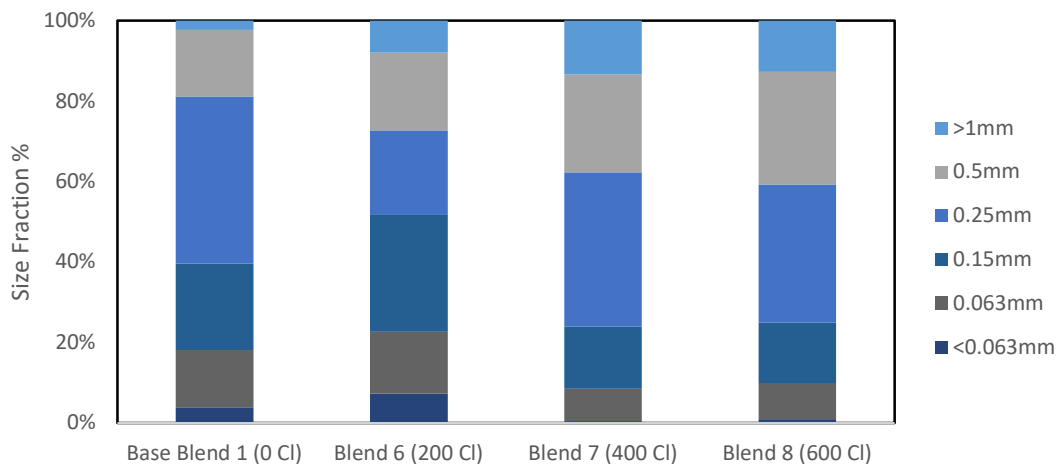
Figure 5.51 - PSD of return fines particulates for the addition of KCl for each blend ranging from 0, 200, 400 and 600 mgC/kg
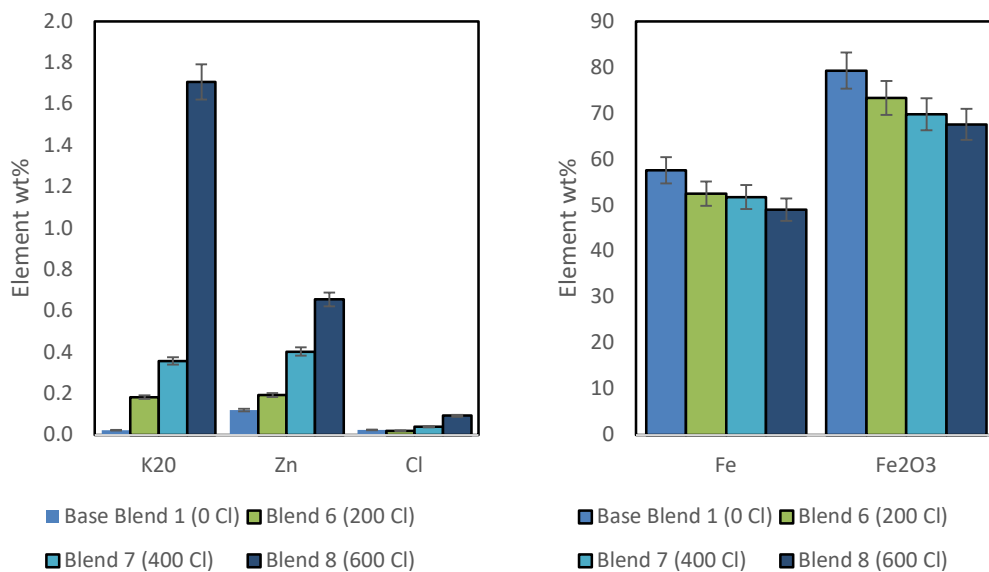
Figure 5.52 – Chemical analysis of return fines particulates (a) and (b) for the addition of KCl for each blend ranging from 0, 200, 400 and 600 mgC/kg

The number of measurable PM emissions and average size for the addition of KCl was shown in Figure 5.53 and displays that the average particle size in the blends decreases and the number of measurable PM emissions increases as the amount of KCl added rises.

The smallest average particle size was 190 μm in blend 8 and is displayed in Figure 5.54. This demonstrates that there was an excess of small particles from the KCl addition and that it is present everywhere, including in PM emissions, return fines, and some even persisting in the sintered product, as previously demonstrated. EDS results shown in Figure 5.55 indicate Fe in high concentration in areas of the sample and S in high concentration in the areas where Fe was low. Cl was uniformly distributed across the sample area, except for a small, constrained region where it was highly concentrated.
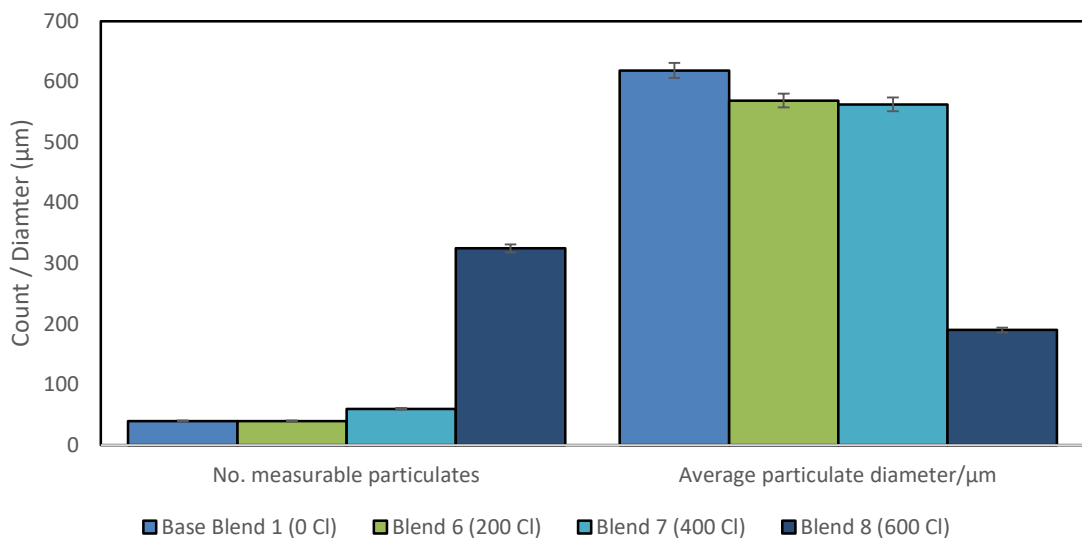
Figure 5.53 – Number of measurable PM emissions and average size for the addition of KCl for each blend ranging from 0, 200, 400 and 600 mgC/kg
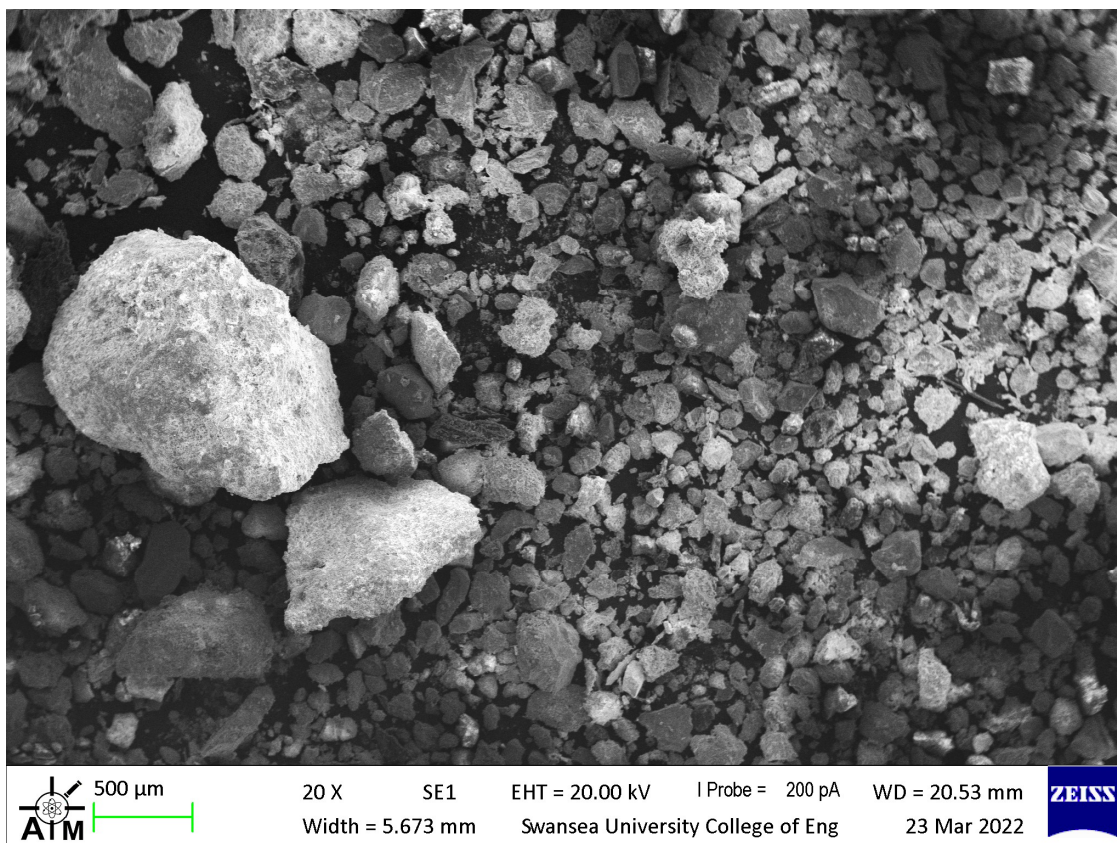
Figure 5.54 – SEM image of Blend 8 (600 Cl) at 20x magnification for the addition of KCl
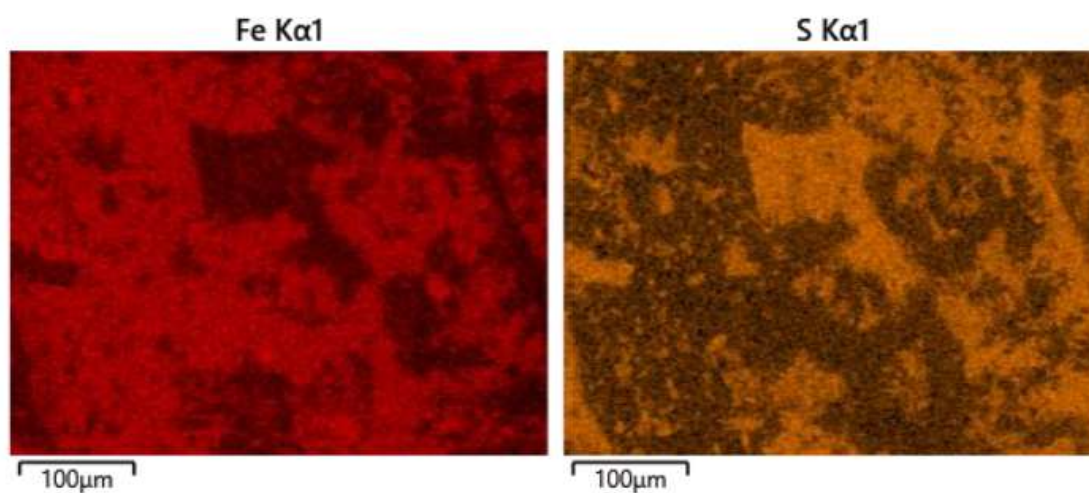
Figure 5.55 – EDS maps showing Fe and S distribution in blend 8 (600 Cl) for the addition of KCl

It was important to connect these findings to the electrostatic precipitator (ESP) to thoroughly analyse the impacts of chloride on PM emissions in a typical sinter plant. ESP abatement struggles to comply with the PM emissions limit values (ELVs) while being

one of the most widely utilised capture technologies because of the high resistance of the released particles. However, since chloride was known to reduce resistivity, the ESP plate's relationship with chloride was needed to understand this to be able to minimise PM emissions. This study has demonstrated that an increase in chloride increases the total PM emissions emitted from sintering procedures in addition to decreasing the particle resistivity. Blend 8 with 600 Cl mg/kg emits significantly more particles while also having significantly smaller particle sizes, which suggests that the ESP would not be able to effectively catch the PM emissions. Figure 5.56 demonstrates by XPS technique how the presence of KCl often increases the suborbital of Cl 2p and this was important in understanding what phase of chloride is released and/or retrained within the sinter bed. The chloride, not volatilising, migrating to the surface, and not evaporating would account for this. Blend 6 demonstrates full saturation of chloride, which was seen in the high concentrations of chloride found in both the returned fine particles and the PM emissions as shown in Figure 5.53. The return fines particulates were continuously recirculated in the process in a closed loop, and over time this would accumulate chloride within the ESP system, which will make the system less efficient and increase the PM emissions over time and this would be a problem for a sinter plant.

To mitigate this, it was important to understand the transformation path for KCl to PM emissions which has been revealed in Figure 5.57. The boiling point of $ZnCl_2$ was 732 °C whilst that of KCl was 1420 °C (the melting point was 770 °C). The boiling point was defined as a temperature at which vapour pressure exceeds 1 atmosphere. Therefore, when approaching the boiling point, the significant vapour pressure of the material and any mixture of $ZnCl_2$ and KCl will have a boiling point between the two which will cause a mass transfer to occur which follows previous research by Zhiyun *et al* who investigated $PM_{2.5}$ release where it was stated that Cl can exist in the speciation of KCl, NaCl and $PbCl_2$ respectively from chlorination reactions. [101]
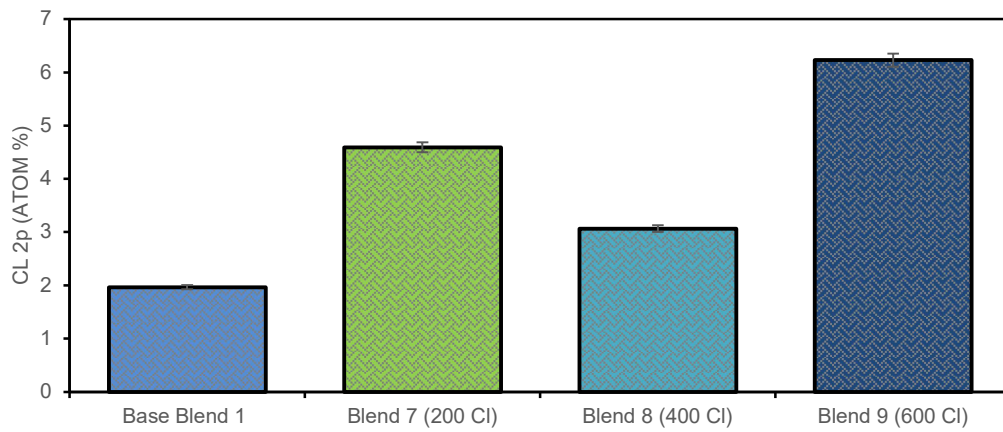
Figure 5.56 – XPS analysis of Cl 2p% for base blend 1, blend 6, blend 7 and blend 8 for the addition of KCl for each blend ranging from 0, 200, 400 and 600 mgC/kg
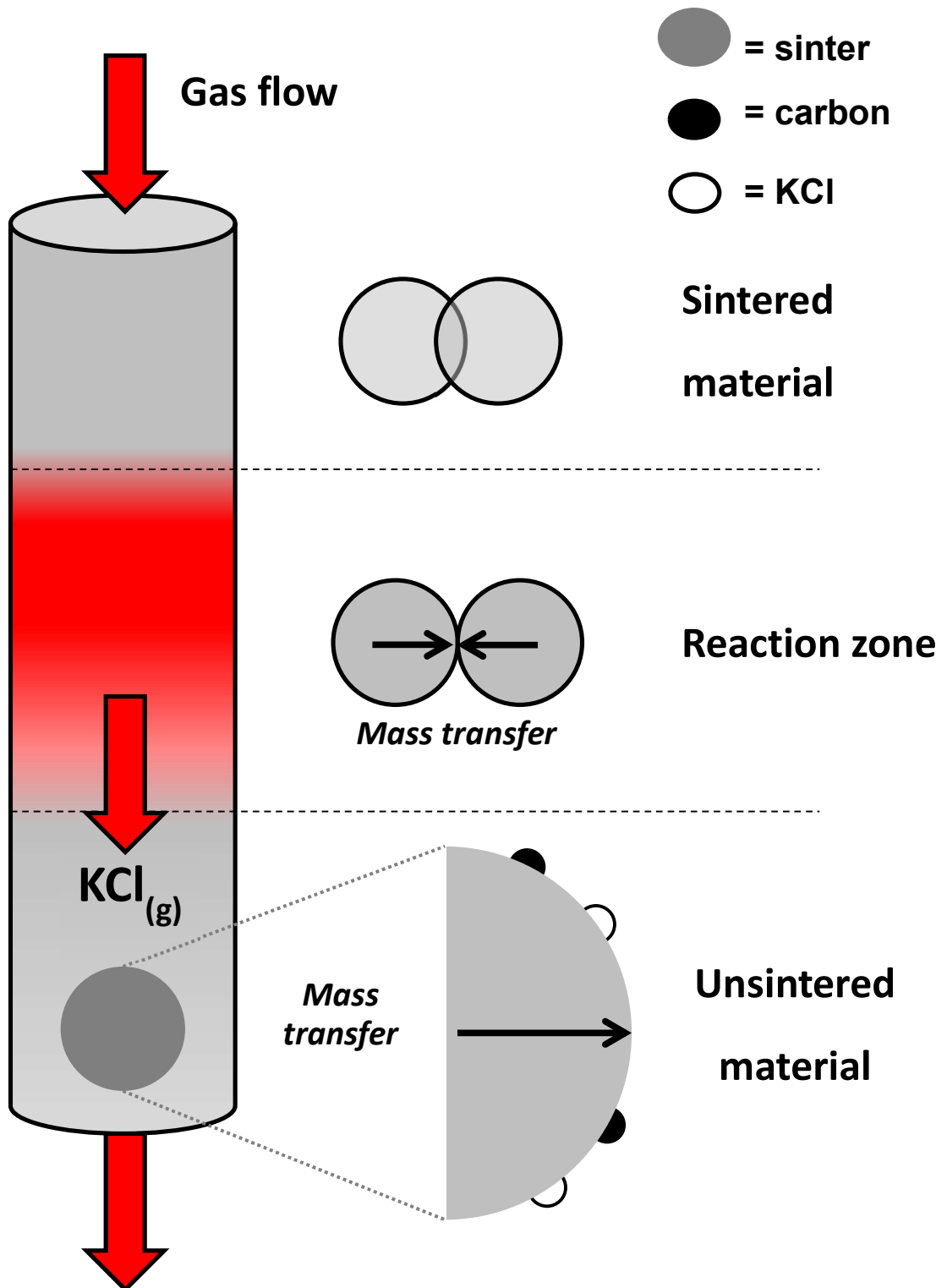
Figure 5.57 – Transformation paths of KCl during sintering operations for the addition of KCl (M.H.Thomas, P.J. Holliam, H.Cockings, Dec 2022, personal communication (paper in preparation))

Summary

- Potassium chloride was added to the sinter blend at increments of 0, 200, 400 and 600mg/kg with no influence on process parameters and sintered product.
- The addition of chloride content to filters causes discolouration of PM emissions.
- The increase in total emission concertation of PM emissions was evident when increasing the amount of chloride addition in each blend.
- The chloride content in the total emission concentration of PM emissions significantly increases with 400 and 600 mg/kg of KCl addition.
- There was a distinct exponential relationship between the total concentration of PM emissions and chloride addition.
- As the amount of KCl trim increases, the size fractions of the return fines particulates rise, resulting in greater PM emissions.
- In contrast, chloride tends to be more evenly distributed throughout the sample, whereas Fe was localised in certain areas of return fines particulates by the EDS technique.
- Due to the overall amount emitted and the average particle size, a typical ESP would not be able to effectively capture the PM emissions with the addition of a KCl above 400 Cl mg/kg.
- XPS results show the suborbital of Cl 2p increasing with the addition of KCl which was important in understating that a mixture of $ZnCl_2$ and KCl will have a boiling point that is halfway between the two, resulting in mass transfer.

5.4.2 Removal of Chloride by Washing of a Revert Material Study

Chemistry analysis was necessary to adjust the blends for these tests before adding ESP dust and washed ESP dust (WESP). The success of washing ESP dust was displayed in Figure 5.58 by XRF and ICP techniques which shows the significant reductions in Na_2O and K_2O in the washed ESP dust and this follows previous research by Peng *et al* whereby K in the ESP dust was mostly presented in the phase of KCl, which was easy to be separated from other elements and stated that it was possible to recover KCl from the ESP dust.[100] It is important to note that every other element remained consistent, proving that the washing method used had little effect on these other chemical elements, as shown by the XRF technique in Table 42. Figure 5.59 compares the size fraction of the ESP dust before and after washing. It reveals a minor increase in the % nuclei particles and a

decrease in % adhering particles, which was as expected given that the procedure used water, which would cause some particles to stick to one another. The ESP dust that has been washed was slightly more reactive, but not substantially as shown in Figure 5.60 for the TGA DT. The TGA DTG results shown in Figure 5.61 illustrates that the washed ESP dust has a second peak in comparison to the ESP dust, which concludes that the KCl was being reactive as it was previously removed by washing.
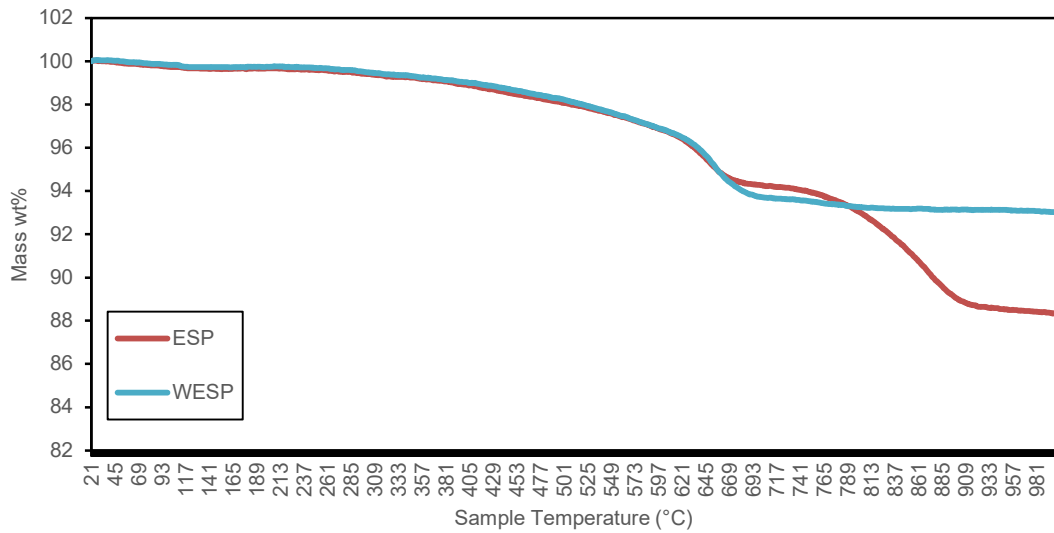

■Raw ESP Dust   ■Washed ESP Dust
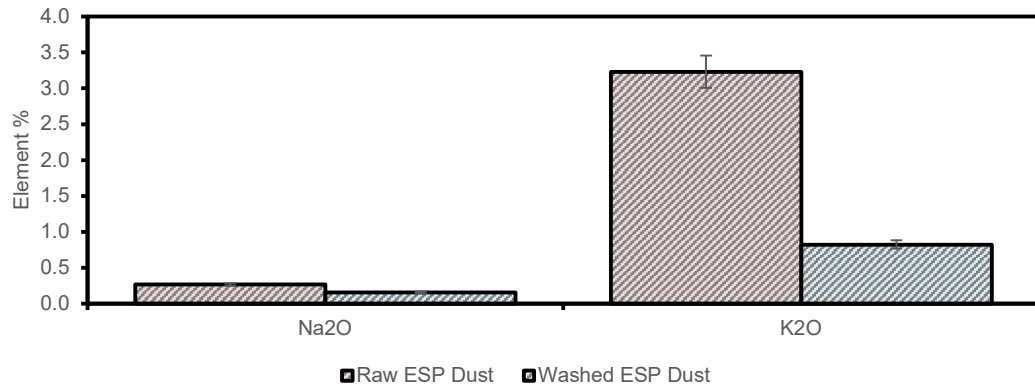
Figure 5.58 - Chemical composition of ESP dust and washed ESP Dust (WESP) that shows a successful technique to remove K_2O and Na_2O via washing

Table 42 – Chemical composition of ESP dust and washed ESP dust (WESP)

Elements %	Raw ESP Dust	Washed ESP Dust
*TFE	43.29	48.25
CaO	8.08	8.05
SiO_2	6.26	6.78
MgO	1.52	1.62
Al_2O_3	1.4	1.46
P	0.026	0.027
Mn	0.16	0.17
S	0.025	0.002
FeO	2.69	2.81
Na_2O	0.268	0.16
K_2O	3.233	0.825
Zn	0.023	0.021
TiO_2	0.1	0.09
LOI	43.29	48.25
H_2O	8.08	8.05
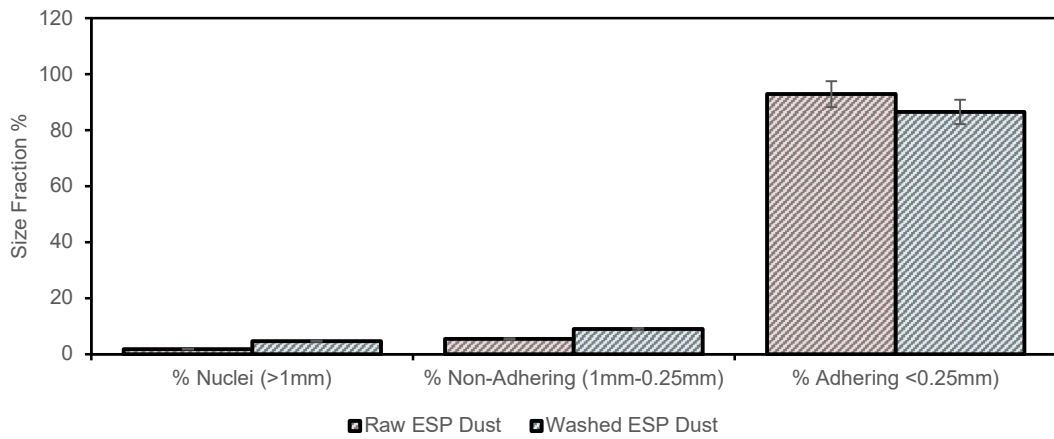
Figure 5.59 – Size fraction of ESP dust and washed ESP dust (WESP) and displays a similar particle size distribution before and after washing

Figure 5.60 - TGA DT of ESP dust and washed ESP dust (WESP) which shows that ESP dust is more reactive than washed ESP dust (WESP)
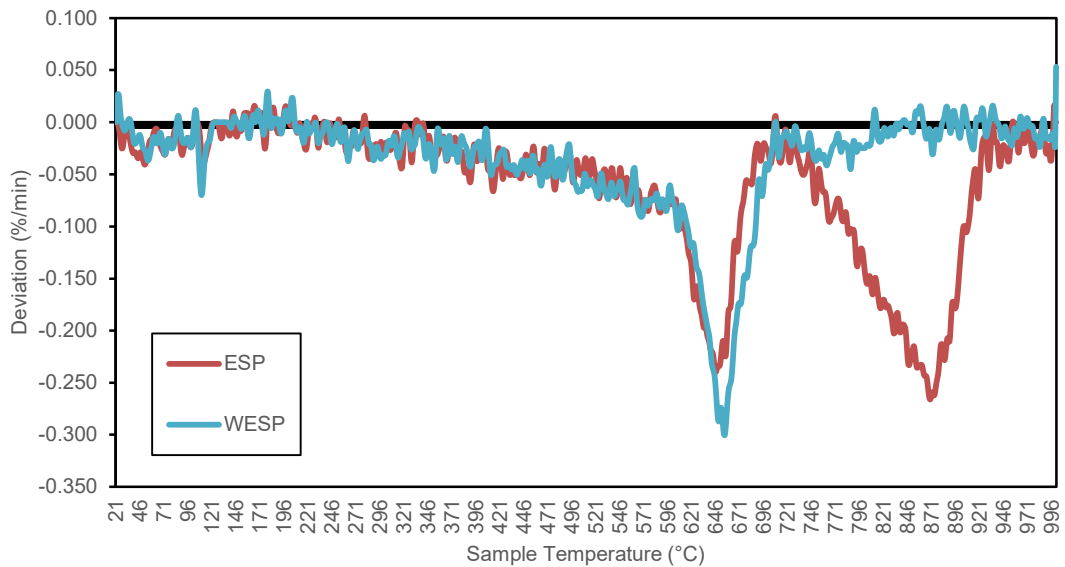
Figure 5.61 - TGA DTG of ESP dust and washed ESP dust (WESP) which shows that washed ESP dust (W ESP) has a single reactive peak compared to ESP dust with two peaks that KCl would have been present if not removed by washing.

Figure 5.62 illustrates that using ESP and WESP dust extended the sintering process. The 5% use of both ESP and WESP dust in blends 12 and 15 resulted in a reduction in hot flow as well as an extension of sintering time. If the hot flow rate was reduced, the sintering time will inevitably increase, as one can anticipate, albeit with little variation. The figure illustrates that the maximum off-gas temperature increases when the use of both ESP and WESP dust was increased. This would impact the release of PM emissions as the efficiency of ESP abatement is sensitive to elevated temperatures. This was also demonstrated in previous research by Fan *et al*, who showed that increasing bed temperature increases the volatilization of hazardous elements, negatively impacting ESP abatement.[77] Additionally, further research has pointed to an exponential relationship, as seen in Figure 5.64, between the amount of Fe_2O_3 present in the return fines particulates and the increase of off-gas temperature. This could mean that the iron oxidation that was occurring would raise the temperature of the waste gas, and the FeO to Fe_2O_3 reaction would provide the heat to cause this increase in temperature. Appendix 8 displays the pilot-scale sinter rig results for all the tests (base blend 7, blend 10, blend 11, blend 12, blend 13, blend 14 and blend 15) including air flow, sintering time, temperature and PM emissions and return fines particulates collected.
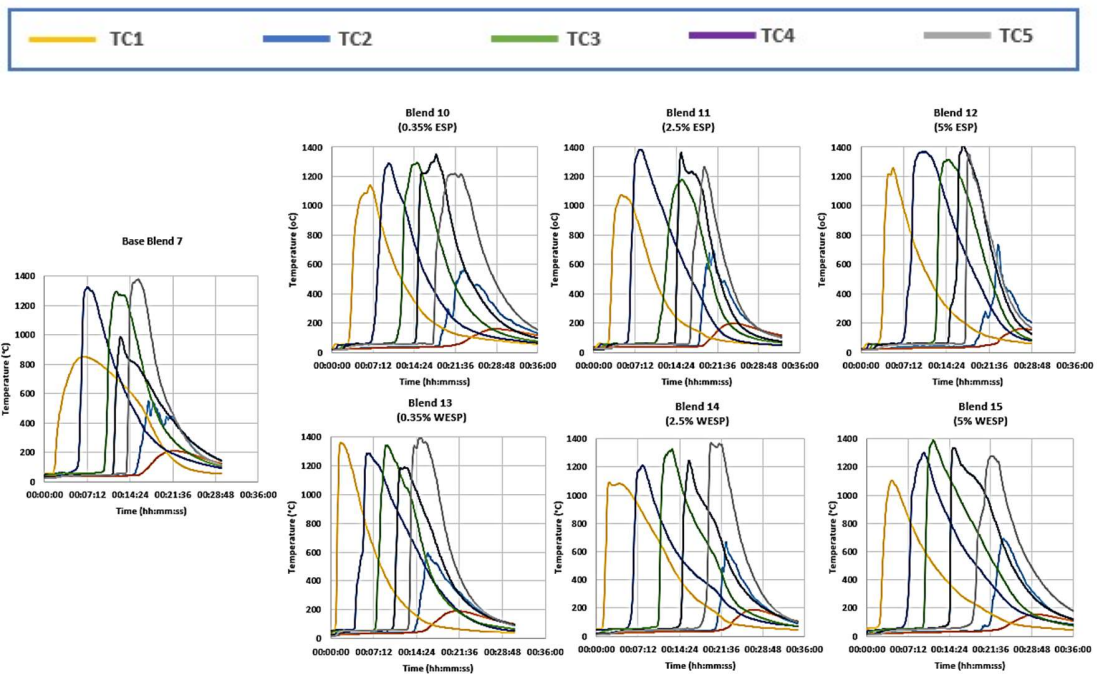
Figure 5.62 - Thermocouple temperature profile during the sintering process for ESP and WESP
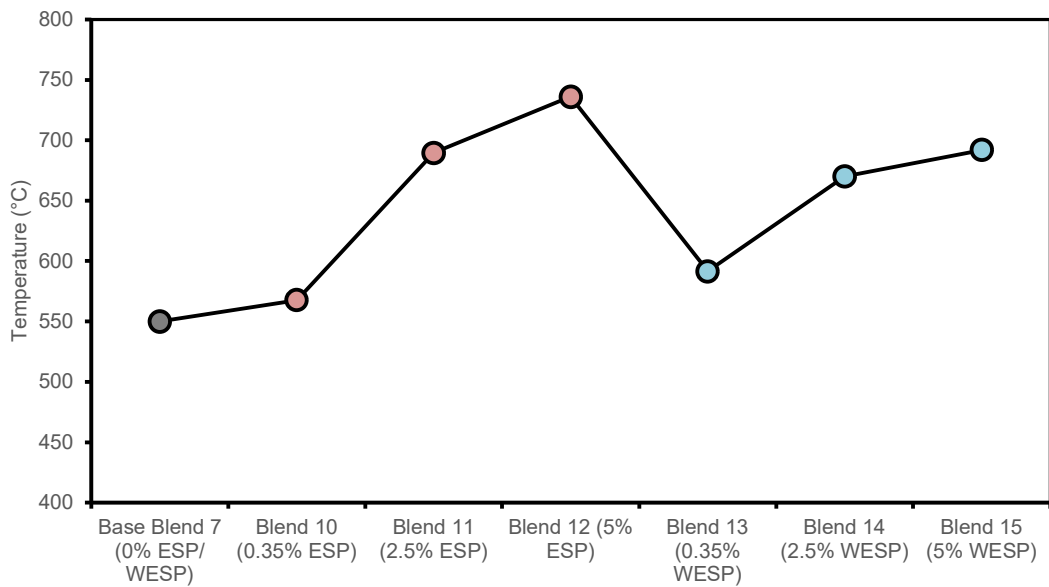
Figure 5.63 – Maximum off-gas temperature for ESP and WESP that highlights that both follow the same trends when increasing in ESP or washed ESP dust quantities
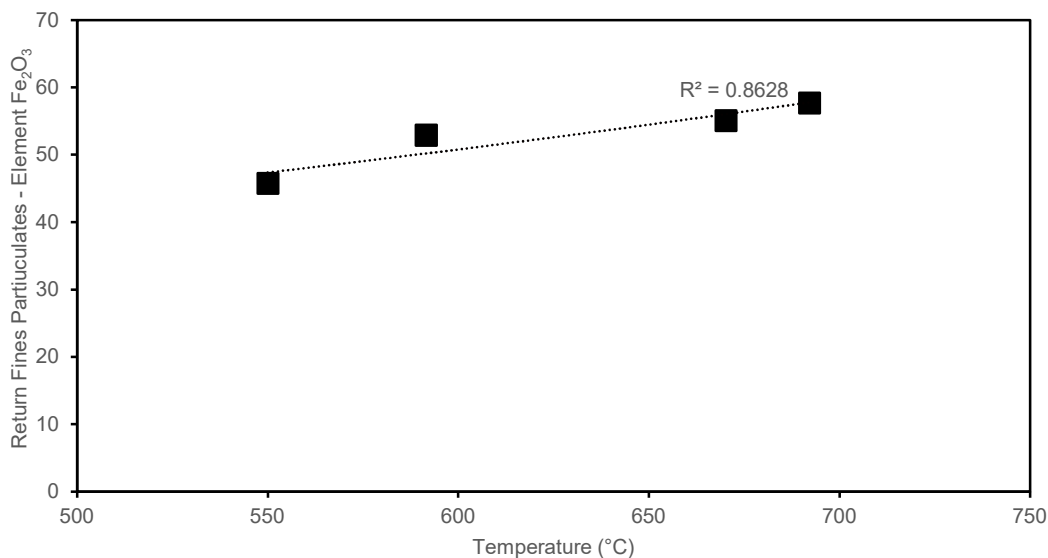
Figure 5.64 – Relationship between off-gas temperature and return fines particulates – Element Fe₂O₃ for WESP

Figure 5.65 shows the mass concentration results for the PM emissions that were collected; it was simple to observe an increase in emissions as additional ESP dust was added to blends 10, 11, and 12, with blend 12 having the highest PM emissions. Debrincat *et al* who used a pilot-scale sinter rig, discovered that most PM emissions had a size of <1.18 mm indicating that it comes mostly from the adhering fines layer of particles in which the KCl particles were present.[43] Similar results can be seen when comparing the washed ESP dust (WESP) in blends 10, 11, 13, and 14. The WESP dust does have a positive influence in minimising the PM emissions but only when a quantity of 5% was used, as shown in blends 12 and 15. Figure 5.66 illustrates how PM emissions rise as ESP dust quantity increases, with blend 12 showing a higher surge in emissions compared to blends 10 and 11. This demonstrates how easily PM emissions can escape into the flue gas as the chloride and volatile components were increased through increasing ESP dust. There was an approximately 50 % reduction in the amount of chloride in the PM emissions when 5% of ESP and WESP dust was compared in blends 12 and 15. Figure 5.67 displays a 5x greater amount of Cl 2p in the ESP return fines particulates (blend 12) compared to WESP return fines particulates (blend 15). This demonstrates how the mass transfer of chloride was increasing as it approaches the boiling point. This can occur because the substance has a high vapour pressure and because any mixture of $ZnCl_2$ and KCl will have a boiling point that lies between the two which can relate to the previous study. It was

optimal to use the washed ESP dust at a rate of 5 % in the sinter bed at the sinter plant, as this would result in lower particle emissions and lower chloride content in the waste gas, improving the effectiveness of the ESP abatement at the sinter plant.
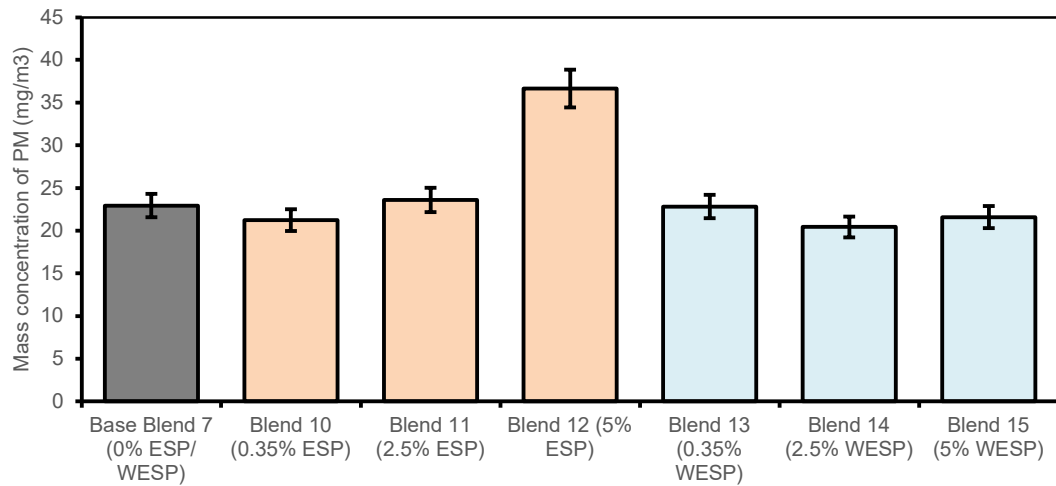
Figure 5.65 - PM emissions collected: total emission concentration for ESP and WESP
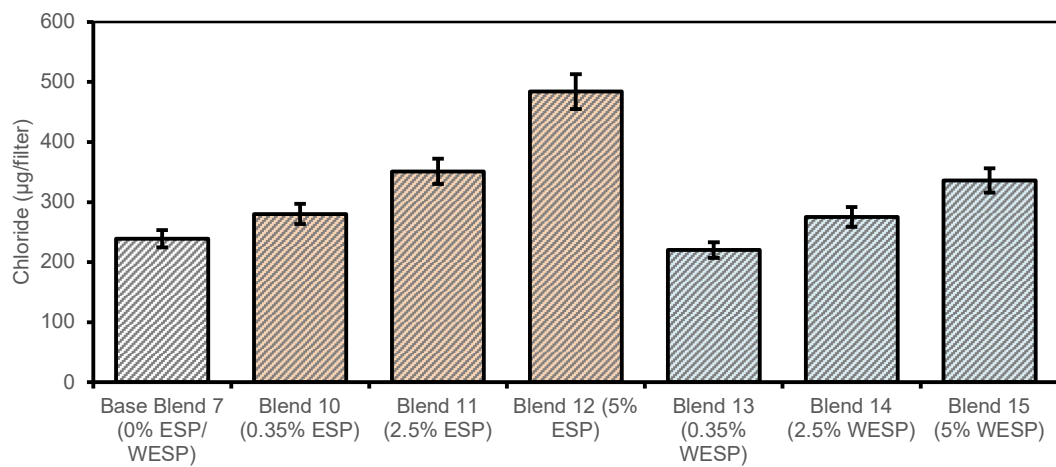
Figure 5.66 – PM emissions collected: chloride content for ESP and WESP
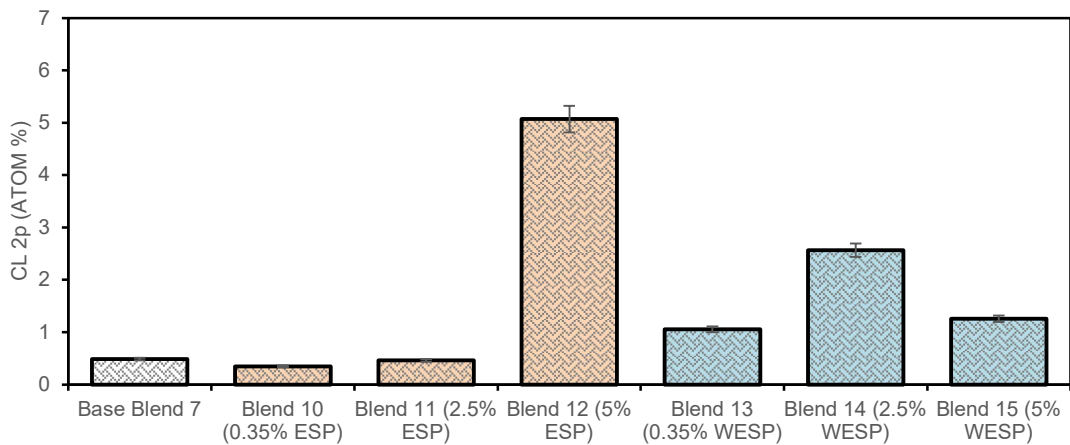
Figure 5.67 - XPS analysis of Cl 2p% of all blends for ESP and WESP

It was important to recognise that the ESP dust's chemistry differs from field to field when washing it because it was known to be non-homogeneous. As a result, the sample of ESP dust only accurately represents the day and field on which it was collected because different fields were recovered at various times. The end fields, however, catch the chlorides and alkali metals while the starting fields was more iron-rich PM emissions (anticipated to be higher than 50-60 % KCl. Since there was no mixing, a slug of high KCl would feed onto the strand, which would account for the sharp spikes in the continuous emissions monitors (CEMs) at the sinter plant. This demonstrates that even a tiny amount of KCl can have a significant impact on the waste gas system because it impacts how undesirable chlorides and alkali metals behave and function in ways that was not proportional to their levels. Although the pilot-scale sinter rig was a technique for pre-abatement, it was well known that the effectiveness of the abatement is increased by lower levels of chloride particles. It was recommended for future experiments that samples be collected from the start of the ESP fields rather than the entire fields with the high alkali materials (at the end of the fields). To ensure a more uniform raw material when reusing it in the sintering process, mixing the ESP dust would be another enhancement. This can eliminate spikes in particle emissions caused by high areas (slugs) of KCl and other alkalis.

Summary

- ESP dust was successfully washed to remove chlorides.

- The washing of ESP dust was a useful tool to decrease PM emissions and it has a large impact when using the quantity of 5% ESP dust compared to 5% WESP dust in the blends.

- The blend consisting of ESP 5% dust has the largest increase in PM emissions due to the highest amount of chloride included.

- Similar results were observed when comparing the quantity of 0.35% and 2.5% levels of ESP and WESP PM emissions in the blends.

- The greater amount of Cl 2p in the 5% ESP compared to 5% WESP return fines particulates demonstrates that the chlorides will also be re-circulated back into the process which will impact the efficiency of the ESP abatement after accumulation over time.

- Maximum off-gas temperature increases when ESP dust increases which may impact the release of PM emissions and decrease the ESP abatement at the sinter plant.

- It was recommended to mix ESP dust for a more homogeneous sample before washing and/or washing the final fields in the ESP abatement as they have the highest levels of chloride and alkali metals.

5.5 Investigation of the Particle Size Distribution of Ultra-fines Iron Ores

In this experiment, iron ore concentrate known as iron ore C concentrate was substituted for iron ore B to evaluate the stability of the sintering process, the sinter quality of sinter ore blends, and its effects on the environment. Although the addition of additional nucleus particles may increase permeability and reduce PM emissions, it is hypothesised that the entire or partial substitution of iron ore with another more affordable iron ore may well improve sintering processes and sintering quality. The ideal ratio of nuclei, non-adhering, and adhering particles may be found by increasing the nuclei-to-layering ratio (NTLR) while adjusting individual size fractions in additional experimental research which could minimise PM emissions.

5.5.1 Displacement of Two Ultra-Fines Iron Ores Study

Base blend 3, blend 16, 17, 18, 19 and 20 produced a stable flame front profile, indicating strong sinter feasibility, and therefore blend process stability. The following effects were produced by gradually adding iron ore C in 5% increments. The maximum sintering temperature was seen to rise across all blends on average while sintering time became shorter up to blend 19, as displayed in Figure 5.68. Figure 5.69 reveals that up to blend 18, both heat and cold permeability rise, after which they both begin to slightly fall. Except for blend 16, sintered airflow was often higher when iron ore was used, which indicates that the sintered structure was more porous, which was good for blast furnace gas permeability. Figure 5.70 depicts a faster sinter cooling rate for blend 18 up to 15% before it slightly declines for blends 19 and 20. The sinter combustion rate increased by over 15% in blend 18 and decreased after this blend. Pilot-scale sinter rig results are shown in Appendix 9.
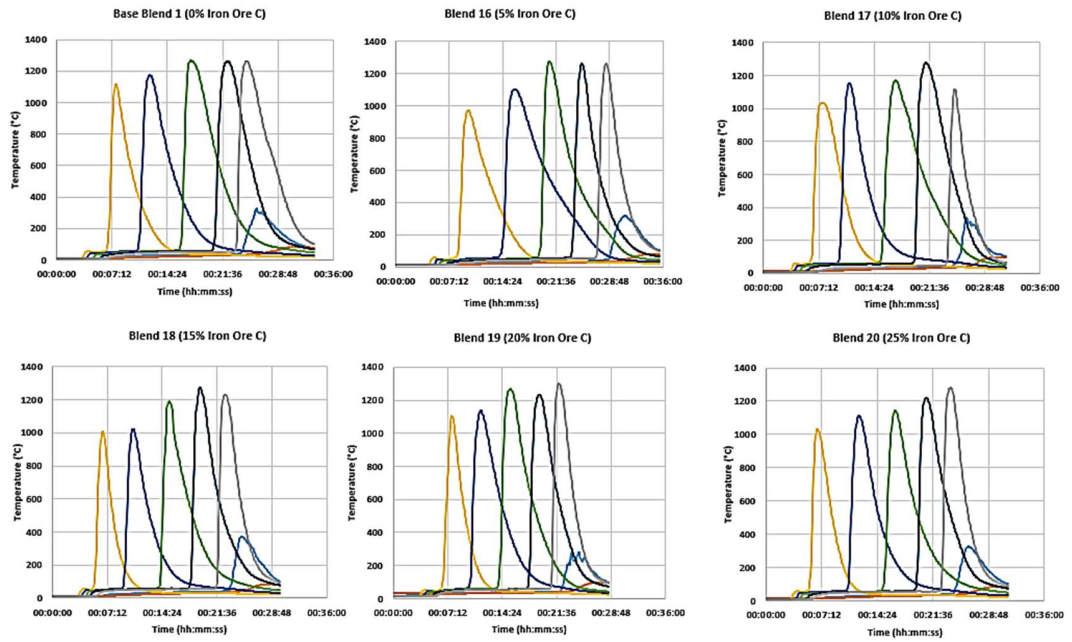
Figure 5.68 - Thermocouple temperature profiles during the sintering process for the displacement of two ultra-fines iron ores
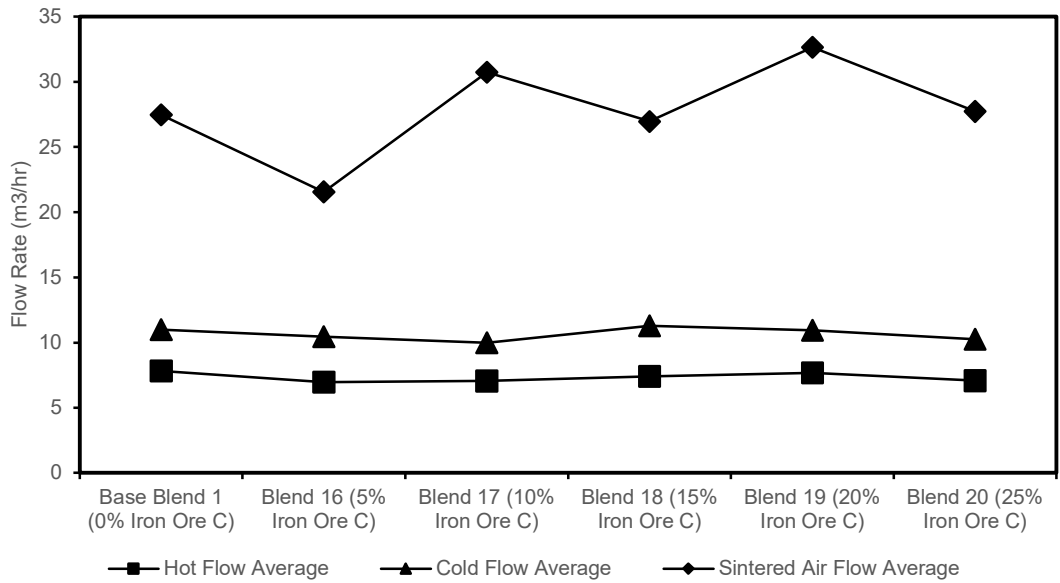
Figure 5.69 – Hot, cold and sintered air flow average rates for the displacement of two ultra-fines iron ores
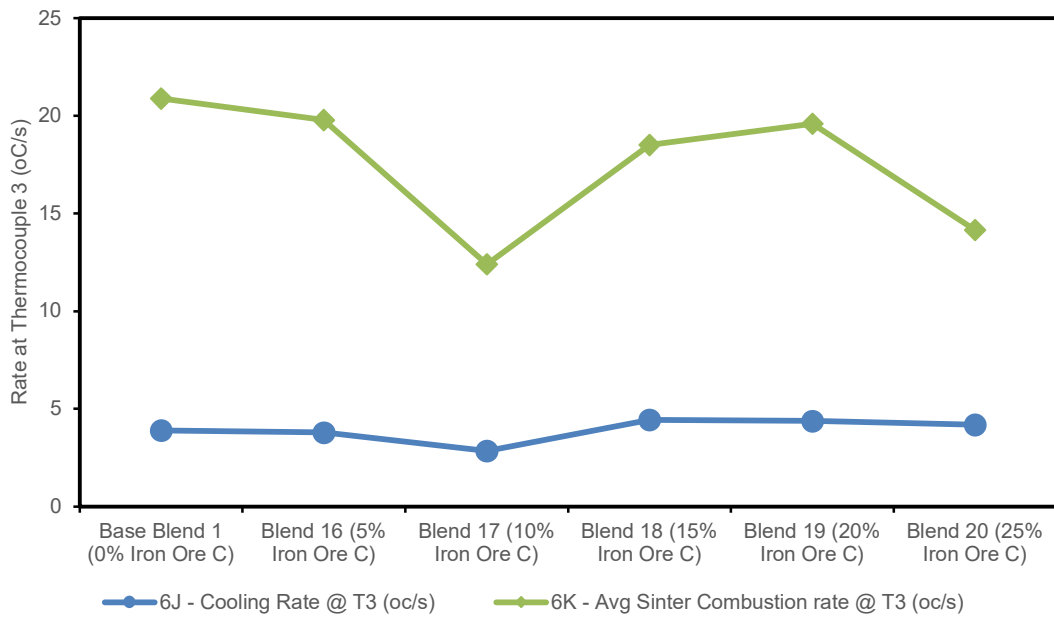
Figure 5.70 – Cooling and sinter combustion average rates for the displacement of two ultra-fines iron ores

Figure 5.71 demonstrates that at increasing iron ore C percentages, iron ore C was marginally preferred over iron ore B for sinter mechanical strength. 48.66% of the sinter base blend was larger than 5 mm after 1 minute of mechanical sieving. Comparatively, it was 53.55% in blend 19 (iron ore C at 20%). When using more iron ore C, the sinter yield remained similar across all blends. However, the RDI 6.3mm results marginally enhanced across all blends. Based on the findings, Blend 19 (20% iron ore C) would be a smart decision due to its higher maximum sintering temperature that supports the formation of SFCA (an increase in strength), a higher cold permeability, a shorter sintering time (increase productivity) a faster sinter cooling rate, better sinter porosity, and a higher hot permeability.
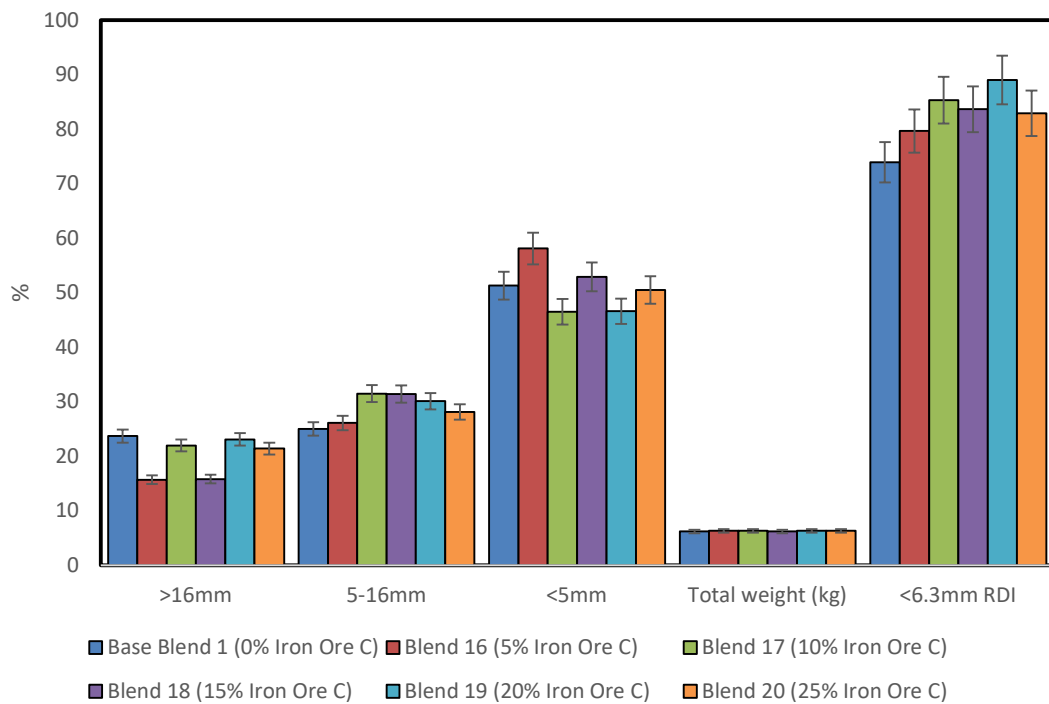
Figure 5.71 – Particle size distribution of the sintered product for the displacement of two ultra-fines iron ores

The particle size distributions of iron ore C and D were different, as was previously mentioned, and the displacement of iron ore D in increments increases the adhesion (fines). Figure 5.72 demonstrates that blends 17 and 18 exhibit the best ratio of both iron ores concerning the volume of PM emissions produced during this investigation and this follows previous research by Fan *et al*. Additionally, Figure 5.73 shows that the blends in question had the lowest levels of chloride that can be detected on the filter which would improve the efficiency of the ESP abatement and minimise the PM emissions released by the sinter plant main stack. It was interesting to note that both blends also produce the most 5–16 mm sinter (Figure 5.71), which may suggest a potential relationship between stronger sinter produced and particle emissions. This can be explained by the fact that more fines aggregate, which reduces the number of free particles released into waste gas steam as PM emissions. Figure 5.74 demonstrates that there were fewer return fine particles in the tray, which may be related to an increase in iron ore C and a decrease in nuclei particles in the blend. Figure 5.75 demonstrates that blends 17 and 18 also have the highest levels of trace metals (Na, K, Zn) which would be returned into the sinter plant system as return fines which would accumulate over time in the closed sinter plant system and would harm sintering operations.
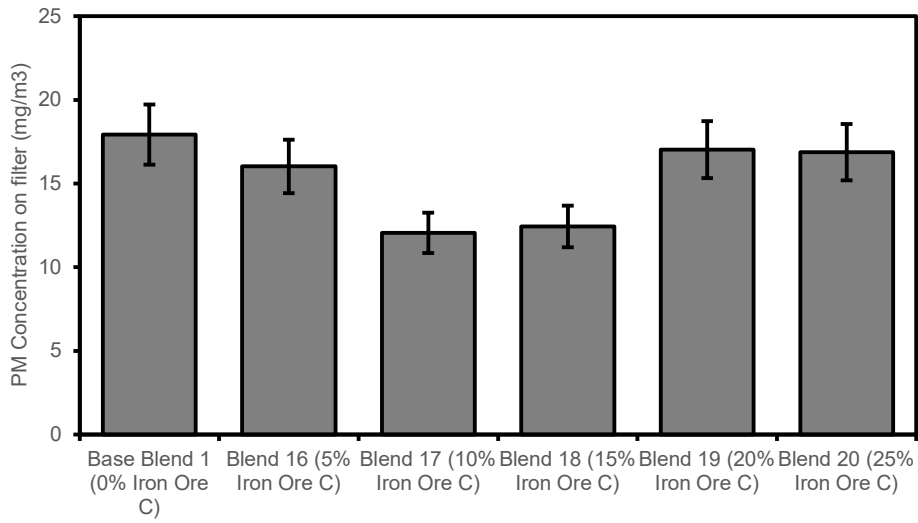
Figure 5.72 - PM emissions collected: total emission concentration for the displacement of two ultra-fines iron ores
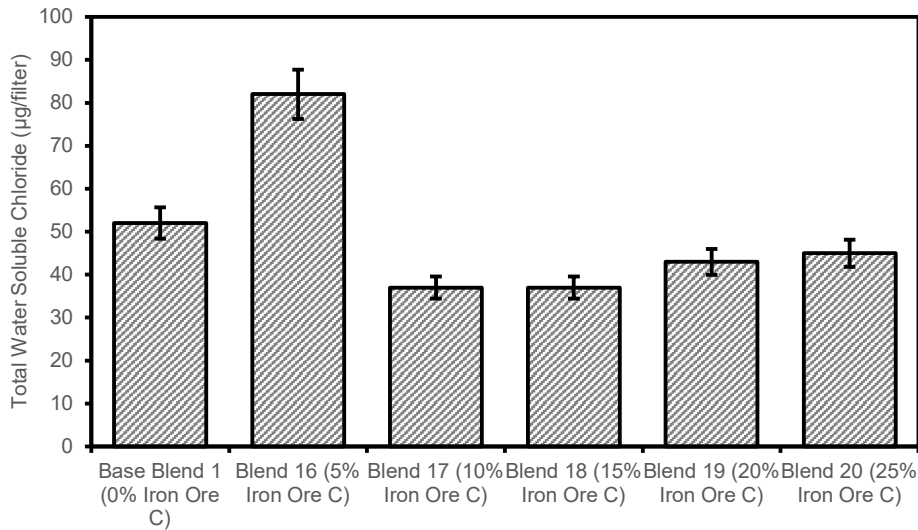
Figure 5.73 - PM emissions collected: chloride content for the displacement of two ultra-fines iron ores
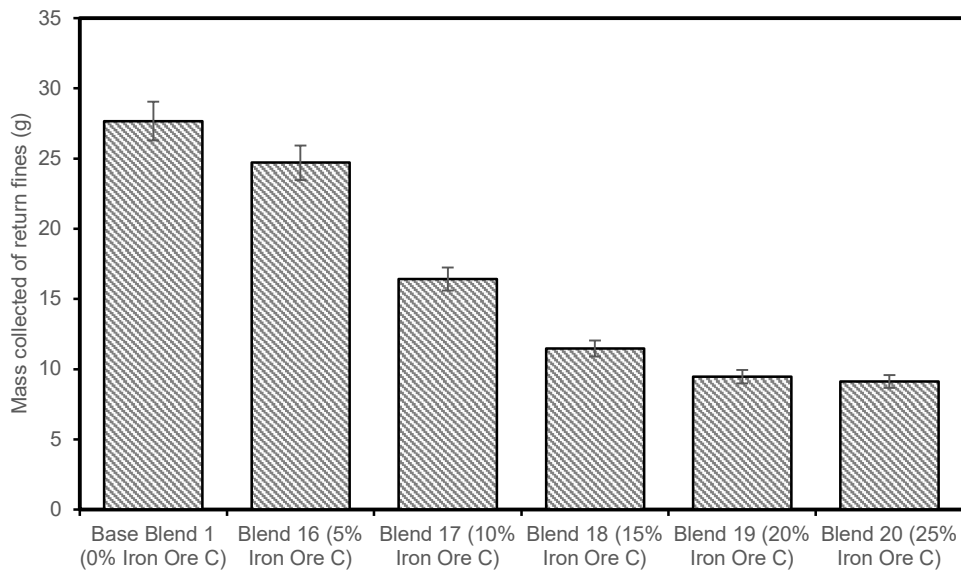
Figure 5.74 - Return fines particulates of the total mass collected for the displacement of two ultra-fines iron ores
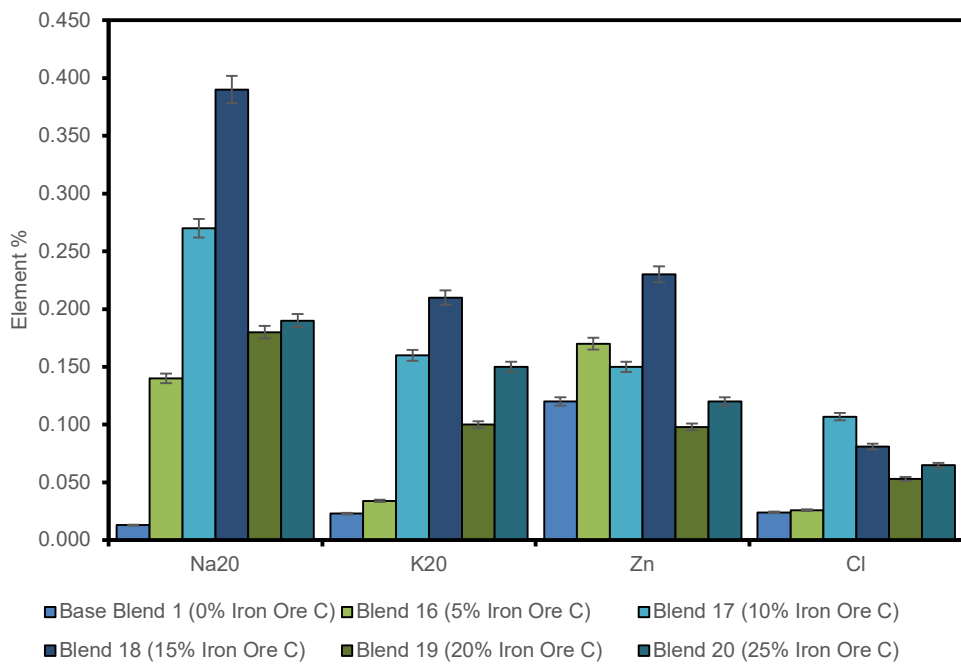
Figure 5.75 - Chemical analysis of return fines particulates for the displacement of two ultra-fines iron ores

Summary

- It was recommended to the sinter plant partially replace iron ore D with a higher percentage of iron ore C. Partial displacement was preferred over complete

displacement due to its impact on process stability, sinter quality produced and PM emissions.

- Based on the process parameters and the sinter produced for the sinter plant with better sinter mechanical and metallurgical qualities for the blast furnace, Blend 19 (20% iron ore C) may be a preferred choice.

- To achieve the environmental benefits and to be able to manufacture a good quality sinter with excellent process parameters, it was suggested to use blend 17 or 18 instead where environmental concerns were met by minimising the PM emissions from the sinter plant main stack.

- It was necessary to conduct a second experiment using manually controlled nuclei of a single iron ore rather than the two iron ores used in the first.

5.5.2   *Varying Absolute Levels of Individual Size Fractions Study*

A representative sample of 1 kg of iron ore E, with different size fractions was separated using sieves of 5 mm, 3 mm, 2 mm, 1 mm, 0.5mm, 0.25 mm 0.15 mm and a receiver. Figure 5.76 indicates the same declining trend as Figure 5.74; when particle size was increased; this has a detrimental effect on the quality of the sinter generated as fewer elements would be present if just employing one size fraction. However, this has a positive impact on PM emissions as there were fewer chlorides present in the larger particles, improving the efficacy of the ESP abatement. Figure 5.77 shows the same downward trend as Figure 4.14 when increasing the particle size. When choosing to employ specific size fractions for iron ore E during sintering, the sinter plant may be able to increase sinter quality while reducing PM emissions.
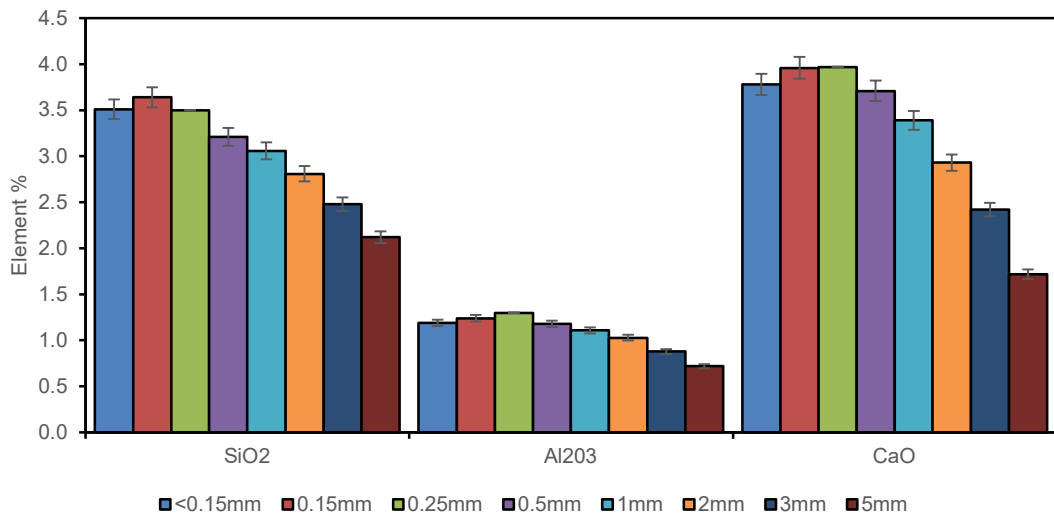
Figure 5.76 - Elements of SiO$_2$, Al$_2$O$_3$ and CaO of iron ore E for size fractions of <0.15, 0.15, 0.5, 1, 2, 3, 4, 5 mm for varying absolute levels of individual size fractions
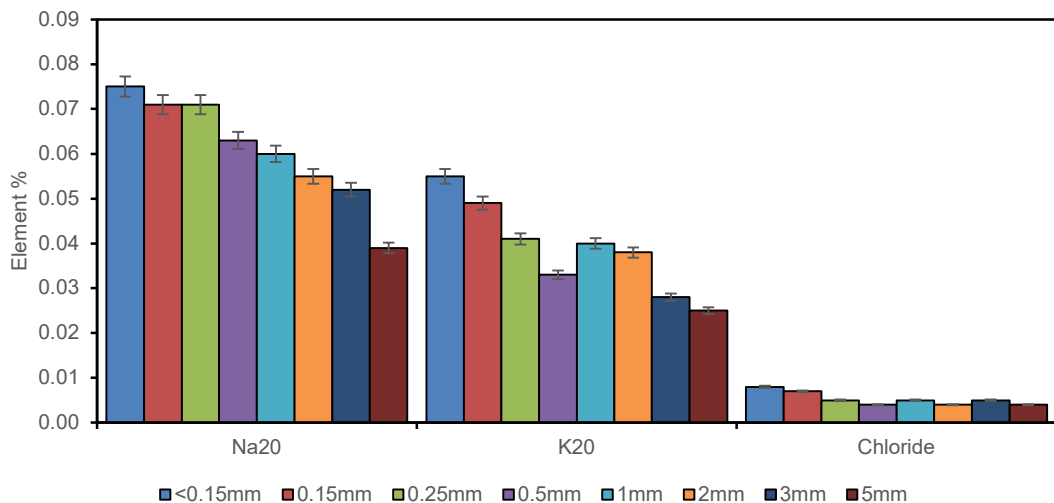
Figure 5.77 - Elements of Na$_2$O, K$_2$O and chloride of iron ore E for size fractions of <0.15, 0.15, 0.5, 1, 2, 3, 4, and 5 mm for varying absolute levels of individual size fractions

Figure 5.78 shows the iron ore E bulk sample's TG (Thermogravimetric) data which indicates a greater mass loss but at a later temperature in a two-stage reaction with iron oxidation at 600ºC, as opposed to the iron ore F bulk sample's one-stage reaction and overall greater stability. The TGA of iron ore F exhibits increased reactivity at lower temperatures, as seen in Figure 5.79 because iron ore E has a wider band and a longer reactivity time and there was greater decomposition. Figure 5.80 displays the TGA results of iron ore E in various size fractions. The smaller particles have a higher surface area to volume ratio, which accounts for an increase in decomposition for the smaller particles in

a two-stage reaction, like the bulk sample of iron ore E. The DTG of iron ore in different size fractions was shown in Figure 5.81. At 227 °C, moisture was lost, and each size fraction undergoes a two-stage reaction because the smaller particles were more receptive to heat. Figure 5.82 displays the DT of different size fractions of iron ore F, all of which follow a similar reactive temperature and durations that signify greater stability and was consistent with iron ore F bulk samples. Figure 5.83 displays the DTG, which similarly follows the aforementioned factors.
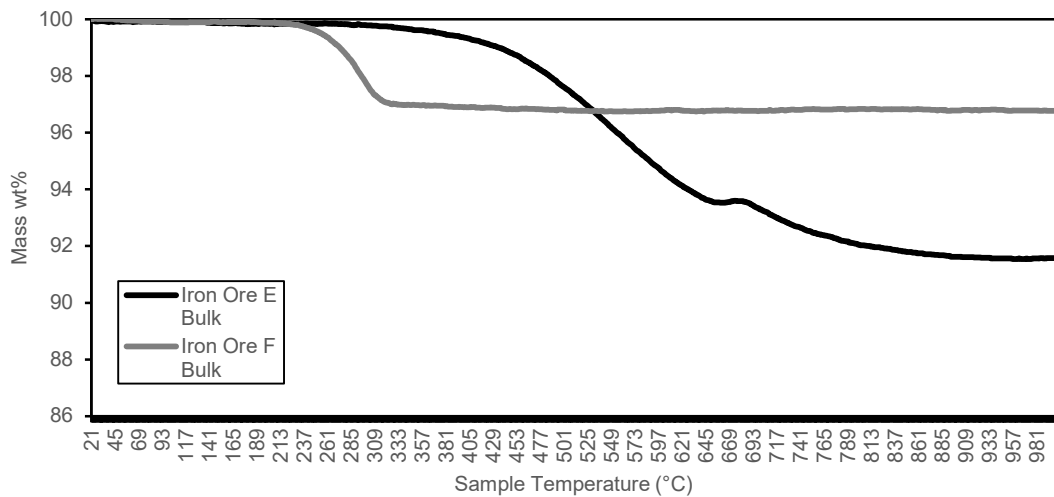
Figure 5.78 - TGA DT analysis of a bulk sample of iron ore E and F for varying absolute levels of individual size fractions
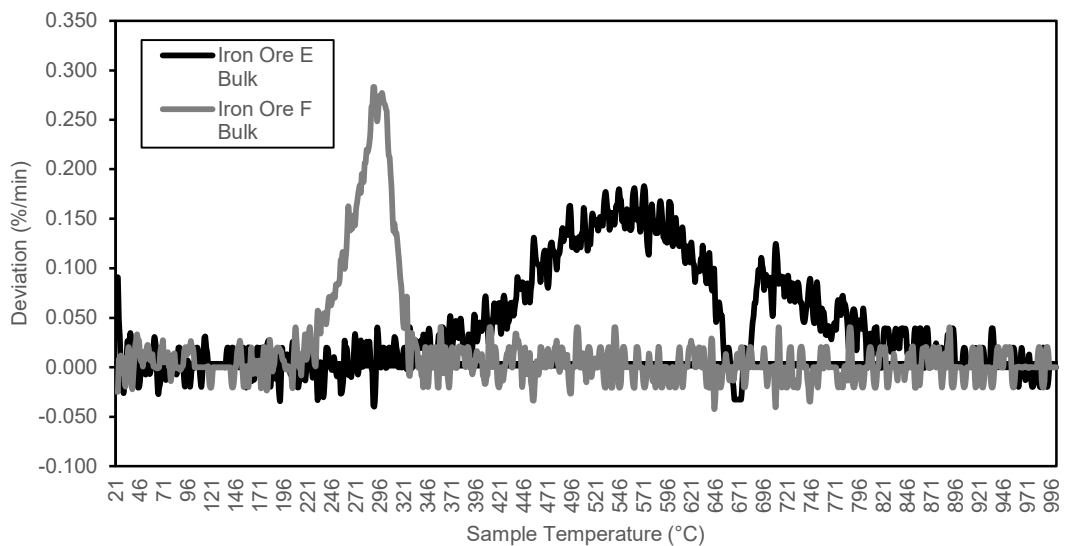
Figure 5.79 - TGA DTG analysis of a bulk sample of iron ore E and F for varying absolute levels of individual size fractions. This demonstrates the temperature at which the reaction is taking place and that iron ore in bulk is proceeding more quickly due to the lower starting temperature.
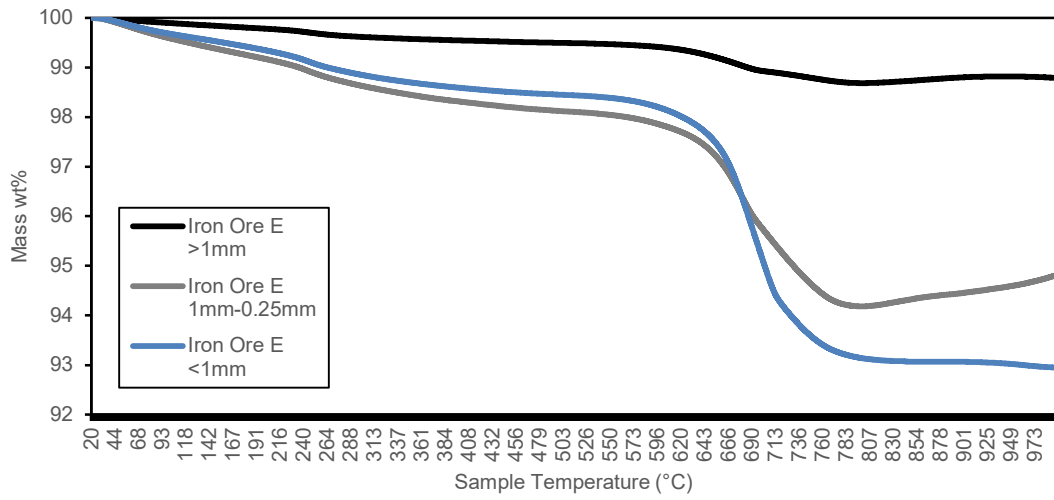
Figure 5.80 – TGA DT analysis of a bulk sample of iron ore E with different size fractions for varying absolute levels of individual size fractions
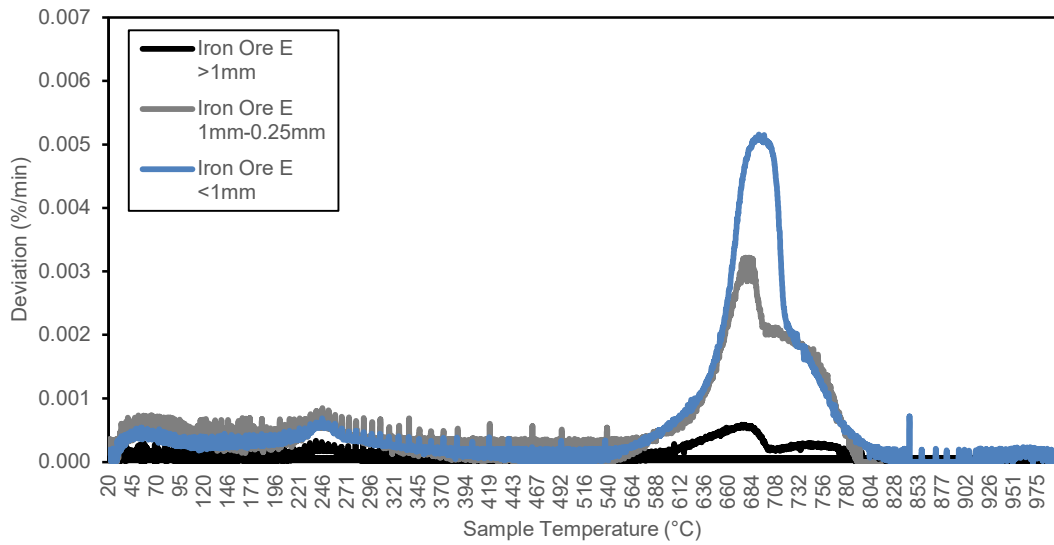
Figure 5.81 – TGA DTG analysis of a bulk sample of iron ore E with different size fractions for varying absolute levels of individual size fractions
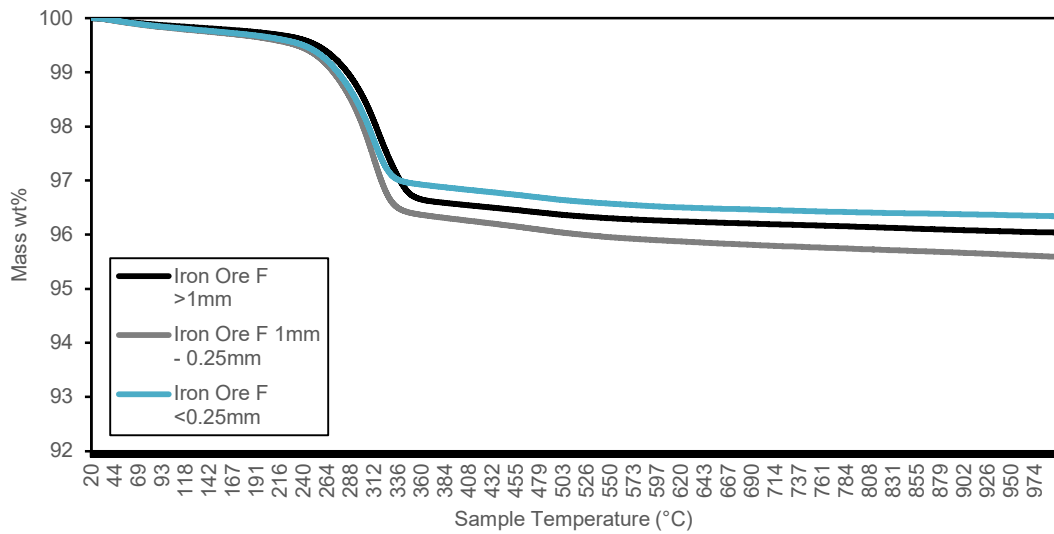
Figure 5.82 – TGA DT analysis of a bulk sample of iron ore F with different size fractions for varying absolute levels of individual size fractions
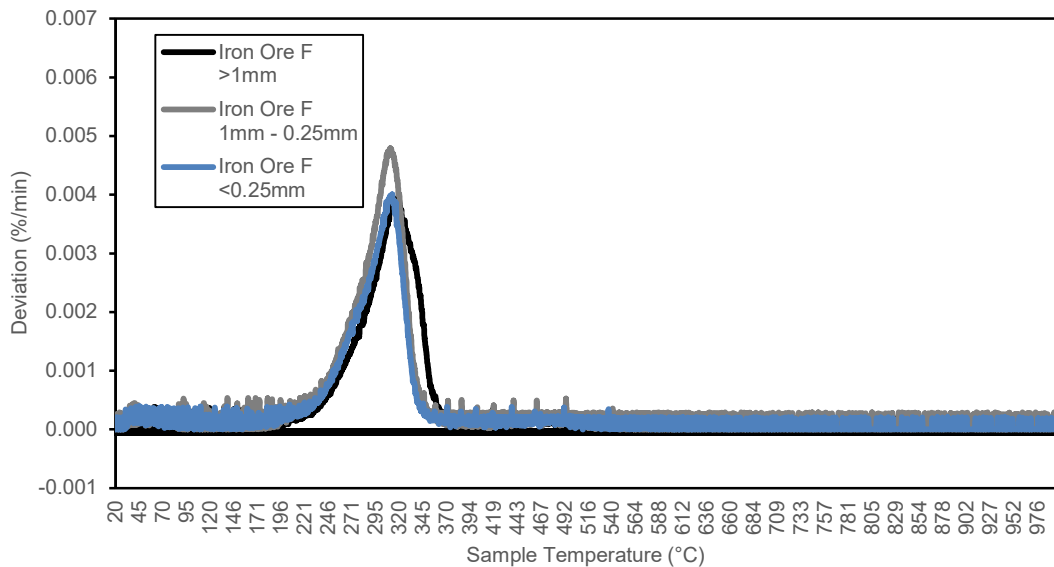
Figure 5.83 – TGA DTG analysis of a bulk sample of iron ore F with different size fractions for varying absolute levels of individual size fractions

Figure 5.84 and Appendix 10 display the blend process stability. Blend 22 (40% nuclei) and blend 23 (45% nuclei) were the most feasible to be sintered with a stable flame front profile whereas blend 21 (35% nuclei) and blend 25 (55% nuclei) did not finish sintering as indicated by the long sintering time, and it was not possible to calculate the flame front width, cooling rate and sintering combustion rate. The sintering time decreases when reaching optimum PSD (particle size distribution) which is shown in blend 23 (45%

nuclei) and the sintering time increases afterwards. Figure 5.85 shows that the maximum sintering temperature appears to rise when nuclei particles were added, and sintered airflow was typically higher until blend 23 (45% nuclei), at which point it starts to decline. This implies that blend 21 (35% nuclei) PSD (particle size distribution) was too fine and that blend 25 (55% nuclei) was too coarse when sintering. nevertheless, blend 22 (40% nuclei) and blend 23 (45% nuclei) has the most optimum PSD concerning process parameters during sintering operations. Figure 5.86 demonstrates that despite the identical yield of sinter produced across the study, blends 21 and 25 produced the greatest amount of sinter with a diameter <5 mm. The yield was calculated with the un-sintered material, which was primarily finer material, in it, indicating, as was previously stated in the thermocouple temperature profiles, that certain blends did not sinter well. The consistent thermocouple temperature profiles predicted that blends 22, 23, and 24 would create strong mechanical sinter. This result demonstrates a good level of nuclei, non-adhering, and adhering particles in those blends, which were neither too coarse nor too fine.
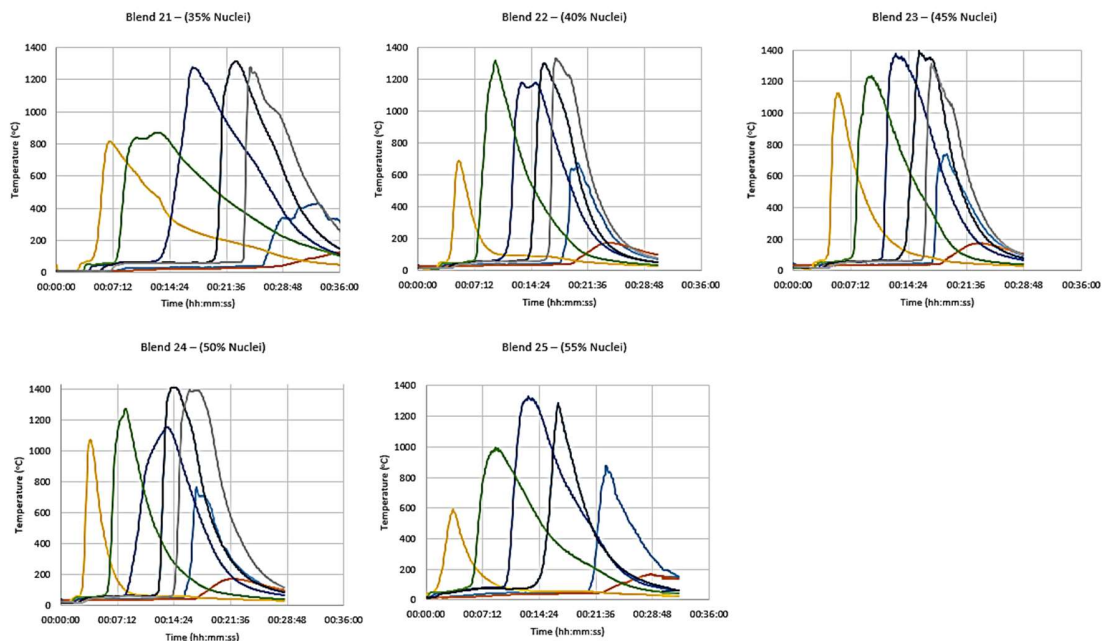
Figure 5.84 - Thermocouple temperature profile during the sintering process for varying absolute levels of individual size fractions
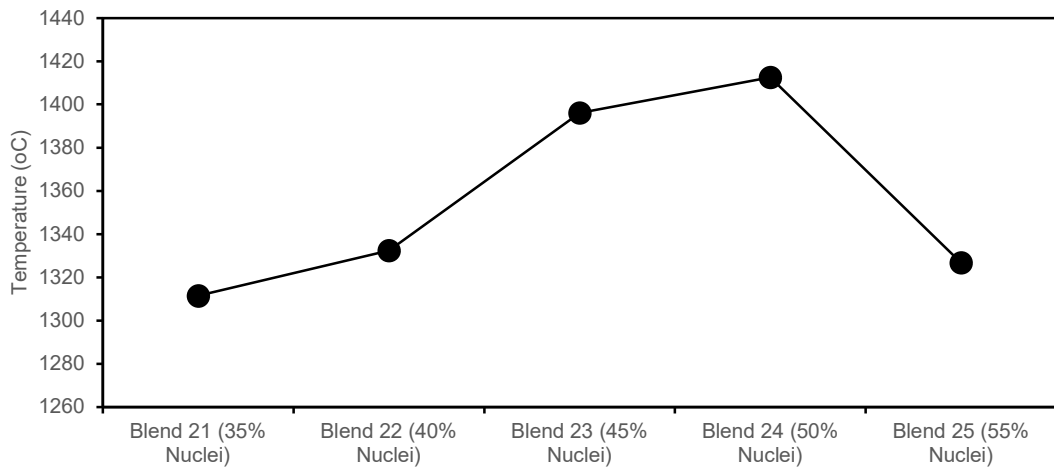
Figure 5.85 - Maximum off-gas temperature for varying absolute levels of individual size fractions
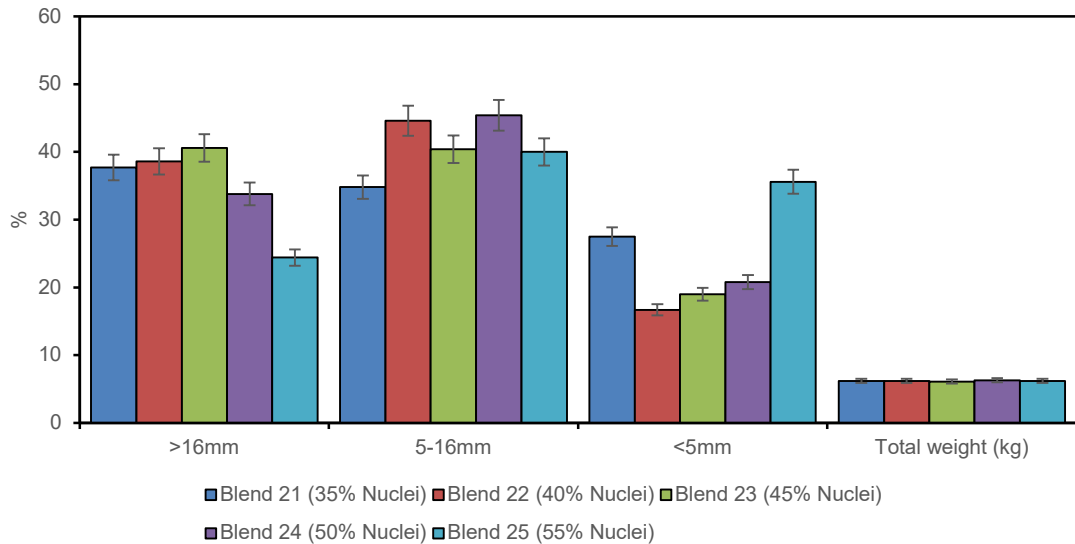
Figure 5.86 - Particle size distribution and RDI for varying absolute levels of individual size fractions

Figure 5.87 shows that blend 23 (45% nuclei) produced the best sinter stability and has the blend's best PSD in terms of the lowest PM emissions. The blends that were found to be too fine and too coarse to sinter, blends 21 and 25, produced the greatest amount of PM emissions. This shows how the finer particles can easily escape into the waste gas stream through their detachment forces during sintering to generate PM emissions, highlighting the significance of good sintering to reduce PM emissions. This would explain why there were always high levels of PM emissions during start-up at the sinter plant as typically all

the settled dust in the process has accumulated during sinter plant downtime. Blend 24 (50% nuclei) has the highest concentration of chloride in the PM emissions, as per Figure 5.88. This would be explained by the fact that blend 24 (50%) contained the highest proportion of adhering fines. This would also explain the significant increase in the chloride content of the PM emissions, as the adhering fines had the highest concentrations of Na_2O, K_2O, and chlorides, as shown previously in Figure 4.14.
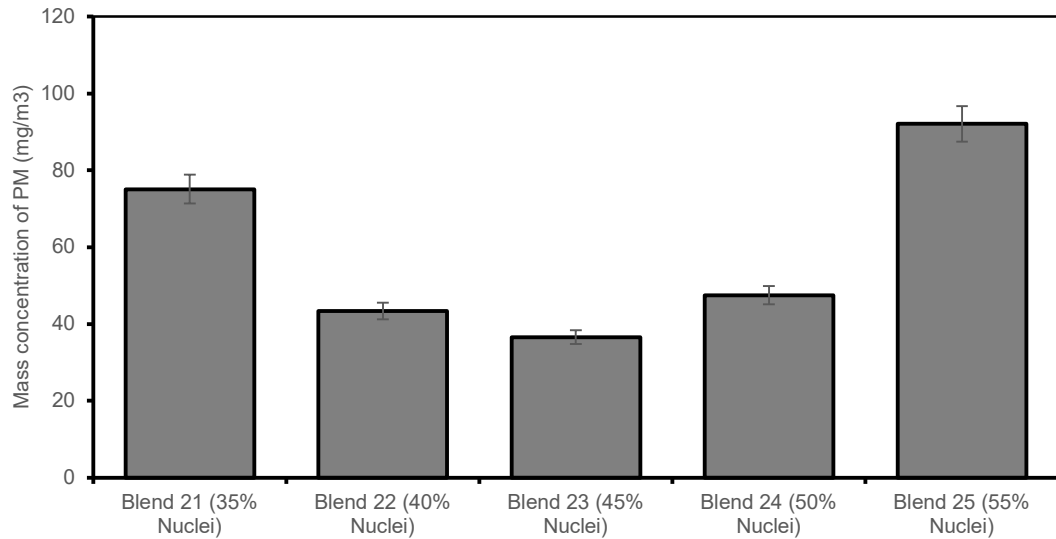
Figure 5.87 - PM emissions collected: total emission concentration for varying absolute levels of individual size fractions
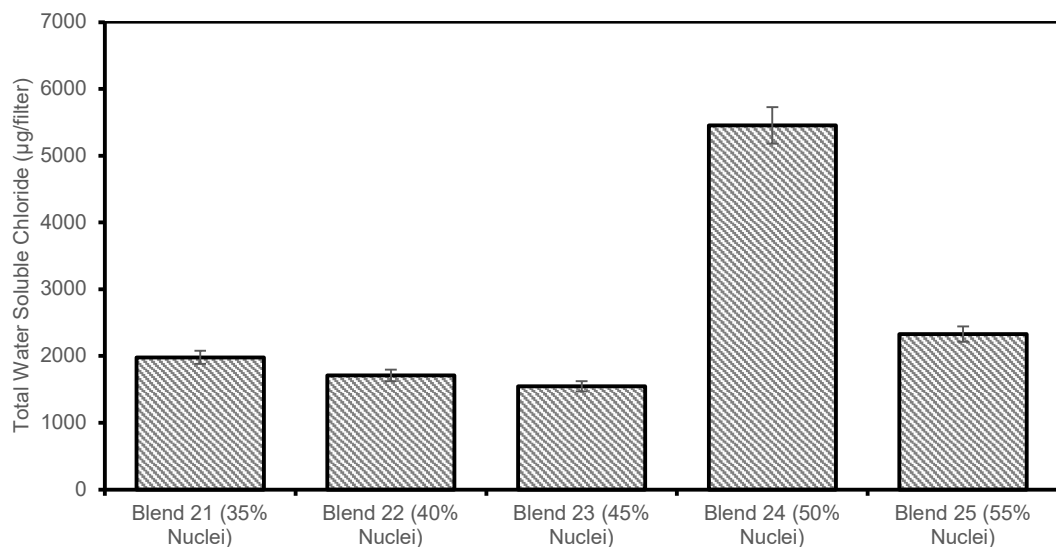
Figure 5.88 - PM emissions collected: chloride content for varying absolute levels of individual size fractions

Summary

- The iron ore E nuclei have the lowest amount of CaO, SiO_2 and trace metals compared to the adhering and non-adhering particles.

- The adhering fines in iron ore E included the highest amounts of Na_2O, K_2O and chlorides. Further investigation proved that the smaller the particle size fraction, the greater amount of Na_2O, K_2O and chlorides that was present.

- Blend 23 (45% nuclei) was shown to have the most optimal PSD concerning the ability to sinter well and have the lowest amount of PM emissions. The ideal number of nuclei, non-adhering and adhering fines in the blend used.

- Blend 25 (55% nuclei) was too coarse while blend 21 (35% nuclei) was too fine for proper sintering and produced the least amount of PM emissions.

- Blend 24 (50% nuclei) had the highest amount of chloride in the PM emissions which was due to the blend being high in adhering fines.

- TGA analysis demonstrates the three different particle sizes for iron ore E reacting at the same time, but the adhering particle size degrades faster for iron ore E which would explain the increased PM emissions.

6   Conclusions

The conclusions of the findings are presented in this chapter. The aims and objectives of the study were reviewed, and their accomplishment was discussed and ranked in order of impact. The research suggests recommendations for future work.

- This thesis shows that by making process adjustments, it is possible to reduce the emission limit values (ELVs) of particle emissions from the sinter plant by 50%. This would improve the local community's air quality while saving £50,000,000 in capital expenditure.

- It is possible to directly influence direct operations by decreasing the quantity of the waste product and producing cleaner/improved quality recycled materials.

- Validation of an in-situ dust capture device has been designed and installed with repeatability analysis to confirm the accuracy of the measurements for the 1st time.

- A full-scale sinter plant trial was successful, and it was shown feasible to use a sinter bed in the pilot-scale sinter rig to foresee the sintering process, the quality of the sinter, and PM emissions by using the sinter plant's pre-abetment online continuous emission monitors (CEMs) for a direct comparison between a pilot-scale sinter rig and the sinter plant.

- It has been recommended to use 3.6% micropellets in the sinter mix with iron ore in the sinter plant to improve sinter productivity and reduce PM emissions by greater than 50%.

- It has been discovered that chloride does not only impact abatement efficiency but also functions as a mass transfer to enhance PM emissions. It was recommended not above 400mg/kg of KCl in the sinter mix in the sinter plant due to the environmental implications. The washing of recycled materials has been proven to remove unwanted volatile elements and the recommendation of only washing electrostatic precipitator (ESP) dust if planned to use over 5% in the sinter plant.

- A combination of iron ore concentrates at 45% was recommended in the sinter mix to have the largest impact on PM emissions in the sinter plant. It has been proven that the amount of nuclei-to-layering ratio (NTLR), nuclei, and non-adhering and adhering particles in each sinter blend was vital to ensure the blend was not too coarse (55% nuclei) or too fine (35% nuclei) when minimising PM emissions during sintering operations.

- Historical data has been analysed to establish what the key levers of PM emissions were from the main stack of the sinter plant.

- A thorough assessment of the literature along with an analysis of the historical data has been conducted to help prioritise the experiments and further understanding.

The pilot-scale sinter rig with the dust capture device has become recognised as an essential experimental instrument for the sintering process and measuring its emissions. In addition to influencing the industrial sector, it has also had a significant impact on academic research and can be used for any future environmental problems, such as the decarbonisation of the steel industry to achieve net zero emissions. In terms of industrial applications, the impact of the work is recognised as follows:

1. The pilot-scale sinter rig is the only operational pilot-scale sinter rig set up in the United Kingdom, as well as the only one known worldwide that can quantify PM emissions. Before the sinter blend is used in the sinter plant, the pilot-scale sinter rig can optimise the sinter blend and make the necessary adjustments that would have a positive impact on the process parameters, sinter quality, *and* emissions.

2. The sinter plant specialists on-site can now make judgments based on facts and experimental data rather than speculation. Making informed choices has included buying more economical raw materials, determining the ideal moisture for each sinter bed, producing the highest quality sinter possible and being able to minimise PM emissions.

3. The micropellets addition to the sinter blend has a significant impact on sintering (process stability and productivity) as well as the environment (emissions). The output of the thesis highlights the feasibility of the use of more recycled materials and allows for finer raw material acquisitions, thus reducing costs of manufacture. Currently, business cases have been developed to suggest a trial of adding more than 4000T of micropellets to a sintering blend.

4. By maximising the recycling resources with additional processing, the steel industry would move toward a more circular economy. This experiment has shown that washing recycled materials in water can eliminate unwanted volatile components that can harm the processes used to make iron. This can result in using less of the high-value iron materials, which would save a significant amount of money. To wash the ESP dust before it was recycled back into the sinter plant, business cases have now been developed.

5. For the first time, it was possible to understand the quantity and characterisation of the return fines particulates that were being recirculated continuously back into

the sinter plant system. It has been determined that the majority were larger particles that were sinter and with a small quantity of smaller particles that were raw mix which had unwanted elements attached.

The following areas have been suggested for further research based on the thesis findings and constraints on the current best available techniques, financial resources, and resources available.

- The establishment of a pilot-scale sinter rig with a dust capture device was part of the research's activities. It was advised that additional equipment be added, including a gaseous species analyser. For example, a completely automated FTIR analyser with a large elemental library that can measure any emission species of interest using ppb level detection such as COx, NOx, SOx etc. With these changes, it will be possible to support the steel industry's decarbonisation through further experimental studies with different biomass and the use of a lower carbon footprint gas as an ignition fuel to support achieving net zero.

- Before using the sinter blend on the sinter plant, the industry will need to understand the sinter stability, sinter quality, and its environmental impact (emissions). This will require recommending the sinter plant for routine bed-to-bed testing on the pilot-scale sinter rig. In the long term, it will be feasible to use this data to build a prediction model for the sinter plant that can forecast emissions before acquiring raw materials.

- This research demonstrated the benefits of adding micropellets into a sintering blend. However, more research was required to optimise the amount of ferrous recycled materials in the micropellets, which can minimise PM emissions to make a circular economy a reality.

- To further advance the circular economy, it has been demonstrated in this thesis that further processing can remove undesired volatile components from recovered materials. Other recycled materials that coould be cleaned, including BOS sludges, etc., would be less damaging to the processes used in iron making and would be used more in more quantity and frequently, leading to further cost reductions. A potential exists to use the washing by-product as a potassium fertiliser.

- Through careful adjustment of the NTLR ratio as this research's work has shown, it was possible to reduce PM emissions. Further research should explore this strategy for various sinter blends as the optimum ratio would vary from blend to blend.

Appendices

Appendix 1 - Safe working procedure: Pilot-scale sinter rig

Warnings and Precautions

- Safety precautions were taken in line with the risk assessment above.
- Handling samples, Full PPE is to be worn as stated above in the risk assessment.
- PPE is to be always worn, also a 4-in-1 gas monitor is to be placed in the laboratory and switched on during all testing. Manual handling procedures were to be always followed.
- Operation of equipment – only trained and competent employees were to use this equipment. Extreme care should be taken when undergoing analysis due to the hazards outlined in the risk assessment above.
- Extraction system to be used during the testing process.
- For use of the cement mixer please ensure the following precautions were taken:
- Constrain loose clothing and long hair.
- Keep hands/fingers away from the rotating drum and drive system.
- Do NOT place the shovel in the drum when rotating.
- Do NOT leave the machine running unattended.
- Ensure the lid is fastened to the cement mixer to avoid dust spilling out.
- Report all machine faults and hazards.
- Make sure all tools and other equipment was removed from the cement mixer before turning it on.
- Do not overload the mixer. An overload can damage the mixer.
- Do not move the cement mixer during operation. The mixer can tip over or the motor can be damaged.
- When transporting the mixer, disconnect the power and make sure the drum is empty of all material/
- Ensure the lid is secure on the cement mixer during use.

Apparatus

- Galvanised Bucket
- Sample trays

- 3001-320-0600-0008-0047 Pickstone oven.
- Riffle box.
- Moisture balance
- Granulation drum
- Pilot-scale sinter rig
- Burner head
- Gas rig
- Type R Thermocouples X 5
- Type K Thermocouples X 3
- Sieves
- Drying oven
- Cement Mixer
- Scoop
- Ceramic sleeves
- Weighing Balance

Drying and storage of sample material

All samples were collected and dried for at least 24 hours at 105˚C.

1) Fill galvanised buckets or sample trays with individual iron ores
2) Using the pickstone oven located in the sampler's building, place the buckets/trays in the oven and leave for a minimum of 24 hours.
3) Retrieve the samples after 24 hours wearing chrome leather heat protective gloves and long sleeves as the bucket/trays will be hot.

Screening

1) Iron ores <5 mm were to be screened out using round 5 mm sieves. The screen-out process can be done manually or by using the vibrating sieve plate.
2) Coke breeze <3 mm to be screened out using round 3 mm sieves. The screen-out process can be done manually or by using the vibrating sieve plate.
3) Flux <3 mm to be screened out using round 3 mm sieves. The screen-out process can be done manually or by using the vibrating sieve plate.

Operating the vibrating sieve plate

1) Pour the full contents of the dried sample into the sieve stack.
2) Turn on the sieve shaker and allow it to shake for 4 minutes.
3) Switch off the sieve shaker and allow it to settle.
4) Pour contents of the <5mm (or <3 mm if screening fuel or flux) sieve in designated sample bins and discard >5mm (or 3mm if screening fuel or flux)

Preparing blend

Using the blend model spreadsheet provided, the user can construct a blend with predicted chemistry. Please ensure to use dry, screened material.

Once correct weights were obtained, proceed to store samples in a storage facility and collect individual constituents i.e., iron ore, flux, fuel

1) Using the weight balance, weigh out the correct amounts stated in the blend model spreadsheet and place them into a bucket.
2) Once all material has been weighed out into a single bucket, the content of the bucket can be poured into a cement mixer.
3) Ensure the cement mixer is fastened at 30 degrees.
4) Ensure the lid is fastened to the cement mixer.
5) Turn the green switch on and allow the cement mixer to rotate for 2 minutes to obtain a dry homogenous mixture.
6) Turn the red switch to stop.
7) Unclamp the lid and slide the mixed blend into a bucket ready for granulation.

Moisture test

The sample can now be brought back into the pilot-scale sinter rig lab. A moisture test is conducted using the moisture balance.

1) Turn on the moisture control balance via the plug socket
2) Wait approximately 30 seconds and open the lid.
3) Ensure the correct metallic dish provided is clean and in the correct position.
4) Close the lid of the moisture control balance and wait until the mass can be seen on the digital screen.
5) Re-open the lid, and place 20g of the sample in the metallic dish when prompted on the digital screen.

6) Close the lid (reading will start to be taken, do not open the lid when in operation) The device will sound once complete. Take 3 readings for accuracy.

Prepare a water spray can before starting the granulation drum. Providing the blend is dry - 1.1 litres of water is placed in the spray can achieve a 5-6.5% moisture reading in the blend.

1) Fill the pressurised spray can with 1.1 litre of water.
2) Pressurise the spray can with 100 pumps
3) When using the spray can, an automatic switch on the nozzle can be used

Granulation

1) Open the cage and pour the contents of the bucket into the granulation drum. Tilt granulation drum for ease.
2) Ensure the lid is fastened to the granulation drum.
3) Pull down the safety cage and ensure it is magnetically interlocked and set the granulation speed to 0.
4) Turn on the granulation drum by pressing the green button and turning the dial from off to on.
5) Once the drum starts to rotate, the nozzle of the spray can be carefully placed into the hole in the cage and the drum.
6) Spray all the water into the rotating granulation drum with a back-and-forth motion to ensure the water is evenly spread across the blend (this process takes approximately 4 minutes).
7) Once all the water is deposited in the granulation drum, leave the drum to rotate for a further 5 minutes.
8) Stop the granulation drum after 5 minutes by pressing the red stop button and turning the dial from on to off.

Once granulation has been completed, the blend can be split into 2 8kg samples using the riffle box. 7kg is used to fill up the reaction vessel and 1 kg is left for further analysis. Ensure the riffle box is free of debris as well as the trays was aligned underneath. Ensure the trays were properly aligned.

1) Safely remove the granulation drum and empty the contents into the clean, closed riffle box. – be cautious that the granulation drum can be heavy.

2) Spread the blend evenly across the riffle box. – ensure even split minimising mechanical noise i.e., not to disrupt particle size or packing.

3) Pull the lever on the side and allow the mixture to fall evenly into the underneath trays. Each tray is enough for 1 furnace run + 1kg for analysis.

Computer Set Up

1) Turn the computer system on with a switch. (Pilot-scale sinter rig control interface should be displayed)

2) Ensure there is a USB drive in the port when switching on the computer as it will not be recognised after this point and the computer system will have to be restarted if a USB is needed.

3) Open the desktop shortcut 'Pilot-scale sinter rig .'

4) Input 'sample name' and 'sample ID' ('time start' and 'time end' will be input automatically when the test starts and ends)

Analysis Procedure

1) Using the leaver in the middle of the two pilot-scale sinter rigs, rotate in a clockwise movement to higher the pilot-scale sinter rigs to enable the operator to rotate the desired pilot-scale sinter rig 180° over the wheelbarrow in a vertical position.

2) Using a metal rod, carefully push into each thermocouple entrance to ensure there was no blockages.

3) Ensure metal mesh is placed at bottom of the pilot-scale sinter rig, held up by bolts.

4) A layer of 400g of hearth layer at a side portion of 10-15mm is evenly spread across the bottom, on top of the metal mesh. (This prevents the blend from binding to the mesh)

5) Scoop by scoop place the 7kg blend into the pilot-scale sinter rig ensuring each scoop is rotated in a different position to prevent preferential packing. (To prevent big particles from falling to one side – which can cause channelling). Fill to the top of the furnace and level off with a ruler to ensure a flat surface minimising packing.

6) Rotate the reaction vessel 180˚still at a vertical position very carefully not to hit the vessel when positioning back in place. (Be aware of trapping points at the bottom of the vessel when positioning).

7) Extreme care should be taken when lowering the reaction furnace into place by turning the middle leaver in a clockwise position.

8) Ensure mechanical noise is kept to a minimum when positioning the pilot-scale sinter rig with blend inside

Cold Permeability Test

1) On the computer system open the 'PID' tab. Set a set point depending on parameters. Usually set at 100mbar.

2) Carefully fasten the flow meter over the top of the reaction vessel and lower using the top leaver turn

3) Plug all the steel thermocouple tubes with rubber seals.

4) Set the computer system to manual and press the 'log' button. (Light will turn from green to red when logging data)

5) Ensure the yellow dial is turned on

6) A red line and a white line will appear on the screen, when the lines meet, the extraction can be turned on by pressing the green 'on' extraction button.

7) Allow the cold permeability test to run for 5 minutes before stopping the recording by repressing the 'log' button and pressing stop.

8) Close the page down and set up new logging data ready for sintering.

1) Note: The white line on the screen indicates the pressure drop. The red line indicates

Sintering Process

1) Unfasten the flow meter head by rotating the top leaver anticlockwise. Rotate the dial to set the burner head in position. (Use extreme care not to hit the furnace and disturb the mixture. Be aware of the trapping point when positioning the burner head). Lower the burner head into position carefully, the ignition pipe should be resting on the edge. (1 inch above the pilot-scale sinter rig).

2) Unplug the rubber seals and poke a measured hole using a metal rod into the steel tube and the bed for the thermocouple to sit into.

3) Plug thermocouples with ceramic sleeves

4) Insert the thermocouple (with ceramic sleeve) into steel tubes and blend ensuring the thermocouples should be at the same depth in the blend.

5) If not, all thermocouples were in use be sure to plug the steel thermocouple entrances with rubber corks.

6) Ensure the burner head is fastened into place. (1 inch above the pilot-scale sinter rig).

2) The pilot-scale sinter rig is not set up and is ready to ignite.

7) Start recording data by switching to automatic control and clicking the green log button (will turn red when recording).

8) Once recording turns the extraction fan on immediately by turning the yellow dial to the 'on' position and pressing the green button.

9) Wait for the pressure to get to 99/100mbar before igniting the burner head.

10) Ensure all gas valves and air supply valves was open apart from the final valves. Once the pressure drop reaches 99/100mbar, the final gas and air valves can be opened, and the red button is pressed to start the ignition process.

11) After 1 minute of ignition, immediately close the gas and air supply valves to turn off the ignition.

12) Unfasten the burner head using the top leaver and turn it anticlockwise. *Extreme care should be taken, and heat-resistant gloves must be worn.*

13) Fasten the flow meter back on.

14) Allow the sintering process to complete. (~30minutes)

15) Stop the test when all 7 thermocouples read <100˚C. This can be seen in the Temperature tab as well as the manual tab.

16) Stop the test by switching back to 'manual control,' press the red 'logging' button to stop recording (will turn green) and press 'stop,' all on the computer program. The red bottom-to-stop extraction fan can be pressed immediately after the data has stopped recording.

17) Raw data is recorded to a memory stick and can be exported to a pilot-scale sinter rig test spreadsheet.

Discharging of Pilot-scale sinter rig

PPE is to be worn throughout. I.e., glasses, overalls, and heat-resistant gloves.

1) Once all thermocouples read <100˚C they were safe to be removed. Remove all thermocouples and place them in the designated area. (If stuck tip the rig horizontally and knock slightly to release the thermocouples. Note: may need assistance if thermocouples were stuck, beware of hot sinter/pilot-scale sinter rig)

2) Unfasten the flow meter by rotating the top leaver anticlockwise.

3) Unclamp the ceramic insulation.

4) Using the leaver positioned in the middle, turn anticlockwise enabling the operator to move the reaction vessel 180˚. Rotate the reaction vessel 180˚ and securely position it over the provided wheelbarrow.

5) Tilt the reaction vessel 180˚ vertically therefore that it is upside down.

6) Using a metal rod gently push the sinter into a wheelbarrow. Please ensure PPE is worn.

7) Place the content of the wheelbarrow into a bucket ready for post-analysis.

Post-Sinter Prep

The sinter should be allowed to cool to room temperature (hour) before sizing analysis takes place. The large sieve shaker shall be used for the size analysis. The various screen sizes shall be set in descending order largest screen at the top +40mm down to the smallest screen at the bottom -5mm.

1) Tip contents of 1 pot test worth into top sieve

2) The large top lid is placed onto the screens and secured in place using threaded bolts, which lock onto the top plate, ensuring the bolts was tight.

3) The mechanical sieve is turned on via the green button and allowed to break the sinter apart for 2 minutes.

4) The mechanical sieve must not be touched when it is in use, after time has elapsed, the machine must be stopped by depressing the emergency stop button.

5) Once the mechanical sieve has been completed, the top plate is removed.

6) Sieve by sieve, the content in each size fraction can be weighed out and noted.

7) 300/500g of the 16-25mm sample is kept for the RDI test. Can be submitted via a single source.

8) 50g of sinter between 16-25mm kept for chemical analysis. Can be submitted via a single source.

Appendix 2 - Safe working procedure: Measurement of PM emissions

Pre-conditioning of filters

1) Turn on the drying oven to 180°C
2) Once the oven has reached 180°C, place the glass dish with the filters in it into the oven for a period not less than 1 hour.
3) Remove the filers from the oven and place them into the desiccator which is situated in the balance room for at least 4 hours (the best practice is overnight).
4) Check balance against a standard weight (1g).
5) Record batch number and type of filters.
6) Label, weigh filters and record.
7) Store filters in an airtight bag.

Use of Dust Capture Device

1) The dust capture device is situated underneath the pilot-scale sinter rig, turning both chamfer locks to unlock the removable door.
2) Clean any previous dust from the tray and filter holder.
3) Place a pre-conditioned filter inside the filter holder using a stainless-steel tweezer tool.
4) Place and turn the chamfer locks into position for an airtight seal.
5) After each test on completion, turn both chamfer locks to unlock the removable door,
6) Remove the filter inside the filter holder using a stainless-steel tweezer tool and place it into individual airtight sealed packets.
7) Collect the deposited dust from the tray using a small brush and place it into individual airtight sealed packets.
8) Conduct sizing on the deposited dust from the tray and record weights for >1mm, 0.5mm, 0.25mm, 0.15mm, 0.063mm, and <0.063mm.
9) Submit each deposited dust from the tray for XRF, ICP (alkalis) and Chloride analysis.

Post-Conditioning of Filters

1) Record BALANCE ID.

2) Check balance against a standard weight (1g).

3) Turn on the drying oven to 160°C.

4) Once the oven has reached 160°C, place the glass dish with the filters in it into the oven for a period not less than 4 hours.

5) Weighing shall be conducted within 3 minutes after removal from the desiccator (not for filters to gain weight from absorbing moisture) and record the weight of filters.

6) Place the filter back into the airtight sealed packet, ready for any future chemical analysis such as ICP-OES for Fe, Sulphur, and Chloride.

Appendix 3 – Raw Data for Historical Data Analysis

Appendix 4 – Pilot-scale sinter rig results for validation that displays minimal variation (1)

Process Parameter	1 - Base blend	2 - Base blend	3 - Base blend	4 - Base blend	5 - Base blend	6 - Base blend	Standard Deviation	% Deviation
Hot Flow Average (m^3/hr)	7.7	7.5	7.3	7.4	7.8	8.4	0.36	5%
Cold Flow Average (m^3/hr)	9.6	8.9	10.5	10.3	11.0	11.1	0.78	8%
Max Sintering Temperature (°C)	1265	1288	1313	1286	1265	1288	16.21	1%
Sintering Time (mm : ss)	00:22:10	00:21:55	00:22:50	00:20:25	00:22:30	00:21:10	00:00:49	4%
Sintered Air Flow (m^3/hr)	32.3	31.5	34.2	34.6	27.5	29.4	2.51	8%
Flame Front Speed Average (mm/s)	0.30	0.31	0.28	0.32	0.30	0.30	0.01	5%
Max off-gas 1 temperature (°C)	370	369	399	358	325	325	26.03	7%
Max off-gas 2 temperature (°C)	94	101	92	99	84	89	5.76	6%
Fraction of sinter >5mm (%)	53	53	51	51	51	52	0.78	2%
Flame Front Width (mm)	10.2	12.6	12.6	10.7	9.8	7.5	1.75	17%
Cooling Rate (°C/s)	3.5	3.4	3.8	3.9	3.9	3.9	0.21	6%
Sinter Combustion rate (°C/s)	19.3	18.9	21.9	17.5	20.9	21.1	1.49	7%
PM emissions Concentration on the filter (mg/m^3)	14.8	16.0	14.7	19.3	17.9	18.4	1.79	11%
PM emissions on the filter (mg)	41.9	43.8	40.7	48.9	51.8	54.2	5.07	11%
Return fines particulates (g)	29.8	18.7	28.6	27.7	27.7	18.3	4.72	19%

Appendix 5 – Pilot-scale sinter rig results for validation

Process Parameter	Bed 1 (NTLR 1.5)	Bed 2 (NTLR 1.6)	Bed 3 (NTLR 1.7)
Hot Flow Average (m^3/hr)	11.8	11.0	11.1
Cold Flow Average (m^3/hr)	14.6	13.7	16.0
Max Sintering Temperature (°C)	1335	1288	1386
Sintering Time (mm : ss)	00:14:20	00:13:55	00:13:35
Sintered Air Flow (m^3/hr)	33.79	34.31	36.82
Flame Front Speed Average (mm/s)	0.15	0.14	0.14
Max off-gas 1 temperature (°C)	638	645	611
Max off-gas 2 temperature (°C)	111	105	99
Fraction of sinter >5mm (%)	28	29	28
Flame Front Width (mm)	5.7	6.6	3.3
Cooling Rate (°C/s)	4.1	4.8	3.9
Sinter Combustion rate (°C/s)	32.8	27.4	24.3
PM emissions Concentration on the filter (mg/m^3)	27.0	31.7	27.1
PM emissions on the filter (mg)	78.0	81.0	68.0
Return fines particulates (g)	9.0	13.1	10.1

Appendix 6 – Pilot-scale sinter rig results for micropellets

Process Parameter	Base blend 7 (0% MP)	Blend 1 (3.63% Initial MP)	Blend 2 (7.27% Initial MP)	Blend 3 (3.63% Recycled MP)	Blend 4 (3.63% IRON ORE A MP)	Blend 5 (3.63% IRON ORE B MP)
Hot Flow Average (m³/hr)	7.7	9.8	11.0	8.40	8.82	9.60
Cold Flow Average (m³/hr)	8.8	11.6	12.6	8.76	10.93	10.33
Max Sintering Temperature	1379	1316	1259	1220.50	1403	1368.02
Sintering Time (mm:ss)	00:17:30	00:13:30	00:13:05	00:21:05	00:15:30	00:15:15
Sintered Air Flow (m3/hr)	50.03	48.2	39.83	45.51	31.9	34.15
Flame Front Speed Average (mm/s)	0.99	0.58	0.54	0.52	0.73	0.44
Max off-gas 1 temperature	550	681	555	709	620	603
Max off-gas 2 temperature	209	187	187	160	165	173
Fraction of sinter >5mm (%)	25	16	15	25	26	24
PM Concentration on the filter (mg/m³)	22.9	8.5	8.5	10.0	7.3	9.2
PM emissions on the filter (mg)	51.8	18.9	20.5	29.4	16.6	22.5
Return fines particulates (g)	13.8	13.6	14.5	26.1	22.3	23.7

Appendix 7 – Pilot-scale sinter rig results for the addition of KCl for each blend ranging from 0, 200, 400 and 600 mgC/kg

Process Parameter	Base Blend 1 (0 Cl)	Blend 6 (200 Cl)	Blend 7 (400 Cl)	Blend 8 (600 Cl)
Hot Flow Average (m^3/hr)	7.8	8.4	8.3	7.9
Cold Flow Average (m^3/hr)	11.0	11.7	11.6	11.9
Max Sintering Temperature	1265	1267	1299	1292
Sintering Time (mm:ss)	00:22:30	00:20:00	00:20:05	00:21:10
Sintered Air Flow (m^3/hr)	27.46	33.04	28.87	28.10
Flame Front Speed Average (mm/s)	0.30	0.33	0.33	0.31
Max off-gas 1 temperature	325	398	386	335
Max off-gas 2 temperature	84	86	86	81
Fraction of sinter >5mm (%)	51	52	47	50
PM Concentration on the filter (mg/m^3)	17.9	20.4	23.2	27.1
PM emissions on the filter (mg)	51.8	57.3	64.2	75.3
Return fines particulates (g)	27.7	14.5	9.8	5.5

Appendix 8 – Pilot-scale sinter rig results for ESP and WESP

Process Parameter	Base Blend 7 (0% ESP/ WESP)	Blend 10 (0.35% ESP)	Blend 11 (2.5% ESP)	Blend 12 (5% ESP)	Blend 13 (0.35% WESP)	Blend 14 (2.5% WESP)	Blend 15 (5% WESP)
Hot Flow Average (m³/hr)	7.7	8.6	7.4	6.6	8.6	6.9	7.3
Cold Flow Average (m³/hr)	8.8	10.2	9.2	8.3	10.01	8.17	8.2
Max Sintering Temperature	1379	1349	1382	1413	1390.1	1369.4	1389
Sintering Time (mm:ss)	00:17:30	00:22:50	00:20:25	00:22:25	00:16:15	00:22:00	00:23:55
Sintered Air Flow (m3/hr)	50.03	34.12	47.0	47.0	40.58	43.57	42.1
Max off-gas 1 temperature	550	568	690	736	592	670	692
Max off-gas 2 temperature	209	160	199	161	192	189	155
Fraction of sinter >5mm (%)	25	22	29	29	19	24	23
PM Concentration on the filter (mg/m³)	22.9	21.2	23.6	36.7	22.8	20.4	21.6
PM emissions on the filter (mg)	51.8	69.2	59.2	89.8	59.0	51.6	63.1
Return fines particulates (g)	13.8	20.3	21.2	20.3	17.9	13.1	18.8

Appendix 9 - Pilot-scale sinter rig results for the displacement of two ultra-fines iron ores

Process Parameter	Base Blend 1 (0% Iron Ore C)	Blend 16 (5% Iron Ore C)	Blend 17 (10% Iron Ore C)	Blend 18 (15% Iron Ore C)	Blend 19 (20% Iron Ore C)	Blend 20 (25% Iron Ore C)
Hot Flow Average (m^3/hr)	7.8	7.0	7.1	7.4	7.7	7.1
Cold Flow Average (m^3/hr)	11.0	10.4	10.0	11.3	10.9	10.3
Max Sintering Temperature	1265	1274	1276	1270	1300	1280
Sintering Time (mm:ss)	00:22:30	00:26:15	00:22:40	00:21:25	00:20:55	00:22:45
Sintered Air Flow (m3/hr)	27.5	21.6	30.8	27.0	32.6	27.7
Flame Front Speed Average (mm/s)	0.30	0.27	0.28	0.30	0.34	0.28
Max off-gas 1 temperature	325	319	336	374	281	326
Max off-gas 2 temperature	84	78	97	85	100	84
Fraction of sinter >5mm (%)	51	58	47	53	47	51
Flame Front Width (mm)	9.8	7.9	8.8	7.1	13.7	7.3
Cooling Rate (°C/s)	3.9	3.8	2.8	4.4	4.4	4.2
Sinter Combustion rate (°C/s)	20.9	19.8	12.4	18.5	19.6	14.2
PM Concentration on the filter (mg/m^3)	17.9	16.0	12.1	12.4	17.0	16.9
PM emissions on the filter (mg)	7.8	7.0	7.1	7.4	7.7	7.1
Return fines particulates (g)	11.0	10.4	10.0	11.3	10.9	10.3

Appendix 10 - Pilot-scale sinter rig results for varying absolute levels of individual size fractions

Process Parameter	Blend 21 (35% Nuclei)	Blend 22 (40% Nuclei)	Blend 23 (45% Nuclei)	Blend 24 (50% Nuclei)	Blend 25 (55% Nuclei)
Hot Flow Average (m³/hr)	6.0	8.5	9.9	11.3	8.8
Cold Flow Average (m³/hr)	13.0	21.4	15.3	23.2	26.6
Max Sintering Temperature	1312	1332	1396	1413	1327
Sintering Time (mm:ss)	00:25:55	00:17:55	00:16:50	00:16:05	00:22:50
Sintered Air Flow (m3/hr)	29.23	53.80	50.66	47.4	37.14
Flame Front Speed Average (mm/s)	0.14	0.18	0.18	0.17	0.02
Max off-gas 1 temperature	430	675	740	768	877
Max off-gas 2 temperature	139	175	175	171	169
Fraction of sinter >5mm (%)	28	17	19	21	36
Flame Front Width (mm)	#N/A	10.4	12.8	11.2	#N/A
Cooling Rate (°C/s)	#N/A	2.9	2.3	3.6	#N/A
Sinter Combustion rate (°C/s)	#N/A	11.2	11.8	13.4	#N/A
PM Concentration on the filter (mg/m³)	30.3	17.0	13.2	16.1	26.9
PM emissions on the filter (mg)	75.1	43.4	36.6	47.5	92.1
Return fines particulates (g)	5.7	5.7	10.2	4.9	3.7

Bibliography

[1]   Fernández-González D, Ruiz-Bustinza I, Mochón J, González-Gasca C, Verdeja LF. Iron Ore Sintering: Process. Mineral Processing and Extractive Metallurgy Review 2017;38:215–27. https://doi.org/10.1080/08827508.2017.1288115.

[2]   Menad N, Tayibi H, Carcedo FG, Hernández A. Minimization methods for emissions generated from sinter strands: A review. J Clean Prod 2006;14:740–7. https://doi.org/10.1016/J.JCLEPRO.2004.03.005.

[3]   Lanzerstorfer C, Fleischanderl A, Plattner T, Lanzerstorfer C. Efficient Reduction of PM 10 / 2.5 emissions at Iron Ore Sinter Plants. 2007.

[4]   Remus R, Aguado-Monsonet Serge Roudier MA, Delgado Sancho L, Aguado Monsonet MA, Roudier S. Best Available Techniques (BAT) Reference Document for Iron and Steel Production 2013. https://doi.org/10.2791/97469.

[5]   Gan M, Ji Z, Fan X, Chen X, Li Q, Yin L, et al. Emission behavior and physicochemical properties of aerosol Particulate Matter (PM10/2.5) from Iron Ore Sintering Process. ISIJ International 2015;55:2582–8. https://doi.org/10.2355/isijinternational.ISIJINT-2015-412.

[6]   Taiwo AM, Harrison RM, Beddows DCS, Shi Z. Source apportionment of single particles sampled at the industrially polluted town of Port Talbot, United Kingdom by ATOFMS. Atmos Environ 2014;97:155–65. https://doi.org/10.1016/J.ATMOSENV.2014.08.009.

[7]   Taiwo AM, Beddows DCS, Calzolai G, Harrison RM, Lucarelli F, Nava S, et al. Receptor modelling of airborne particulate matter in the vicinity of a major steelworks site. Science of The Total Environment 2014;490:488–500. https://doi.org/10.1016/J.SCITOTENV.2014.04.118.

[8]   Thermo. TEOM 1405F Operator's Manual. 2007.

[9]   Evrard D, Laforest V, Villot J, Gaucher R. Best Available Technique assessment methods: A literature review from sector to installation level. J Clean Prod 2016;121:72–83. https://doi.org/10.1016/j.jclepro.2016.01.096.

[10]   Report on Carcinogens (12th Ed.) - Nat. Toxicology Program (NTP) (NIH) - Google Books n.d. https://books.google.co.uk/books?id=raW5FLj408QC&pg=PA122&lpg=PA122&dq=-

+Kaegi,+D.,+Addes,+V.,+Valia,+H.+and+Grant,+M.+(2000).+Coal+Conversion +Processes,+Carbonization.+Kirk-

Othmer+Encyclopedia+of+Chemical+Technology.&source=bl&ots=5xW5Uh82P I&sig=ACfU3U1UPR6bg_l_Vn-qDwKYPtF-

3J_EYQ&hl=en&sa=X&ved=2ahUKEwiVj8j084_mAhVlSxUIHfQfAMIQ6AEw AnoECAoQAQ#v=onepage&q=- Kaegi%2C D.%2C Addes%2C V.%2C Valia%2C H. and Grant%2C M. (2000). Coal Conversion Processes%2C Carbonization. Kirk-Othmer Encyclopedia of Chemical Technology.&f=false (accessed November 29, 2019).

[11]   Okosun T, Street SJ, Zhao J, Wu B, Zhou CQ. Influence of conveyance methods for pulverised coal injection in a blast furnace. Ironmaking and Steelmaking 2017;44:513–25. https://doi.org/10.1080/03019233.2016.1217116.

[12]   Association ST. MCerts Level 2 Training Booklet. 2017.

[13]   National Resources Wales. EPR/BL7108IM Permit. 2010.

[14]   Kubat C, Taşkin H, Artir R, Yilmaz A. Bofy-fuzzy logic control for the basic oxygen furnace (BOF). Rob Auton Syst 2004;49:193–205. https://doi.org/10.1016/j.robot.2004.09.007.

[15]   Clout JMF, Manuel JR. Mineralogical, chemical, and physical characteristics of iron ore. 2015. https://doi.org/10.1016/B978-1-78242-156-6.00002-2.

[16]   Materials Education Training and Learning. Burdening Course, 2015.

[17]   Lanzerstorfer C. Emission reduction for iron ore sinter plants 2016.

[18]   TATA Steel. Knowledge document Processes Heavy End at IJmuiden 2016.

[19]   Air Quality Group. Understanding PM10 in Port Talbot. 2011.

[20]   Loo CE, Wong DJ. Fundamental factors determining laboratory sintering results. ISIJ International 2005;45:449–58. https://doi.org/10.2355/isijinternational.45.449.

[21]   Yang W, Ryu C, Choi S, Choi E, Ri DW, Huh W. Mathematical model of thermal processes in an iron ore sintering bed. Metals and Materials International 2004;10:493–500. https://doi.org/10.1007/BF03027355.

[22]   Lu L, Ishiyama O. Iron ore sintering. 2015. https://doi.org/10.1016/B978-1-78242-156-6.00014-9.

[23]   Mochón J, Verdeja LF. IRON ORE SINTERING PART 2. QUALITY INDICES AND PRODUCTIVITY SINTERIZACIÓN DE MINERALES DE HIERRO

PARTE 2. ÍNDICES DE CALIDAD Y PRODUCTIVIDAD ALEJANDRO CORES ÍÑIGO RUIZ-BUSTINZA JOSÉ IGNACIO ROBLA FERNANDO GARCIA-CARCEDO 2014;81:168–77.

[24] Lu L, Holmes RJ, Manuel JR. Effects of Alumina on Sintering Performance of Hematite Iron Ores. ISIJ International 2007;47:349–58. https://doi.org/10.2355/isijinternational.47.349.

[25] Bhagat RP, Chattoraj US, Sil SK. Porosity of Sinter and Its Relation with the Sintering Indices. ISIJ International 2006;46:1728–30. https://doi.org/10.2355/isijinternational.46.1728.

[26] Jeans B. Research and Development of a High Temperature Pot for the Sintering of Iron Ores 2014.

[27] Biswas AK. Principles of blast furnace ironmaking: Theory and Pratice. 1981.

[28] C. Price and D. Wasse. Iron Ore Sintering. Conf Iron and Steel Institute 1972.

[29] P F. Journal of Iron and Steel Research. Research International 2011.

[30] Shen Huiguo, Du Jianxin W shengli. Experimental Research on Basic Sintering Features of Iron Ore powder. Metallurgical Research 2005.

[31] He Litang QFengming. Characteristics and Applications of Sinter waste gas ESP. Academic Discussion 2003.

[32] SASAKI M, HIDA Y. Consideration on the Properties of Sinter from the Point of Sintering Reaction. Tetsu-to-Hagane 1982;68:563–71. https://doi.org/10.2355/tetsutohagane1955.68.6_563.

[33] Mumme W, Clout J, Gable R. The crystal structure of SFCA-I, Ca3.18Fe3 14.66Al1.34Fe 2 0.82O28, a homologue of the aenigmatite structure type, and new crystal structure refinements of β-CFF, Ca2.99Fe3 14.30Fe2 0.55O25. Neues Jahrbuch Fur Mineralogie, Abhandlungen 1998;173.

[34] Ahsan, S.N. / Mukherjee, T. / Whiteman JA. Structure of fluxed sinter. Ironmaking and Steelmaking 1983:54–69.

[35] Pownceby MI, Clout JMF. The Importance of Fine Ore Chemical Composition and High Temperature Phase Relations - Applications Ton Iron Ore Sintering and Pelletising. Australasian Institute of Mining and Metallurgy Publication Series 2002;9553:209–15. https://doi.org/10.1179/037195503225011402.

[36] Umadevi T, Naik DK, Sah R, Brahmacharyulu A, Marutiram K, Mahapatra PC. Studies on parameters affecting sinter strength and prediction through artificial

neural network model. Transactions of the Institutions of Mining and Metallurgy, Section C: Mineral Processing and Extractive Metallurgy 2016;125:32–8. https://doi.org/10.1179/1743285515Y.0000000020.

[37] Umadevi T, Brahmacharyulu A, Sah R, Mahapatra PC, Prabhu M. Optimisation of MgO addition in low and high silica iron ore sinter to improve sinter reducibility. Ironmaking and Steelmaking 2014;41:270–8. https://doi.org/10.1179/1743281213Y.0000000124.

[38] Yadav US, Pandey BD, Das BK, Jena DN. Influence of magnesia on sintering characteristics of iron ore. Ironmaking and Steelmaking 2002;29:91–5. https://doi.org/10.1179/030192302225002018.

[39] Li T, Sun C, Liu X, Song S, Wang Q. The effects of MgO and Al2O3 behaviours on softening–melting properties of high basicity sinter. Ironmaking and Steelmaking 2018;45:755–63. https://doi.org/10.1080/03019233.2017.1337263.

[40] Donskoi E, Hapugoda S, Manuel JR, Poliakov A, Peterson MJ, Mali H, et al. Automated optical image analysis of iron ore sinter. Minerals 2021;11. https://doi.org/10.3390/MIN11060562.

[41] Lu L, Ooi TC, Li X. Sintering emissions and their mitigation technologies. Iron Ore 2015:551–79. https://doi.org/10.1016/B978-1-78242-156-6.00018-6.

[42] Khosa J, Manuel J, Trudu A. Results From a Preliminary Investigation of Particulate Emission During the Sintering of Iron Ore. Australasian Institute of Mining and Metallurgy Publication Series 2002;112:291–8. https://doi.org/10.1179/037195503225011367.

[43] Debrincat D, Loo CE. Factors Influencing Particulate Emissions during Iron Ore Sintering. ISIJ International 2007;47:652–8. https://doi.org/10.2355/isijinternational.47.652.

[44] M. te Lindert. Demonstration plant for sintering with reduced volume of flue gases. Hoogovens 1996:1–7.

[45] Passant NR, Peirce M, Rudd HJ, Scott DW, Marlowe I, Watterson JD. UK Particulate and Heavy Metal Emissions from Industrial Processes. 2002.

[46] D. Poole, E. Aries, D. Ciaparra, D.R. Anderson, S. Johnston, N. Schofield, A. Horne DH. Investigations into the parameters influencing plume visability at UK sinter plants 2011.

[47] Chen Y-C, Kuo Y-C, Chen M-R, Wang Y-F, Chen C-H, Lin M-Y, et al. Reducing polychlorinated dibenzo-p-dioxins and dibenzofurans (PCDD/F) emissions from a real-scale iron ore sinter plant by adjusting its sinter raw mix. J Clean Prod 2016;112:1184–9. https://doi.org/10.1016/J.JCLEPRO.2015.07.013.

[48] Anderson DR, Fisher R. Sources of dioxins in the United Kingdom: the steel industry and other sources. Chemosphere 2002;46:371–81. https://doi.org/10.1016/S0045-6535(01)00178-3.

[49] WHO | Ambient air pollution. WHO 2018.

[50] Lelieveld J, Evans JS, Fnais M, Giannadaki D, Pozzer & A. The contribution of outdoor air pollution sources to premature mortality on a global scale n.d. https://doi.org/10.1038/nature15371.

[51] Moreno T, Jones TP, Richards RJ. Characterisation of aerosol particulate matter from urban and industrial environments: examples from Cardiff and Port Talbot, South Wales, UK. Science of The Total Environment 2004;334–335:337–46. https://doi.org/10.1016/J.SCITOTENV.2004.04.074.

[52] WHO. Health Aspects of Air Pollution with Particulate Matter, Ozone and Nitrogen Dioxide Report. 2003.

[53] Putaud J-P, Van Dingenen R, Alastuey A, Bauer H, Birmili W, Cyrys J, et al. A European aerosol phenomenology – 3: Physical and chemical characteristics of particulate matter from 60 rural, urban, and kerbside sites across Europe. Atmos Environ 2010;44:1308–20. https://doi.org/10.1016/J.ATMOSENV.2009.12.011.

[54] Monitoring PM 10 and PM 2.5 Environment Agency. 2012.

[55] El Morabet R. Effects of Outdoor Air Pollution on Human Health. Reference Module in Earth Systems and Environmental Sciences 2018. https://doi.org/10.1016/B978-0-12-409548-9.11012-7.

[56] Tang HP on. Recent development in analysis of persistent organic pollutants under the Stockholm Convention. TrAC - Trends in Analytical Chemistry 2013;45:48–66. https://doi.org/10.1016/j.trac.2013.01.005.

[57] Davis ML, Cornwell DA. Introduction to environmental engineering. McGraw-Hill; 2013.

[58] Naik S, Wesorick S, Cotton S, Plegue T, Hoffman N, TerBeek E. Visual Encyclopedia of Chemical Engineering 2016.

http://encyclopedia.che.engin.umich.edu/Pages/SeparationsChemical/Absorbers/
Absorbers.html (accessed December 2, 2019).

[59] Hanna SR, Paine RJ. Hybrid plume dispersion model (HPDM) development and evaluation. Journal of Applied Meteorology 1989;28:206–24. https://doi.org/10.1175/1520-0450(1989)028<0206:HPDMDA>2.0.CO;2.

[60] Air Quality News. High air pollution hits Port Talbot 2015. http://airqualitynews.com/2015/08/05/high-air-pollution-hits-port-talbot/ (accessed December 2, 2019).

[61] Tata Steel Group Health S and E. Assessment of the impact of emissions from Port Talbot sinter plant dedust stack 2018.

[62] Evrard D, Laforest V, Villot J, Gaucher R. Best Available Technique assessment methods: A literature review from sector to installation level. J Clean Prod 2016;121:72–83. https://doi.org/10.1016/j.jclepro.2016.01.096.

[63] Woodard MK. Stationary Source Control Techniques Document for Fine Particulate Matter. 1998.

[64] Schnelle KB, Brown CA. Air pollution control technology handbook. CRC Press; 2016. https://doi.org/10.1016/s0304-3894(02)00253-4.

[65] Visual Encyclopedia of Chemical Engineering n.d. http://encyclopedia.che.engin.umich.edu/Pages/SeparationsChemical/Absorbers/
Absorbers.html (accessed November 28, 2019).

[66] Buonicore AJ, Davis WT, Air & Waste Management Association. Air pollution engineering manual. Van Nostrand Reinhold; 1992.

[67] (PDF) The Effect of Vortex Finder Diameter on Cyclone Separator Performance and Flow Field n.d. https://www.researchgate.net/publication/215715864_The_Effect_of_Vortex_Fin
der_Diameter_on_Cyclone_Separator_Performance_and_Flow_Field (accessed November 28, 2019).

[68] Author JR, Richards PE. Air Pollution Training Institute (APTI). 2000.

[69] Demir S. A practical model for estimating pressure drop in cyclone separators: An experimental study. Powder Technol 2014;268:329–38. https://doi.org/10.1016/j.powtec.2014.08.024.

[70] Deltoid. The cyclone / chip separator from the HR-D / V-D series 2016.

[71] Bag Filter Design Software - Buy Bag Filter Product on Alibaba.com n.d. https://www.alibaba.com/product-detail/Bag-Filter-Design-Software_109265835.html (accessed November 28, 2019).

[72] Parliament E. Establishing the best available techniques (BAT) conclusions under Directive 2010/75/EU. Industrial emissions for iron and steel production. 2012.

[73] Mizuno A. Electrostatic precipitation. IEEE Transactions on Dielectrics and Electrical Insulation 2000;7:615–24. https://doi.org/10.1109/94.879357.

[74] Avis KE, DeLuca PP. Particulate Matter in the UK. Pharmaceutical Dosage Forms 2018:117–230. https://doi.org/10.1201/9780203743676-3.

[75] Sadeghbeigi R. Fluid Catalytic Cracking Handbook. Elsevier Inc.; 2012. https://doi.org/10.1016/C2010-0-67291-9.

[76] Hall HJ. History of pulse energization in electrostatic precipitation. J Electrostat 1990;25:1–22. https://doi.org/10.1016/0304-3886(90)90034-S.

[77] Ji Z, Fan X, Gan M, Chen X, Li Q, Tian Y, et al. Influence factors on PM2.5 and PM10 emissions in iron ore sintering process. ISIJ International 2016;56:1580–7. https://doi.org/10.2355/isijinternational.ISIJINT-2016-169.

[78] Gan M, Ji Z, Fan X, Chen X, Li Q, Yin L, et al. Emission behavior and physicochemical properties of aerosol Particulate Matter (PM10/2.5) from Iron Ore Sintering Process. ISIJ International 2015;55:2582–8. https://doi.org/10.2355/isijinternational.ISIJINT-2015-412.

[79] C. E. Loo: Porgress in Understanding the Science of Iron Ore Sintering,. Ironmaking Division of the Iron and Steel Society, Warrendale 1998.

[80] Jiang T, Hwang J-Y, Dean D, An G, Zhiwei G, Peng Z, et al. High-Temperature Metallurgical Processing Processing. 2019.

[81] Ji Z, Fan X, Gan M, Li Q, Chen X, Tian Y, et al. Speciation of PM2.5 released from iron ore sintering process and calculation of elemental equilibrium. ISIJ International 2017;57:673–80. https://doi.org/10.2355/isijinternational.ISIJINT-2016-650.

[82] Ji Z, Fan X, Gan M, Chen X, Li Q, Tian Y, et al. Influence Factors on PM2.5 and PM10 Emissions in Iron Ore Sintering Process. ISIJ International 2016;56:1580–7. https://doi.org/10.2355/isijinternational.ISIJINT-2016-169.

[83] Chen YC, Sun YM, Mou JL, Tsai PJ. Application of orthogonal array tests method to optimize operating conditions for iron ore sintering. ISIJ International 2009;49:743–8. https://doi.org/10.2355/isijinternational.49.743.

[84] Pietruck R, Janz J, Unland E, Ventrella G, Fray TAT, Martinez Pacebo M, et al. Alternate carbon sources for sintering of iron ore (Acasos). 2013.

[85] Findorák R, Legemza J, Fröhlichová M, Fabriciová G, Džupková M. New Utilization of Specific Biomass: Lignin in the Iron Ore Sintering Process. Metals (Basel) 2020;10:1170. https://doi.org/10.3390/met10091170.

[86] D. F. Ball AFB and AG. Minerals and the environment. Institution of Mining and Metallurgy 1975:453.

[87] Gao-yuan SHA, Feng-qing HUA. Influence of Sinter Raw Mix on Sinter Dust Emissions at Baosteel 2019:1–3.

[88] Fan X, Ji Z, Gan M, Li Q, Chen X, Jiang T. Participating patterns of trace elements in PM2.5 formation during iron ore sintering process. Ironmaking and Steelmaking 2018;45:288–94. https://doi.org/10.1080/03019233.2016.1262575.

[89] Harp G, Möhring S, Hillman C, Bsirske W. Alternative Processing Sinter Plant Recycling Materials. 2005.

[90] Gan M, Ji Z, Fan X, Chen X, Zhou Y, Wang G, et al. Clean recycle and utilization of hazardous iron-bearing waste in iron ore sintering process. vol. 353. Elsevier B.V.; 2018. https://doi.org/10.1016/j.jhazmat.2018.04.032.

[91] Cheng Z, Yang J, Zhou L, Liu Y, Guo Z, Wang Q. Experimental study of commercial charcoal as alternative fuel for coke breeze in iron ore sintering process. Energy Convers Manag 2016;125:254–63. https://doi.org/10.1016/J.ENCONMAN.2016.06.074.

[92] Tariq Al-Haji. Developments In Iron Ore Sintering Using A Laboratory Scaled Development Platform 2022.

[93] Post J. TATA Steel Europe - Imjuiden Research. Internal TATA Steel 2018.

[94] Assembly N, Executive S, Ireland N. UK Fine Particulate Emissions from Industrial Processes 2000.

[95] Agency E. M2 Monitoring of stack emissions to air. 2017.

[96] Dadolab. Isokinetic Sampling line configuration 2016:2–4.

[97] Pal J, Ghorai S, Venkatesh P, Goswami MC, Bandyopadhyay D, Ghosh & S, et al. Ironmaking & Steelmaking Processes, Products and Applications Development of

fluxed micropellets for sintering utilising iron oxide waste fines Development of fluxed micropellets for sintering utilising iron oxide waste fines 2013. https://doi.org/10.1179/1743281212Y.0000000069.

[98] Nyembwe AM, Cromarty RD, Garbers-Craig AM. Effect of concentrate and micropellet additions on iron ore sinter bed permeability. Https://DoiOrg/101080/0371955320161180033 2016;125:178–86. https://doi.org/10.1080/03719553.2016.1180033.

[99] Pal J, Ghorai S, Das A. Development of carbon composite iron ore micropellets by using the microfines of iron ore and carbon-bearing materials in iron making. International Journal of Minerals, Metallurgy and Materials 2015;22. https://doi.org/10.1007/s12613-015-1053-7.

[100] Peng C, Guo Z, Zhang F. Discovery of Potassium Chloride in the Sintering Dust by Chemical and Physical Characterization. ISIJ International 2008;48:1398–403. https://doi.org/10.2355/ISIJINTERNATIONAL.48.1398.

[101] Ji Z, Fan X, Gan M, Li Q, Chen X, Tian Y, et al. Speciation of PM2.5 released from iron ore sintering process and calculation of elemental equilibrium. ISIJ International 2017;57:673–80. https://doi.org/10.2355/isijinternational.ISIJINT-2016-650.

[102] Tchounwou PB, Yedjou CG, Patlolla AK, Sutton DJ. Heavy Metal Toxicity and the Environment, 2012, p. 133–64. https://doi.org/10.1007/978-3-7643-8340-4_6.